Ultrafast photo-switching of spin crossover crystals : coherence and cooperativity

Roman Bertoni

▶ **To cite this version:**

Roman Bertoni. Ultrafast photo-switching of spin crossover crystals : coherence and cooperativity. Other [cond-mat.other]. Université de Rennes, 2013. English. NNT : 2013REN1S048 . tel-01016162

HAL Id: tel-01016162
https://theses.hal.science/tel-01016162

Submitted on 28 Jun 2014

THÈSE / UNIVERSITÉ DE RENNES 1
sous le sceau de l'Université Européenne de Bretagne

pour le grade de

DOCTEUR DE L'UNIVERSITÉ DE RENNES 1

Mention : Physique

Ecole doctorale « Science de la Matière »

présentée par

Roman Bertoni

Préparée à l'unité de recherche :
Institut de Physique de Rennes
UMR CNRS 6251

Ultrafast Photo-switching of Spin Crossover Crystals: Coherence and Cooperativity

**Thèse soutenue à l'Université de Rennes 1
le 27 Juin 2013**

devant le jury composé de :

Andreas HAUSER
Professeur, Université de Genève / *rapporteur*

Pascal RUELLO
Professeur, Université du Maine / *rapporteur*

Michel VERDAGUER
Professeur Emérite, Université Pierre et Marie Curie
/ *examinateur*

Eric COLLET
Professeur, Université de Rennes 1
/ *directeur de thèse*

Maciej LORENC
Chargé de Recherche, Université de Rennes1
/ *directeur de thèse*

TABLE OF CONTENTS

Résumé

Commutation photo-induite ultra-rapide de cristaux à transition de spin : Coopérativité et Cohérence.

Le travail de thèse a pour objectif principal d'étudier la commutation ultrarapide de matériaux à transition de spin. Ces composés sont des prototypes de systèmes moléculaires bistables possédant deux états électroniques nommés Haut Spin (HS) et Bas Spin (LS). Ce changement d'états électroniques s'accompagne de changements structuraux principalement autour de l'ion métallique central. Nous nous sommes particulièrement intéressés à deux classes de systèmes moléculaires à base de Fer: Fe^{II}(LS→S=0 ; HS→S=2) et Fe^{III}(LS→S=1/2 ; HS→S=5/2).

L'état de l'art des recherches résolues en temps sur de tels systèmes est principalement divisé en deux catégories : les expériences femtosecondes effectuées sur des molécules en solution et des mesures sur des matériaux solides allant de la centaine de femtosecondes à la milliseconde pour couvrir toute la dynamique hors équilibre du système. Ces recherches s'inscrivent dans le cadre plus général des transitions de phases photo-induites (**Fig 1**). Ce champ particulièrement nouveau essaie de comprendre comment, par irradiation lumineuse, un système peut atteindre une nouvelle phase avec de nouvelles propriétés structurales et électroniques. Cela pourrait être vu comme l'application de la femtochimie à l'échelle du matériau où de nouveaux effets peuvent apparaître dus au caractère actif de l'environnement. De fameux exemples sont ceux de la transition isolant-métallique (**Chollet 2005**) ou neutro-ionique (**Collet 2003**).
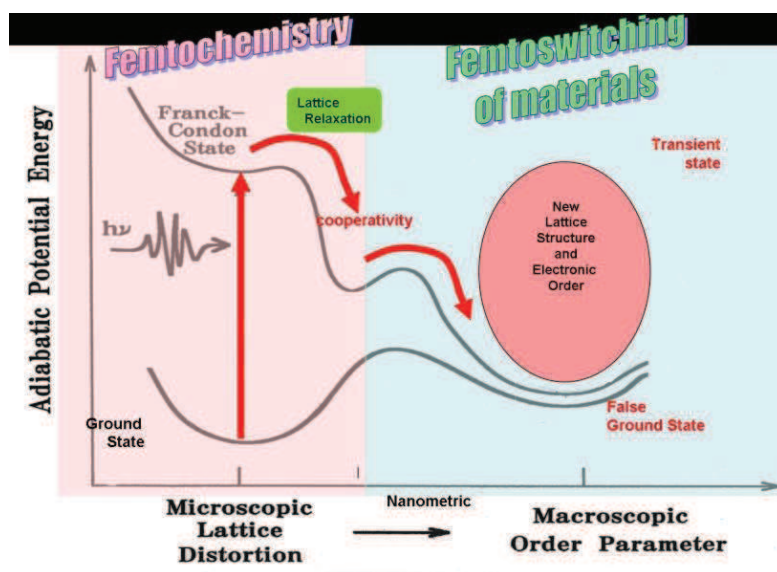
Fig 1 *Concept de la transition de phase photo-induite.*

Pour étudier ce changement, nous avons utilisé tout un panel de techniques ultrarapides reposant toutes sur le même principe : la méthode pompe-sonde. Une impulsion lumineuse, nommée pompe, excite le système à une longueur choisie. Une seconde impulsion sonde le système à différents délais de façon à reconstruire son évolution en fonction du temps. La majeure partie des résultats présentés repose sur les mesures de spectroscopie optique ultrarapide effectuées sur la plateforme laser ultrarapide de l'Institut de Physique de Rennes. De telles mesures permettent de suivre la variation d'absorption ou de réflectivité optique du composé avec une résolution temporelle de l'ordre de la centaine de femtosecondes. Ces mesures sont particulièrement utiles car elles permettent de déceler la formation d'états excités transitoires générés durant le processus de photo-commutation et nous renseigne sur la présence d'une éventuelle dynamique cohérente.

Ces résultats sont complétés par des mesures de diffraction résolues en temps effectués au synchrotron Advanced Photon Sources (APS, Argonne, USA) qui nous permettent de reconstruire la structure transitoire du cristal avec une résolution de 100 picosecondes. Pour suivre des changements structuraux locaux à l'échelle de la femtoseconde, la technique du XANES est aussi particulièrement appropriée car elle est sensible à l'environnement direct de l'atome de Fer. Elle permet d'avoir une mesure directe de l'élongation de la liaison Fe-Ligand qui est un marqueur de la transition de spin. De telles mesures de XANES avec une résolution femtoseconde ne sont possibles qu'à peu d'endroits dans le monde et ont été effectuées dans notre cas au premier laser électron-libre à rayons X opérationnel au monde; le X-FEL Linac Coherent Light Source (LCLS, Stanford, USA).

Les résultats obtenus durant cette thèse sont divisés en deux parties : la première partie s'intéresse à la commutation ultrarapide, c'est-à-dire essaie d'élargir notre compréhension du mécanisme de base à l'échelle moléculaire. La seconde partie est consacrée à la dynamique hors équilibre à l'échelle macroscopique. Il s'agît d'étudier comment le système constitué de molécules bistables va évoluer suite à cette perturbation initiale et les différents degrés de libertés mis en jeu durant le processus.

Durant cette thèse, deux composés ont été principalement étudiés :

Le composé de [$Fe^{II}(phen)_2(NCS)_2$], présentant une transition de phase du premier ordre aux alentours de 180K entre un état diamagnétique (LS, S=0) et un état paramagnétique (HS, S=2).

Le composé de [$Fe^{III}(3\text{-MeO-SalEen})$]$PF_6$, présentant une transition de phase du premier ordre aux alentours de 162K entre deux états paramagnétiques de spin différents (LS→S=1/2 et HS→S=5/2).

Le processus de commutation induite par la lumière a été étudié depuis plus d'une décennie sur des molécules en solution (**Gawelda 2006**, **Smeigh 2008**). L'absorption du photon par une bande de transfert de charge mène à un état Franck Condom instantané (^{1}MLCT ou ^{2}LMCT) qui va relaxer via un croisement inter-système (ISC). Cette première étape s'effectue sur des temps très courts de l'ordre de la dizaine de femtosecondes. Ensuite le système va traverser un ou plusieurs états excités pour finalement arriver dans le potentiel de l'état HS.

Dans le cas du [$Fe^{III}(3\text{-MeO-SalEen})$]$PF_6$, le composé est excité avec une impulsion de pompe centrée vers 800 nm sur une bande de transfert de charge. Cette bande, nommée Transfert de Charge du Ligand vers le Métal (LMCT en anglais) dans la littérature, est connue pour permettre une conversion quasi complète des molécules irradiées LS vers l'état HS.
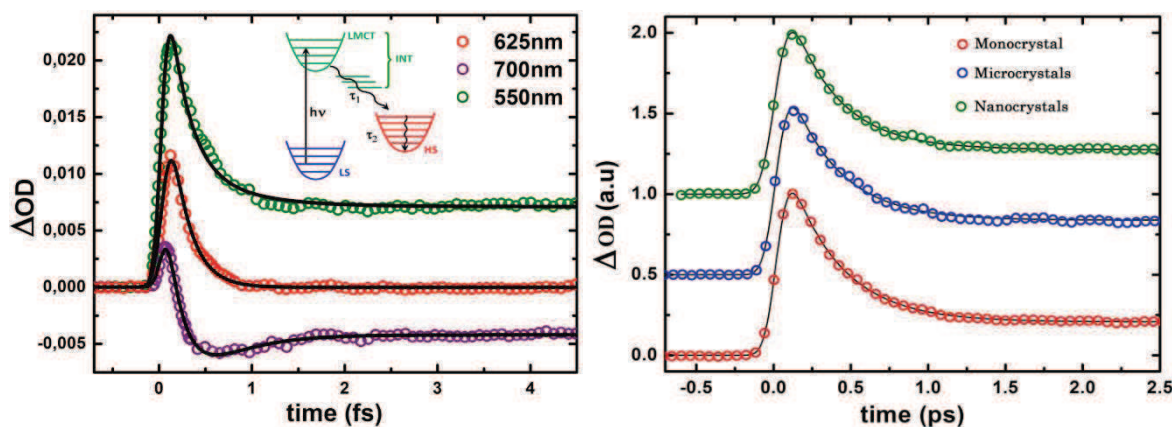
Fig 2 *Réponse de nanocristaux à une excitation femtoseconde pour différentes longueurs d'onde de pompe (gauche),*

Reponse de différentes tailles d'échantillons à la même longueur d'onde de sonde (droite).

Les résultats obtenus (**Fig 2**) montrent que la génération de molécules HS se fait à une échelle sub-picoseconde. En analysant plus précisément la dynamique, il a été extrait deux constantes de temps à ce processus. La première constante de temps de 200 ± 20 fs correspond à la population de l'état HS par les états électroniques excités. Le second processus plus lent (500 – 800 fs) est associé à un phénomène d'affinement spectral caractéristique du processus de refroidissement vibrationnel. Il traduit le fait que lorsque la molécule arrive dans le potentiel HS, il reste des états vibrationnels excités qui vont relaxer pour que le système atteigne le fond du potentiel HS.

Ce type de mesure a été fait avec des échantillons de différentes tailles allant du mono-cristal standard à des échantillons nanométriques. Dans tous les cas, les dynamiques observées ont été les mêmes quelque soit la taille ou l'environnement du système. De plus, le nombre de molécules photo-converties est linéaire avec la puissance de pompe, donc avec le nombre de photons incidents. Ces deux faits prouvent que la commutation de spin par la lumière est un phénomène purement local où les molécules agissent indépendamment les unes des autres. Bien que nous ayons étudié des systèmes fortement coopératifs, aucun effet coopératif n'a été détecté sur les échelles de temps picoseconde.

Pour photo-exciter le [$Fe^{II}(phen)_2(NCS)_2$], on utilise une impulsion de pompe à 650 nm dans une bande de transfert de charge. Dans ce cas de figure, à l'inverse du [$Fe^{III}(3-MeO-SalEen)]PF_6$, il s'agit d'un transfert de charge du métal vers le ligand, ce qui signifie que l'électron excité est envoyé d'une orbitale du Fer vers une orbitale du ligand. Les dynamiques ultra-rapides observées (**Fig 3**) diffèrent dans le sens où une dynamique oscillatoire correspondante à plusieurs phonons optiques est observée. De plus, le temps de relaxation des états excités, connus sous le nom de MLCT, est inférieur à 50 fs ce qui est trop court pour pouvoir être déterminé par notre système.
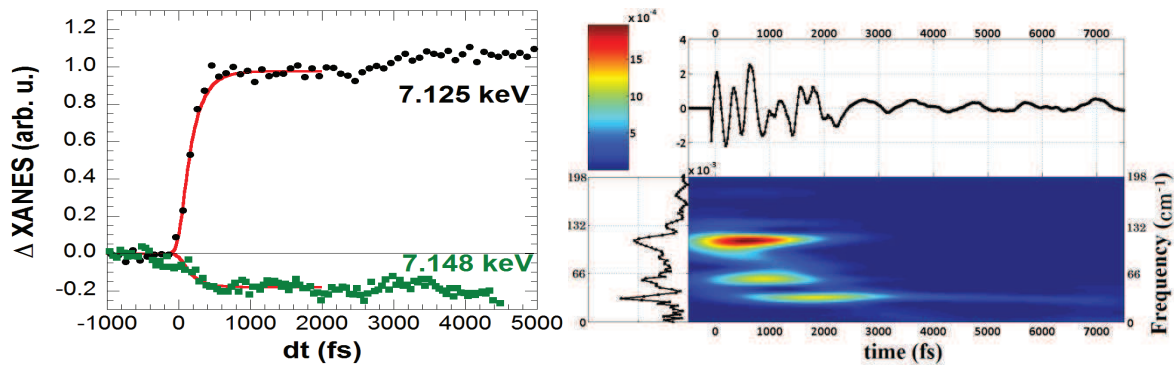
Fig 3 *Mesure de XANES femtoseconde sur le [Fe^{II}(phen)₂(NCS)₂] (gauche),*

Dynamique oscillante et sa Transformé de Fourier dépendante du temps (droite).

En parallèle de ces mesures optiques nous avons effectué des mesures de XANES femtoseconde au X-FEL LCLS. Ces mesures nous permettent d'avoir une signature structurale du processus avec une résolution de l'ordre de la centaine de femtosecondes. Cela a permis de déterminer un temps d'élongation de la liaison Fer-Ligand de   170 ± 10fs. Cela signifie que dans un tel processus, les degrés de liberté électroniques et structuraux sont dissociés. De plus l'analyse par transformée de Fourier du signal oscillant nous a permis d'extraire plusieurs fréquences correspondant à des modes propres de l'état Haut Spin. Un premier phonon (113cm^{-1}) est activé à temps zéro et correspond à un mode de respiration des liaisons Fe-ligand mettant en jeu principalement les liaisons avec les groupements phenantronlines. Ensuite d'autres phonons sont activés avec un certains délai par rapport au temps zéro : principalement un phonon correspondant à un mode de torsion du ligand qui apparaît vers 500 fs et des modes de basses fréquences (59cm^{-1} et 33cm^{-1}) correspondant à des modes de réseaux.

L'ensemble de ces résultats nous permet de mettre en évidence le caractère séquentiel de la commutation ultrarapide avec l'activation à différents délais de divers degrés de liberté. Il semble aussi que l'amortissement rapide des phonons optiques (300 fs) activés à temps zéro soit un paramètre clé dans la stabilisation de l'état HS photo-induit. Contrairement aux composés de Fe^{III}, une réponse cohérente impliquant plusieurs phonons optiques est observée. Cela est peut être dû à la vitesse du croisement inter-système qui permet de garder la cohérence sur des modes rapides.

La réponse de tels cristaux à transition de spin à une excitation femtoseconde est un processus multi-échelles faisant intervenir différents degrés de liberté sur une gamme temporelle de dix décades (**Lorenc 2012**). D'abord a lieu la photo-commutation à une échelle sub-picoseconde. Les molécules HS ayant un volume supérieur à celles LS, cela produit un gradient de pression dans le cristal. Ce gradient va relaxer en entraînant une dilatation du réseau concomitante avec une nouvelle création de molécules HS. Ce processus met en jeu les couplages élastiques inter-moléculaires et apparaît à l'échelle de la nanoseconde qui est le temps nécessaire à la vitesse du son pour parcourir les dimensions typiques du cristal. Ensuite, l'énergie résiduelle déposée par le laser augmente la température du cristal ce qui a pour effet de peupler thermiquement l'état HS. Ce processus prend effet à l'échelle de la microseconde et s'accompagne d'une homogénéisation du cristal en température et en pression. A l'échelle de la centaine de microsecondes, le cristal est homogène en température et en pression mais n'est pas à l'équilibre thermique avec son environnement. Le système relaxe vers son état d'équilibre avec des constantes de temps de l'ordre de la milliseconde.
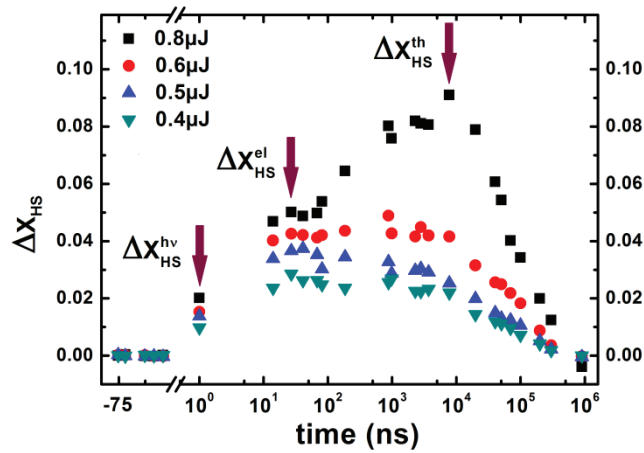
Fig 4 *Dynamique hors équilibre du [Fe^{II}(phen)$_2$(NCS)$_2$] après une excitation femtoseconde.*

Dans le cas du [Fe^{II}(phen)$_2$(NCS)$_2$], on retrouve bien les trois étapes (**Fig 4**) précédemment observées pour des composés de Fe^{III} faiblement coopératifs mais la dernière étape n'apparaît qu'au-delà d'une densité d'excitation critique. En effet, le peuplement thermique à l'échelle de la microseconde n'est pas présent à faible densité d'excitation et le système ne fait que relaxer après la dizaine de nanosecondes. Ce peuplement thermique n'est le fruit que d'une augmentation transitoire de température
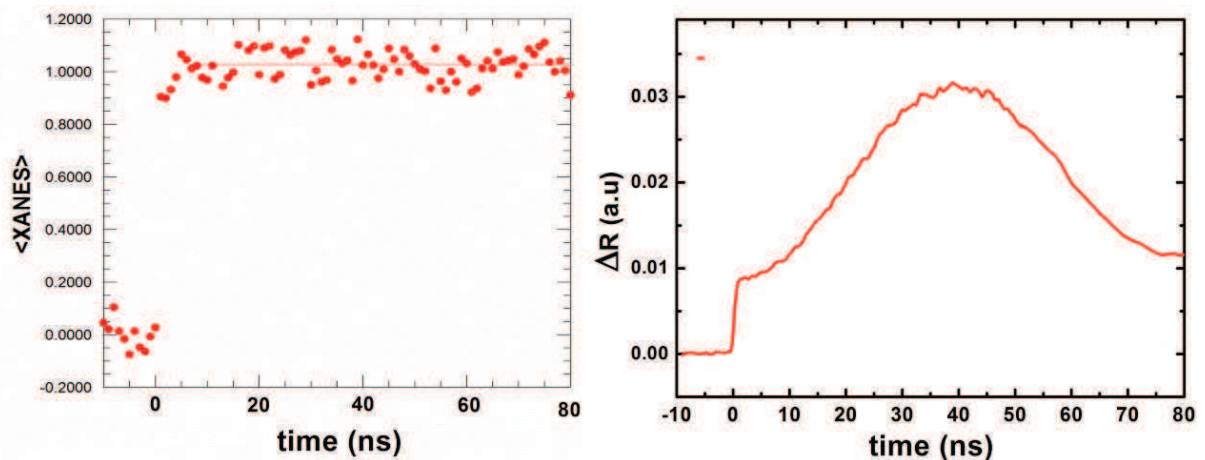
Fig 5 *XANES et réflectivité du [Fe^{II}(phen)$_2$(NCS)$_2$] dans la gamme temporelle 0-80 ps.*

De plus les molécules HS créées à l'échelle de la picosecondes se comportent comme des génératrices d'ondes acoustiques. Ces ondes entrainent une modulation périodique de la fonction diélectrique du cristal et nous avons donc pu les détecter à l'aide de mesures de réflectivité. Mais pour autant ces phonons acoustiques n'entrainent pas une modulation de la fraction HS comme le montre les mesures de XANES (**Fig 5**). La variation de fraction HS à l'échelle de la nanoseconde est corrélée à une dilatation d'ensemble du cristal et réfère à un phénomène macroscopique au lieu d'une commutation locale microscopique.
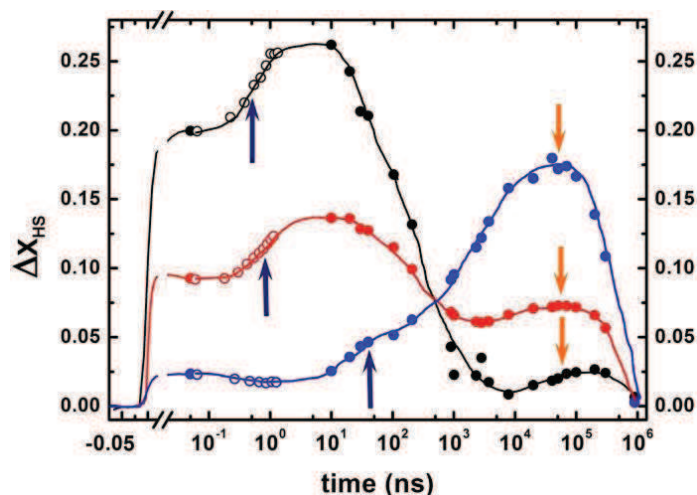
Fig 6 *Dynamique hors équilibre pour différentes tailles d'échantillons.*

Le fait de posséder plusieurs tailles d'échantillon de [Fe^{III}(3-MeO-SalEen)]PF$_6$ nous a permis d'observer l'influence de la taille des cristaux sur l'ensemble du processus. Les mesures ont été effectués sur trois catégories d'échantillons : Nanocristaux [(950±150)×(270±40) ×(35±7) nm^3], microcristaux [(7.5±2.1) ×(0.64±0.15) ×(0.21±0.03) µm^3] et mono-cristal[(200±50)×(300±50) ×(10±5) µm^3]. De précédentes mesures avaient mis en évidence le lien direct entre la taille de l'échantillon et le temps de dilatation (**Collet 2012**). Dans notre cas de figure, les épaisseurs des échantillons de nanocristaux (noir) et le mono-cristal (bleu) changent de deux ordres de grandeur, ce qui se traduit par un décalage de la réponse élastique vers les temps courts par plus de deux décades (**Fig 6**).

La réponse à une impulsion femtoseconde de tels systèmes comporte 3 étapes comme vu précédemment dans des composés de Fe^{III} faiblement coopératif. A l'échelle de la picoseconde à lieu la commutation photo-induite avec une meilleure conversion dans le cas de nanocristaux. Cela s'explique par une excitation très homogène de tels échantillons qui sont beaucoup plus petit que la longueur de pénétration de la pompe. Ensuite on peut remarquer un décalage de deux décades dans le front acoustique schématisé par une flèche bleu. Cette valeur est en accord avec le rapport de taille entre les nanocristaux et le mono-cristal pointant clairement le caractère propagatif de ce processus. Enfin à l'échelle de la microseconde, on retrouve le peuplement thermique par effet de chauffage.

Ce processus est indépendant de la taille et est seulement piloté par une constante cinétique sensible à la pression et à la température. Mais dans le cas des échantillons de petites tailles, cet effet est presque supprimé. Cela peut s'expliquer par une meilleure dissipation de l'énergie déposée par le laser due à deux facteurs. En premier lieu, le rapport surface sur volume est plus favorable pour nanocristaux ce qui doit faciliter la dissipation. En second lieu, dans le cas des microcristaux et nanocristaux, ceux-ci sont piégés dans une matrice polymérique inerte qui dissipe mieux l'énergie que le jet d'azote dans le cas du mono-cristal.

Ces études ont donc apporté de nouvelles compréhensions sur les processus photo-induits multi-échelle dans les matériaux moléculaires photo-actifs. Tout d'abord au niveau de la réponse moléculaire puis ensuite au niveau de la réponse au matériau. En dégageant les mécanismes fondamentaux jouant un rôle important dans ces processus, ces études ouvrent la voie à de nouveaux dispositifs photo-actifs basés sur de nouveau design moléculaire et de nouvelles mises en forme

__Introduction__

Photo-induced phase transitions are a fascinating field of material science and a new great challenge for controlling materials by light at ultrafast time scale.

The ensemble of work presented in this manuscript is based on the investigations of ultrafast photo-switching of Spin Crossover Molecular Crystals, considered prototypes of molecular bistability in the solid state. Owing to the tremendous progress in chemical engineering, it's now possible to tune at will the properties and the scale of a chosen material for switching its physical properties (color, magnetism...) under various control parameters such as temperature, pressure, magnetic field... Some cooperative properties may emerge, and another important question is being asked whether these properties e nanoscale. The trapping of light-excited states opens the doorway to developing light-activated functions. All these features result from complicated couplings between different degrees of freedom, such as electronic and structural ones.

The ultrafast photoswitching study of SCO materials presented here benefit from the growing knowledge and new experimental facilities developed to serve the more general filed, namely the ultrafast science. Nowadays, table top laser systems open at laboratory scale the femtosecond frontier (10^{-15}s), where a completely different science emerges with new non trivial processes such as coherence. For instance, femtochemistry shows that time obtaining ultrafast time resolution is rewarded by a phenomenal amount of new information. However, the new challenge is not only the watch the system but also to gain control over physical properties at extreme time scales. In order to understand which degrees of freedom are involved in ultrafast processes, new "cameras" have been built relying on optical spectroscopy and X-ray diffraction or absorption. The construction of large-scale facilities and the advent of new light sources, such as X-ray Free Electron Laser, provide ultrashort and ultrabright X-ray pulses are likely to revolutionize the ultrafast structural science. Taking a picture of atomic motion at femtosecond time scale is no more a dream but a reality achievable at a laboratory scale. By combining spectroscopy and structural techniques, an accurate picture of the out-of-equilibrium processes in SCO materials is presented.

This manuscript is divided in four chapters:

The first chapter is a general introduction to the Photo-Induced Phase Transitions and Ultrafast Science. In addition, it presents general aspects of Spin Crossover Systems and the state of the art of ultrafast spin state switching.

The second chapter is dedicated to experimental tools I used during my thesis. The ultrafast optical spectroscopy experiment at the Institut de Physique de Rennes allows investigating with high accuracy photo-induced phenomena in the fs-ms time window. I also used complementary time-resolved techniques on large-scale facilities, a synchrotron and X-FEL, on which I performed X-ray diffraction and XANES measurements.

The third chapter focuses on the ultrafast spin state photo-switching in the solid state. The inter system crossing and the structural trapping of the photoinduced state are discussed. The coherent breathing of the ligand is revealed, and the trapping of the excited state is discussed in terms of an efficient damping process.

In the fourth and last chapter, we investigate the complete out of equilibrium dynamics of SCO crystals. The femtosecond molecular photo-switching triggers a sequence of additional switching between LS and HS states observed at longer delays. The latter processes are discussed in terms of elastic interactions as crystal volume expands (ns), and thermal population of the HS state (ms). We attempt a mechanistic description of the underlying physical processes.

Chapter1: Photo-Induced Phase Transition and Multi-stability

1.1 Phase Transition and Multistability

One of the major concepts in condensed matter physic and more generally in science is the concept of phase transition (**Landau 1980, Diu 1989**). The striking force of this concept lies in its universal nature allowing describing the evolution of different systems with a limited number of parameters. Numerous systems undergo a classical phase transition cascade (gas→liquid→solid) and equilibrium phases are defined for given values of external parameters {T,P,V,…}. Numerous tools exist to investigate and understand phase transition phenomena. The equilibrium state is determined by the free energy of the system G, which must take the lowest value. It may correspond to a unique phase (liquid, solid, gas), but sometimes several phases can coexist with the same free energy. A simple case is the liquid-gas transition where beyond the critical point both liquid and gas phases become indiscernible. And in solid state the same kind of situation may occur at larger scale.

Indeed, in the case of solid state material, the potential energy landscape is quite complex and numerous quantities of local free energy minimum may exist. This complex landscape allowed in certain cases presents several minimums of free energy which corresponds to different macroscopic phases with completely new structural and electronic orders. It refers to a mutlistable situation where solid-solid phase transition exists in the same compound. This concept of mutlistability goes hand to hand with increase of material functionality. Indeed, numerous materials present phase transition between two phases of completely different characters like para- to ferro-magnetic, or metal-insulator transition. Thanks to a tremendous progress of material chemistry, it is achievable to get material with properties on demand like photo-magnetism, photo-conductivity, photo-magnetism, etc... By triggering the transition in this system with an external parameter, the control of pertinent physical properties is achieved.

1.2 The case study of Spin-Crossover Materials

1.2.1 The two electronic states of the molecular system

The spin crossover (SCO) compounds are acclaimed as prototypes of molecular bistability in the solid state. Indeed, such compounds with transition metal ions of $3d^4 - 3d^7$ configuration in octahedral surroundings (or even $3d^8$ with lower symmetry) exhibit a change of spin multiplicity (**Gütlich & Goodwin 2004**). A spin state of a metal ion can be switched between a high spin HS state and a low spin LS state (even dia-magnetic if S=0) depending on the external conditions, such as temperature, pressure, the presence of magnetic or electric fields, of light, *etc.* This change of spin (electronic) state is accompanied by an electronic redistribution in a molecule which brings out a change of optical properties and of molecular geometry (notably a change of metal-ligand bond lengths; see **Fig 1.1**). In particular, variations in molecular geometry can manifest themselves as a change of volume, which triggers pressure effects, and as a change of vibrationnal frequencies, which triggers entropic effects. This observation has been reported for the first time with the pioneering

work of Cambi (**Cambi 1931**) who has noticed an unusual magnetic behavior in a Fe^{III} compounds under thermal variation. More often this type of phenomena is observed on Fe^{II} or Fe^{III} complexes, but nowadays similar observations are reported in system with Cobalt, Nickel, Copper, etc. (**Gütlich & Goodwin 2004**).

For describing this phenomenon, it's necessary to take care about some ligand field considerations. In the case of metal transition systems with 5 electrons in the d-shell and having an octahedral environment, theory predicts a splitting of the d orbitals with t$_{2g}$ and e$_g$ levels and two possible electronic ground states. In the electronic distribution of the Low Spin (LS) state, electrons populate the t$_{2g}$ orbital only. By opposition, in the High Spin (HS) state electrons populate both t$_{2g}$ and e$_g$ orbitals as the Hund Rules is fulfilled. The t$_{2g}$ being bonding orbitals and the e$_g$ being antibonding, the switch between these two states leads to a structural reorganization of the molecules.
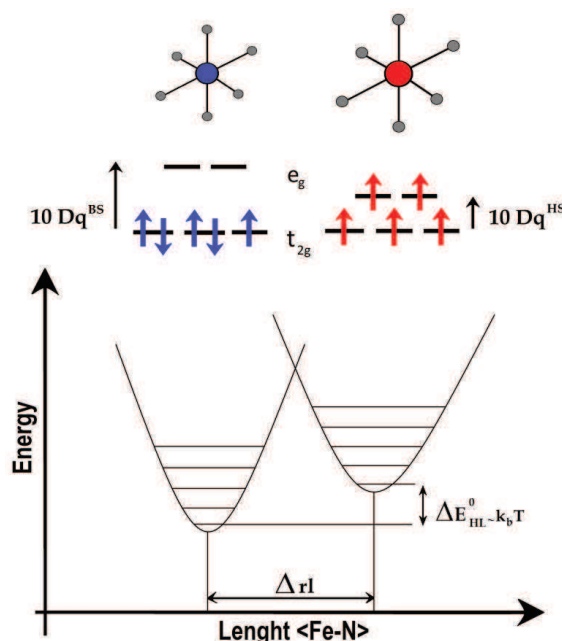
Fig 1.1 Energy diagram for LS State and HS State and the associated structural change.

In the O$_h$ representation n$_d$ orbital are split into two groups, t$_{2g}$ assigned to d_{xy}, d_{yz}, and d_{zx} and e$_g$ assigned to d_{z^2} and $d_{x^2-y^2}$. The energy splitting between these two groups is linked to the ligand field strength, usually referred in the literature as 10 Dq (**Fig 1.1**). 10 Dq translates the influence that ligand field exerts on the electron distribution and may change the possibility of occupying one of the two electronic configurations. This effect competes with the electron pairing energy π. Increasing the ligand field tends to stabilize the low spin configuration because it costs more energy to occupy the e$_g$ orbital.

The 10 Dq value must remain between two critical values in order to present some bi-stability under accessible conditions by playing on temperature or pressure for example. If not, the barrier between the two states is so high that it is impossible to switch between these two states with these external parameters.

In order to estimate the possibility of such conversion between LS and HS states, the energy difference between the two LS and HS states $\Delta E_{HL}^0 = E_{HS}^0 - E_{LS}^0$ should be of the order of the thermal energy $k_B T$.
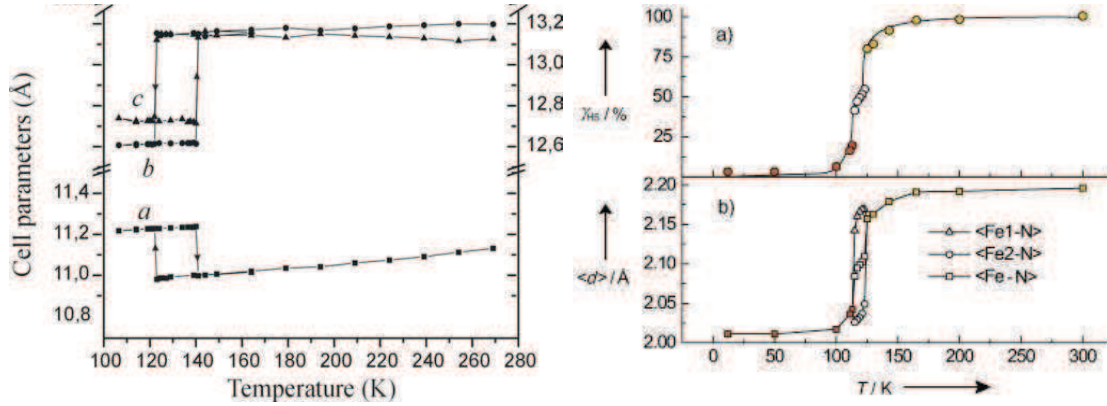
Fig 1.2 *X-ray diffraction of unit cell parameter **a** (**Pillet 2004**) and bong length <Fe-N> in different Fe^{II} systems during the thermal transition, (**Chernyshov 2003**).*

The spin state change from LS to HS leads to structural rearrangement at molecular level but also at macroscopic level (volume and shape of the crystal) (**Fig 1.2**). Indeed, the orbital populate during the transition in HS state e$_g$ are antibonding and generate an increase of bond length <Fe-N>. In addition to the bond length elongation other structural parameters like distortion can be involved during the transition (**Buron 2012**). This change of the molecular structure is concomitant with change of the lattice cell parameters. New cell parameters are of higher values and lead to crystal expansion. The conventional values for Fe^{II} systems are an increase of 10% in volume unit cell and 10% in the bond length <Fe-N>. These ratios are smaller in Fe^{III} compound (**Van Koningsbruggen 2004**).

1.2.2 Phase Transition and Spin Conversion

SCO systems are not only of interest for potentials applications as storage devices but the prototype bistability character of such systems make them useful case studies in order to test theoretical tools in the phase transition fields. The two levels aspect of SCO systems made it a good candidate for Ising like model (**Wajnflasz 1971**), able to predict the apparition of 1st order transition in SCO system. It considers a square lattice with particles at each node i or j and two different states accessible characterized by the eigenvalues S_i, for HS S_i = +1 and LS S_i = -1. The Hamiltonian of such system is:

$$H = -J \sum_{\langle i,j \rangle} S_i S_J - h_{eff} \sum_i S_i$$

The two states +1 and -1 are of degeneracy g$_+$ and g$_-$; J corresponds to the inter-sites coupling between the nearest neighbors and h$_{eff}$ is mean-field proportional to temperature expressed like :

$$h_{eff} = -\frac{1}{2}\left(\Delta - k_b T \ln(g)\right) \text{ with } g = \frac{g_+}{g_-}, \quad \text{which gives } H = -\sum_{\langle i,j \rangle} J_i S_i S_j + \frac{1}{2}\sum_i \left[\Delta_i - k_b T \ln(g)\right] S_i$$
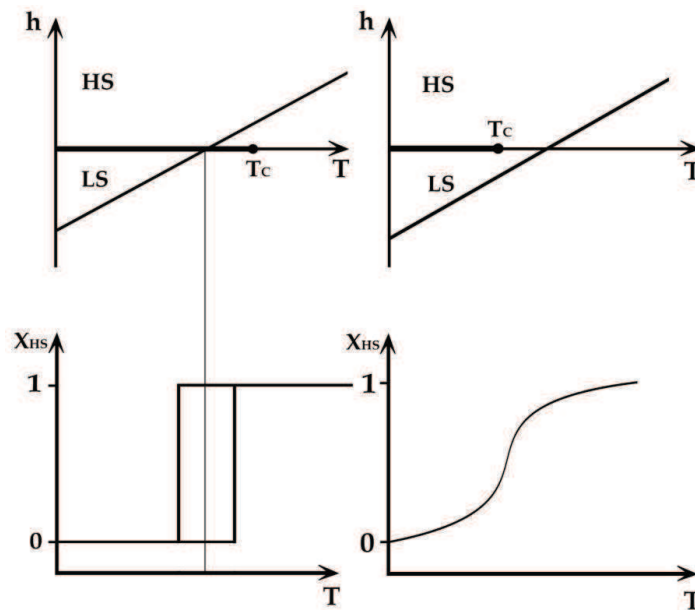
Fig 1.3 *Phase diagram for classical Ising Model.*

The phase diagram of such Ising-like model is universal model (**Fig 1.3**), with a key parameter named T_c. It refers to a critical temperature $T_C = \dfrac{qJ}{k_B}$ that depends on the intensity of the inter-sites coupling J and the number of first neighbors q. $T_{1/2}$ is defined as temperature corresponding to an equal repartition of molecules between HS and LS : $T_{1/2} = \dfrac{2\Delta}{k_B \ln(g)}$

Below T_c, 1st transition occurs with an abrupt change of the HS fraction around $T_{1/2}$. This transition involves a hysteresis centered at $T_{1/2}$ whose the width depends on the intermolecular coupling. Under T_c, the transition is 2nd order kind with a gradual change of HS fraction.
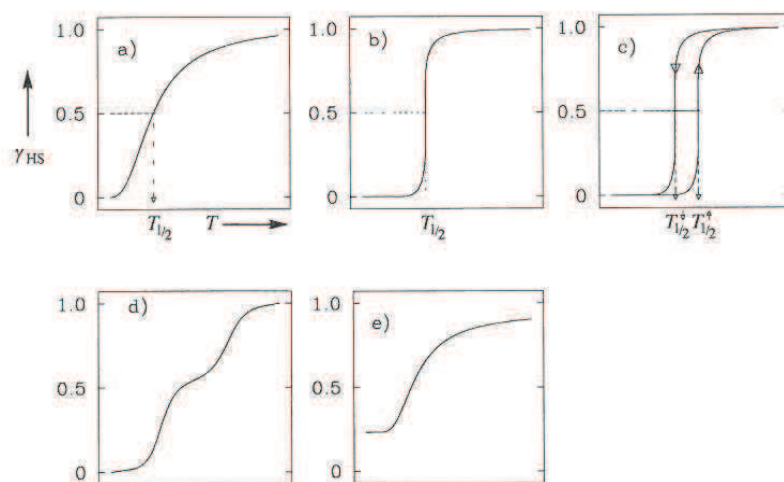
Fig 1.4 *Different transitions observed in SCO systems (*Gutlich 1994*).*

But the discovering of two-steps transition, as many others kind of transitions (**Fig 1.4**), required to develop new concepts. It reveals the importance of the competition between short range and long-range interaction in SCO systems. Introduction of short range antiferro interactions allows solving this problem in terms of Ising-like model (**Bousseksou 1992, Nishino 2003**). It considers two sublattices interacting each other via the crystalline field *h* of each :

$$H = -J_{AA}\sum_{\langle i,j \rangle} S_i^A S_j^A - J_{BB}\sum_{\langle i,j \rangle} S_i^B S_j^B - J_{AB}\sum_{\langle i,j \rangle} S_i^A S_j^B - h\sum_i \left(S_i^A + S_i^B \right)$$

J_{AA} and J_{BB} are intrasublattice coupling and J_{AB} intersublattice coupling with : J_{AA}, J_{BB} > 0 (ferro-like) and J_{AB} < 0 (antiferro-like).

But SCO transition may be also understood in terms of elastic interactions (**Slitcher 1972**). Indeed, the transition is concomitant with a lattice change of volume, shape and elasticity. This problem can be solved in terms of mean field model where the associated field refers to a pressure field (**Spiering 1989 & 2004**).
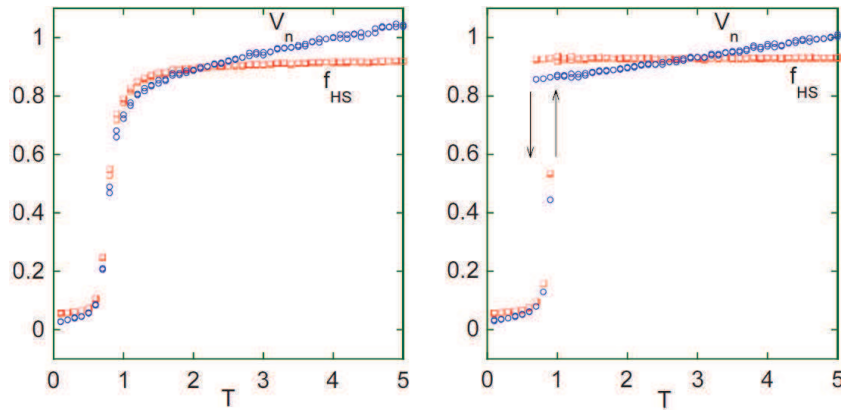
Fig 1.5 *Simulation of SCO transitions for different intermolecular interactions (**Nishino 2009**).*

More recently, a new kind of SCO cooperative model goes beyond the classical mean field approach and is based on ball and spring concept. In this case elastic interactions arise from lattice distortion resulting to the volume difference between HS and LS (**Nishino 2007, Stoleriu 2008**). This model uses both Monte Carlo and Molecular Dynamics computational techniques with different Hamiltonians. It succeeds to reproduce different transition behaviors and cooperative effect (**Nishino 2009** & **Fig 1.5**).
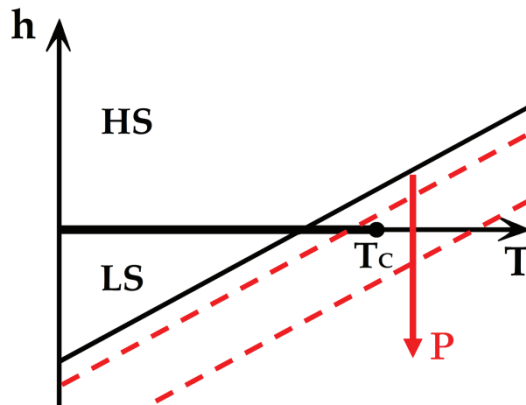
Fig 1.6 *Influence of Pressure on SCO transition.*

It is possible to shift the transition temperature by applying an external field on the system, such as pressure for example (**Fig 1.6**). In addition to change the transition temperature $T_{1/2}$, it also modifies the transition from a 1st order to a crossover above the critical point (**Bousseksou 2003, Ksenofontov 2004**). Indeed, the enthalpy will change and favor the LS state of smaller volume. On contrary, a decompression or negative pressure will favor the HS state and it is analog to lattice dilatation.

The origin of spin state may be investigated in terms of energy (**Sorai 2004, Sorai 1974**). The driving process that is responsible of spin transition is the huge increase of entropy during the LS→ HS conversion. This term can be split into two parts : an electronic one due to spin state and a vibrationnal one, each having different weights in the process. In the case of Fe^{II} systems, when the spin state switches between HS (S=2) and LS (S=0), we can estimate the two entropic terms related respectively to electronic distribution and lattice vibration. The electronic term is

$\Delta S_{spin} = k_B \ln\left(\dfrac{g_{HS}}{g_{LS}}\right)$ where g is spin multiplicity of one molecule. And the vibrationnal one is:

$\Delta S_{vib} = S_{HS} - S_{LS}$ which leads in harmonic oscillator approximation to

$F = -k_B T \ln\left(\dfrac{k_B T}{\hbar \omega}\right)$ ... S ... $k_B\left[1 + \ln\left(\dfrac{k_B T}{\quad}\right)\right]$ so $\Delta_{vib} = k_B \ln\left(\dfrac{\hbar \blacksquare}{\hbar \blacksquare}\right)^6$ for one molecule.

We can approximate the solid state with N oscillator:

$\Delta S_{vib} = k_B \ln\left(\displaystyle\prod_{i=1}^{R} \dfrac{\omega_{iLS}}{\omega_{iHS}}\right)$

The heat capacity in solid state can be decomposed in several parts (**Sorai 1974**):

$$C_v(normal) = C(g(v)) + \sum g_i C_E(v_i) + C_{magn}$$

The two first terms take into account lattice vibrations and the last one refers to the electronic aspect of the transition. And depending on the transition order, the heat capacity may change dramatically (**Fig 1.7**).
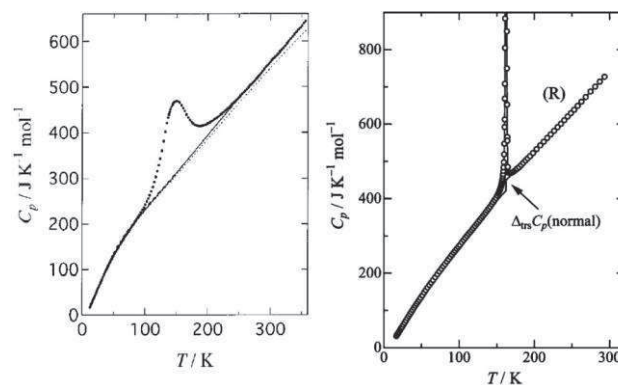
Fig 1.7 *Heat capacity in 2nd order system (left) and 1st order system (right), (**Sorai 2004**).*

In a case of a first order transition, an anomaly like a Dirac peak occurs at the transition temperature corresponding to a latent heat like liquid-gas transition. In the case of a crossover, a small deviation exists compared to pure lattice during the entire crossover. In both case, it is a Schottky anomaly that refers to the two level aspect of SCO system.

1.2.3 LIESST effect : SCO as prototype photo-switchable materials

At the end of the seventies, on one hand it was admitted that pressure, magnetic field, and temperature can switch the spin state of such SCO system. On the other hand, some studies on molecules in solutions have shown the possibility to perform spin state photo-switching and to create short-lived HS excited state that relaxes with ns time scale (**Lawthers 1984**). But crucial step arrives with the capacity to trap the HS state of SCO in solid state under continuous irradiation at low temperature. First proof has been reported on the Fe^{II} compound $[Fe(ptz)_6]$ $(BF_4)_2$ (**Decurtins 1984**).
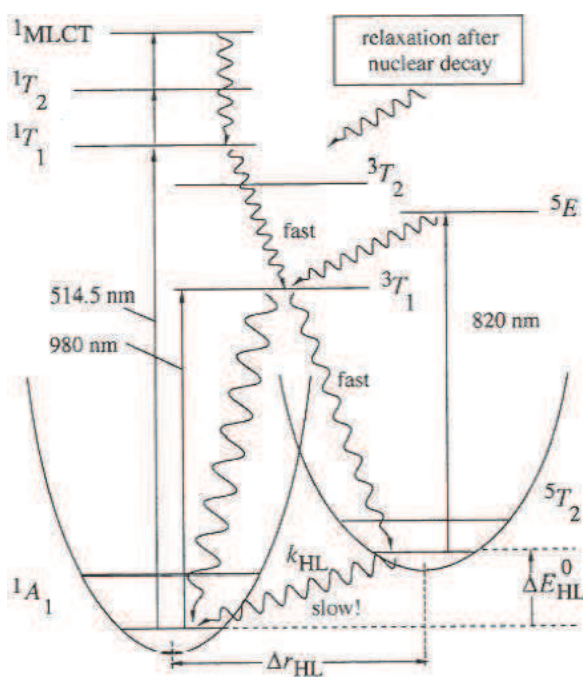
Fig 1.8 *Schematic diagram of LIESST effect (**Hauser 1986**).*

By irradiating LS molecules with visible light, HS molecule can be generated because of the efficient electronic decay of excited state via Inter System Crossing towards HS state (**Fig 1.8**). This effect is now referred as LIESST (Light Induced Electronic Spin State Trapping) in the literature. Once irradiation is stopped, the system relaxes to the thermal equilibrium state LS. But depending on the temperature, the mechanisms involved during the relaxation process can differ and the lifetime of metastable HS varies from ms to several days. At really low temperature, the thermal energy is not large enough to overpass the potential barrier between the two states and the relaxation mainly occurs through quantum tunneling effect. At higher temperature, thermal energy allows passing the barrier through classical vibrationnal process and molecules relax on s-ms time scale (**Hauser 2004**). Due to the different nature of the processes involved during the relaxation, the time constant for the same compound may change of several orders of magnitude, depending on temperature (**Krivokapic 2010**).
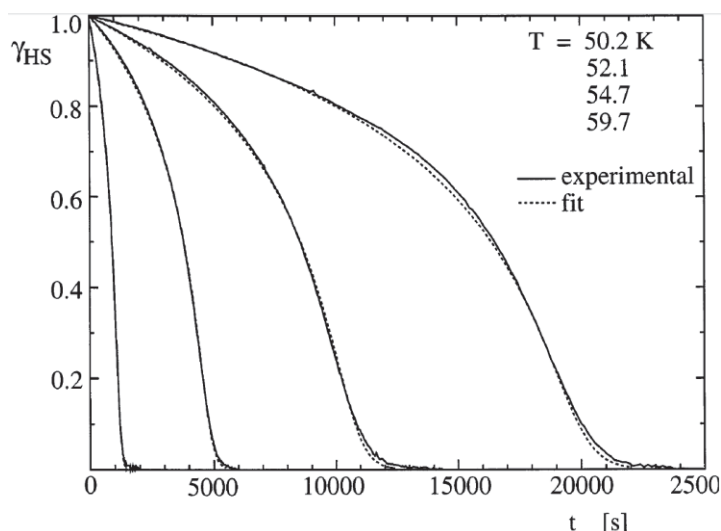
Fig 1.9 *Relaxation of HS state is cooperative system (**Hauser 1999**).*

After, with the discovery of the LIESST, ns laser were used to investigate the relaxation in solid state where cooperative effect may occur. Because of the intermolecular coupling, relaxation may differ from the classical single exponential decay (**Hauser 1992**). Indeed, the variation of HS fraction modifies the kinetic constant and leads to a self accelerated relaxation giving sigmoid shape (**Fig 1.9**). The relaxation rate in addition to HS fraction dependence is modulated by the crystal temperature and the strength of the intermolecular coupling (**Hauser 1999**). Such behaviors have been reproduced by theoretical calculation (**Boukheddaden 2000**).

Not only the relaxation of the metasable HS state but also its stability has been investigated. The efficiency of spin state trapping is quantified by a characteristic temperature *T* (LIESST). It is defined as the limit temperature above which the HS state, photoinduced at 10 K has thermally relaxed using a heating rate of 0.3 K· min^{-1}. A high T_{LIESST} value indicates a high stability of the trapped HS state (**Letard 2006**). Several parameters play a role in this stabilization of the photoinduced HS state and especially the molecular structure reorganization (**Buron-Le Cointe 2012**).

The opposite switching process from HS to LS is also possible in some cases, by irradiating at another energy the HS species formed at low temperature. This process is known as reverse-LIESST (**Hauser 1986**). But in this case, the quantum efficiency of the ISC is weaker than the one in LIESST. These first studies of LIESST and reverse LIESST processes were performed at low temperature with weak *cw* light excitation and were investigating the kinetic population or relaxation of photo-excited states. First time resolved experiments in spin crossover system were performed with ns laser to determinate the relaxation constant of metastable HS state in solution (**Lawthers 1984**). Nowadays, nanosecond (ns) lasers are used to perform single shot experiment in solid state outside and inside hysteresis (**Bonhommeau 2005**, **Galle 2010**) and also to catch fast relaxation in weakly cooperative system (**Enaschescu 2006**). Due to the huge amount of photons in a single ns pulse, a complete spin state switching of a crystal with a single shot is performed (**Cobo 2008**).

The high flexibility of spin crossover systems and its photo-switchable character leads to new concept : light-based control science, as transition between different excited states are possible as illustrated in bi-nuclear systems (**Trzop 2007**). This electronic configuration change goes with a change of color, volume, heat capacity and magnetic susceptibility. So light may control numerous physical properties of the system thanks to the molecular bistability or multi-stability. Fundamentally the study of such out-of-equilibrium processes driven by light in SCO systems can be discussed in the more general field of Photo Induced Phase Transition.

1.3 Photo-induced Phase Transition : Ultrafast Light Control

1.3.1 Photo Induced Phase Transition Concept

Even in solid state, some materials undergo transition between two phases of different properties with or without symmetry changes (**Le Cointe 1995**, **McWhan 1969**). These phases may have different macroscopic properties and the key parameter which drives the transition and selects a configuration is the free energy G of the system. The potential energy landscape may exhibit some local minimum that cannot be reached with thermal energy, because the amount of energy available is not large enough to overpass potential barriers. These local minima may be associated to new macroscopic phases with different electronic and structural orders providing a hidden multi-stability. A new approach emerges at the end of the 80's with the concept of Self Trapped Excitons and Photo Induced Structural Change (**Song & Williams 1993**). Excitons are referring to photon absorption by electrons that will lead to transient excited state. This transient state induces electronic density change and lattice distortion in response to sudden charge redistribution. People start to be convinced that such phenomenon can generate a new macroscopic phase by spreading of instabilities (**Fig 1.10**). At that time, the term Photo Induced Structural Transition has been used to describe such effect (**Nasu 1997**).
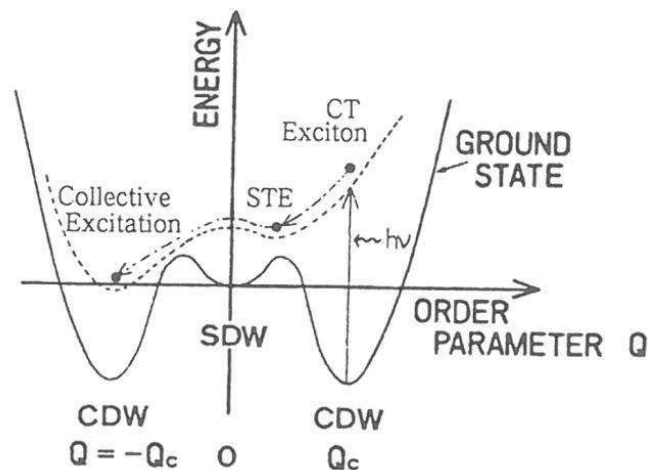
Fig 1.10 *Schematic view of Photo induced Structural Change (**Nasu 1997**).*

Using light is a powerful tool to explore potential energy landscape and try to find new local minimum. Indeed, thermal energy is on the order of $k_B T$ so only a small part of the phase space is explored. The typical photon energy in the eV range deposited by a photon, allows the system to explore a larger phase space. The main idea behind Photo Induced Phase Transition is to reach hidden false ground state by surfing on potential energy surface towards new local minima. If the false ground state reached has potential energy barriers high enough to trap the excited state for days and nullify thermal energy, the new phase may be seen as a metastable state.
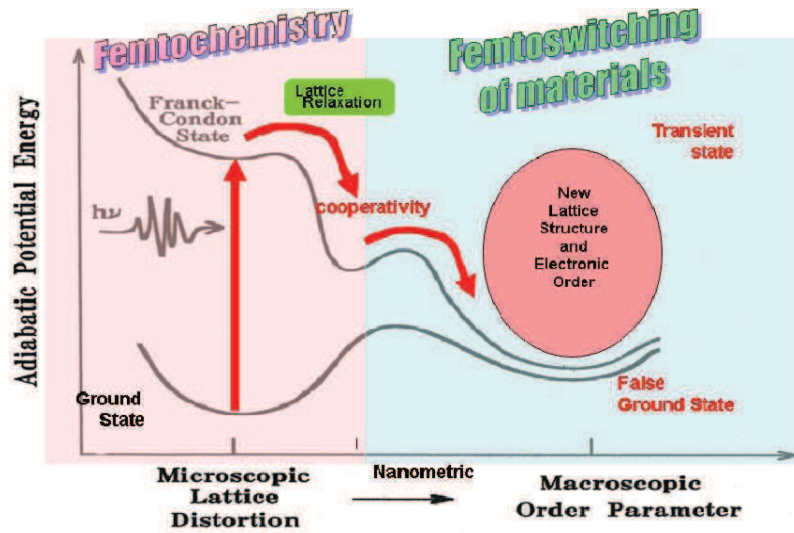
Fig 1.11 *Idea behind the concept of Photo Induced Phase Transition (**Nasu 2004**).*

The pathway following on potential energy surface decides what phase is reached after photo-excitation. Some complex interactions with lattice exist and added to cooperative effects; it can lead to new macroscopic order (**Fig 1.11**). Here again the photoinduced phase may possess different lattice structures and electronic order compared to the initial one (**Nasu 2004**). Photo-excitations sometimes can also lead to irreversible process (when bonds are broken or formed) but this case refers to photochemistry because the PIPT strength is the reversible character of this process. The PIPT field is associated with the material control by light that increases the functionality. Another important goal is also to shorten the time needed to act on the system. This is done now with the use of ultrashort light pulses as short as few femtosecond (fs = 10^{-15}s).

One striking force of light-based science is the possibility to use different photon energies to act on the system, from X-ray to THz (keV to meV) that covers six decades on energy. Depending on the photon energy range used as transition trigger, different structural and electronic degrees of freedom are activated. X-ray or UV photons act more on core shell of the atom to allow PIPT (**Vanko 2007**). Visible and near infrared photons impact the valence shell and trig macroscopic transition (**Collet 2003, Chollet 2005**). Infrared range allows the possibility to act directly on molecular vibrationnal modes without passing through electronic excited transient state. The last and newest excitation method deals with THz radiation (1 THz – 300 μm). In this low energy range, it is possible to excite directly lattice mode (**Rini 2007**).

When a new phase is generated by light irradiation, the pathway followed by the system is unclear, neither the physical process involved in the emergence of new structural and electronic order. But it's obvious that such process is driven by atoms or molecules and more probably by electrons motions. So by looking at pertinent time and pertinent space scales, one can hope to watch in real time all the relevant processes involved for increasing our understanding of this new field of physics.

1.3.2 Pioneer studies on PIPT

Now the concept of PIPT is well established and subject to a rich literature (**Buron & Collet 2005 / Tanaka, et al, 2009**). The new metastable state may be generated by different methods, regarding the energy range of the photon used, or the degrees of freedom involved during the transition.

A case study of PIPT is the VO_2 system which undergoes a solid-solid phase transition after light excitation. Like several oxide of vanadium, VO_2 exhibits an insulator to metal transition (340 K) coupled to symmetry change between low temperature-monoclinic and high temperature-rutile. It has been demonstrated that such phase transition can be triggered by an intense laser irradiation of visible light (**Cavalleri 2001**). The laser impacts the LT phase that will relax to a new phase characterized as the high temperature one. This transition is associated to a change of structure that can be caught by X-ray diffraction. This structural signature made no doubt on the creation of a new macroscopic phase.

An interesting fact is that there are lots of organic systems that undergo photo-induced phase transition. One of the most studied organic systems which presents a PIPT is the TTF-CA compound. This system undergoes a neutral-to-ionic phase transition evidenced by the creation of long range ferroelectric ordering below 81 K. It has been demonstrated that by irradiating the neutral phase at temperature just above T$_c$, the metastable ionic phase is generated (**Koshihara 1999, Collet 2003, Uemura 2010**). The emergence of the ionic phase is confirmed by the apparition of Bragg peak normally forbidden due to symmetry consideration and referring to the ionic phase structure. This new diffraction pattern points out the long range order of the new phase obtained by this way.

Another interesting system is the charge transfer system (EDO-TTF)PF$_6$, undergoing a metal-insulator transition at 278 K. At high temperature the system is metallic with a charge ordering pattern as $\left(1/2, 1/2, 1/2, 1/2\right)$. By cooling the system, the symmetry changes and cell doubling occurs. Simple physical considerations link this symmetry change to a new charge ordering $\left(1, 0, 0, 1\right)$ which gives birth to an insulating phase. Experiments have proved that irradiation may restore the conductivity in the insulator phase by restoring the high symmetry (**Chollet 2005, Gao 2013**). By this way, material conductivity is controlled by light irradiation and the structural transition occurs on the picosecond time scale. It shows how complex are all these systems where electronic and structural degrees of freedom are coupled.

Light pulse can also be used as an indirect trigger for the new phase. In the field of ultrafast acoustic, the pulse acts like a hammer to generate shock wave (**Temnov 2013, Pezeril 2011**). This pressure front may modify the material properties like magnetism (**Kim 2012**). To increase the understanding of such effects that involve electron, phonon, lattice etc…, it is pertinent to look at the different time scales of physical process (**Fig 1.12**).
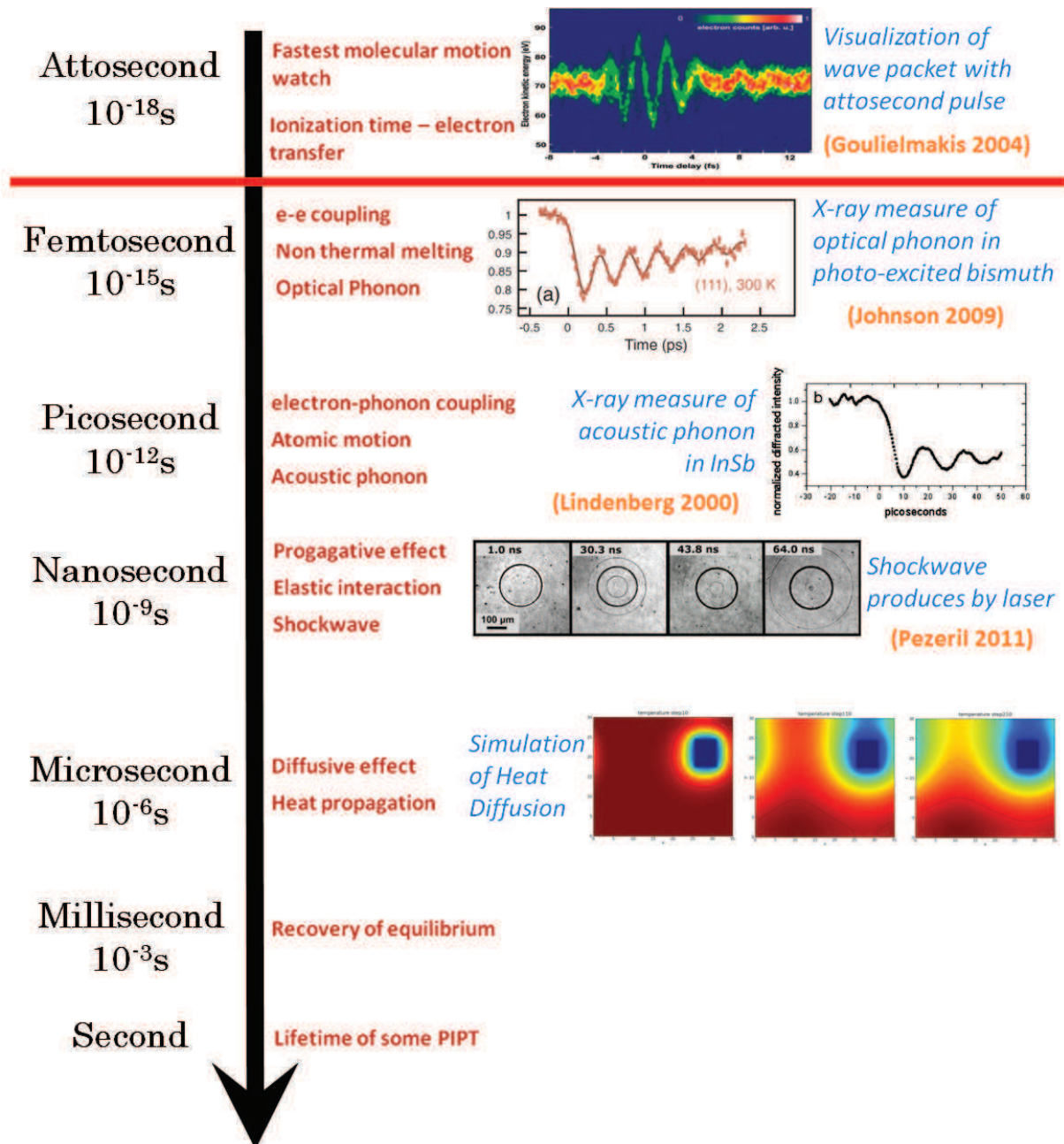
Fig 1.12 *Time Scale VS Physical Process.*

During a PIPT in solid state, a superposition of different physical process at different time scales might happen. Several degrees of freedom inside the material are involved during the emergence of new macroscopic order. Electrons which drive the system to new order have typical motion around fs time scale. The red line denotes the temporal limit of the results I will present in this manuscript.

All the couplings in systems previously presented involve electronic and structural dynamics that may be ultrafast. In order to increase material control, determining the potential energy surface of excited state is the goal of ultrafast studies to increase the understanding on light triggered transitions. Indeed, PES determines which kind of new phase is reached after the excitation. So tools are needed with time resolution high enough to follow in real time all these dynamics.

1.4 Ultrafast Science : Seeing is Believing

1.4.1 General consideration about ultrafast : How, Why?

Now technology allows watching quantum effect like ionization with time resolution as good as 100 attosecond (10^{-16}s) (**Baker 2006**). 100 attosecond was the world shortest observable in 2006 but obtaining such time resolution is still a big experimental challenge. On contrary, at lab scale with simple system, fs (10^{-15}s) time resolution is easily achievable. At the beginning of the 20th century, the best time resolution was around few ms, so technology had gained a factor of 10^{14} in one century. It's probably one of the most spectacular increases in terms of technology and opens new gates in the understanding of fundamentals process. The Nobel Prize of Zewail for his work on femtochemistry puts under light the necessity to get ultrashort time resolution to understand key mechanism of nature. Now, it is possible to follow in real time all primary process and to get clear signature of transient species or transient states. The term "ultrafast" should be used when coherence is observed and it is possible to play with primary effect of nature like chemical reaction (**Zewail 2000**).

It's crucial to assimilate the fact that ultrafast science differs from conventional macroscopic physics. For example, at ultra short time scale, atoms look frozen and temperature cannot be defined. In a sense one has to deal with deterministic systems because time duration is too short to explore the phase space and it corresponds to a kind of ergodicity breaking. New concepts have to be created in order to understand and interpret things watched with fs time resolution (**Bloembergen 1999**). For instance, sometimes ultrafast excitation leads to non trivial effects that cannot be done in nature. The relaxation channels used by the system to dissipate energy depend of the duration of the external trigger and it can lead to completely different physical effect.
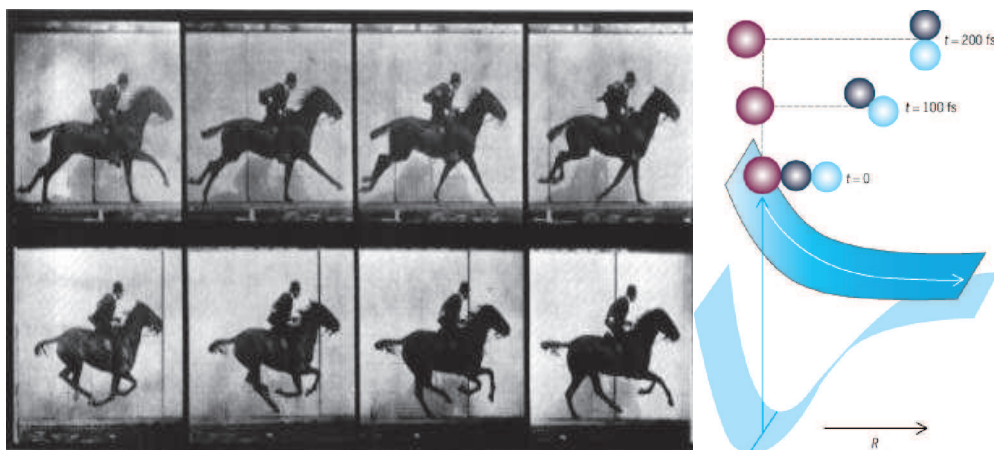
Fig 1.13 *Time resolved movies of the beginning of 20th and 21thcentury.*

Since the invention of camera, humanity has realized the omnipresence of processes so fast that they cannot be watched by human eye (**Fig 1.13**). The possibilities of catching more general process like how atoms move or the pertinent time scale for chemical reactions became conceivable with the emergence of new techniques and tools. To catch fast events, the major criterion is to get a camera that takes pictures fastest than relevant time scale of the process studied. By doing this, it's easy to separate the different steps of the process and reconstruct the complete pathway. For instance, the concept of phonon (quantifications of lattice oscillation mode) was introduced by Einstein at the beginning of the 20th century but watching some coherent lattice motion in real time was not performed until the eighties (**Zeiger 1992**).

To observe coherent dynamic, we need to excite the system with pulse duration shorter than pulsation of vibrationnal modes or phonon modes (3000-30 cm^{-1})→10 fs-1 ps (**Uemura 2010**). By doing this, all molecules are impacted at the same time by the pump compared to the phonon period. So initially they have the same phase and the whole oscillation superposes like positive interferences. Now, coherent control of organic system is possible (**Iwai 2006**) and in this case the response of the system is non linear and may be suppressed or exalted.
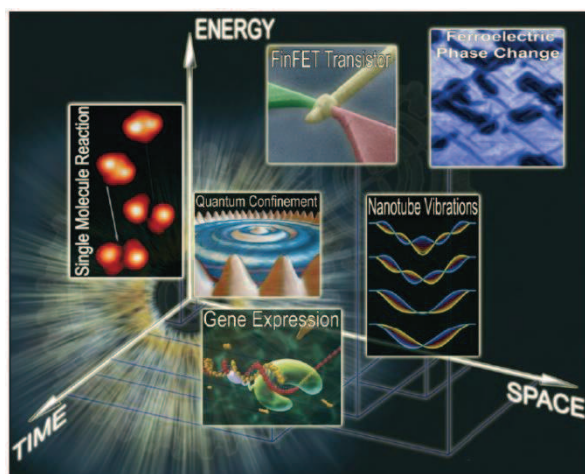
Fig 1.14 *Time VS Energy VS Space.*

One great advance in ultrafast science is the possibility to control the system at extreme time scale not for watching but impacting the system in order to reach the desired configuration. The optimal control is not only to act at relevant time scale but also to use pertinent energy (**Fig 1.14**). Another possibility in ultrafast science is to follow a complete out of equilibrium dynamics. By looking with enough time accuracy, it is easy to decorrelate the different degrees of freedom involved during PIPT like electronic effect or elastic effect (**Cailleau 2010**) and to study how they interact with each other.

1.4.2 State of the Art on Ultrafast Tools

Development of ultrafast tools was tremendous during the 20th century and is still ongoing. Until the sixties, the best experimental time resolution was around few microseconds with flash photolysis techniques. Porter, Eigen and Norrish received the Nobel Prize in 1967 for having developed this technique.

But two tools will break the barrier of microseconds time scale. The first one is mode locked laser that produces fes (10^{-15}s) light pulses. The second one is the new generation of synchrotron that produces short and bright X-ray pulse (100 ps). Femtosecond X-ray pulse may be obtained at lab scale with plasma source or in synchrotron facilities with the slicing method. All these issues will be detailed later in chapter 2. And now, X-Ray Free Electron Laser X-FEL produce ultra bright X-ray fs pulse (>40 fs). With all these tools, it's possible to measure structural dynamic in a material with fs time resolution. A large literature exists on ultrafast structural science with a large scope of techniques (**Collet 2010**).

Femtosecond optical spectroscopy is used to detect all the processes which modify the dielectric function of the system (and therefore the electronic state). With such setup, the all visible spectra from UV to near infrared can be probed with hundreds of fs time resolution. The light is used both as probe and pump. The pump impacts the system for triggering the transition and the probe records the modifications created by the new phase. Femtosecond transient absorption

spectroscopy provides clear fingerprints on the generation of transient excited states (**Van der Veen 2011, Yeh 2000**) that may be coupled to coherent wave packet motion. Instead of chemistry, optical investigations are also done in solid state and may reveal coupling between light and coherent lattice vibrations (**Wall 2009**). New development of these techniques makes it now possible to get 10 fs time resolution giving access to primary photo-chemical reaction (**Polli 2010**).

Nevertheless, optical spectroscopy only gives an indirect proof of coherent atomic or molecular motions and to truly observe such process, diffraction is mandatory. Indeed, the structure factor is directly linked to the atomic positions. The generation of fs X-ray pulses provides an essential tool in order to catch in real time atomic motion (**R.W Schoenlein 2000**). With a K_α source, the photon fluency is very weak and allows only recording few Bragg peaks dynamics. But still, a complete coherent motion of solid following a fs excitation can be observed (**Sokolowski-Tinten 2003**). K_α sources start now to be applied to molecular materials (**Freyer 2013**). The Slicing source is more tunable in energy and increases the flexibility of experiment. It allows to performed fs X-ray Spectroscopy in these facilities (**Bressler 2009, Huse 2011**). A full cell motion following a fs excitation has been reconstructed with slicing techniques (**Johnson 2009**). And by coupling THz pulse to X-ray probe, it is possible to observe in real time a polariton which refers to a coherent coupling between light pulse and lattice mode propagate at light speed in the material (**Cavalleri 2006**).

X-ray is not the only way to perform diffraction and ultrafast electron diffraction seems to be a serious alternative for ultrafast structural science. Compact electron gun producing fs electron bunch is a table top system providing a view of the reciprocal space. The limitations of such facilities lie in two parameters. The first one is the Columbian repulsion that destroys the time duration of the electron pulse and the second one is the huge cross section of electron in scattering process. It imposes to deal with electron bunch compression and samples of nanometric thickness. That is the reason why most experiments were performed on hard matter systems (**Siwick 2003, Scaini 2009, Ernstorfer 2009**). In hard matter, ultrafast processes like non thermal melting or bond hardening are observed. Today, the improvement on this kind of source has made it possible to deal with organic system with good diffraction patterns. This use of electron diffraction has evidenced a transient structural state which has not been observed with optical results (**Gao 2013**).

Another new but fascinating technique is time-resolved ARPES (Angle Resolved Photo Electron Spectroscopy). Photo-electron spectroscopy is useful to investigate electron dynamics in strongly correlated system. An UV light pulse impacts the system and generates photo-electron emission. By resolving this emission in angle, a complete view of the system band structure is possible. With such measure, the evolution of electronic band structure following an ultrafast excitation may be recorded (**Schmitt 2008**). It is also possible to decorrelate the electronic states of surface and bulk and observed their dynamics independently (**Papalazarou 2012**). With this technique, the direct modulation of the band structure by phonon activation is caught.

1.5 Ultrafast Spin State Switching

Continuous irradiation is known as the easiest way to perform spin state photo-switching. As Bloembergen says in his review (**Bloembergen 2009**), the advent of femtosecond time resolution opens the possibility to follow a complete chemical reaction or electronic process and photo-induced spin state switching suited well to this definition.

Pioneering time resolved studies have dealt with ns laser mainly to probe the relaxation time of transient HS state (**Lawthers 1984, Creutz 1979**). New step has been reached at the end of the

90's with the emergence of femtochemistry. Studies have put under light the possibility to generate HS molecules by irradiation with ultrashort laser pulse of hundreds of fs (**Monat 2000, Canizzo 2006**). This time resolution opens the possibility to follow in real time the pathway from LS to HS and increase the understanding of this ultrafast process.

1.5.1 SCO Molecules in Solutions: Femtosecond Time Scale

In Fe^{II} systems, due to forbidden character of the direct transition $\Delta S=2$, such change of spin state involves one or several transient states referred in the literature as MLCT (Metal-to-Ligand-Charge-Transfer). First the photon absorption leads to an instantaneous Franck Condom state named ^{1}MLCT which corresponds to the transfer of the excited electron on ligand molecular orbitals. After excited states cascade with MLCT and/or Ligand Field characters occurs toward the HS potential (**Fig 1.15**). This new electronic state has new absorption spectra so absorption spectroscopy is well suited to study the overall process. Furthermore, the spin state switching also leads to structural reorganization. It is due to the less bonding character of HS state resulting to an increase of the average bond length <Fe-N>. It should be possible to record this structural change if a probe sensitive to <Fe-N> is used.

One big step has been done with the work of McCusker et al, who report that such ISC occurs at sub-picosecond time scale but this observation was limited by the experimental time resolution (**McCusker 1992**). At the dawn of the 21th century, amazing progresses have been made with fs laser and now table top systems with fs time resolution are rather common.
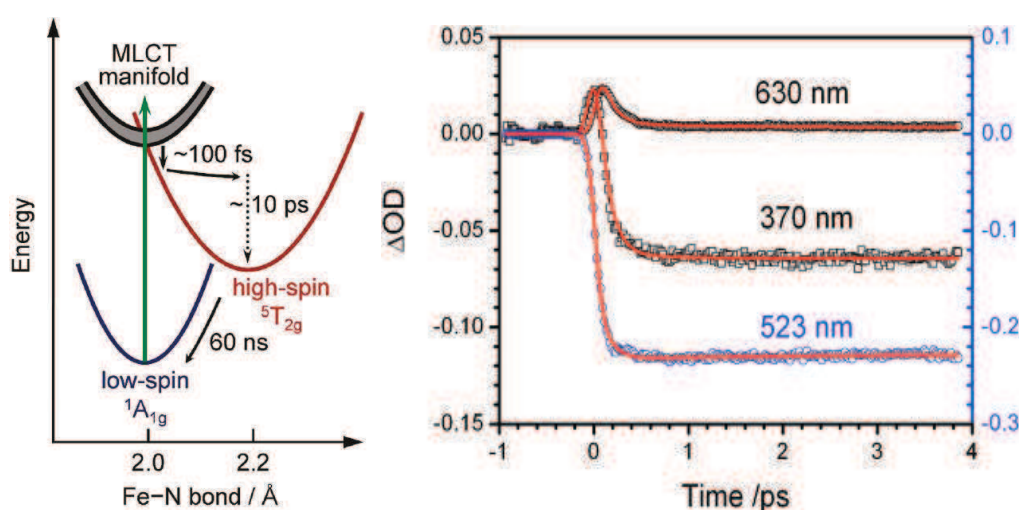
Fig 1.15 *transient absorption of solution of SCO molecules following a laser excitation (**Gawelda 2007**).*

Optical pump probe spectroscopy is the most common way to perform time resolved experiment with fs resolution. A light pulse referred as pump will impact the system in order to generate HS state. This excitation creates transient excited state that relaxes into the HS state and such process is watched in real time (**Fig 1.15**) (**Canizzo 2006, Smeigh 2008, Tribollet 2010**). The dynamics of the ultrafast relaxation process is fit by single exponential decay which gives a time constant of 120 ± 10 fs in $[Fe^{II}(bpy)_2]^{2+}$ for example (**Gawelda 2007**). All these experiments deal with molecules in solutions for convenience because solid state spectroscopy is much more difficult. A

complete painting of this photo-switching has not been done yet and the excited states cascade is still unclear (**Juban 2006**).
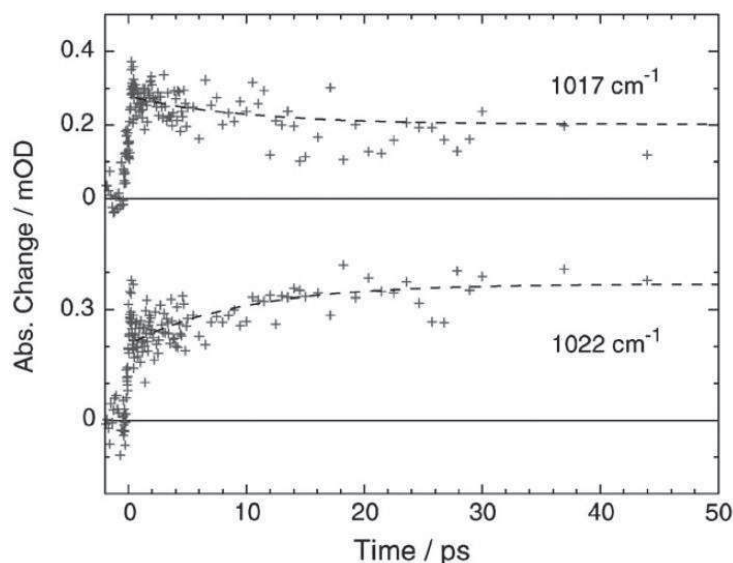
Fig 1.16 *Infrared absorption transients of [Fe(btpa)]$^{2+}$* (**M.N Wolf 2007**).

Once the system arrives in the HS state potential, there are still some excited rotational and vibrationnal levels. This transient state is Hot because a lot of energy is localized on the HS molecule at this time scale, and the relaxation towards the bottom of the potential might take several ps (**M.N Wolf 2008, Gawelda 2007 & Fig 1.16**). Relaxation occurs via coupling with the surrounding environment, solvent in the main case. To truly investigate this process, infrared experiments are required in order to probe small energy levels.

As previously mentioned the switching modifies both the electronic state of the system, in addition to the molecular structure. In order to follow this structural dynamic, the X-ray Absorption Near Edge Spectroscopy is a powerful tool because in the X-ray regime it probes directly the atomic core. On contrary, visible and near infrared fs experiment have the disadvantage to be sensitive not only to HS and LS state but also to transient states and vibrationnal process.
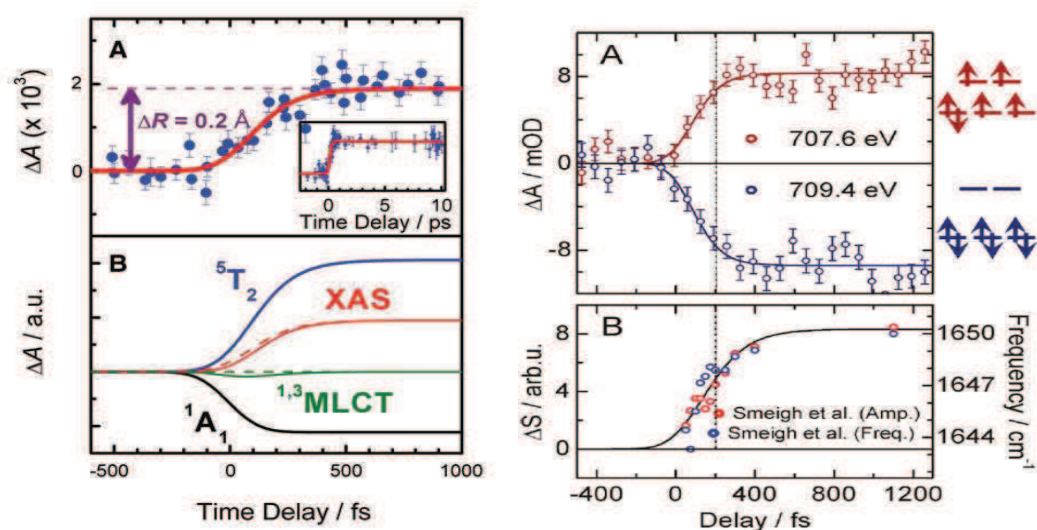
Fig 1.17 *Femtosecond XANES at K-edge (right,* **Bressler 2009**) *and L-edge (left,* **Huse 2011**).

The local change of structure during the LS to HS transition modifies the position of edge absorption in the X-ray spectra (Chapter 2). By probing the system in function of times at given photon energy, corresponding to the maximum change between HS and LS, the structural dynamics of spin state switching is recorded (**Fig 1.17**). These kinds of experiments are really difficult and made only in few places in the world because it implies a tunable X-ray source. The first attempt was performed by Bressler and co-workers in the slicing source of SLS at the Fe K-edge (**Br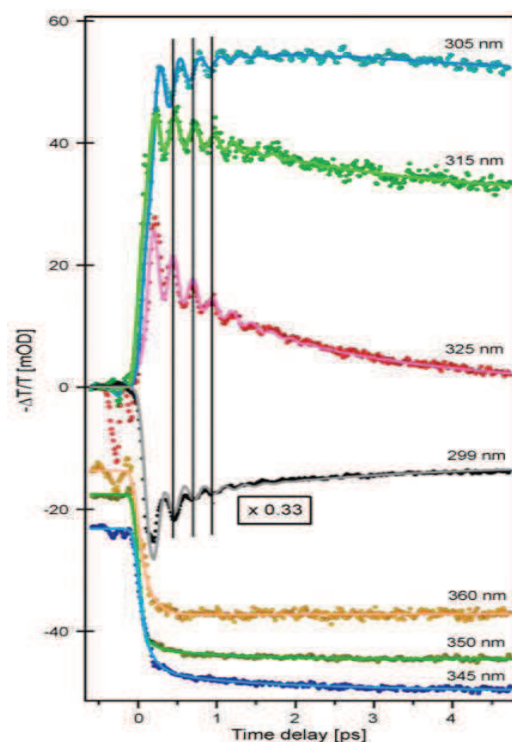essler 2009, Lemke 2012**). Results reveal an elongation time constant of the <Fe-N> bond length of 140 fs. Other experiments have been performed on the Fe L-edge a give same dynamics (**Huse 2012**).

Fig 1.18 *Coherent wave packet motion in [Fe^{II}(bpy)$_3$]$^{2+}$ (*Consani 2009*).*

Numerous optical studies on SCO systems have been done but coherent vibrationnal motion of excited HS state has only been reported once (**Consani 2009**). In this paper, authors report a coherent wave packet motion observed after the excitation of [Fe^{II}(bpy)$_3$]$^{2+}$ aqueous solution (**Fig 1.18**). Only one coherent mode of low frequency (128 cm^{-1}) is detected and linked to ligand vibrationnal mode.

The overall description of the ultrafast spin state switching of Fe^{II} SCO molecules in solution can be summarized in this way :

The photon absorption leads to an instantaneous Franck Condon state referred as ^{1}MLCT. This state relaxes to the HS state via ultrafast ISC (tens of fs) (**Van Veenendal 2010, Gawelda 2007**) with a new spin multiplicity. Until now, it's not clear if there are intermediate MLCTstates like ^{3}MLCT or a cascading process involving MLCT and/or LF states (**Brady 2004**). After HS potential state is reached within less than ≈ 100 fs, a correlated with structural elongation of the Fe-N bonds is observed to occur within ≈ 140 fs. And the last step consists in vibrationnal cooling towards the HS potential bottom, which occurs during several ps, depending on the solvent (Tribolet). It's during this process that coherent phonons are emitted and strong interaction between the photo-excited and his environment occurs.

In the frame of the what is discussed in the literature of ultrafast spin-state switching in SCO molecules, several important questions have not being addressed yet :

Are there clear differences between Fe^{II} and Fe^{III} compounds in the ultrafast photo-switching and on the different excitation processes which can be used (LMCT, MLCT, d-d...)?

Is this pertinent to consider only one parameter to explain the process (<Fe-N>) or are other degrees of freedom involved in such process?

How do molecules respond in a solid and is it possible to take advantage of cooperative interactions?

1.5.2 Ultrafast Spin State Switching in Molecular Crystals

1.5.2.1 Femtosecond time scale study

Solid state studies of ultrafast SCO photoswitching were only recently started in Rennes. The first relevant limiting parameter in order to perform 1 kHz pump-probe study at fs time scale in solid state is to find a system able to relax within one millisecond time scale. It happens that some Fe^{III} system were found in the literature as undergoing a fast enough relaxation (**Enachescu 2006**) and were therefore the first potential candidates for such experiments.
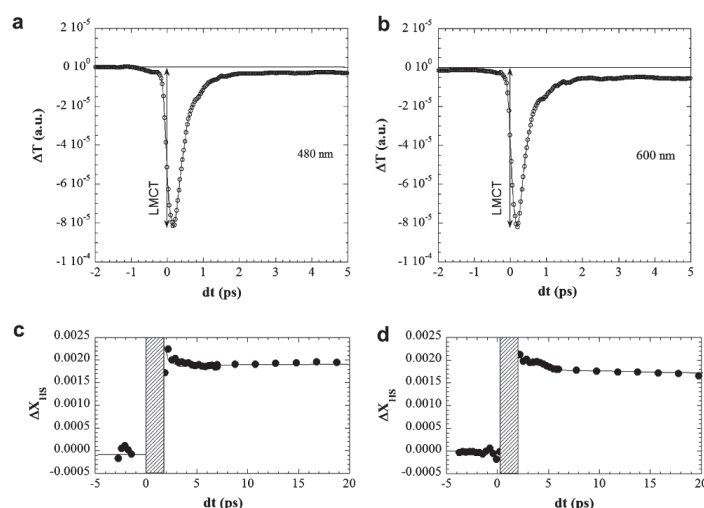
Fig 1.19 *Femtosecond spin state switching in solids state of [(TPA)Fe^{III}(TCC)]PF_6 crystal (**Moisan 2008**).*

First attempt of fs spin state switching in solid state has been performed by Moisan on $[(TPA)Fe^{III}(TCC)]PF_6$ compounds (**Moisan 2008**). Due to the Fe^{III} character of the system, the pump was set to a LMCT (Ligand to Metal Charge Transfer) and the probe in a spectral area sensitive to the LS→H transition. The observed dynamic looks similar to the ones performed in solution with the occurrence of instantaneous electronic peak assigned to LMCT excitation (**Fig 1.19**). This transient state relaxes like single exponential decay with less than 300 fs. But the fraction of molecules generated in this way was weak (0.2%) and made detailed analysis difficult.

1.5.2.2 Out of equilibrium dynamics from molecular to material scale

If photo-switching process seems understood at the molecular level, no studies have been performed on solid state system to track macroscopic response, cooperative phenomena or out-of-equilibrium dynamics. Obviously, it's understandable to wish slightly difference in the mechanism/process because in the SCO crystal the surrounding molecules are active (lattice effect) in contrast with molecules in solutions where the solvent is passive. For instance, the electronic switching remains the same, which means photon absorption generates an instantaneous frank Condon state (MLCT or LMCT) and a relaxation via ISC towards metastable HS state. But in solid state other phenomena that generate spin state switching occur during the out of equilibrium process.
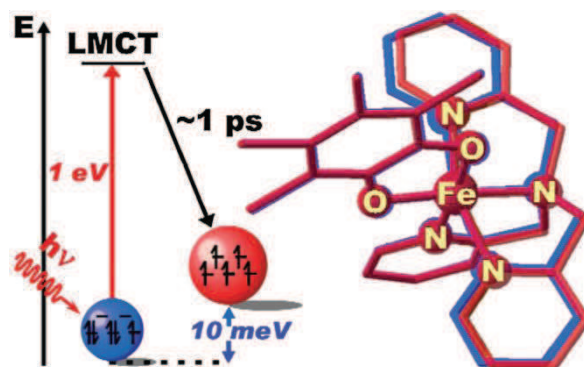
Fig 1.20 Schema of LMCT process with the relevant energy.

The pump pulse contains a number of photons much small than the number of SCO molecules in the crystal. So the first step is a photo-switching of a small fraction of molecules towards the trapped HS state. Basically, few percent of HS are generated at picosecond time scale. The ground state energy difference is around tens of meV but the photon energy classically used (800 nm = 1.55 eV) is much higher (**Fig 1.20**). This process leads to huge redistribution of energy, first localized around the Fe atoms and transferred by electron-phonon coupling to the lattice. This lattice heating may generate some non linear effect at longer time scale.
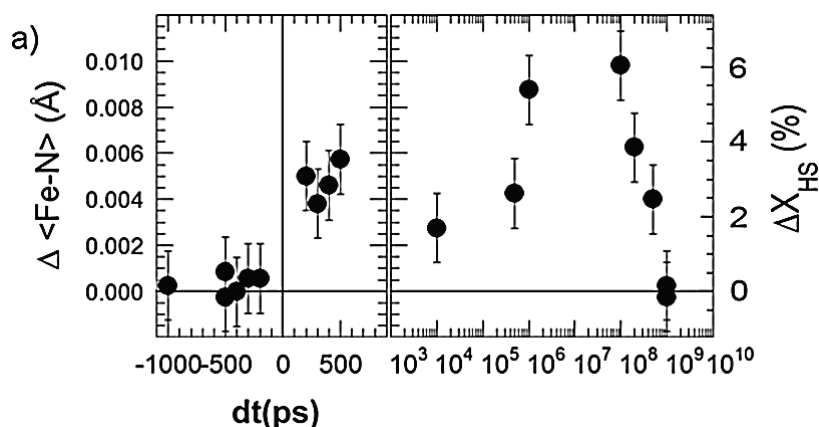
Fig 1.21 Time evolution of <Fe-N> caught by X-ray diffraction (*Lorenc 2009*).

The detection of this fraction is made possible by ultrafast optical spectroscopy via change in optical density or by time resolved x-ray diffraction via elongation of the bond length <Fe-N> (**Fig 1.21**). For conventional single crystal, the system state is invariant during hundreds of

picoseconds and is now referred as picosecond plateau. It shows that the fs spin state photoswitching (step 1) occurs at constant volume in solid state and the lattice parameters remains unchanged during several nanoseconds.
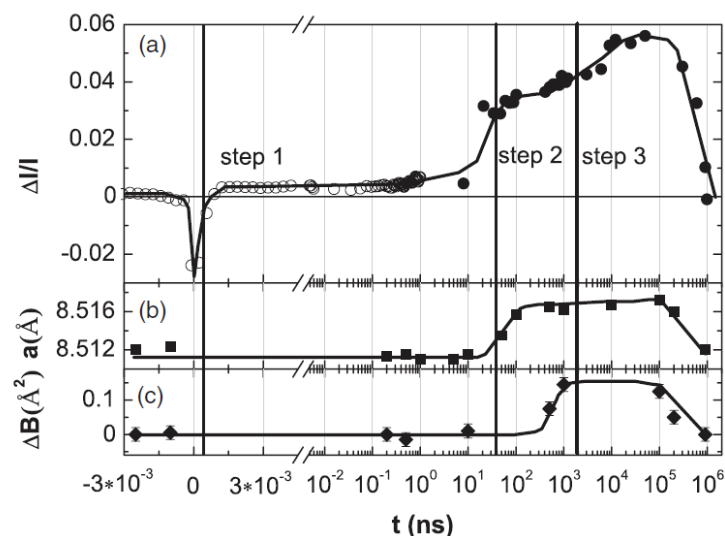
*Fig 1.22 Temporal evolution of Transient Absorption, **a** cell parameter and Debye-Waller following a femtosecond excitation (**Lorenc 2012**).*

After, due to the fact that HS molecules possess higher volume than LS ones, the internal pressure of the crystal increase. It generates a strain field that will relax through elastic coupling between molecules. As a matter of fact, a lattice expansion occurs and is analog to macroscopic crystal expansion. This expansion takes place at the nanosecond scale which corresponds to the ratio between crystal size and the speed of sound in the material. This expansion is concomitant with a creation of HS molecules characterized by a change of transient absorption. Such process is also observed by X-ray diffraction with a time dependent change in lattice parameters refer as an elastic step (step 2) in **Fig 1.22**.
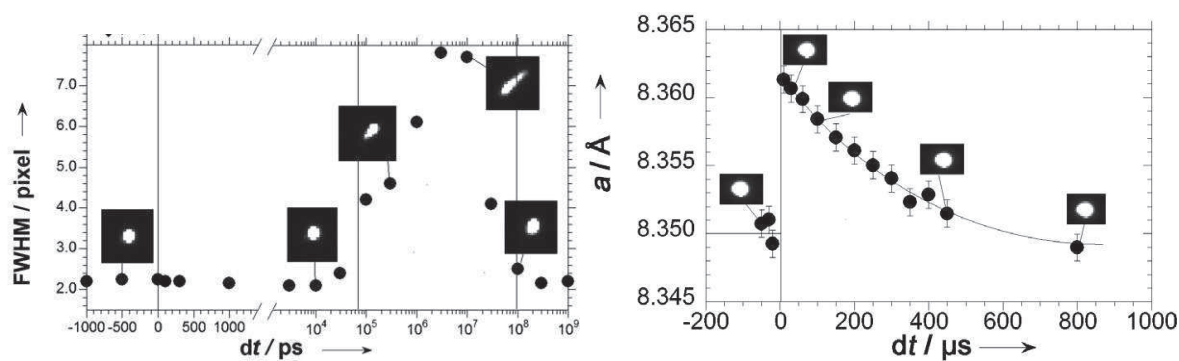
*Fig 1.23 Bragg peak shape during the out of equilibrium process (**Collet 2012**).*

And finally, the energy deposited by laser pulse can be mainly converted into thermal energy because only few percent correspond to energy gap between HS and LS. Expressing this in terms of heat capacity $E_{Laser} = C_P \Delta T$, it corresponds to an increase of temperature around 5-10 K. In case of spin crossover complex, a 5-10 K increase of temperature around $T_{1/2}$ leads to few percent of molecules converted by thermal population. This process is referred as the thermal step (step 3) on **Fig 1.22**.

Another important information at macroscopic scale is the broadening of Bragg peak shape (**Fig 1.23**). This fact is due to a gradient of energy through the sample thickness that leads to inhomogeneous distribution of local temperature. Such fingerprints make no doubt to the inhomogeneous character of the transient crystal structure until 100 μs. At this stage (100 μs), the system is homogeneous in terms of pressure and temperature but not at thermal equilibrium testify by the Bragg peak shape (**Collet 2012**). After, the system relaxes towards its equilibrium state with millisecond time scale.

From a general point of view, the most fascinating feature in this painting is the multi scale effect. It starts from a local electronic excitation which follows pure deterministic dynamic and ends with thermal diffusive process undergoing stochastic behavior:

1. fs purely electronic, local trapping effect
2. elastic interaction ns, propagative effect
3. thermal conversion, diffusive process of heat and thermal energy barrier

1.6 Goal of this research project

The goal of my research is to increase the understanding of ultrafast spin state switching in solid state, for understanding how the material evolves from the local molecular switching to the global response of a crystal made of a macroscopic number of molecules.

These processes occurring during different steps involve a lot of degree of freedom, playing their role on different time scales. Therefore it is of interest to understand the limiting parameters on the switching dynamics and its efficiency. This is what is investigated in this thesis, thanks to the use of ultrafast tools. The ultrafast techniques used and developed for this project are presented in Chapter 2.

The use of these ultrafast techniques, with time resolution shorter than the elementary structural reorganization time scales (<100 fs), allows tracking new information on the ISC process and on the structural degrees of freedom involved, making it possible to discuss the role of structural coherence during ISC process. These results will be presented in chapter 3.

The possibility to take advantage of the active crystal medium for generating and controlling cooperative effects will be presented in chapter 4. We will show that non-linear effects can be induced by light and the associated out of equilibrium process will be discussed. As propagating elastic and diffusive thermal effects compete, we will also investigate size effect, and show the influence of the environment in the ultrafast spin state switching resulting from crystal downsizing and confinement in a passive polymer matrix.

Chapter 2: Ultrafast Techniques applied to SCO Materials

Nowadays technology allows femtosecond (fs) time resolved experiments with compact table top laser systems. Paradoxically, numerous time-resolved beamlines capable of ultrafast resolutions proliferate on large-scale facilities. But almost all these time resolved experiments have one thing in common: the pump-probe method. The method goes by a simple principle, whereby the first pulse called pump impacts the system and another pulse called probe monitors the system at a given time delay (negative or positive) (**Fig 2.1**). The pulse type can vary from hard X-ray (**Collet 2003, Rousse 2001, Sokolowski-Tinten 2003**) to THz (**Perfetti 2006, Tani 2012**), or even bunches of electrons (**Siwick 2003, Baum 2007**). Depending on the nature of the pump and the probe, different dynamics and physical processes are investigated. For example, X-ray pulse will probe the atomic positions (**Fritz 2007, S. L. Johnson 2009**), whereas infrared pulse will probe the frequencies of vibrations (**Kubicki 2010 & 2011, Zhang 2009**). From the low energy photon in the THz range (few meV) to hard X-ray (15 keV), there is a factor 10^7 in energy. It puts a number on the range of physical processes that can be seen with pump probe techniques.
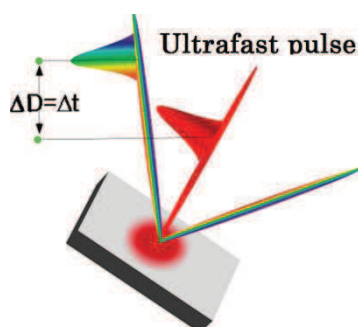
Fig 2.1 The Pump-Probe Way.

The measurements are typically based on the stroboscopic principle, which means they are made at a given repetition rate (typically 1 kHz) with fixed delay time between pump and probe (**Fig 2.2**). But this imposes a limitation on the range of systems amenable to study, as it requires that systems relax in a time shorter than the laser pulse period (1 ms). Of course, alternative methods exist for probing slowly relaxing or irreversible systems, such as single shot method (**Poulin 2006**).
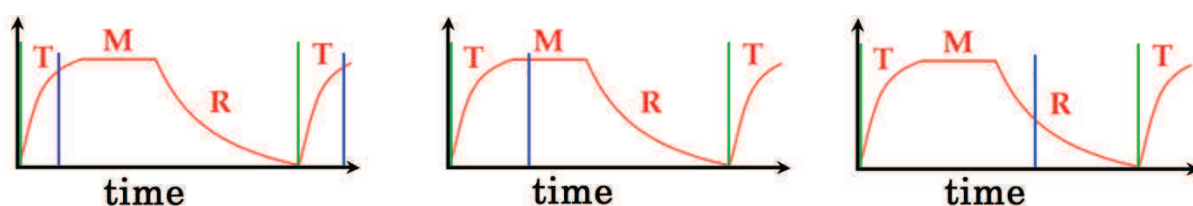
Fig 2.2 Schematic principle of pump (green) probe (blue) measurements.

The time resolution of any experiment is determined both by the pulse duration and the geometry of the setup. If we make a simple calculation with two co-propagating Gaussian pulses (laser pulse often shows Gaussian distribution) in perfectly parallel geometry :

$$f(t) = e^{-\frac{t^2}{2\sigma_f^2}} \text{ and } g(t) = e^{-\frac{t^2}{2\sigma_g^2}}$$

The convolution product is $f(t) \otimes g(t) = \int_{-\infty}^{-\infty} f(t-x)g(x)dx \rightarrow P_{f\otimes g}(t) \propto e^{-\frac{t^2}{2(\sigma_f^2+\sigma_g^2)}}$

So for two Gaussian distributions σ_1 and σ_2, the temporal resolution is $\sigma_{tot} = \sqrt{\sigma_f^2 + \sigma_g^2}$, which simplifies to $\sqrt{2}\sigma$ for identical pulses. Setup geometry may also affect the experimental time resolution.
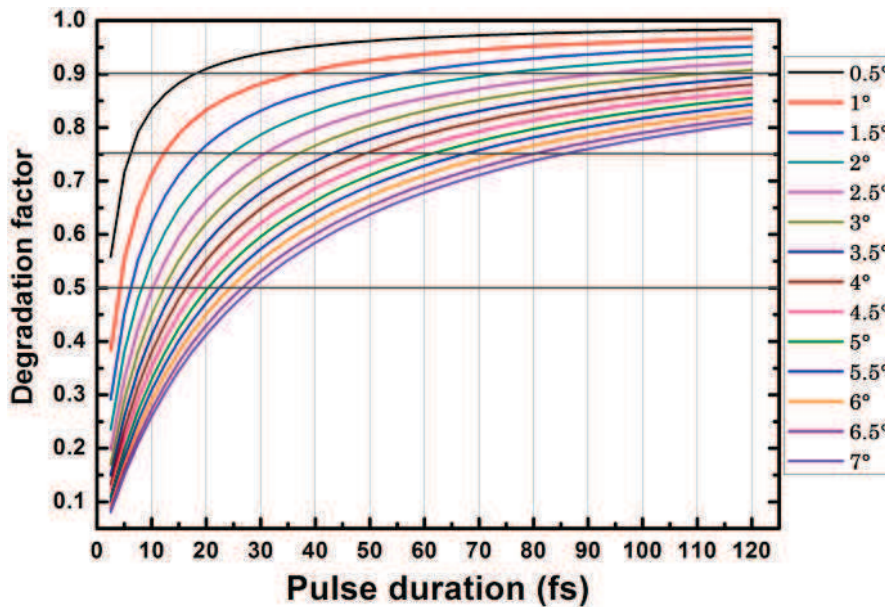
Fig 2.3 Degradation of time resolution in function of pulse duration and angle between pump and probe.

Fig 2.3 shows simulation of the time resolution loss as a function of angle between pump and probe compared to perfectly parallel beams (100 μm diameter). The time resolution of the experiment, taking into account the angle and pulse duration, is given by $IRF = \frac{\sqrt{\sigma_1^2 + \sigma_2^2}}{D_f}$ where

IRF is the instrumental response function, σ the distribution of the pulse and D the degradation factor proportional to the angle. For pulses longer than 80 fs, such geometrical factor is less critical. For ultrashort (<20 fs) pulses, geometry has to be almost parallel to prevent severe loss of resolution.
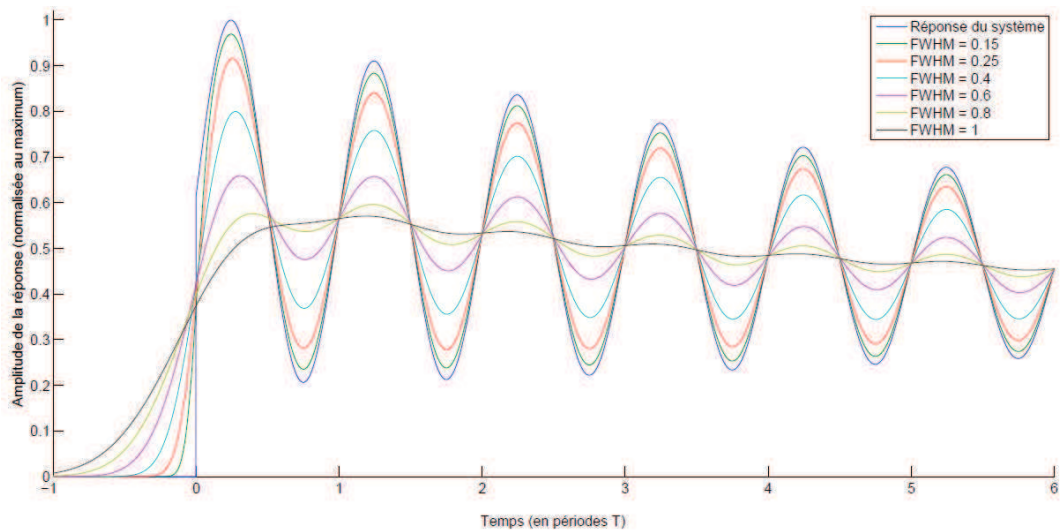
Fig 2.4 *Signal of the measure of oscillating signal with different IRF.*

The signal detected of such pump-probe system is : $M(t) = S(t) \otimes IRF$ .The impact of the time resolution on the detection of fast oscillation process like optical phonon can be dramatic. **Fig 2.4** shows the convolution of pulse of different time duration and a simulated phonon. The amplitude of the oscillation are directly link to the time resolution and beyond a critical time resolution, the information is lost.

During my thesis, the experiments have brought me to use different tools, and I will now present them with more details :

- Optical pump-probe experiments with fs laser pulses.
- Time resolved diffraction studies with 100 ps X-ray pulse generated in the storage ring of a synchrotron.
- Ultrafast XANES with fs X-ray pulses generated by X-ray Free Electron Laser (X-FEL).

2.1 Ultrafast laser spectroscopy

Here, at the Institute of Physics of Rennes, a fs laser spectroscopy system was set-up in 2005, and then rebuilt in 2010 into a multi-experimental platform. Basically, it consists of a fs oscillator (Coherent MIRA) which seeds two regenerative amplifiers (Coherent USP and Coherent ELITE) (**Fig 2.5**). Then each amplifier seeds two Optical Parametric Amplifiers (Light Conversion TOPAS).
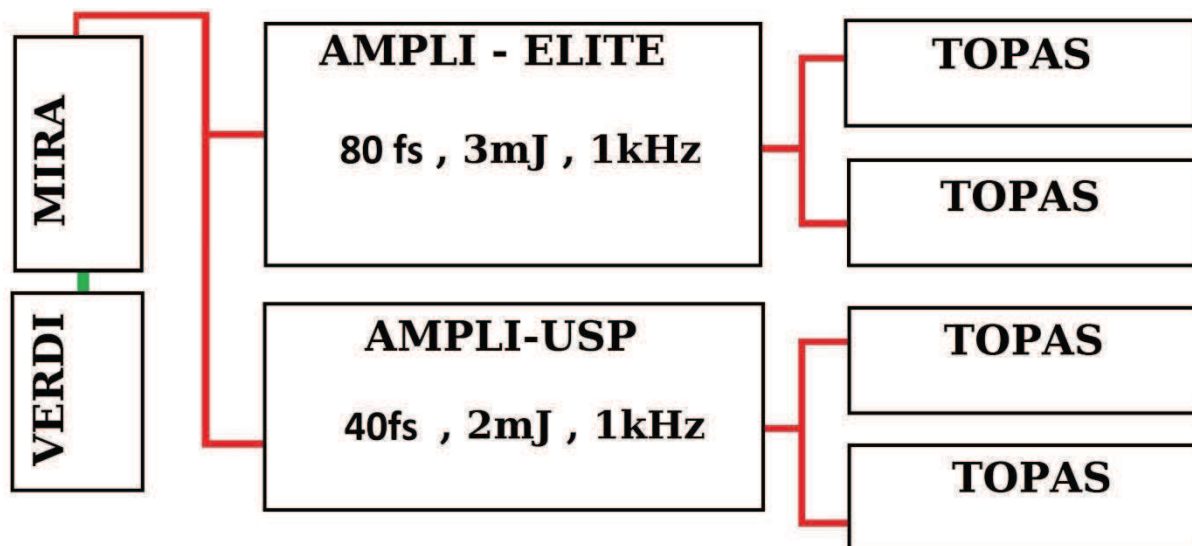
Fig 2.5 *Schema of the laser system in the laboratory.*

The generation process begins with a continuous wave (CW) laser Verdi that pumps the oscillator cavity with 4.5 W power at 532 nm. This oscillator is the seed and the clock of the entire laser system. At the output there is a train of pulse with 76 MHz repetition rate (radio frequency for the clock) with the following properties : all pulses are centered at 800 nm wavelength and have 40 nm bandwidth, which translates to pulse duration of 35 fs in Fourier transform limit. The 40 nm bandwidth fits the spectral transfer function of two amplifiers, especially the more stringent USP. These pulses have low energy (around 6 nJ) and by consequence are not suitable for pump probe experiments where significant number of excited states has to be populated in a linear process by a single laser pulse. So this train is split in two and seeds two regenerative CPA (Chirped Pulse Amplification) amplifiers in order to obtain pulses with mJ energy.

Before the mid-80's pulse amplification was stopped due to damage inflicted on the amplifying media. To overcome this limitation the Chirped Amplification technique was introduced (**Strickland 1985**) which is based on simple yet clever concept. Pulses are stretched in time prior to amplification and recompressed after, thereby lowering the peak power in the amplifier medium and allowing to reach higher gain. To stretch the pulse, gratings are typically used to introduce spatial dispersion, thus typically permitting stretching factors of as much as 10^4 inside the laser cavity. The recompression is simply a reverse process. With these techniques, reaching mJ pulses has become common. The amplifiers are called regenerative because two Pockels cells lock the cavity for a determined period of time so the pulse can be trapped and makes as many round trips as determined. Normally once the gain is saturated, the cavity is unlocked and the pulse released.
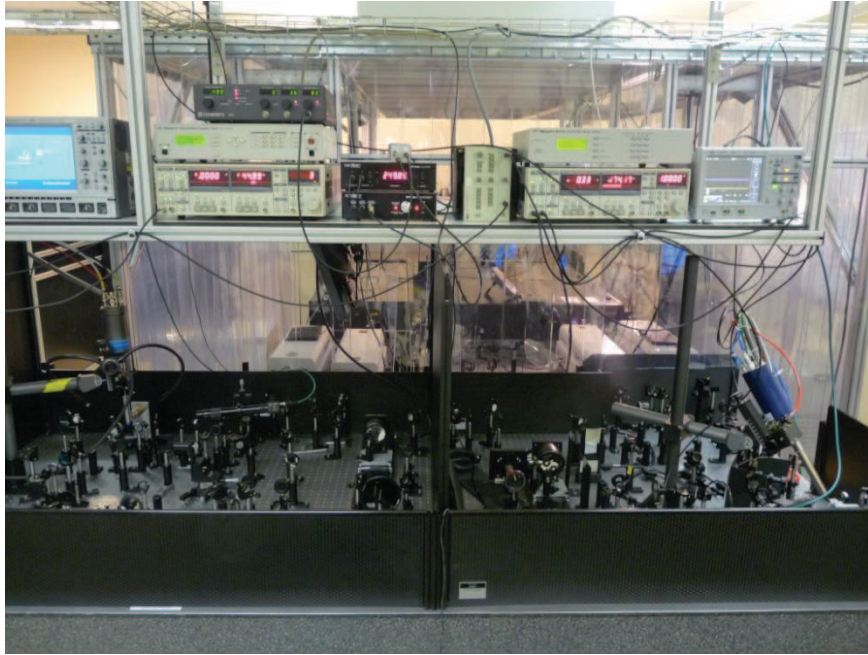
Fig 2.6 *Picture of the Laser System.*

Then, the output beam is again split into two parts and seeds two TOPAS to generate pulses at desired wavelengths, within the spectral range from UV (300 nm) to near infrared (2.5 μm). The generation of all these different wavelengths is based on several non linear optical processes. The entire laser system is enclosed in a pressurized hutch to prevent dust and ensure stable temperature (**Fig 2.6**).

During my thesis, I have performed three kinds of experiments with this laser system, and below I will explain in more detail these experiments:

- Two color pump-probe (heterodyne detection).
- White light spectroscopy (CCD detection).
- Synchronized amplifiers (electronic delay control).

2.1.1 Two color pump probe experiment for time resolved optical absorption

The simplest experiment to set up with a fs laser is transient absorption for recording transient optical density with fs time resolution. To do this, two TOPAS generating two pulses of different wavelength are used as the probe and the pump. To increase the sensitivity of this measurement, the synchronous detection with a lock-in amplifier is used and allows detection of very small signals.
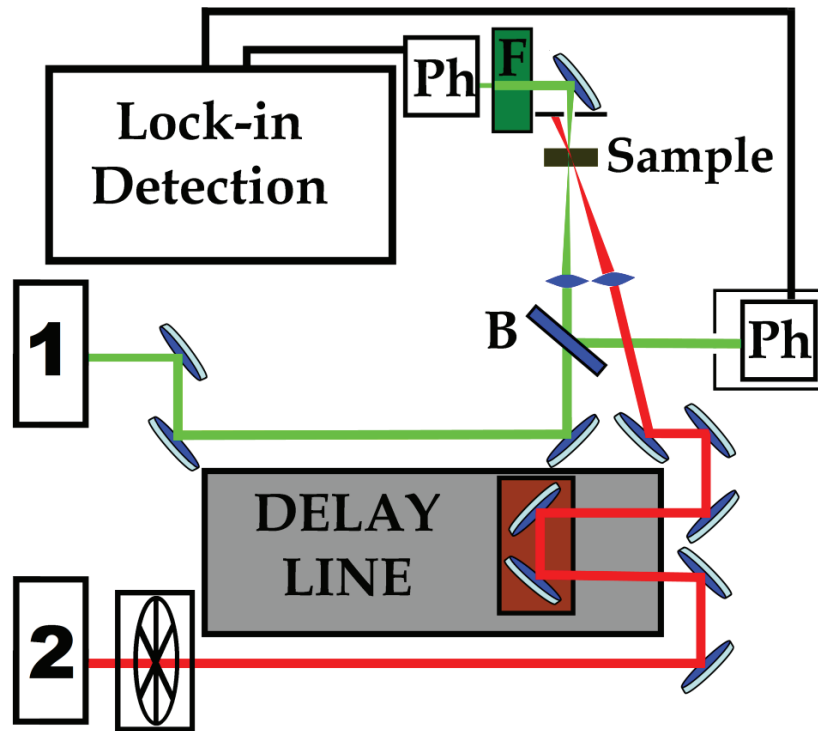
Fig 2.7 Scheme of the two color pump (red), probe (green) setup.

As shown in **Fig 2.7**, the probe beam in green is split in two parts : one is sent on the sample as a probe, and the other one goes straight to a photodetector and serves as intensity reference. The photocurrents from both photodiodes are fed to the lock-in amplifier. The pump beam in red is passed first through a chopper in order to divide its frequency by two and then onto the delay stage for the desired delay. The mechanical delay line is simply made of a hollow corner cube fixed to a mechanical stage driven by a stepper motor. The need to divide the frequency by two takes all its meaning with the lock-in detection scheme (see below). After the sample, the pump light having the right modulation frequency for the detector is suppressed spatially with an iris and spectrally with optical bandpass filters.

This setup can cover spectral range from UV (300 nm) to infrared (2.5 µm), and by combining sensitivity of the lock-in with stability of the amplifier (<1% RMS) it allows detection of signals of which $\Delta I/I = 10^{-5}$, to the best we have achieved. Both pump and probe have 80 fs pulse duration without geometrical consideration. The beam waist at the focal plane is about 80 µm and the angle between pump and probe is 7° all of which eventually result in 140 fs of temporal resolution. The loss of time resolution by Group Velocity Dispersion inside the sample for such pulses is almost negligible. As previously mentioned the photo-signal is collected and sent to the lock-in amplifier. It gives the possibility to detect a weak signal on top of a huge background.
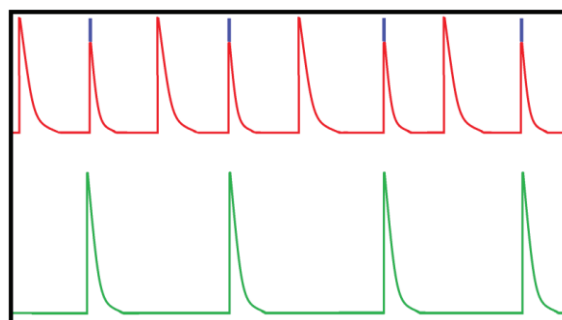
Fig 2.8 Schematic view of the experiment method.

With this kind of detection the sensibility is at 10^{-4} but with higher frequency like MHz, 10^{-6} is possible. The pattern is the following : the probe (in red) will see alternately a stable state and an excited state generated by the pump pulse (in green). The detector locks on the photo-induced (differential) signal (in blue) (**Fig 2.8**) if suitable reference frequency is provided (that of the pump). By doing so, all components of the signal that do not oscillate at the reference frequency are discarded. This detection acts like Fourier filter that keeps only the components modulated by the pump frequency.

A crucial condition is to have the two pulses overlap in time and space. The spatial length of a 100 fs is only 30 µm and it is necessary to superimpose both pump and probe. A common way of checking is with optical bleaching effect (of a semiconductor, optical density filter, etc.) (**Fig 2.9**). Impacting a neutral optical filter with an intense pulse will lead to a transient phenomenon called bleaching. To optimize the spatial overlap, we maximize the signal on the first absorption peak.
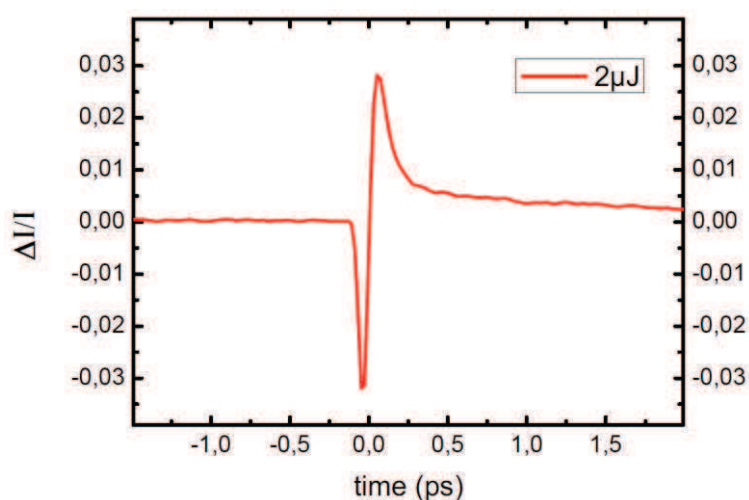
Fig 2.9 Bleaching of neutral filter (OD 0.5) by 800 nm pulse.

First the pulse will lead to instantaneous depopulation of the ground state (GS), thus decreasing the absorption of GS, and population of transient species with lifetime of few ps or shorter, depending on the nature of the excited state (ES) : fs for electron-hole recombination in a semiconductor, ps for Singlet or ns for Triplet molecular states.

We can go as far as to say that this convenient perturbation can be provided by various physical processes, such as atomic motion or photo-induced phase transition. The experiment can run in transmission configuration but also in reflectivity configuration, when the optical density of the sample is too high.

For example, it is possible to observe weak variation of dielectric constant caused by a small atomic motion. One widely known example of this case is the Bismuth (**Boschetto 2008**) where a laser pump generates a coherent motion via the excitation of the totally symmetric A1 mode. This phonon modulates the reflectivity of bismuth and can be conveniently recorded by lock-in detection.

It is also possible with a more elaborated setup to perform coherent control with a two-pump experiment (**Wall 2012, Iwai 2006**). In this case not one but two pump pulses are used with a controllable delay between them. By choosing this delay according to the phase of the phonon, it is possible to suppress or enhance the coherent dynamics resulting from the first excitation.

Recent achievements in THz radiation allow the use of such pulses either as pump or probe. For example, with a THz pump, it is possible to send an electric field of MVcm^{-1} and drive huge carrier dynamics (**Hirori 2011**). It is also possible to perform time resolved THz spectroscopy to investigate the suppression and recovery of a superconducting gap (**Beck 2011**). Not only purely electronic process but also acoustic phenomena can be investigated with such optical techniques (**Kim 2012**).

2.1.2 White Light Experiment

Another experiment we built is the fs white light spectroscopy with supercontinuum generation (**Alfano 2006**). This setup covers an extended spectral range and is also used to record optical density changes induced by temperature.
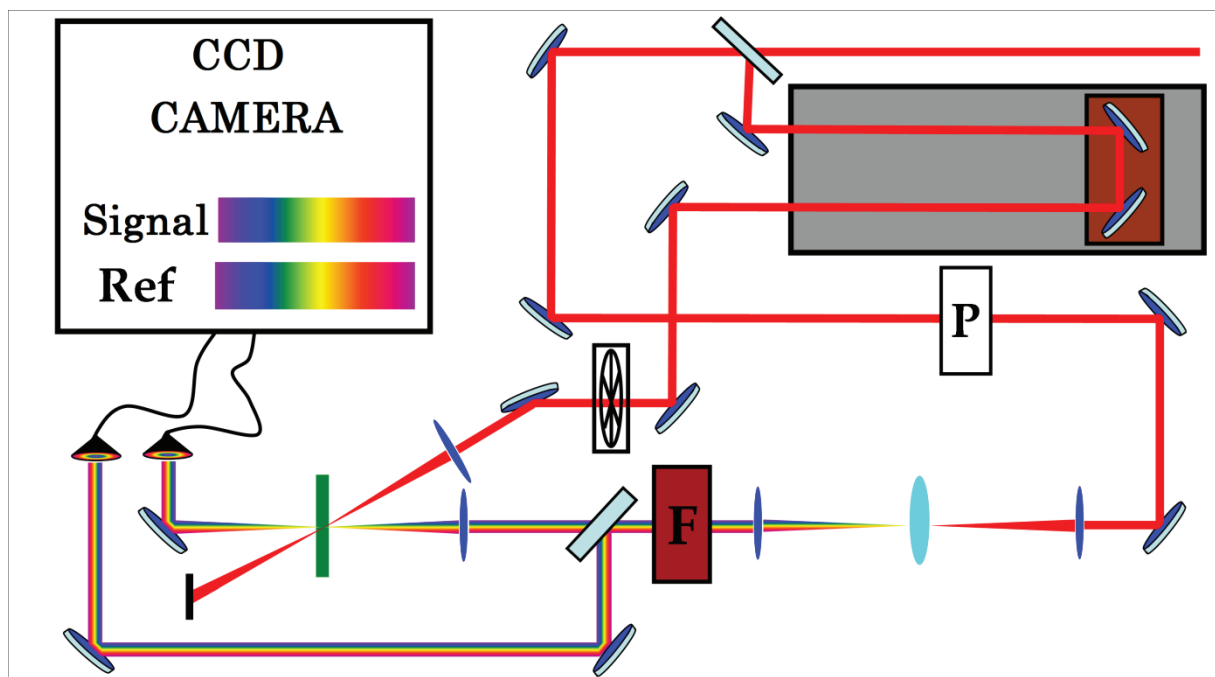
Fig 2.10 *Schema of the White Light experiment.*

The setup of this experiment is presented in **Fig 2.10**. The main piece of this experiment is a CCD camera that is cooled down to -75°C by a Pelletier system to reduce dark current and to accelerate the chip dynamics. By coupling this CCD to a grating polychromator, we obtain a spectrometer with detection range from 450 nm to 720 nm, and read-out time of 1.45 ms. Dividing the laser repetition rate by two, to 500 Hz for probe and 250 Hz for pump, permits recording single spectra without averaging on the chip in order to perform single shot spectroscopy (**Kaszub in preparation**). The main idea was very simple : a 800 nm pulse coming from the ELITE amplifier is split into two parts. One part generates the supercontinuum in a sapphire plate and the other one is used as pump. The supercontinuum pulse itself is split into a probe and a reference, like the two-color system. Photons above 720 nm are suppressed by optical filters because most of the energy remains at 800 nm and around (3-4 orders of magnitude), so the photons from the pulse tail may cause charge spill-out on the detector. More technical details are presented in the thesis of W.Kaszub (**Kaszub 2012**).
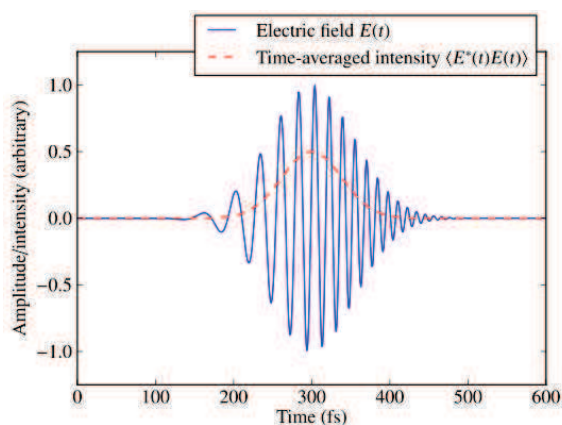
Fig 2.11 *Chirped femtosecond impulsion.*

When the system is operated in the time resolved mode, one more parameter has to be taken into account : the pulse chirp (**Fig 2.11**). Due to group velocity dispersion, the white light pulse on the sample has no longer 100 fs of duration but approximately 2 ps. It means that the red part of the pulse comes first followed by the blue part. So there is a temporal distribution of the wavelengths arriving on the sample, and thus smearing of the time-zero.
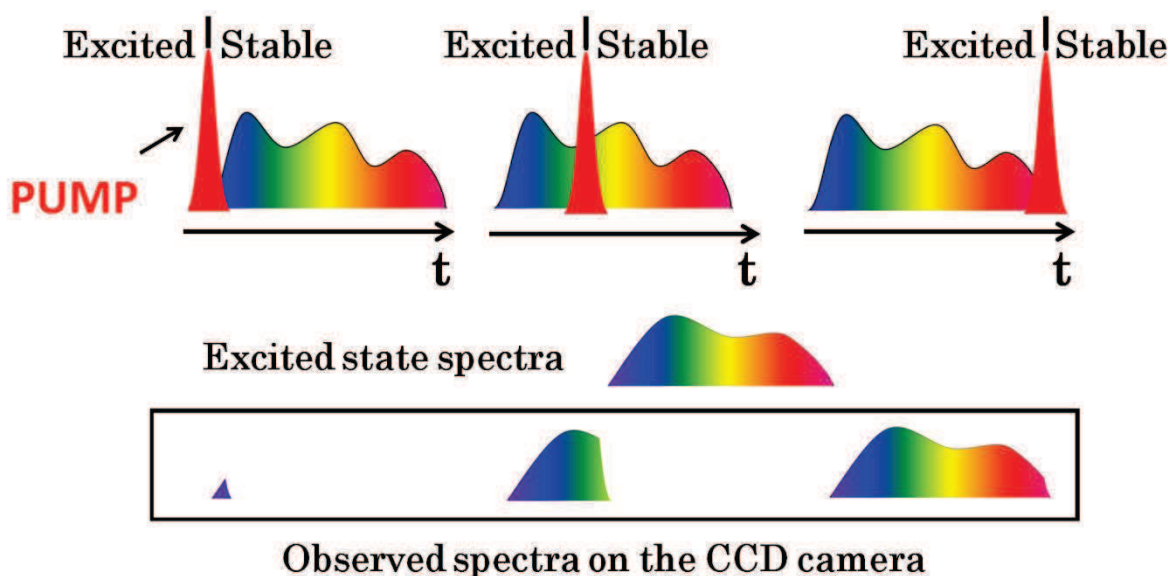
Fig 2.12 *Simulation of chirp influence on the excited spectra detected on CCD.*

As explained in **Fig 2.12**, the blue part of the excited spectra appears first on the CCD. Because there is a correlation between the wavelength and the arrival time, the interpretation of the data at shortest times is possible. It is possible to use temporal or spectral gating and to correct for the chirp in the data (**Polli 2010**). That means that if the spectral resolution is good enough, the system keeps time resolution around ≈ 100 fs.

This setup is particularly suited for the photo-chemistry because it gives direct access to complete spectra of the excited states in the visible range. This spectral bonus is obtained by somewhat compromising the statistics of the signal. Numerous experiments benefit from this kind of setup to explore transient excited states of chemical groups (**D'amico 2012**). It provides a better signature of transient excited state than the two-color studies.

It can also be used to investigate phase transitions, such as the metal-insulator transition in a charge transfer system (**Chollet 2005**). In this work, authors investigate the photoinduced charge transfer of an organic conductor, which undergoes charge ordering under thermal transition. With a good precision on the pulse chirp and a spectral resolution provided by the spectrometer, they were able to reconstruct monochromatic kinetic traces and observe coherent phonons.

2.1.3 Experiment with two synchronized amplifiers

Conventional mechanical delay stage allows covering in the best case few nanoseconds. So this way is not suitable for covering the entire out of equilibrium dynamics spanning over ten decades. We therefore suggested an alternative approach (**Lorenc 2012**).
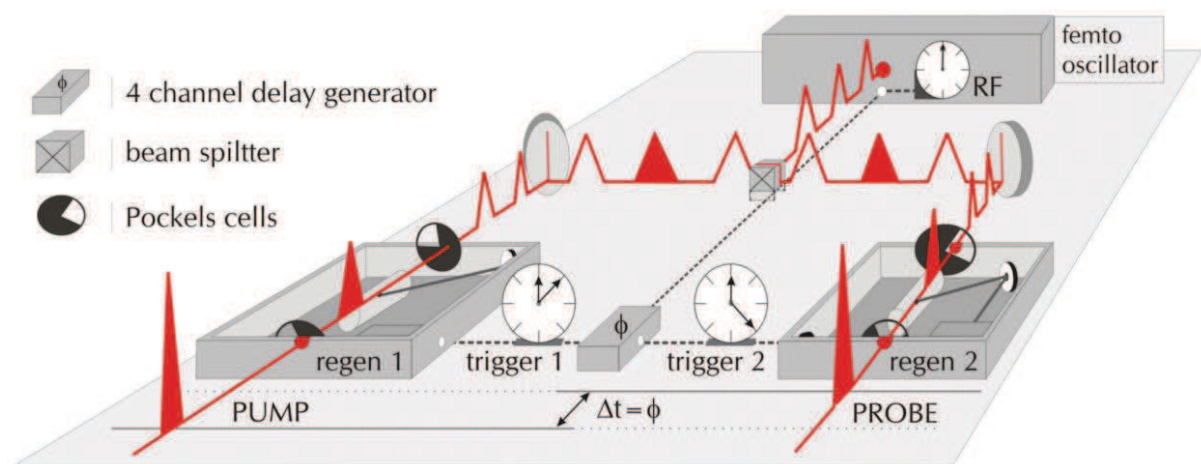
Fig 2.13 Operating mode of the synchronized system.

The key is to lock two regenerative amplifiers to a trigger signal provided by a digital delay pulse generator (**Fig 2.13**). Femtosecond oscillator provides a train of pulse at 76 MHz, thus spaced by 13 ns. By electronically controlling the Pockels cell's opening time, any pulse from that train can be selected for amplification. As a result, each amplifier can trap a different pulse, and the spacing between the trapped pulses is a multiple of 13 ns. This is a more elegant way to reach µs range than to put 500 delay lines in series. At very long delays (long time-base), the electronic jitter being proportional to the time-base of the delay generator, the jitter becomes critical.
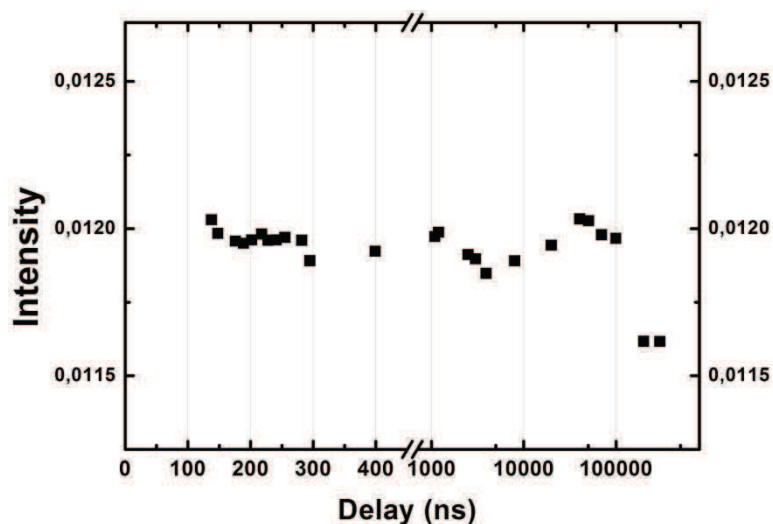
Fig 2.14 Evolution of the pulse intensity in function of the delay imposed to the amplifier.

The Pockels cells ideally should be fired midway through the period of the laser pulse train, otherwise more than pulse may be trapped when the timer jitter brings the gating signal near the confusion zone (exactly on the pulse, where the electronics may slip and lock onto the neighbouring pulse). **Fig 2.14** shows that with a good set of delays, a stability of few percent is available but at long delay (>100 μs), it's harder to conserve stability and the quality decreases quickly. This can be remedied by a delay generator with less jitter.

2.2 X-ray studies using large-scale facilities

Experiments relying on optical spectroscopy, besides providing some crucial information on mechanisms and time scales of molecular changes, are used as starting point for experiments on large-scale facilities. Diffraction provides more detailed information on the mechanisms and processes involved in the formation of photoinduced phases and the associated structural dynamics. Indeed, a change of atomic position in a crystal will modify the structure factor F_{hkl} and by consequence the diffraction pattern. Also scattering factor from molecules in solution provides information about the local molecular conformations (**Ihee 2005**).

In the X-ray regime (500 eV-50 keV), generation of sub-nanosecond X-ray pulses can be accomplished either by using table top experiments (betatron and X-ray plasma) or by using the so called large-scale facilities like synchrotrons and X-FELs (X-ray Free Electron Laser).

2.2.1 Synchrotron Radiation

According to Maxwell equations, all accelerated charged particles emit an electromagnetic radiation. And when a charged particle travels at relativistic speed $v \approx c$, the emission is called synchrotron radiation (**Fig 2.15**). The main interest of accelerating particles at such speed is to concentrate all emissions in a narrow cone with an angle of $1/\gamma$ ($\approx$ few mrad) and to obtain photon in the X-ray regime. The key parameters of synchrotron radiation are the synchrotron frequency ω_0

(number of turns per second) and electron energy expressed in function of their own rest mass:

$$\gamma = \frac{\varepsilon_e}{mc^2}$$

$v = 0$ $v = 0.9c$
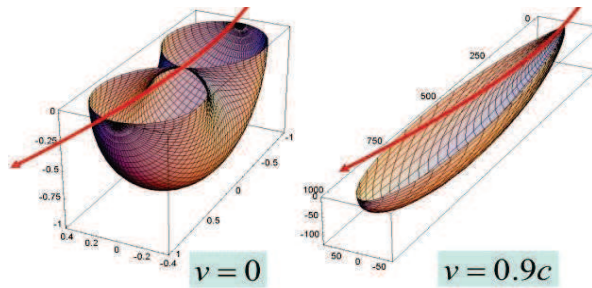
Fig 2.15 Simulation of X-ray emission in function of electron speed.

In order to quantify the beam quality, a useful parameter is the synchrotron brilliance:

$$Brilliance = \frac{Photons/\sec}{(mrad)^2 (mm)^2 (0.1\% bandwidth)}$$

In third generation synchrotrons, in addition to conventional bending magnets (used to keep electrons in almost circular orbits), magnetic structures are inserted in the straight sections of the ring.
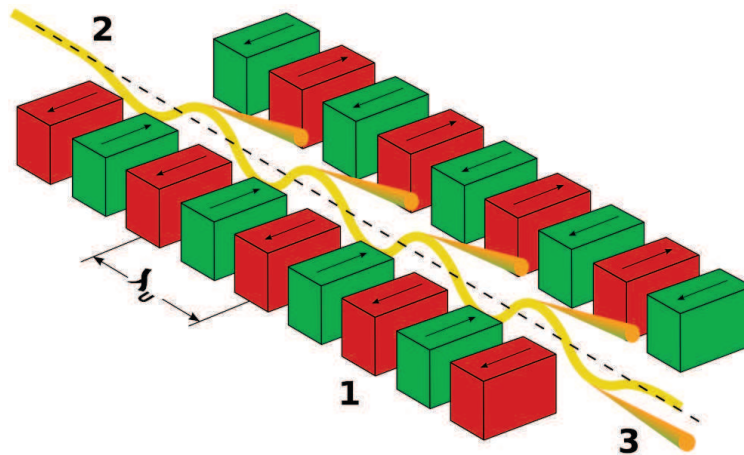
Fig 2.16 Plan of an insertion device.

The goal of such devices is to increase the photon flux .They are classified in two categories: undulator and wiggler (**Fig 2.16**)**.** Each time the electron is deviated; there is emission of electromagnetic radiation. By the use of Lorentz force, magnetic field can bend electron trajectory and by playing with the field shape a fast oscillation of electron is obtained. A wiggler provides higher flux and a rather large bandwidth (several tens of percent). On the other hand, an undulator "concentrates" the emitted photons in only few harmonics, each with a bandwidth of few percent. Obtaining a monochromatic beam is achieved with monochromator as silicon crystal to get almost $\Delta E / E \approx 10^{-4}$.

Pioneering works on time resolved diffraction in synchrotron have been done on ID09b beamline at ESRF (Grenoble) where the first 100 ps time resolved diffraction on organic system

(**Techert 2001**) has been obtained, although some studies with nanosecond resolution had already been performed at that time (**Perman 1998**). Taking a picture of transient crystal structure within a 100 ps temporal resolution is now available and opens new doors in structural dynamics (**Collet 2010**).
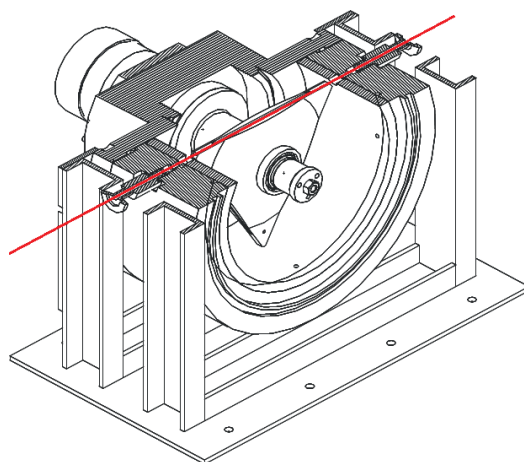
Fig 2.17 Drawing of the Jullich Chopper.

The possibilities of this kind of experiment rely on synchronizing the synchrotron "cavity" and the laser cavity. To do this, active feedback on laser cavity is mandatory and done by piezzo electrical mirrors that match laser frequency with a harmonic of the synchrotron frequency. When using slow detectors, X-ray choppers (**Fig 2.17**) are used in order to select only one pulse every millisecond to match the repetition rate of ultrafast high power amplifiers. Finally, the temporal overlap is checked with an ultrafast diode which can detect both visible and X-ray radiation.

Fig 2.18 Aerial view of the APS Synchrotron.

Following these pioneering works, several time resolved beam lines have emerged all over the world, such as Biocars beam line at APS (USA)(**Fig 2.18**) and NW14 at PFAR-KEK. On the Biocars beamline, physical (**Collet 2012**), structural chemistry (**Coppens 2010**) and biological (**Jung 2013**) time resolved experiment can be performed.
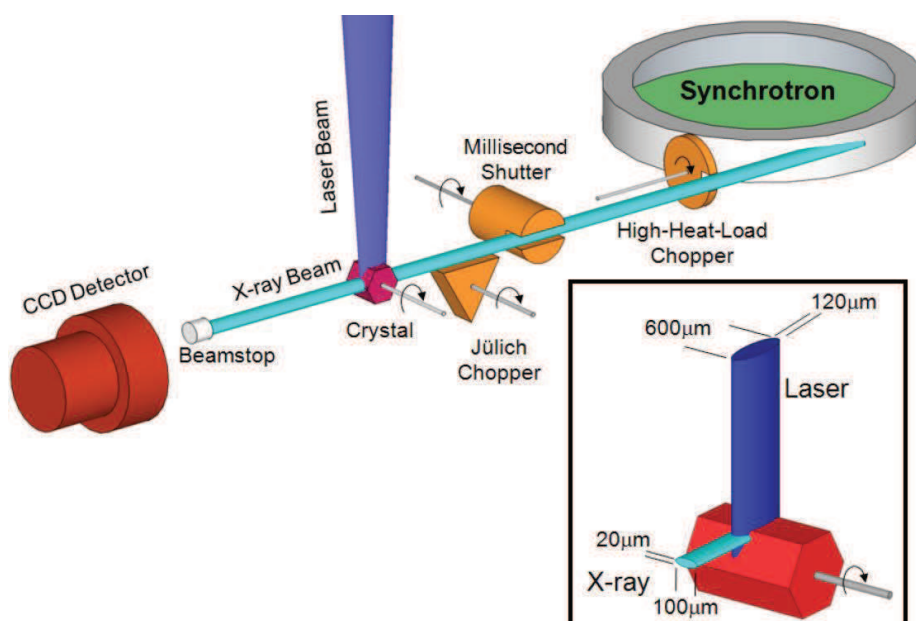
Fig 2.19 *Setup of the Biocars beamline at APS Synchrotron.*

The setup at Biocars beamline is typical for time resolved diffraction (**Fig 2.19**). The X-ray pulse of 100 ps produced in undulators is monochromatized by silicon crystal. The range X-ray energy for goes from 7 to 20 keV and pink beam is also available for Laue Diffraction (**Benedict 2011**). A series of choppers and shutters ensure that only single x-ray pulses are sent to the sample at 40 Hz. At the same time, laser pulse of 1 ps coming from the laser hutch is sent on the top of the sample. Pump wavelength is tunable in the 290-800 nm range thanks to OPA. Diffraction patterns are recorded on a MAR CCD system. This frequency is really suitable for our system because sometimes the relaxation is not complete under 1ms. All the technical specifications are discussed in *J. Synchrotron Rad.* **18 658-670 (2011)**.

Femtosecond X-ray pulses can be obtained in synchrotrons facilities by the slicing method (**R. W. Schoenlein 2000**). An intense ultra-short laser pulse interacts with the electron bunch and locally modulates electrons's energy. The energy of electrons within the laser pulse envelope is modulated and energy dispersive electron optics elements allow selecting only those electrons from the bunch (~100 ps long). At the end, a 100 fs sub-bunch is obtained, yet it contains only few tens of photons. This technique has been implemented on ALS synchrotron (USA) and SLS synchrotron (Switzerland). Slicing method is useful for strongly diffracting systems with only few atoms per unit cell that can be understood by looking only at few Bragg reflections. Molecular systems (often degraded by laser excitation after few hours of experiments) are not suited for such sources where the exposure times are often of the order of several days.

2.2.2 Free Electron Lasers

The X-ray sources have undergone a huge transformation during the 20th century with synchrotron facilities, and are now at the dawn of a new era with an unprecedented x-ray source : Free Electron Laser (FEL).
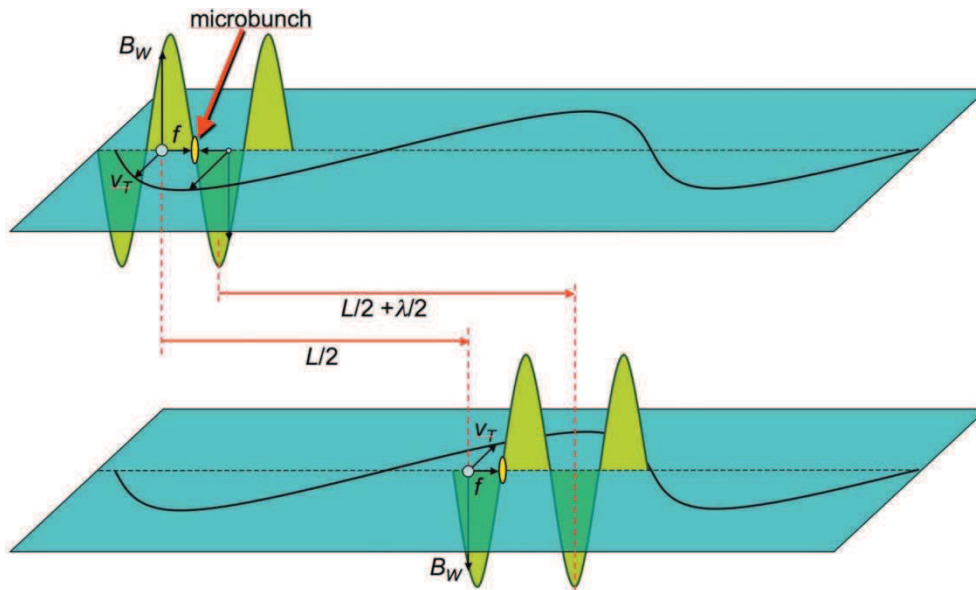
Fig 2.20 *Diagram of the microbunching process (Margaritondo 2011).*

In a typical synchrotron, electrons radiate in non coherent way one with respect to another, so global intensity at the output is proportional to the number of electrons N. In a FEL, electrons radiate in coherent way and the intensity is proportional to N^2. Key point of coherent emission is a process called microbunching. When electron travels through an undulator, electromagnetic wave is emitted each time electron's trajectory is deviated so that the relativistic electron and its wave may interact. The B-filed of the already existing wave and the transverse electron velocity generate Lorentz force that pushes the electrons to form a bunch (**Fig 2.20**).
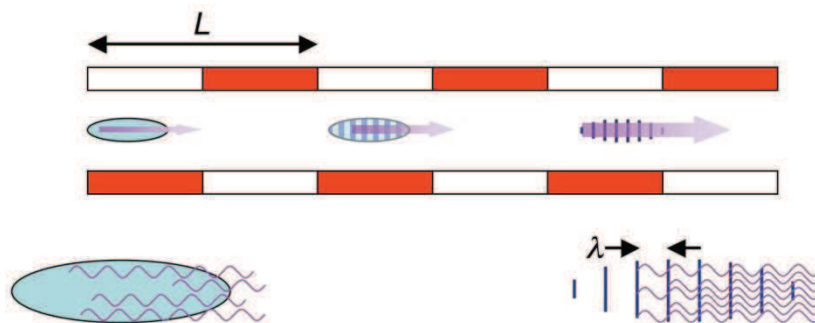
Fig 2.21 *During the pathway, due to Lorentz force, electrons form bunch with X-ray periodicity.*

In such fashion, electrons start to behave coherently but it takes a long time to reach full microbunching. Beam intensity increases exponentially with length and energy saturation is reached at a critical length name saturation length. First, the bunch of electrons is spatially spread but the undulator with typical length L forces electron to emit electromagnetic radiation. Due to positive feedback between electron and electromagnetic field the electrons form microbunches with a periodicity equal to the emitted wavelength λ (**Fig 2.21**). Due to the fact that electrons within a microbunch oscillate all together with the same phase, the resulting intensity is proportional to N^2 instead of N. Nowadays there is no mirror that can reflect photon in the X-ray regime at normal incidence, so single pass strategy is the only way to achieve microbunching. In simple terms, it explains the length and the geometry of such facilities.

Another way to obtain microbunching is to get separately X-ray and electron bunch and send them together to an undulator. In this case X-rays act like a seed to accelerate the microbunching process. In the case where the process appears freely, like in LCLS, it is called SASE (Self Amplified Spontaneous Emission). The world's first operational hard X-ray FEL is LCLS at SLAC (USA), opened since 2009 :

Fig 2.22 *Aerial view of the LINEAC in SLAC facility.*

It is a 3 km long linear accelerator with and ~100 m undulator for generation of X-FEL radiation (**Fig 2.22**). Beam is sent to 6 beam lines split into two experimental halls. The beam line especially devoted to the ultrafast pump probe studies is named X-ray Pump and Probe (XPP) (**Fig 2.23**).
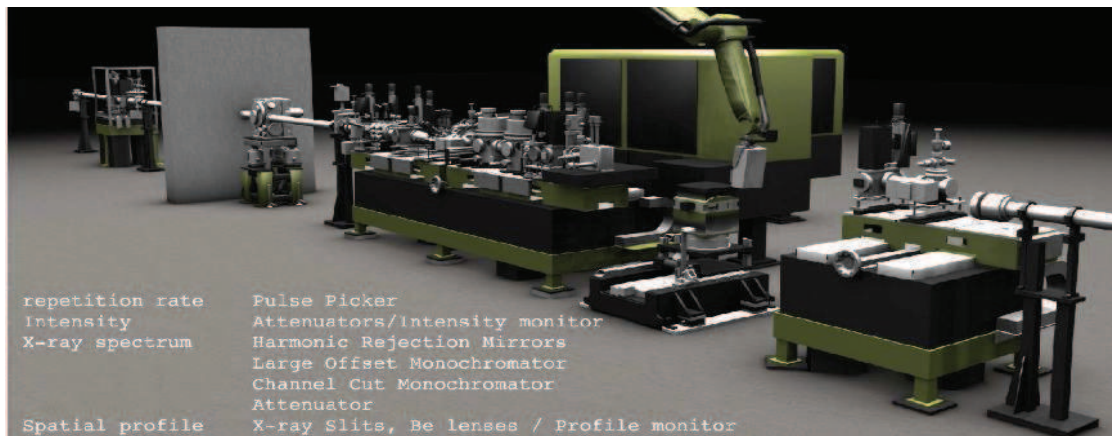
Fig 2.23 *3D drawing of the XPP beam line.*

With this new technology, fs X-ray pulses with duration as short as 20 fs are accessible. X-ray beam can be focused onto few microns with beryllium lenses. The beam line is equipped with a Si (111) monochromator $\left(\frac{\Delta E}{E} = 1.14 * 10^{-4}\right)$ and can work in energy range of 4-10 keV of the fundamental wavelength, and 10-25 keV using the third harmonic (with a factor 100 loss in intensity).

Contrary to synchrotrons where the same electron bunches are used billions of times, current XFELS uses a new electron bunch for every X-ray pulse thus introducing shot-to-shot fluctuations of X-ray beam properties like position, intensity, arrival, time, etc. To overcome this problem, numerous diagnostic tools which quantify the above are present in the beamline to

measure as many parameters as possible for every single pulse. Timing jitter between X-Ray and laser pulse is 200 fs r.m.s compared to 50 fs for the laser duration and 30 fs for X-ray duration. To avoid such jitter problem and improve the time resolution, so called timing tools have been built and now allow 6 fs r.m.s jitter correction (**Harmand 2013**).
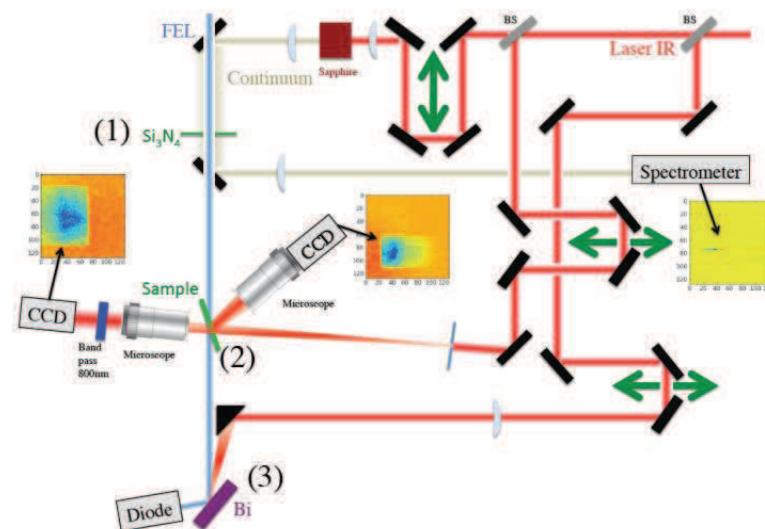
Fig 2.24 Plan of the timing tool on XPP beamline.

Induced ultrafast optical switching of bulk refractive indices is a common cross-correlation technique and can be used as timing tool for FEL hard X-ray source (**Fig 2.24**). The method goes by the following principle. The laser pump pulse is divided into two parts. One part is used as a pump for the pump probe experiment, whereas the other part is used to generate a supercontinuum and is sent to a Si_4N_3 membrane. After crossing the membrane, the white light pulse is sent on a grating where it is spectrally dispersed and collected on a CCD camera. Due to the chirped character of this continuum, it is possible to map out time with wavelength. The impacting X-ray will instantaneously modify the optical properties of the membrane, which in turn modifies the spectrum of supercontinuum probe, leaving a time stamp at only one wavelength.

Time resolved diffraction at this time scale poses a huge technical challenge as it entails exploring as much of reciprocal space as possible while keeping the femtosecond time resolution. The difference in refractive index between x ray and visible pulse is such that the samples have to be only few microns thick to avoid loss of time resolution.

2.3 Time Resolved Diffraction (at APS Synchrotron)

2.1 Introduction to Diffraction

Scattering techniques of X-rays (as well as of neutrons and electrons) represent a fundamental tool to investigate structural aspects of matter and its transformations (**Als-Nielsen & McMorrow 2001, Hercules 1993**). From diffraction patterns a wealth of information can be extracted by following the positions of peaks, the intensities of peaks, the shapes of peaks and the spread of diffuse scattering in the reciprocal space. **Fig 2.25** shows a typical diffraction pattern obtained by using monochromatic X-ray diffraction on a single crystal.

Bragg peaks :
Position: average lattice
Shape: domain size
Intensity: average structure factor

Diffuse scattering :
Position: local periodic structure
Shape: correlation of local order
Intensity: deviation from the average structure
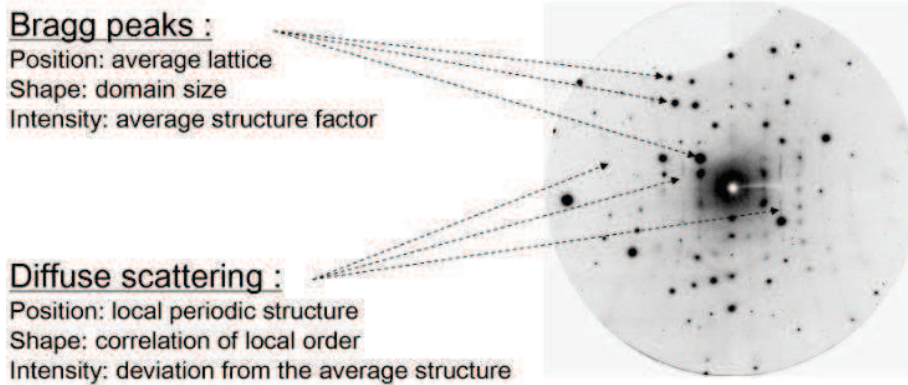
Fig2.25 Monochromatic X-ray scattering pattern recorded on a 2D CCD camera.

In the kinematical approximation, the intensity of the X-ray diffracted by a crystal is proportional to the square modulus of the coherent addition of the amplitudes scattered by all the electrons in the diffracting crystal.

$$R_{uvw}$$
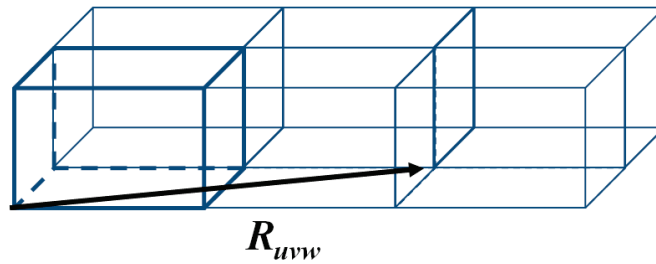
Fig 2.26 Simple view of lattice periodic pattern

Thus in the simplest case of a crystal built with NxNxN identical unit cells on a 3D periodic lattice (**Fig 2.26**) the scattered intensity in a direction defined by a scattering vector $Q=k_d-k_i$, where k_d and k_i are respectively the diffracted and incident wave vector, takes on the form :

$$I(Q) = \left| \sum_{u=1}^{N} \sum_{v=1}^{N} \sum_{w=1}^{N} F(Q) e^{-iQ.R_{uvw}} \right|^2$$

where $F(Q)$ is the scattered amplitude along Q for one unit cell, and the position of each unit cell in the crystal is defined by $R_{uvw} = ua + vb + wc$. The periodic summation leads to

$$I(Q) = \frac{\sin^2(\pi Nh)}{\sin^2(\pi h)} \times \frac{\sin^2(\pi Nk)}{\sin^2(\pi k)} \times \frac{\sin^2(\pi Nl)}{\sin^2(\pi l)} |F(Q)|^2$$

where the scattering wave vector Q has been decomposed on the reciprocal space basis a^*, b^* and c^*: $Q = ha^* + kb^* + lc^*$.

Constructive interferences from the different unit cells constituting the crystal is only observed around integer values of the *(hkl)* coordinates, which correspond to the nodes of the

reciprocal lattice. This condition for Bragg scattering gives rise to sharp peaks in the diffraction pattern around the different nodes. The intensity of every Bragg peak is proportional to the square modulus of the amplitude scattered by all the electrons of a unit cell.

By considering a spherical distribution of electrons around atoms at rest a structure factor of the unit cell can be introduced:

$$F(Q) = F(hkl) = \sum_j f_j e^{-Q \cdot r_i} = \sum_j f_j e^{-2i\pi(hx_j + ky_j + lz_j)}$$

where f_j is the atomic scattering factor (form factor) of spherical atom j, at position r_j. The integrated intensity of a Bragg peak on the *(hkl)* node is then determined by *F(hkl)*. Thus the information about the distribution of atoms within the unit cell is contained in the structure factor associated with the various nodes of the reciprocal lattice.

These different basic features of X-ray diffraction are illustrated in **Fig 2.27**, for a simple case where every unit cell contains one small molecule: the position of Bragg peaks in the reciprocal space is related to the 3D periodic lattice (unit cell parameters), their intensity to the atomic structure, and their shape to the size of diffracting volume, in general controlled by the imperfections of the crystal.
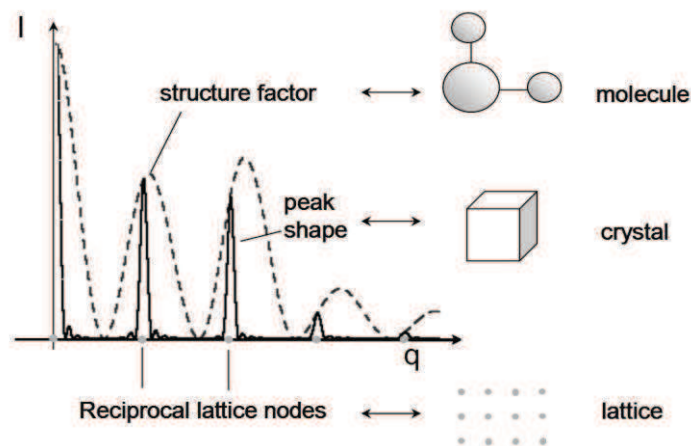
Fig 2.27 Relations between the reciprocal space (left) and real space (right).

2.2 Time resolved studies

Time resolved diffraction in synchrotron enabled following structural dynamics in biological, chemical and physical systems with a sub-angstroms resolution. It is possible to catch a transient structure of crystal and to detect change of 10^{-2} Å in the molecular structure (**Lorenc 2009**). Studies on biological systems have been performed and ligand migration into a complex system observed with 150 ps time resolution (**Schotte 2003**). The possibility to track a new phase generated by photo-excitation is also possible. Due to selection rules, when a system undergoes a phase transition with symmetry breaking some Bragg peaks may vanish. The creation of a new photo-induced phase may change the diffraction pattern if long range order appears or vanish. By looking at some reflections, a new transient state can be observed (**Cavalleri 2001**).

The first attempt of fs time resolved diffraction has been made with plasma sources producing fs X-ray pulses. When a metal is excited by an intense fs laser, atomic recombination leads to X-ray emission at K_α line but this emission is weak and isotropic.
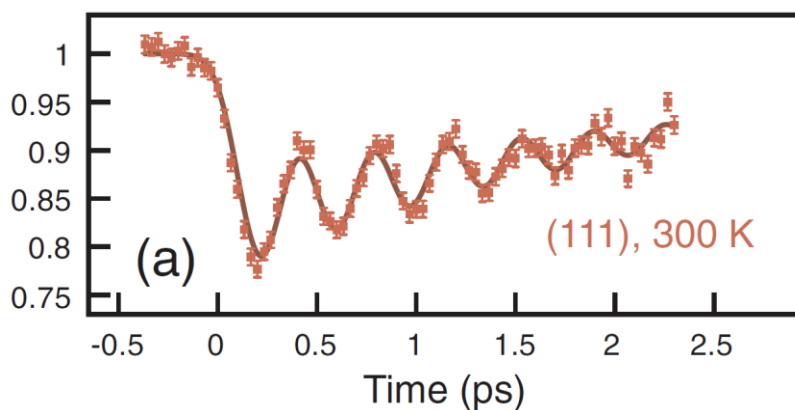
*Fig 2.28 Evolution of the (111) reflection of Bismuth after irradiation by fs laser pulse (**Johnson 2009**).*

It is still possible to follow the change of structure by recording one specific Bragg peak because its intensity gives directly the structure factor. For example, by following the (111) Bragg peak of bismuth (**Fig 2.28**), it has been found that a modulation of intensity monitors the phonon dynamics of the total symmetric mode A_1 (**Sokolowski-Tinten 2003**). The slicing technique provides flexibilty and higher fluency than plasma source .With this kind of source, it is possible for instance to reconstruct a full cell motion on fs time scale (**Johnson 2009**). Slicing and FEL facilities have also been used to perform fs XANES measurements (**Bressler 2009, Lemke 2013**) which can give information about the local structure of molecules around a specific atom.

2.4 Time resolved XANES

X-ray absorption spectroscopy quantifies the probability for a sample to absorb photon as a function of the photon energy. Each element on the periodic table has its own characteristic absorption spectrum.
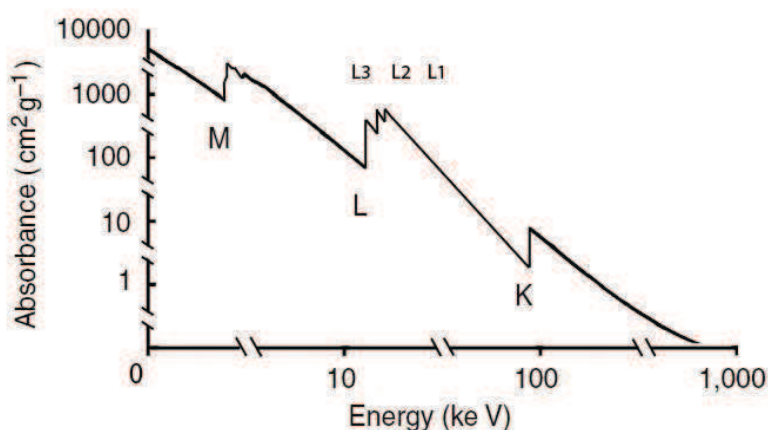
Fig 2.29 X-ray absorption spectra of transition metal species.

Such spectra provide not only information about the electronic configuration of the system but also structural information in the condensed phase (crystals or liquids), as the photo-electron scatters backs on the neighboring atoms and modifies the absorption cross-sections. Local molecular configurations are given by X-ray absorption spectra. A typical X-ray absorption spectrum is showed **Fig 2.29**, illustrating sudden absorption near ionization energy of core binding electrons. These edges refer to electrons ionization of n=1 shell for K-edge and n=2 for L-edge. Near the edge, there is an oscillating feature which carries information on the local structure (**Fig 2.30**).
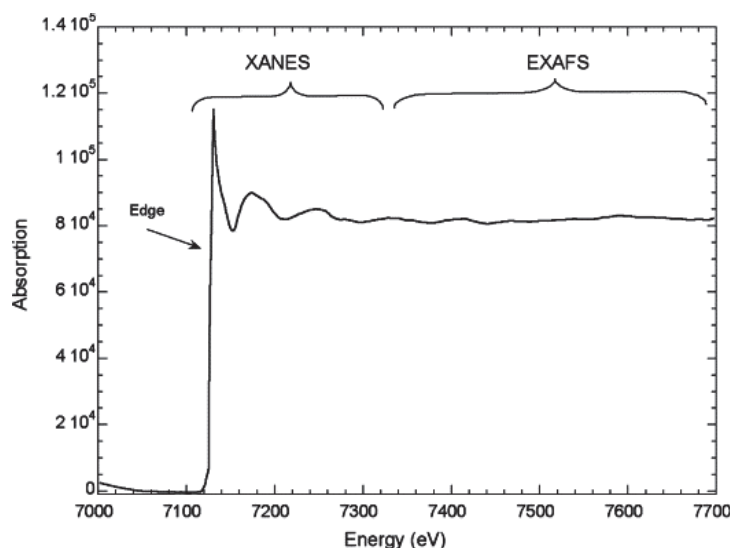
Fig 2.30 *Classical X-ray Absorption Near Edge.*

The area above ionization threshold is divided into two parts : XANES (X-ray Absorption Near Edge Spectroscopy) which covers first ~100 eV above the edge and contains both structural and electronic information. The second part called EXAFS (Extended X-Ray Absorption Fine Structure) starts from 150 eV above the edge and provides more detailed information on the structure. There are two ways to do XANES experiments : absorption or fluorescence. Absorption is a straightforward detection of the amount of absorbed photon by a system obeying the classical Beer-Lambert law. If the crystal length is known, the fraction of the photoinduced species can be easily extracted. But when the absorption is too high, such detection is not suitable and it is better to perform fluorescence detection. Fluorescence results from the emission of high energetic photo-electron after the ionization via recombination processes.
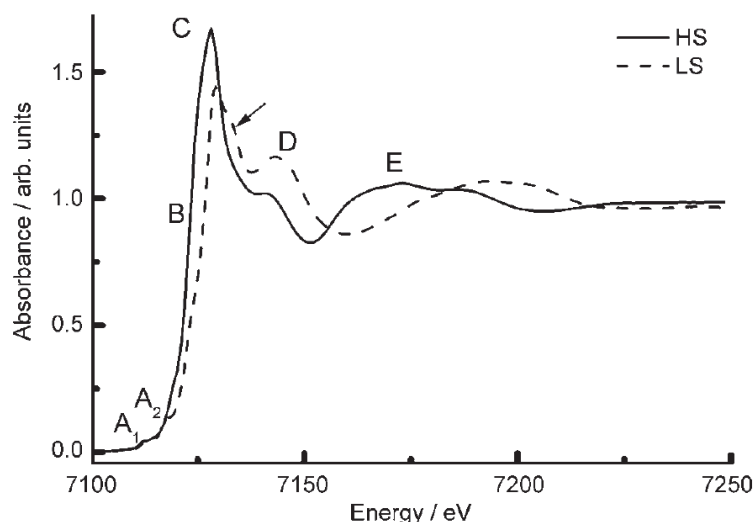
Fig 2.31 *K edge XANES spectra in the HS and LS state of the [Fe^{II}(phen)$_2$(NCS)$_2$] compound (**Arezki 2011**).*

For instance, in SCO system, the changes of structure and electronic configuration modify the XANES spectra on the K edge of iron (**Roux 1996, Arezki 2011**)(**Fig 2.31**). This energy shift of the edge is correlated both with electronic and structural properties. By recording at fixed energy close to the edge, the evolution of fluorescence intensity in time gives a fingerprint on the creation of HS molecules. Because XANES probes atoms core-shell, the signature observed is directly linked to the elongation of the bond length <Fe-N> in the case of SCO system. Like with diffraction, XANES measurements observe directly the structural dynamic of the LS to HS transition.
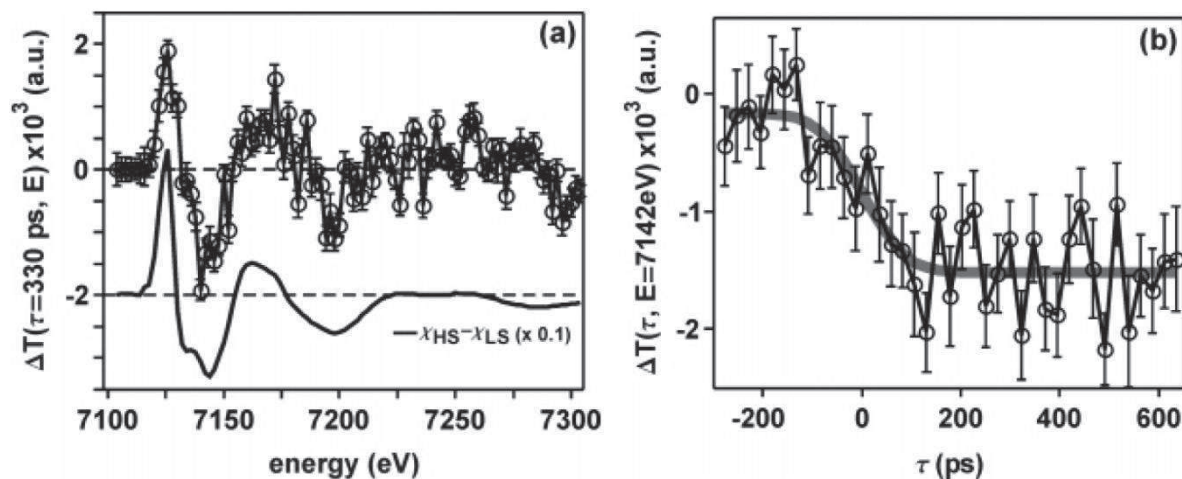
Fig 2.32 *Difference between LS and HS XANES spectra in [Fe(tren(py)$_3$)](PF$_6$)$_2$ (left). Evolution in time of the fluorescence intensity at 7,142 keV following fs laser excitation (right). (**Khalil 2006**).*

One great advantage of XANES studies compared to diffraction resides in simplicity of the former, dispensing with need to record vast sections of reciprocal space. It can be also applied to molecules in solution. If the change of absorption between HS and LS is known, by choosing wisely the photon energy, the structural dynamic is recorded (**Fig 2.32**). XANES was the first method used to watch picoseconds structural dynamics in SCO systems (**Khalil 2006**) and nowadays several studies with femtosecond time resolution have been carried out (**Bressler 2009, Lemke 2013, Huse 2012**).

Chapter 3: Ultrafast spin-state Photo-switching in Solid State

Switching the macroscopic physical properties of a material with an ultrashort laser pulse through interconversion of molecular states is an important goal in ultrafast science. Understanding molecular photo-switching in the solid state requires answers to a number of fundamental questions regarding the relevant physical parameters involved and the role of the active crystal made of switchable molecules. Spin-crossover compounds promise bright perspectives as acclaimed prototypes of photoactive molecular bistability. Several investigations of the ultrafast photo-switching of spin crossover systems have already been reported by others groups with a rich literature. Most of this work deals with molecules in solution as introduced in chapter 1 (**Gawelda 2006, Smeigh 2008, Huse 2011**). Nanosecond laser excitation was used to photo-switch solids in several studies below and inside the thermal hysteresis (**Galle 2010, Cobo 2008**) and more recently fs optical laser pulses were used in solid state in weakly cooperative systems, mainly for investigating the out-of-equilibrium dynamics in the ps-ms range (**Moisan 2008,Lorenc 2009**). But no detailed study of ultrafast spin state switching in solid state has been reported so far. In the solid state, the influences of cooperativity or size effects are of interest for understanding how the different phenomena involved play their role. To explore these different points, I have studied two types of different cooperative SCO solids : a Fe^{III} compound $[Fe^{III}(3\text{-MeO-SalEen)}]PF_6$ which shows a 1st order transition and which is available in several crystal sizes as well as the prototype Fe^{II} compound $[Fe(phen)_2(NCS)_2]$ which also undergoes a 1st order transition.

One of the most interesting aspects of the LIESST process is that the Inter System Crossing (ISC) is of high quantum efficiency (close to 1), as almost all the molecules reaching an electronic excited state switch towards the high spin state, if the correct pump wavelength is used. To investigate this process in detail, a fs time resolution is needed. Most of the investigations I performed used fs optical pump-probe spectroscopy in the fs laser platform at the Institut de Physique de Rennes (**Lorenc 2012**). We also performed a fs X-ray study, by using XANES at the XPP beamline of the LCLS X-ray Free Electron Laser (X-FEL) (**Lemke 2012**). Part of these results are included in Publication N°1, 3 , 4 and 5.

3.1 Investigation of the $[Fe^{III}(3\text{-MeO-SalEen)}]PF_6$ complex

The first system studied during my thesis was the Fe^{III} complexe : $[Fe^{III}(3\text{-MeO-SalEen)}]PF_6$ (**M.S. Haddad 1981**), in the frame of the ANR project with Marie-Laure Boillot and Antoine Tissot. Indeed, the group of A. Hauser (**Enaschescu 2006**) demonstrated that in Fe^{III} complexes the relaxation of photo-excited HS state can be the order of 1 ms, what is required for pump-probe studies with our experimental set-up.

3.1.1 Thermal Switching : Single Crystal vs Nanocrystals

3.1.1.1 Single crytal

The molecular structure of this compound, synthesized for the first time in 1981, is shown in **Fig 3.1**. The unique independent cation observed in the asymmetric unit is a six-coordinated Fe^{III} ion with tridentate Schiff-Base ligands. At 300 K, the bond lengths to the Fe^{III} atom (mean value <Fe–L>= 2.094 Å) and bond angles measured fall within the range of expected values for a high-spin $[FeN_4O_2]$ complex with this type of ligand (**Hayami 2006, Summerton 1978, Sim 1981**). It is one of the few cooperative Fe^{III} systems showing a 1st order phase transition. Such behavior is rather unusual in Fe^{III} systems, which switch between two electronic states:

- A low spin one (LS) with S= 1/2 corresponding to the electronic distribution $t_{2g}^5 e_g^0$

- A high spin one (HS) with S= 5/2 corresponding to the electronic distribution $t_{2g}^3 e_g^2$

The transition from LS to HS states can be probed by magnetic susceptibility measurements, as the $\chi_m T$ product (χ_m = molar magnetic susceptibility) is the weighted contribution of magnetic susceptibility of molecules in the HS and in the LS states. **Fig 3.2** shows that this compound undergoes a 1st order transition around 163 K, with a 3 K width hysteresis (T^{down}=162.5 K, T^{up}=165.5 K). Such measure is a straightforward marker of the spin state of the system.
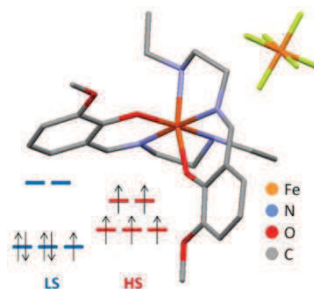
Fig 3.1 [Fe^{III}(3-O-MeSalEen)$_2$] PF$_6$ structure.
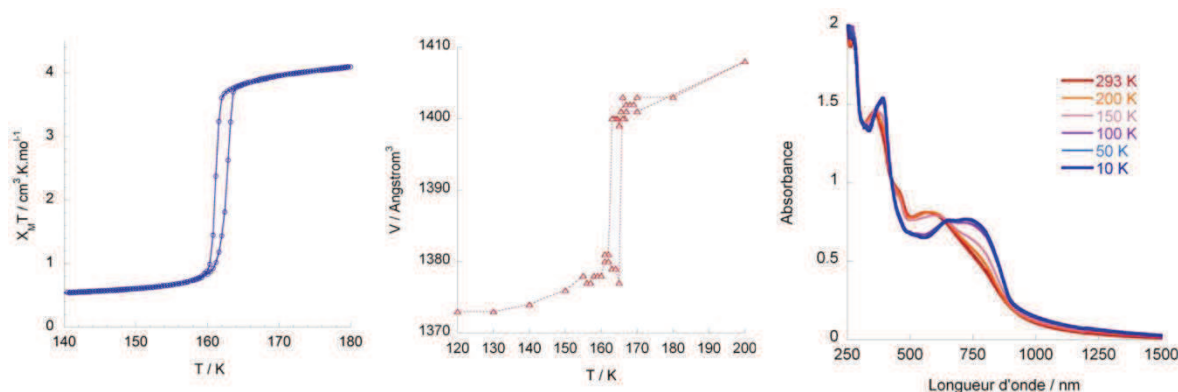
Fig 3.2 Signature of the thermal transition by SQUID, X-ray diffraction and optical absorption.

Like many spin crossover systems, the central Fe atom is caged in a nearly octahedral ligand field (here made of 4 Nitrogen atoms and 2 Oxygen atoms) (**Fig 3.1**). This system crystallizes in the triclinic P$_{-1}$ space group and undergoes an isostructural transition as it is often the case in spin

transition systems. This transition is also linked to structural change that can be observed by X-ray diffraction with a discontinuous expansion of the volume of the lattice cell and an increase of <Fe-N>, the average <Fe-N> bond length, from the LS (T<163 K) to the HS phases (T>163 K). The 0.15 Å <Fe-N> elongation is rather common in Fe[III] system (**Tissot 2011**). X-ray data analysis tends to explain the cooperativity by an extensive 3D network of intermolecular interaction.
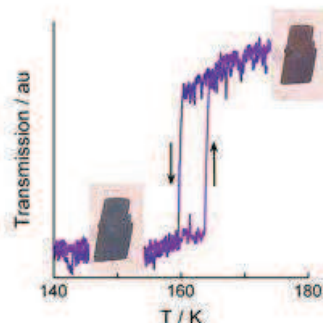
Fig 3.3 *Optical absorption on single crystal during thermal transition at 760nm.*

Because of the different electronic and structural states, the optical absorption must differ between HS and LS. This is clearly observed in the visible range in **Fig 3.2** with a LS LMCT band centered around 800 nm. By looking at the crystal under a microscope (**Fig 3.3**) in the transmission mode, a change of color from orange 285 K (HS) to dark green 90 K (LS) is observed in agreement with the change of absorption.

3.1.1.2 Nanocrystals and Microcrystals

For investigating size effects, we also studied nano-crystals, as our chemist collaborators have the possibility to synthesize crystals of different sizes of this compound. Now formidable progresses in the chemistry of nano-patterning and nanoscale assembling allow such thing (**Coronado 2007, Boldog 2008, Molnar 2007**). Nanoparticles of this compound are obtained by fast precipitation method (**Tissot 2012**) and embedded in a polymeric matrix of PVP (polyvinylpyrrolidone). This mixture is dropped off on a subtract plate by spin coating. The crystallinity of such nanocrystals trapped in the polymer is confirmed by X-ray diffraction and Raman spectroscopy.
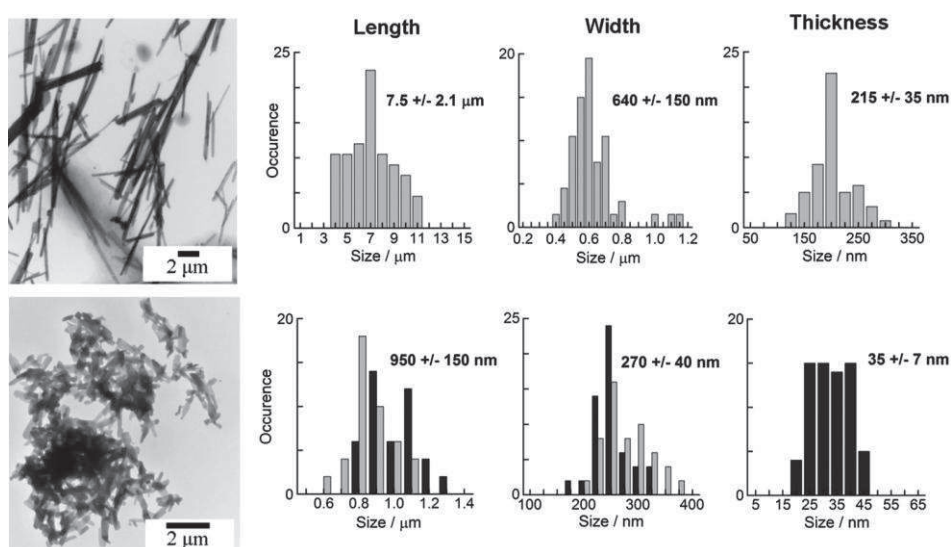
These needle-shape nanocrystals have the typical dimension of $(950\pm150)\times(270\pm40)\times(35\pm7)nm^3$ with a good size dispersion estimated via TEM (**Fig 3.4**). In the same way, bigger crystals of µm size have been synthesized and characterized. The size dispersion of the microcrystals is also reasonable and gives typical dimension of $(7.5\pm2.1)\times(0.64\pm0.15)\times(0.21\pm0.03)\mu m^3$. Microcrystals are an order of magnitude larger in the three directions of space than nanocrystals.
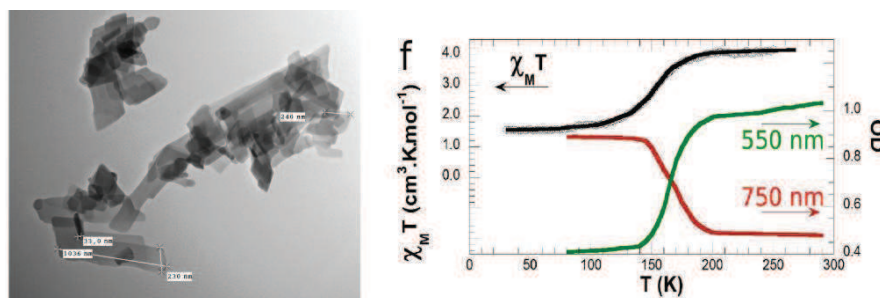
Fig 3.5 TEM image of nanocrystals with typical size (left),

SQUID and Optical transmission during thermal transition (right).

The thermal spin conversion of these two systems has been investigated via magnetic and optical measurements. They look globally similar (**Tissot 2012**) and only the behavior of nanocrystals will be discussed here. On contrary to single crystal, the transition appears now more gradual with a crossover spanning over 40 K and centered around 165 K. This crossover is well characterized by SQUID (**Fig 3.5**). Below 100 K, the system remains fully LS and above 200 K fully HS. The origin of the loss of cooperativity is currently under investigation. Some new experiments on similar systems (**Tissot 2013**) tend to link this process with both chemical bonding to the polymer and anchoring effects. Like monocrystal, a good agreement between magnetic and optical measure (**Fig 3.5**), allowing to use optical absorption spectroscopy for tracking the evolution of the HS fraction of molecules in the system (**Bertoni 2012**).
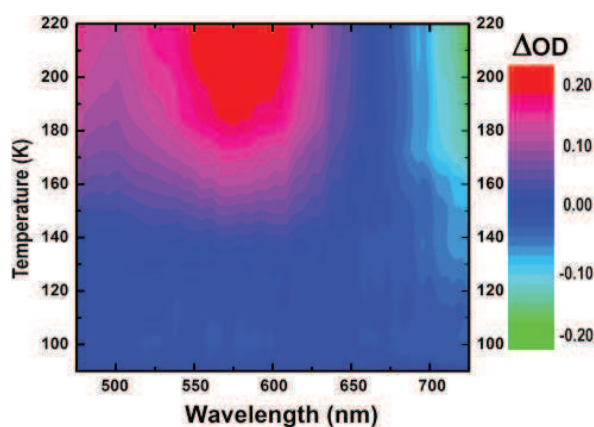
Fig 3.6 Change in optical density during the thermal transition from LS to HS.

A detailed inspection of the absorption spectra during the LS→HS conversion (**Fig 3.6**), some clear fingerprints are revealed. An absorption band appears at around 550 nm and bleaching in the NIR (Near Infrared). There is also an interesting feature provided by an isobestic point at 670 nm. An isobestic point is referring to a wavelength where low spin and high spin states have same optical density. So absorption at this wavelength does not vary between the two spin states. These strong optical fingerprints of LS to HS conversion are interesting for performing time resolved optical studies. The orientation of nanocrystals in the matrix is random which means that we are not sensitive to polarization effect but only probing an average change. The same isotropic orientation of the crystals also exists in the microcrystals matrix. The polymer does not absorb in the visible range or in NIR range so all changes measured here during the thermal transition, and later in time-resolved mode, are only due to the change of spin state.

3.1.2 Femtosecond response of single crystal

The first attempt of ultrafast spin state photo-switching has been performed on single crystals. It involves the use of classical pump probe setup in absorption mode presented in chapter 2. The setup runs at 1 kHz for the probe and 500 Hz for the pump and is linked to a lock-in detection. The probe is set to 760 nm, where the change of optical transmission between LS and HS states is large, and the pump to 850 nm, on the LMCT band. Both pulses have 80 fs duration so that the overall time resolution of the experiment is 140 fs. Both pump and probe are polarized on the long axis of the crystal were the penetration depth is larger. For scaling the number of molecules converted by light from LS to HS state, the measured change of optical density (OD) in the time domain is scaled to the change of optical density observed during the thermal crossover. The crystal is cooled down via cryostream jet (liquid nitrogen) in pure LS state and the fs pump-probe experiment is performed at 140 K. This temperature is well below the spin transition to avoid residual laser heating effect, but high enough to ensure a fast relaxation of the photo-excited HS state, required for stroboscopic pump-probe experiment. A well marked 1st order transition is observed in the temperature dependence of optical transmission measured with our experimental set-up (**Fig 3.7**).
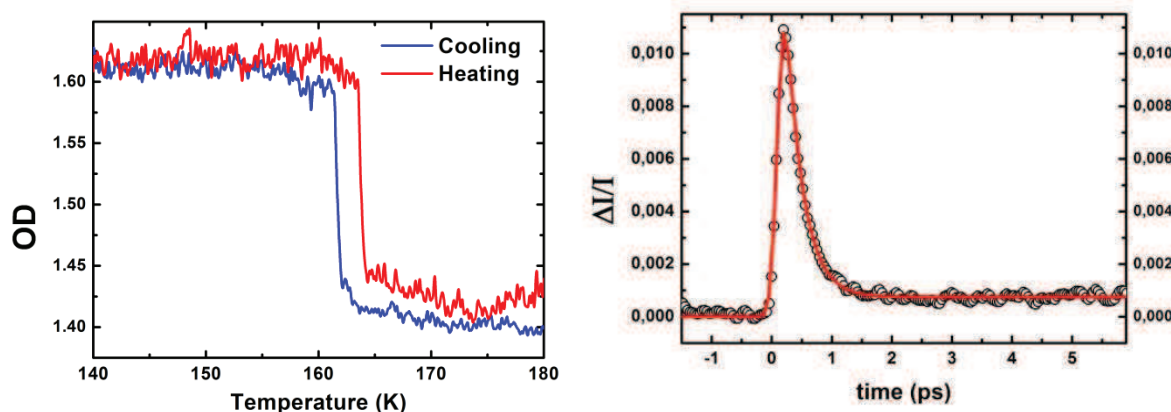
Fig 3.7 *Thermal signature (left) and the associated time resolved data (right) at 760 nm.*

A typical time-resolved optical pump-probe result is also presented in **Fig 3.7**. It shows a sub picoseconds peak which relaxes on an extremely short time-scale towards a small plateau. The increase of transmission agrees with the expected decrease of OD at 760 nm when HS state forms. The increase of transmission peak can be attributed to the bleaching of the initial LS state after the excitation by the pump beam of the LMCT band. By fitting the relaxation of this LMCT state with a single exponential decay, a time constant of 170 ± 50 fs is found which is close to with typical

timescale observed for Fe^{II} molecules in solution (**Smeigh 2008, Gawelda 2007**). But the fraction of photo-switched molecules is really low, approximatively 0.2%. It is mainly due to the low excitation density which has to be used in order to prevent sample damage. The laser penetration depth (5 μm) is indeed the limiting parameter for investigating these single crystals 20-50 μm thick.
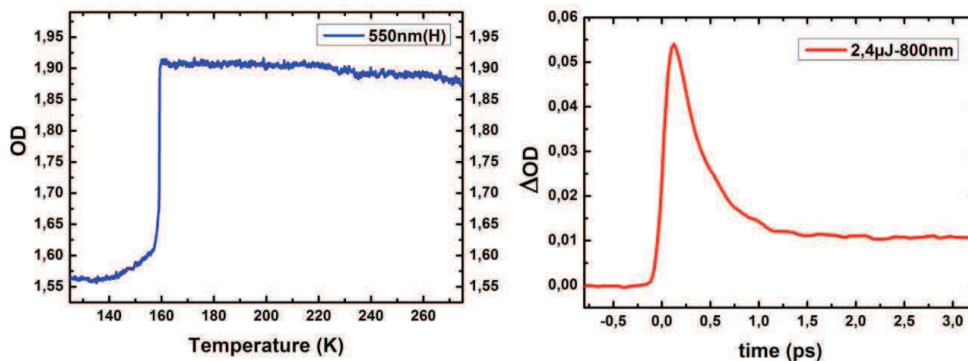
Fig 3.8 *Thermal signature (left) and the associated time resolved data (right) at 550nm.*

Other experiments were performed on 20 μm thick with a probe set to 550 nm, where the OD change is larger and in opposite sign compared to 760 nm (**Fig 3.8**). A conversion of 2.5% is reached with laser pulse energy near threshold damage. Both time dependent signals in **Fig 3.7** and **Fig 3.8** have signs in agreement with the thermal variation of OD during the LS to HS conversion. It's a clear fingerprint of photoinduced spin state switching at fs time scale in the solid state, with a time constant of ≈ 200 fs for reaching the HS state. For overcoming the problem of penetration depth and reaching larger conversion rate, it was therefore necessary to study smaller crystals.

3.1.3 Femtosecond switching in Nanocrystals

For overcoming the problem of sample damage and of the penetration depth of pump and probe in order to cover the all visible spectra, the same kind of pump-probe experiments were performed on the nanocrystals in polymeric matrix shown in **Fig 3.9**.
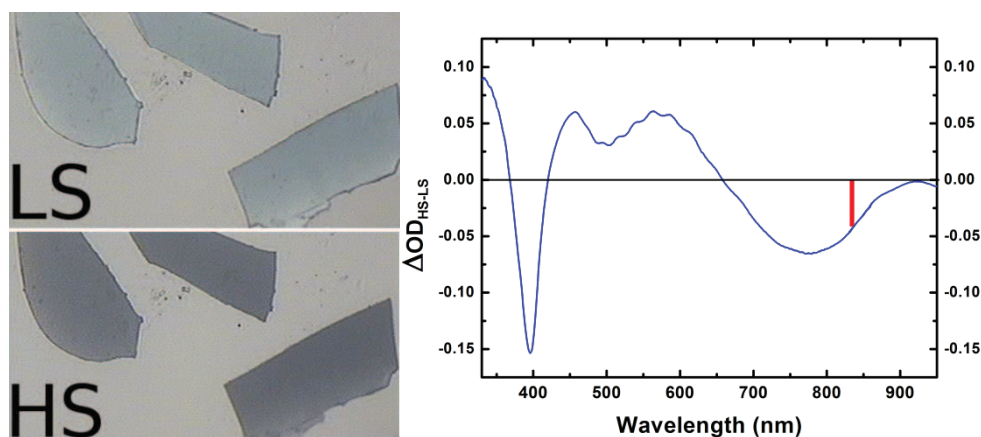
Fig3.9 *Picture of film of polymer in HS and LS state (left)*

Difference in optical density between Pure HS and Pure LS (right).

Due to the thickness of the crystals and the transparency of the polymer, the optical density in the visible range is small, between 0.5 and 1, depending on the crystals concentration in the film. The pump wavelength was set around 840 nm where it efficiently induces LS to HS transition from pure LS state at 100 K. The thermal transition involves a clear change of color in the visible range (**Fig 3.9**). For this study two kinds of optical pump-probe techniques have been used. The first one, similar to the one used in 3.1.2, is a two-color pump-probe set-up, which uses different probe wavelengths covering a 475 -750 nm spectral range, with a high signal/noise ratio for probing the time-course of the probe over versatile time domain. The other one using white light spectroscopy (CF chapter 2) probes a broad spectral range at different time delays, but with more limited statistic and time steps. The overall instantaneous response function (IRF) of these experiments is ca. 140 fs.
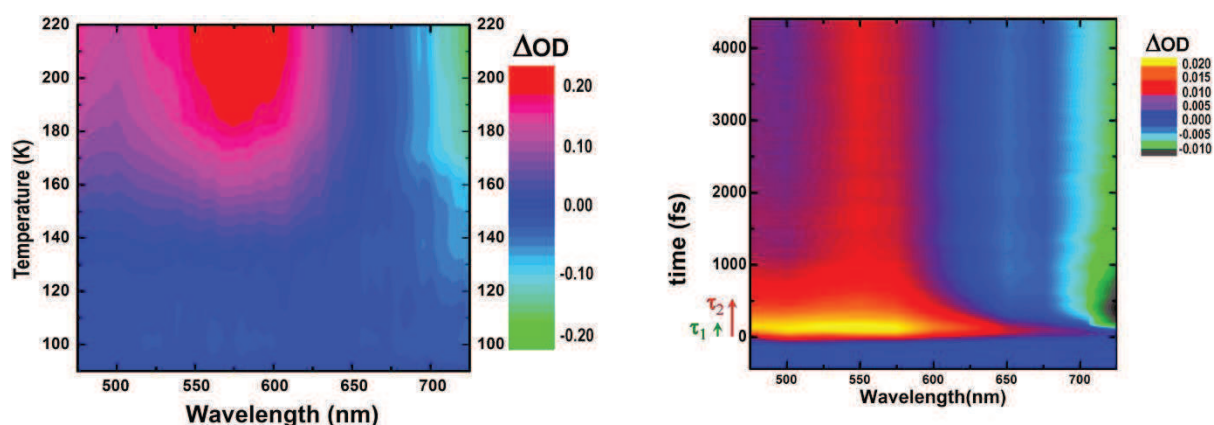
Fig 3.10 *Thermal ΔOD (left) VS time resolved ΔOD (right).*

The two dimensional time-wavelength plot of ΔOD is presented in **Fig 3.10**. It is obvious, by comparing the thermal fingerprint and the time resolved result, that HS species are created in less than 1 ps, as the characteristic HS absorption in the visible part and bleaching in the NIR are observed. But the transient OD immediately after the photo-excitation differs significantly from the HS and LS states. Our data show a broad and strong absorption in the visible part which is clearly the sign of an excited transient state. This fact clearly suggests the generation of LMCT state with femtosecond lifetime that will relax within less than 1 ps in the HS state.
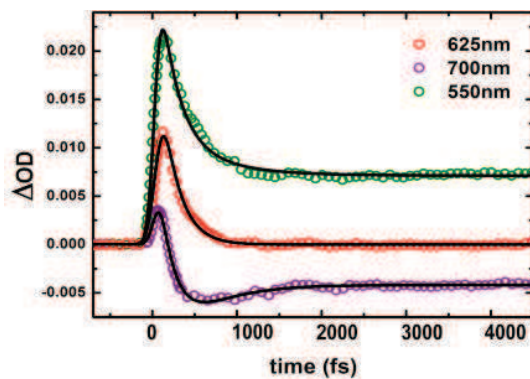
Fig 3.11 *Time resolved data at 550 nm, 650 nm and 700 nm.*

By analyzing more carefully selected time traces, presented here at different wavelengths, it is possible to go deeper in the understanding of such ultrafast process (**Fig 3.11**). The traces at 625 nm show a ΔOD that tends to nullify at picoseconds time scale (around the isobestic point). This wavelength is a good candidate in order to follow the dynamics of excited intermediate state as initial LS and final HS states are optically silent at this wavelength. The kinetic trace shows, first, a rapid rise in the absorption corresponding to the generation of instantaneous Franck Condom state. It is followed by a fast decay of this transient state. In Fe^{II} compounds intensively studied in the literature, this ultrashort excited state is referred to as a metal-to-ligand charge-transfer state (MLCT). In our case of Fe^{III} compound, the excitation at 840 nm corresponds to a ligand-to-metal charge-transfer state (LMCT). Thus, LMCT intermediate (INT) states are the bottleneck for the relaxation process and we use here a time constant τ_1 for describing the exponential population of HS state from the LMCT state. By fitting the data with a single exponential decay convoluted with the Gaussian IRF of our experiment, we found τ_1= 200 ± 20 fs. As for single crystal investigations, this value is again of the same order as previous results reported in the literature for Fe^{II} systems.

For the other measurements with probe wavelengths out of the isobestic point, the single exponential model fails to reproduce the observed dynamics as a slower dynamics is observed on the ps time-scale. Thus we used a two-exponential decay model for fitting both dynamics. In all the data, the first time constant is fixed to τ_1= 200 fs. Depending on the probe wavelength the second time constant τ_2 varies between 500 fs to 800 fs. This second time constant is concomitant with a spectral narrowing observed in the 2D time-wavelength plot (**Fig 3.10**). These two observations put together make no doubt about the nature of this second dynamic which is a vibrationnal cooling (**Gawelda 2007, M.N Wolf 2008**).
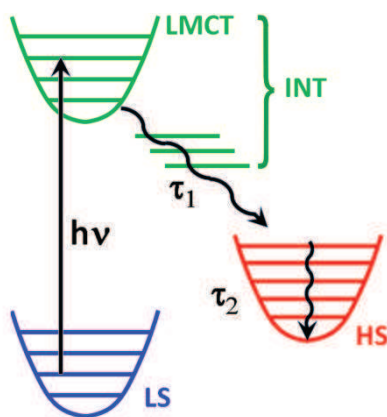
Fig 3.12 Schematic drawing of the ultrafast photo-switching.

The term vibrationnal cooling refers to the relaxation of the hot HS state into the HS potential (**Fig 3.12**). When the HS potential is reached after ISC there are still many vibrationnal and rotational excited levels. These excited states will relax as the molecule reaches to the bottom of the HS potential. This vibrationnal cooling process in the crystals is significantly faster than the ones observed for molecules in solution, for which the energy is dissipated by collision with the solvent and is also solvent dependent for the same molecule (**Tribollet 2011**). In the present case it can be explained by a better cooling in solid state due to electron-phonon and phonon-phonon coupling which allows a fast dissipation of the energy as the solid constitutes an effective surroundings for dissipating energy from the local molecular system. By combining all these observations, it is possible to draw a schematic picture of such ultrafast spin state switching in solid state, as schematically represented in **Fig 3.12**. Such process involves two different dynamics which are the relaxation of transient INT excited state (200 ± 20 fs) followed by the vibrationnal cooling (>500 fs).

For learning more about these states, we used a white light experiment for catching the transient optical spectra. As explained in chapter 2 this white light pulse is positively chirped, meaning that red part of the spectrum arrives first and blue part last. Because the pump comes from negative delay the blue part of the spectrum of the excited state is probed first. The diagram in **Fig 3.13** shows the envelop of the signal measured at different time steps of the white light pulse. By making fine step with the pump pulse, it is possible to slice the white light pulse and to obtain complete spectra of the transient state.
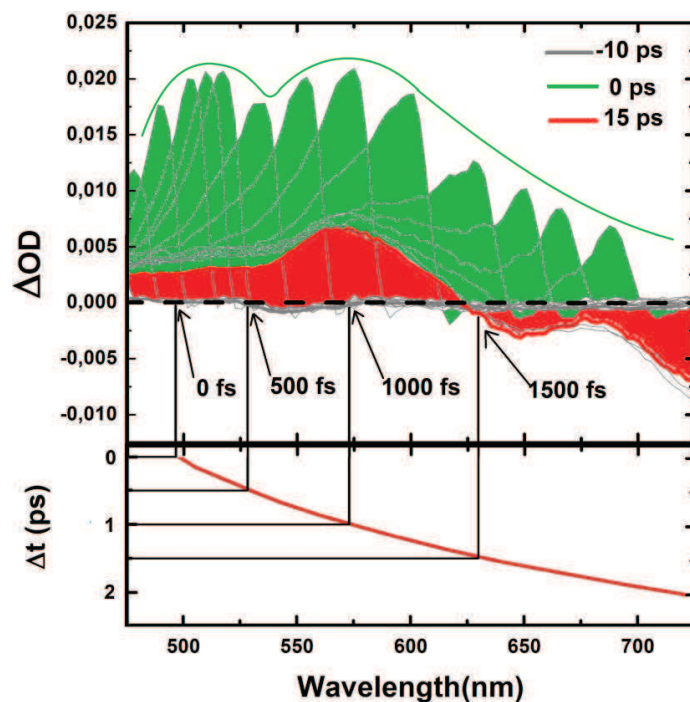
Fig 3.13 Time resolved data on white light system, (up)

Associated chirp of the white light pulse (bottom).

In such a way, we obtained the complete time zero spectra corresponding to intermediate excited state (**Fig 3.13**), given by the green envelop. It differs from the spectra of the photo excited HS specie. All these data represent a complete optical study in the visible range of spin state switching in solid state.
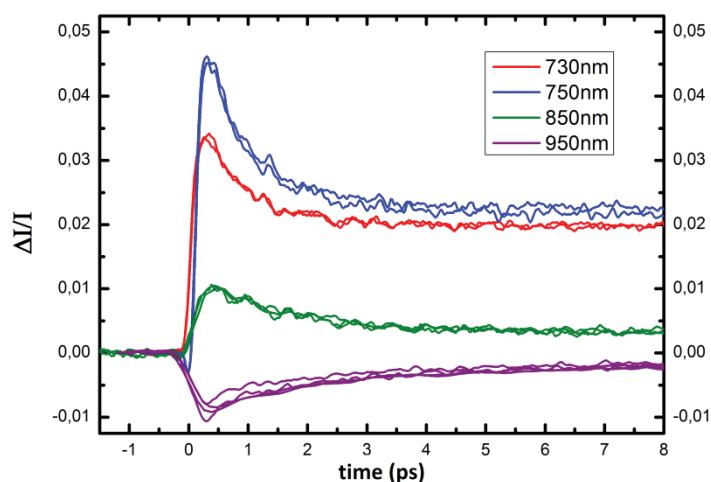
Fig 3.14 Time resolved data in near infrared.

Some complementary experiments were performed in the infrared region (**Fig 3.14**) where the sensitivity to the vibrationnal cooling is even larger when lower energetic levels are probed. In this case the relaxation time τ_2 is in the order of few picoseconds. This is again similar to what was reported for Fe^{II} molecules in solution, for which the relaxation reaches up to ten's of picoseconds in far infrared (**M.N Wolf 2008**).

3.1.4 Comparison of the ultrafast dynamics in single and nanocrystals

The method described above can be applied to the samples of different sizes of $[Fe^{III}(3\text{-MeO-}SalEen)]PF_6$ crystals we have. From single macroscopic crystal down to nanocrystals, in the three sizes of sample, we investigate the ultrafast response for looking to existence or not of size effect on the ultrafast dynamics.
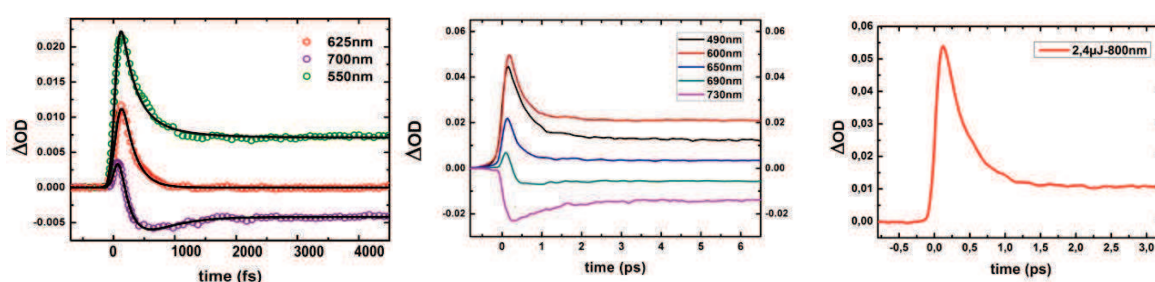
Fig 3.16 *From left to right, time resolved data in Nanocrystals, Microcrystals and Single Crystal.*
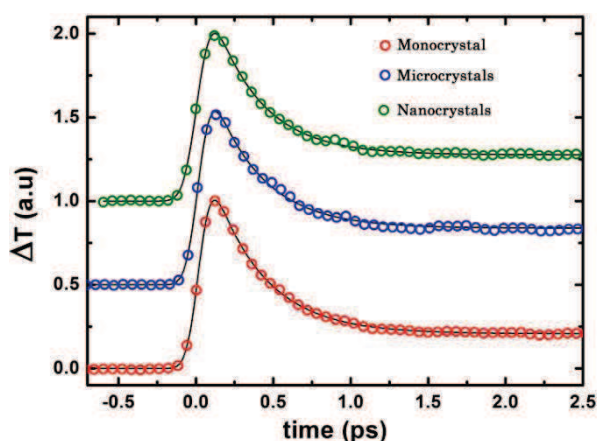
Fig 3.17 *Time resolved data at 550nm for 3 sizes of sample.*

The dynamics for the 3 samples studied are presented in **Fig 3.16** and look pretty much similar. **Fig 3.17** shows the comparison of the 3 sizes for a 550 nm probe and evidences clearly the same dynamics as these curves use the same fit constants (τ_1 = 200 fs and τ_2 > 500 fs). It means that the size of sample has no effect in the ultrafast photo-switching. This is in agreement with the current picture we have of local spin state trapping at the molecular level, which is not sensitive to the environment. Because the elastic coupling, known as the driving force of SCO transition in materials is unable to propagate on such short time-scales. That is the reason why the dynamics is very similar to the one reported for molecules in solution. The only difference deals with vibrationnal cooling, where the environment (crystal lattice *vs* solution) plays a role and may couple in a more or less efficient way for cooling the photo-excited molecule.
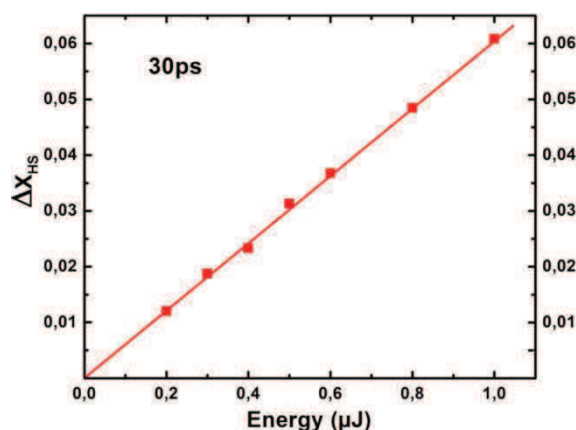
Fig 3.18 *Plot of the fraction of HS molecules in function of the pump energy.*

This idea of local switching without interaction with the environment is supported by the response of the crystal to the excitation density. The fraction of molecules photo-switched varies linearly with the excitation density as shown in **Fig 3.18**. Each photo-switching is an isolated event at the fsd time-scale as molecules do not see each other and the response of independent molecules in the solid corresponds to the response of independent molecules in solution. It will be shown in Chapter 4 that cooperative effects appear on longer time scales.

3.2 Investigation of the [Fe^{II}(phen)$_2$NCS$_2$] complex

Fe^{III} compounds, such as the one presented above in 3.1, are switching between two paramagnetic states. But Fe^{II} systems show a more important change of electronic state because they switch from diamagnetic (S=0) to paramegnetic (S=2) states. It is interesting to compare the ultrafast switching dynamics to the one observed in Fe^{III} systems, as the excitation scheme is different (MLCT instead of LMCT). In addition, the structural changes are more important in Fe^{II} with 0.2 Å <Fe-N> elongation instead of 0.15 Å for Fe^{III}. These different aspects should show in the ultrafast dynamics at some point. We have chosen a cooperative Fe^{II} system; the prototype [Fe^{II}(phen)$_2$(NCS)$_2$] system, for which a large literature exists regarding thermal equilibrium conversion as well as *cw* light excitation at low temperature (**Konig 1966, Granier 1993, Marchivie 2002**).

3.2.1 Thermal switching

[Fe^{II}(phen)$_2$(NCS)$_2$] (phen=1,10-phenanthroline, **Fig. 3.19**) is one of the most studied Fe^{II} SCO systems involving bi-stability between two electronic configurations : the diamagnetic LS (S=0, $t_{2g}{}^6 e_g{}^0$) and paramagnetic HS (S=2, $t_{2g}{}^4 e_g{}^2$) states. Single crystal and films of thin powder of this system were synthesized in the group of J-F.Létard (ICMCB) in the framework of an ANR project.
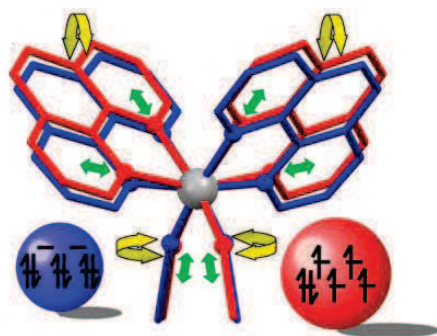
Fig 3.19 Structure of [Fe^{II}(phen)_2(NCS)_2].

The molecular structure is based on the center iron atom located on a 2 fold symmetry axis (**Fig 3.19**). The Fe atom is bonded to two N atoms of the two NCS group and also to four N atoms of the two phenantroline groups (**Gallois 1996, Marchivie 2002**). The compound crystallizes in the Pbcn (orthorhombic) space group, where the molecules are located on the two fold axis. Thin single crystals have red color due to the huge optical absorption in the visible range up to 700 nm. The crystals have a form of a lozenge (**Fig 3.20**) where *a* and *b* axis are respectively the smallest and the longest diagonal. The *c* axis corresponds to the crystal thickness.
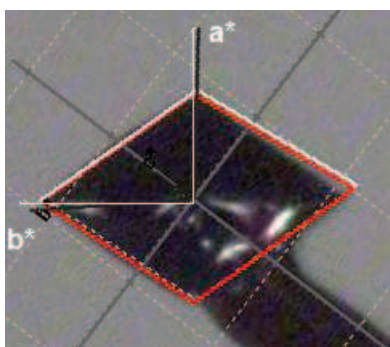
Fig 3.20 Single crystals of [Fe^{II}(phen)_2(NCS)_2] of dark red color. The crystal axes are shown.

73
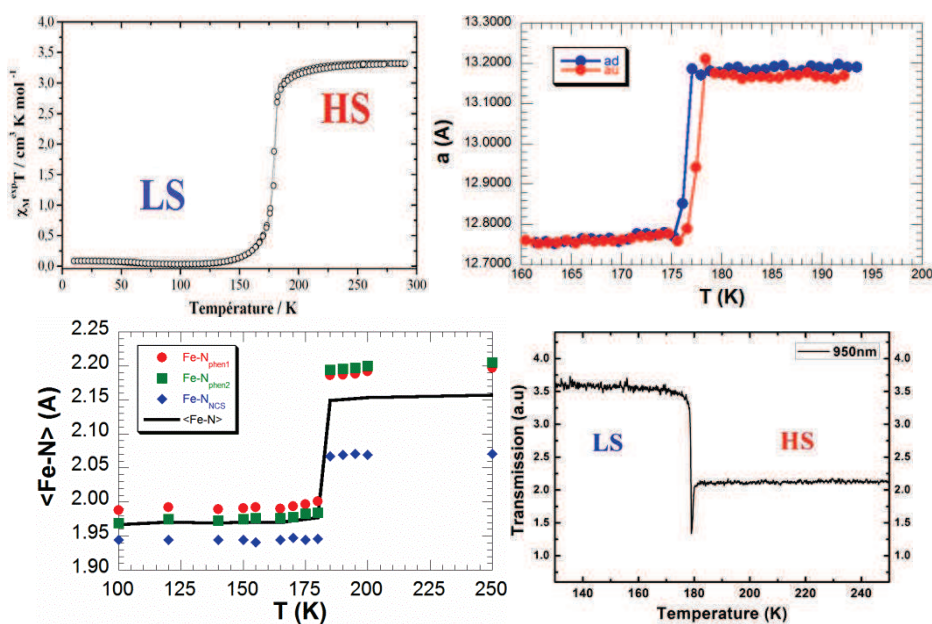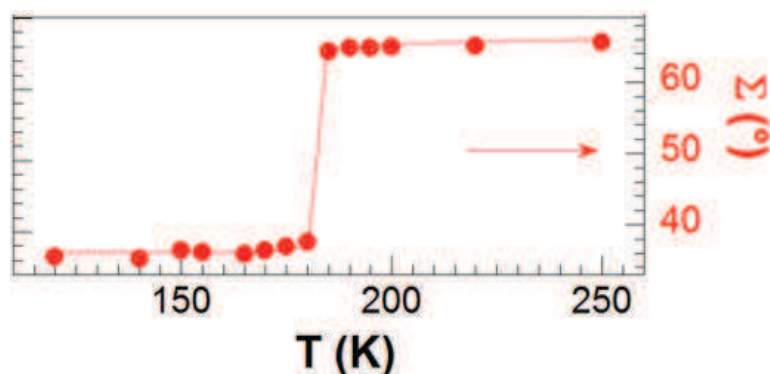
Fig 3.21 Signature of the thermal transition by SQUID, X-ray diffraction and optical absorption.

[Fe^{II}(phen)$_2$(NCS)$_2$] undergoes a first-order isostructural phase transition around 176 K, clearly observed by SQUID (**Fig 3.21**), with a small hysteresis. These measurements of the evolution of the χ_MT product (χ_M being the molar magnetic susceptibility and T the temperature) indicate that the low temperature phase is diamagnetic (LS, S=0) and that the high temperature paramagnetic phase is HS (S=2) with χ_MT approaching 3.5 cm^{3}Kmol^{-1} (**Baldé 2008**).

The strong coupling between the electronic and structural degrees of freedom drives important structural reorganization of the constituting molecules (**Fig 3.21**), mainly around the central Fe atom and the six N atoms bonding to the ligand. We present here new temperature dependence x-ray diffraction studies performed in our laboratory. The lattice parameters measured on cooling and heating also show a small hysteresis (2 K). At the intra-molecular level, a well-known marker is the variation of the average distance between the Fe and the bonded N atoms. Because the molecule lies on a twofold axis there are 3 independent Fe-N bonds. One with the NCS group (Fe-N$_{NCS}$) and two with the phen group (Fe-N$_{phen}$). The two Fe-N$_{phen}$ bonds are similar but the Fe-N$_{NCS}$ is smaller because of the ionic character of this bond (2 electrons are transferred from the Fe to the 2 NCS groups making it a Fe^{II} system). All these Fe-N bonds expand by $\approx$ 10% between LS and HS states

(**Fig 3.21**). The average distance D between Fe and N atoms is given by $D = \dfrac{1}{6}\sum\limits_{i=1}^{6} Fe - N_i$ expands

between LS and HS states (**Fig 3.21**) from D_{LS}= 1.97 Å to D_{HS}=2.16 Å. This well-known effect results from the less bonding character of the HS electronic distribution. This value is in agreement with typical value of 0.2 Å for bond length elongation in Fe^{II} system (**Guionneau 2004**).

A second parameter, identified more recently as playing an important role in the stabilization of the photoinduced HS state (**Buron 2012**), is the distortion Σ of the FeN$_6$ octahedron. It is defined by the sum of the deviation from 90° of the 12 N-Fe-N cis angles in the coordination sphere:

$$\Sigma = \sum\limits_{i=1}^{12} \left|90 - \phi_i\right|$$ and in the case of [Fe^{II}(phen)$_2$(NCS)$_2$] Σ changes from 35° for LS to 65° for HS. The

first order phase transition from LS to HS phases is associated with a discontinuous variation of D and Σ without any significant temperature dependence in the HS or in the LS phases (**Fig 3.21**).

Like all SCO systems, the change of electronic state modifies the absorption spectra at the transition. So it can be used to probe the LS-HS conversion. Our optical measurement presented in **Fig 3.21** and performed on a single crystal shows that the absorption is stronger at 950 nm in the HS state, as observed previously by Konig (**Konig 1966**). The peak associated with a decrease of transmission observed in the hysteresis of the phase transition is due to a huge light scattering linked

to domain growing. This phenomenon was also reported by detailed optical microscopy for other SCO system (**Varret 2011**). For our studies performed on single crystals, we could not detect significant effect with regard to the orientation of light polarization with respect to the crystal axis in the (a,b) plan. All these measurements performed on single crystals confirm the first order character of the phase transition and correlate for describing a phase transition between LS and HS states.
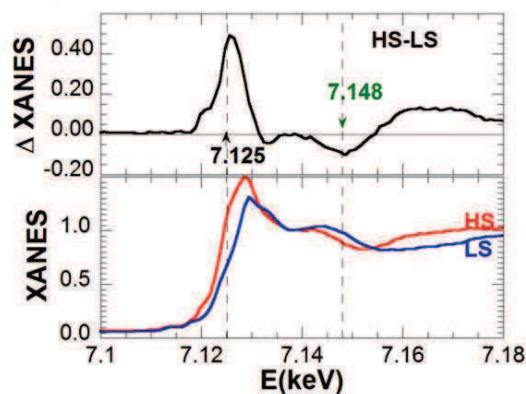
Fig 3.22 XANES spectra of the LS and HS phases and the difference of both.

The change of the molecular structure around the Fe atom accompanying the spin state change can also be monitored by XANES (X-ray Absorption Near-Edge Structure) spectroscopy at the K-edge (**Gawelda 2007 ,Boillot 2002**), as it modifies the energy position of the edge and the amplitude of different absorption features. XANES can be measured both in X-ray absorption or X-ray fluorescence. For our time-resolved studies it was easier to measure XANES through fluorescence because only a small fraction of the molecules will be photo-switched. In the W-ray transmission mode it is more difficult to extract the signal from the huge noisy background. XANES measured at XPP beamline of the LCLS differs significantly between the HS and LS species (**Fig 3.22**). The most important changes in XANES from LS to HS states correspond to a higher absorption at 7.125 keV and a decrease at 7.148 keV, agreeing well with the documented XAS literature on this compound (**Arezki 2011, Roux 1996**).

All our measurements presented here, consistent with the reach literature on this compound, show that several probes sensitive to the change between molecular spin states can be used in the time domain (X-ray, optics...), as they provide clear fingerprint of LS-to-HS switching, and open the possibility to combine them to study the ultrafast spin state switching of [Fe^{II}(phen)$_2$(NCS)$_2$]. Even though this compound is among the most widely investigated SCO solids, nothing is known about its ultrafast photo-switching dynamics. Therefore, we have used two complementary pump-probe methods to investigate the photo-switching from LS to HS state via a Metal-to-Ligand Charge-Transfer process (MLCT). On one hand, fs optical laser pulses were used for measuring transient optical reflectivity (OR) and transmission (OT). On the other hand, fs x-ray laser pulses were used as probe for measuring XANES at the XPP station of the LCLS X-ray Free Electron Laser (X-FEL). X-ray diffraction was used on longer delays (100 ps-1 ms) and this will be presented in chapter 4 as the present chapter focus on the molecular photoswitching process only.

3.2.2 Ultrafast Optical spectroscopy

Optical pump-probe studies were performed in the fs laser platform at IPR in Rennes, as described in part 3.1 (cf also chapter 2), with an instrumental response function of 140 fs. Spectroscopic studies are performed on single crystals (20-30 µm thick) in both reflection and transmission configuration. The crystal is cooled down by a nitrogen flow cryostat at 140 K where it remains in the pure LS phase but relax fast enough to performed pump-probe studies

From a theoretical point of view, it is known that such system cannot switch from the LS to the HS state straight after photon absorption because the change of spin multiplicity $\Delta S = 2$ is a forbidden direct transition. As a matter of fact, the electronic excited state just after the photon absorption is the MLCT[1] $\left(t_{2g}^6 e_g^0 L^0 \xrightarrow{h\nu} t_{2g}^5 e_g^0 L^1 \right)$ where L represents an orbital of the ligand. The ultrafast studies of the spin-state switching of such Fe^{II} molecules in solution give a conventional scheme with a cascade of excited state.

In any case, the ISC between Charge Transfer states and the triplet state is very fast (<30 fs).

By performing detailed time-resolved studies, the first step is to determine the optimal pump wavelength for promoting efficiently the system from the LS to the HS states. In its paper, Konig (**Konig 1966**) assigns the band around 650 nm to a MLCT transition.

S. Matar from ICMCB performed Density Of State (DOS) calculations on this compound in the LS phase (**Matar 2010**) and in the framework of a collaborative work he extended his calculation to the HS phase (**Cammarata 2013**). The main results are presented in **Fig 3.23**.
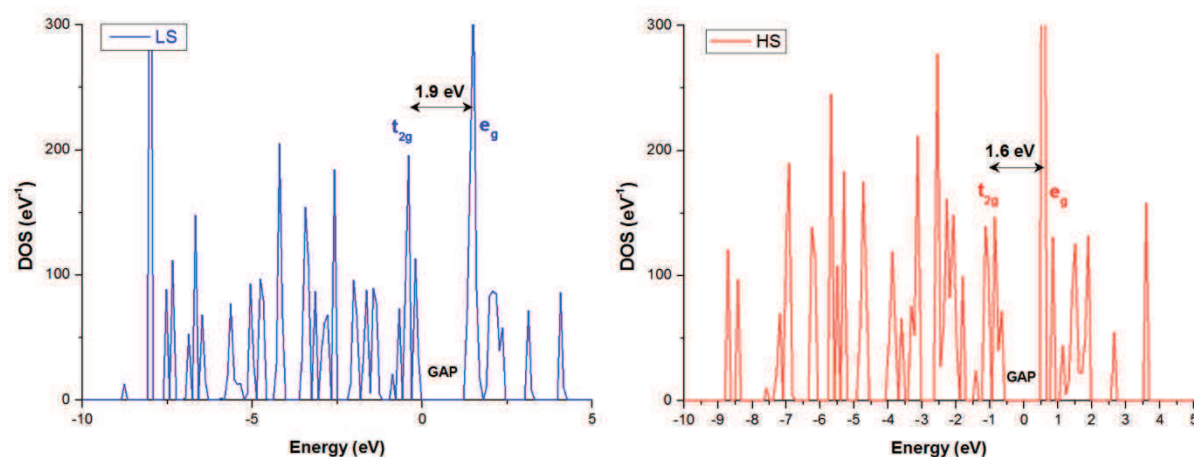
Fig 3.23 *Total DOS for [Fe^{II}(phen)$_2$(NCS)$_2$] in its LS (blue) and HS (red) states.*

An important feature is the low dispersion of the bands, which is characteristic of a molecular system with small transfer integral between the molecules, *i.e.* in opposition to a metal or an intermetallic system where the DOS are broadened. Somehow, even in the organized periodic solid state, [Fe^{II}(phen)$_2$(NCS)$_2$] exhibits a kind of molecular behavior because there is a weak overlap between orbitals of the different molecules. The key information regarding the time-resolved optical studies presented here is that on either side of the gap the DOS correspond the Fe-*d* states which are respectively t_{2g} and e_g like. The DOS calculations indicate that :

- in the LS state the t_{2g}-e_g energy difference is centered around 1.9 eV, with a gap around 1.6 eV

- in the HS state the t_{2g}-e_g energy difference is centered around 1.6 eV, with a gap around 1.3 eV

This decrease of the gap in the solid state is analogous to the decrease of the 10 Dq ligand field between the *d* orbitals for the isolated molecule. Therefore, these results provides an important feature that the photon with energy around 1.3-1.6 eV can probe the gap narrowing as the system switches from LS to HS states, as absorption will be higher in the HS state. This is what is observed at 950 nm (1.31 eV) during the thermal conversion in **Fig 3.21**.

In order to define the best excitation scheme, several trials with different pump wavelengths were performed. The probe was set to 950 nm, for which a decrease transmission is expected if HS molecules form, as observed during thermal conversion (**Fig 3.21**).
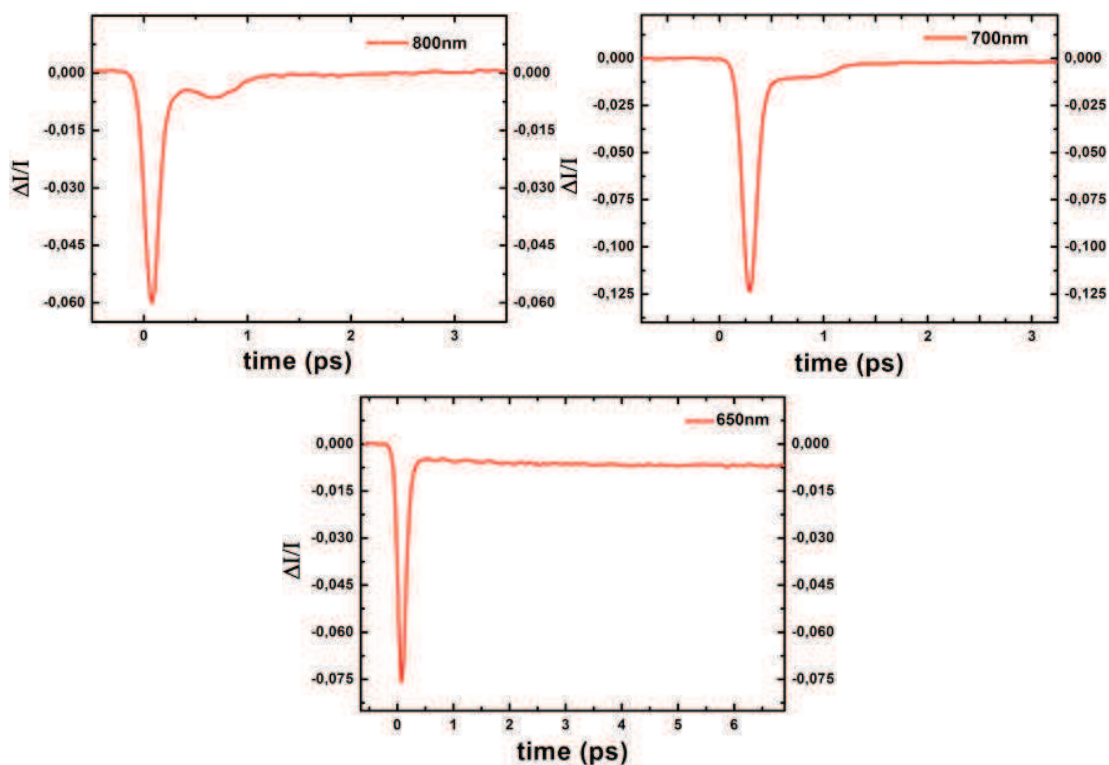
Fig 3.24 *Time resolved data for different pump wavelength.*

According to the expectations, **Fig 3.24**, a pump set to 650 nm promotes efficiently LS to HS via MLCT states, as there is a non-zero change of transmission in the photo-induced state few ps times after excitation. This is not the case when 700 nm and 800 nm radiation are used for pumping the system (**Fig 3.24**) as the excited electronic state relaxes rapidly to the LS state, omitting the modes leading to ISC. Konig reported that a weak d-d band exist above 800 nm (**Konig 1966**). Using pump wavelength below 650 nm (such as 530 nm) resulted in surface damage of the sample because the OD is intolerably high in the visible part compared to the infrared. We therefore excite the tail of the MLCT band for ensuring the maximum penetration depth of the laser, since at 650 nm, the OD is tolerable and generates a homogeneous excitation of the crystal.
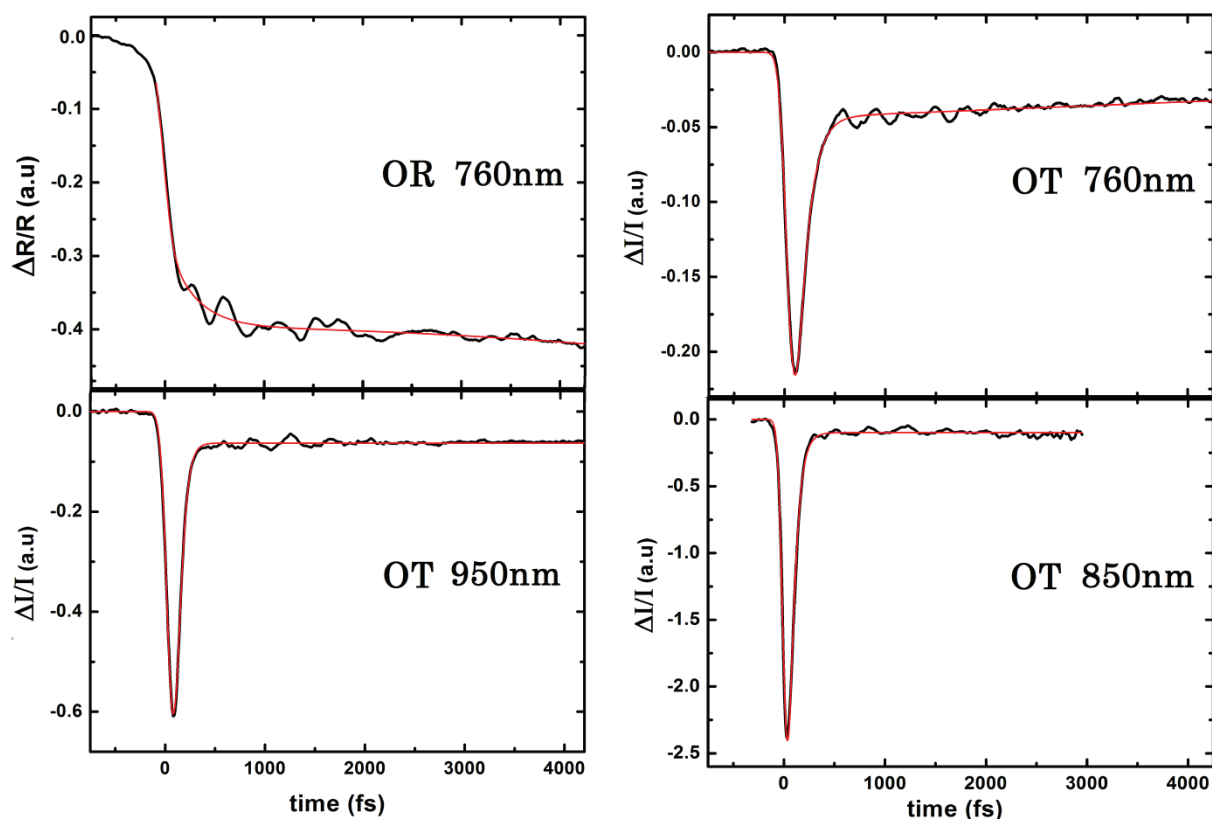
Fig 3.25 *Time resolved data in transmission (OT 760, 850 and 950 nm) and in reflectivity (OR 760 nm).*

Single-wavelength measurements probed the resulting photo-switching dynamics through optical reflectivity (OR) change at 760 nm and optical transmission (OT) at 760, 850 and 950 nm and the data are shown in **Fig 3.25**. Two main steps are revealed in the variation of optical transmission ΔOT : a transient peak appearing at 950, 850 and 760 nm immediately after laser excitation followed by a relaxation towards a plateau. The transient peak is the signature of excited electronic states including the photo-excited ^{1}MLCT state ($t_{2g}^5 e_g^0 L^1$) and other possible intermediates (INT) such as ^{3}MLCT and ^{5}MLCT which are difficult to identify because they are short-lived and impossible to distinguish IR signatures. Data at 950 nm indicates that the intersystem crossing (ISC) between MLCT states and HS potential corresponds to a time constant shorter than 50 fs, which is too fast to be accurately determined with our time-resolution.

The increase of optical absorption on the plateau, which translates into a simultaneous decrease of OT and OR at 760 nm, is another fingerprint of LS-to-HS photo-conversion. The stronger absorption of the HS state at 760 nm (*i.e.* 1.6 eV) results from the gap narrowing as the ligand field (t_{2g}-e_g splitting) decreases when Fe-N distance increases. The OT and OR data at 760 nm point a $\approx$ 140 fs time constant for reaching the HS plateau. This is the direct signature of the gap closing in the HS state, which is driven by the Fe-N elongation dynamics $\tau_1 \approx$ 170 fs (see XANES hereafter).
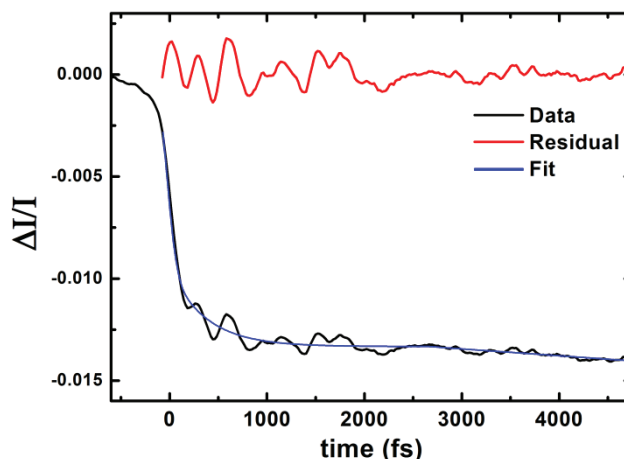
Fig 3.26 Time resolved data with the associated fit and the residual part.

An important feature is the observation of oscillating components in all the data, which appear once the system reaches the HS potential. For extracting these residual components, data are here also fit with a single or bi-exponential model convoluted with the Gaussian pulse like plotted in **Fig 3.26**.
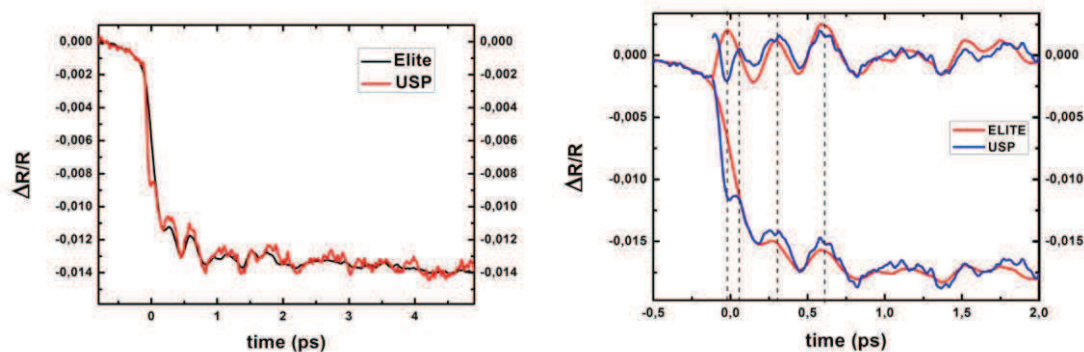
Fig 3.27 Comparison between USP setup (45 fs pulse) and Elite setup (80 fs pulse).

Some other experiments were performed on the faster fs system (45 fs pulses) which allows a better time resolution by somewhat compromising the signal/noise ratio. The results (**Fig 3.27**) do not show clear difference at the exception of small electronic peak in the first instant of the photo-switching. This peak can be due for example to the bleaching of the LS state caused by a depopulation of this state into [1]MLCT.

Once all these oscillating components are extracted, a complete analysis by Fourier transform and time-dependent Fourier transform provides us essential information on the mechanism involved (**Fig 3.28 and 3.29**).
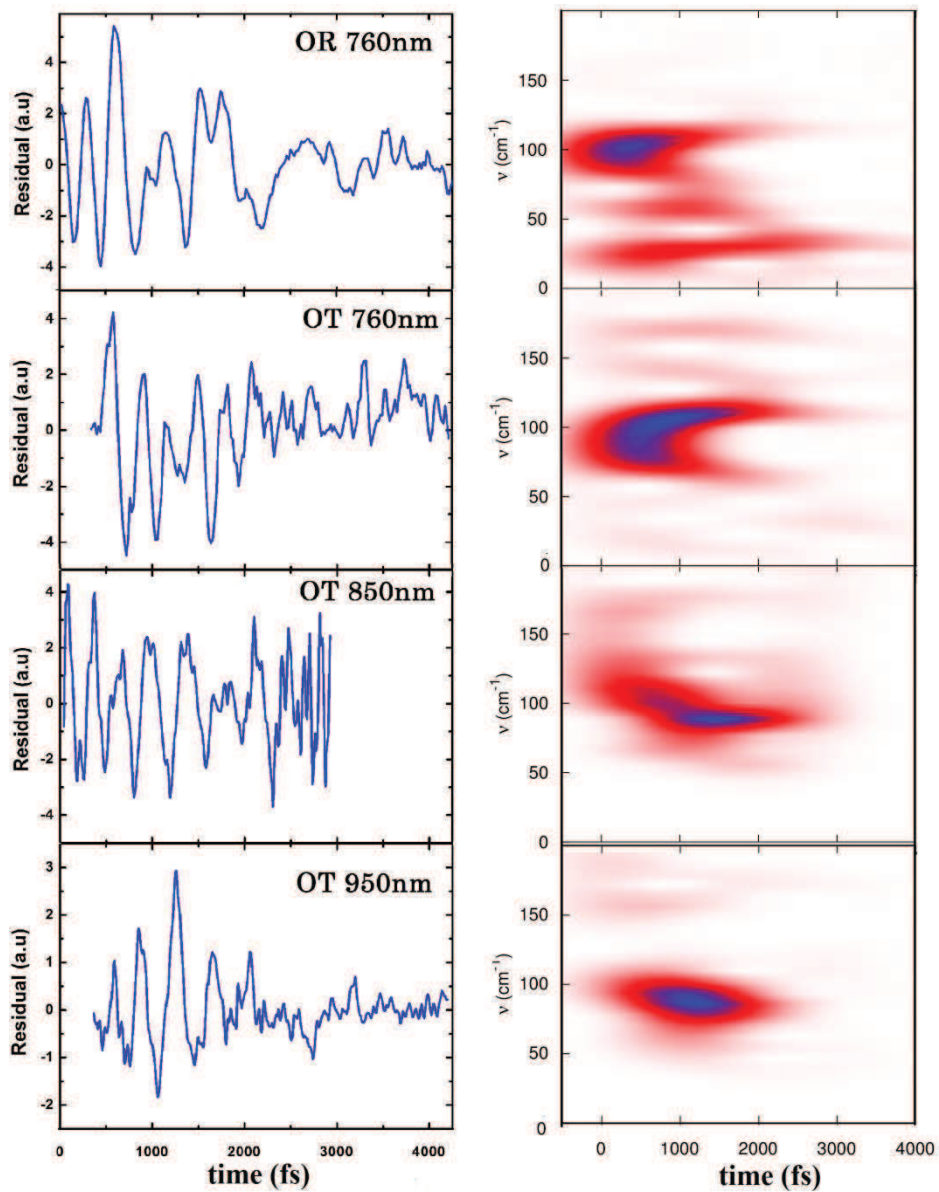
Fig 3.28 *Oscillating part of the time resolved data (left) and the associated time dependent Fourier transform (right).*
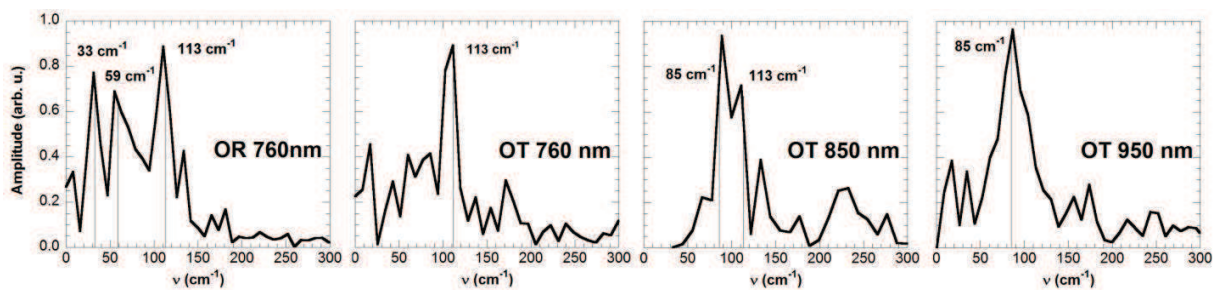
Fig 3.29 *Fourier transform of the residual part for all optical data.*

Data at 760 nm both in transmission and reflectivity indicate a main frequency at around 113 cm^{-1} (3.3 Thz). The reflectivity data allows the observation of slower mode at 59 cm^{-1} and 33 cm^{-1}. On the contrary, the optical transmission at 950 nm reveals a main frequency at 85 cm^{-1} (2.6 THz). At last, optical transmission at 850 nm possesses both frequency at 113 cm^{-1} and 85 cm^{-1}.

The coherent mode around 113 cm^{-1} in OT and OR data at 760 nm and OT at 850 nm is sensitive to the amplitude of the ligand field, because this mode is identified in the literature as the breathing mode of the FeN_6 octahedron. It is characterized by a stretching in phase of the Fe-N bonds, and involves mainly the 4 Nitrogens atoms linked to phenantroline groups. It is schematically represented by green arrows in **Fig 3.19**. It is the strong modulation of the t_{2g}-e_g gap by the Fe-N elongation that makes it possible to observe this breathing mode in optical data. It is important to underline that the rich literature on [Fe^{II}(phen)$_2$(NCS)$_2$] (**Ronayne 2006, Baranovic 2004**) allows assigning the 113 cm^{-1} frequency to the breathing mode of the HS state, as the frequency of this mode in the LS state is significantly higher ($\approx$150 cm^{-1}). The Fe-N stretching mode is activated immediately after photo-excitation and corresponds to the first oscillations in **Fig 3.28** (OR and OT 760 nm) also shown in Time Dependent Fourier Transform.

The 85 cm^{-1} mode is identified as the butterfly mode. It involves bending of the rigid phenantroline about central ring without significant change of Fe-N distance, but we should underline that contrary to the breathing mode the amplitude of the bending mode rises only after $\approx$ 500 fs and is maximum around 1300 fs (**Fig 3.28**). Such coherent ligand vibration was also observed for another molecular system in solution (**Consani 2009**).

The OT data below the gap (950 nm) are not so modulated by the ligand field and better probe the ISC dynamics (τ_0<50 fs) but they are modulated by the coherent vibration around 85 cm^{-1} referred as butterfly mode. Data at 850 nm are close to the gap and in occurrence sensitive to both butterfly and breathing mode. The TD-FT evidences a spectral weight transfer in time from the breathing mode (113 cm^{-1}) to the butterfly mode (85 cm^{-1}). This is due to the delayed activation of the butterfly mode suggesting a multi-step process in the ultrafast photo-switching.
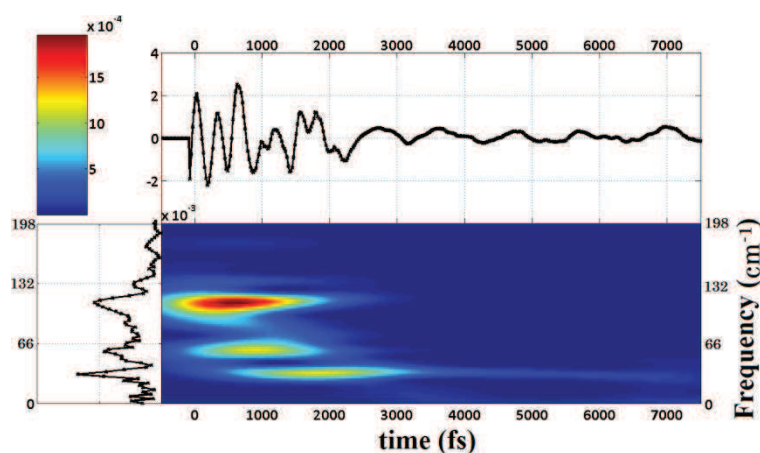
Fig 3.30 *Average of time resolved data and time dependant Fourier transform with 900 fs window.*

The reflectivity data at 760 nm were analyzed by performing a Fourier frequency filter to decrease the noise and obtain oscillating components of very high quality (**Fig 3.30**). The TD-FFT shows clearly the spectral weight transfer in time from the high frequency (113 cm^{-1}) to the low frequency (59 cm^{-1} and 33 cm^{-1}). The slowest component at 33 cm^{-1} remains activated until 7 ps. These modes are described in the literature as lattice mode involving large molecular motions. All

these results seem to indicate a multi step process involving different structural parameters such as stretching and bending.

A slower dynamic is observed in optical data, especially in the OT and OR data at 760nm (**Fig 3.25**). Probing the structural dynamic at fs time scale is needed to go deeper in the understanding of this process.

3.2.3 Femtosecond XANES

Femtosecond XANES studies were performed by using fs X-ray at the XPP station of the LCLS x-ray free electron laser (X-FEL)(**Lemke 2012**), presented in chapter 2. The time course of the XANES signal presented in **Fig 3.30** was measured at the two energies identified as most sensitive to the change of spin state (**Fig 3.22**), by varying the time delay between the laser pump and the X-ray probe pulses. A timing tool (**Harmand 2013**) was used for synchronizing optical laser and X-ray pulses. The time-resolved XANES signal (**Fig. 3.31**) shows an increase (respectively decrease) of XANES at 7.125 keV (resp. 7.148 keV), which represent clear fingerprints of the photo-switching dynamics between LS and HS states. The rising time trace was fitted by convolving a Gaussian temporal Instrument Response Function (IRF) with an exponential rise (with a time constant τ_1). The results give a 140 ± 10 fs FWHM IRF allowing an accurate determination of τ_1= 170 ± 10 fs. After the rapid rising, a second slower increase occurs around ≈ 2 ps and do not evolve anymore up to 100 ps (cf Chp. 4). A similar slower change around 2 ps is also observed in OT data at 760 nm (**Fig. 3.25**)
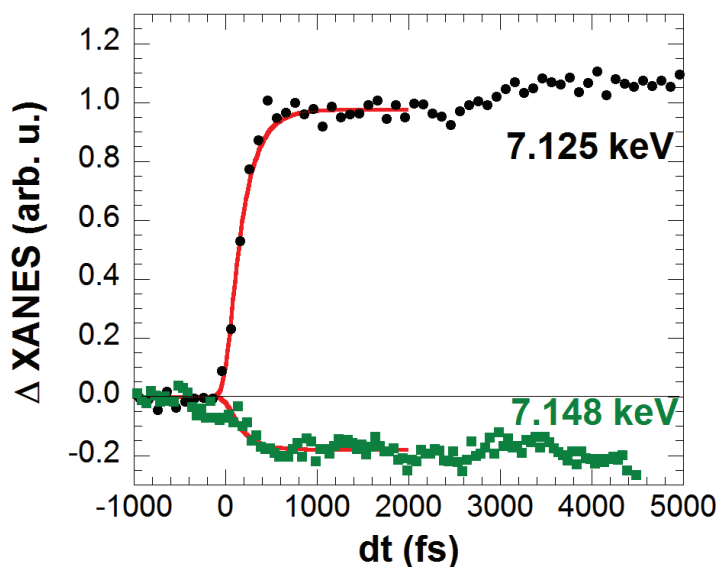
Fig 3.31 *time resolved XANES with 2 different energies.*

These results in the solid state showing an ultrafast ISC (< 50 fs) followed by a structural elongation of Fe-N distance within 170 fs, are in good agreement with previous reports for similar Fe[II] molecules in solution (**Bressler 2009, Huse 2011**). The analysis presented hereafter allows learning more about the basic mechanisms that allow efficient trapping of the photo-excited HS state.

3.2.4 Discussion on the ultrafast photo-switching dynamics:

The results presented above show that in the [Fe^{II}(phen)$_2$(NCS)$_2$] complex studied here the inter-system crossing is as fast as in other Fe^{II} systems studied in solution. But the coherent dynamics involving different modes and the apparent two-step change in XANES (within 170 fs and after 2 ps) differs from what was reported so far. Before going deeper in the analysis, we should stress here that in SCO materials the elongation of the average Fe-N distance D during LS-to-HS conversion are very similar. But it has been earlier reported that the relative stability of LS and HS states is governed by the torsion Σ of the ligand (**Buron 2012**).

We draw a scenario explaining the ultrafast photoswitching pathway, by taking into account these two relevant structural changes and the associated phonon modes. **Fig 3.32** represents the trajectory across the potential energy surface (PES) in the (D,Σ) space. For [Fe^{II}(phen)$_2$(NCS)$_2$] the structural analysis (**Fig 3.21**) indicates that the energy potential of the LS ground state is centered at coordinates (D_{LS}=1.97 Å, Σ_{LS}=35°), whereas the one of the distorted HS state is centered at coordinates (D_{HS}=2.17 Å, Σ_{HS}=65°). The very first step is the electronic photo-excitation of the $^1A_1$ ground LS state, with initial electronic configuration $t_{2g}^6 e_g^0 L^0$. Since the photo-excitation conserves spin, the initial photoexcited state is a ^{1}MLCT associated with an electron transfer from the metal to the ligand ($t_{2g}^5 e_g^0 L^1$). The transient CT step, which may involve other INT states like ^{3}MLCT (**Gawelda 2007, Hauser 1990**), is characterized by the transient absorption peak (**Fig 3.25**) and the ISC for reaching the $t_{2g}^4 e_g^2 L^0$ HS potential is very fast (<50 fs).
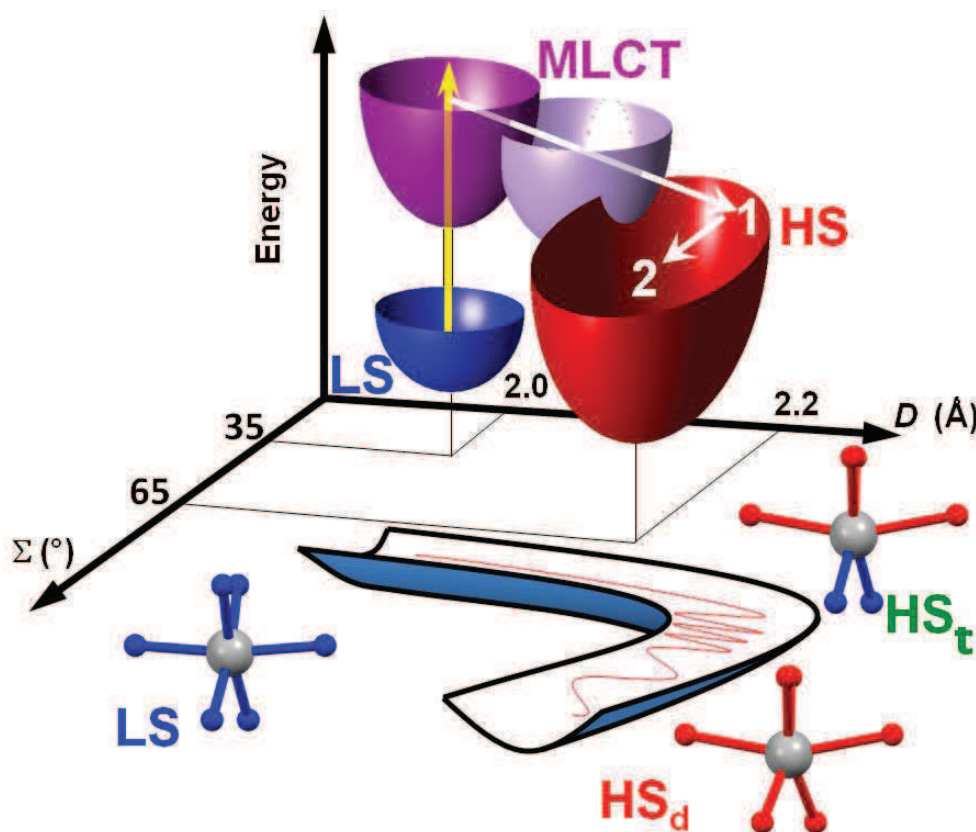
Fig 3.32 *Classical trajectory in the (D,Σ) space. Molecules in the LS potential reach MLCT state by light excitation. Fast ISC through possible INT states towards the HS potential occurs as D elongates during step 1 with the breathing mode. The equilibrium position in the HS potential is reached by generation of distortion phonons activating Σ coordinate during step 2. (B) Schematic representation of the elongation and stretching of D accompanied by damping.*

The electronic distribution in the HS state corresponds to a less bonding state and consequently the Fe-N distance elongates in a first step within 170 fs as the HS potential is reached. A recent theoretical work (**Van Veenendal 2010**) underlined that an ISC of tens of fs is compatible with a structural elongation in 100 – 200 fs. This is made possible by dephasing of MLCT state by HS phonon states. This is what we observe here, with the activation of breathing mode of the HS state within our experimental time resolution, as the breathing mode is directly coupled to the change of spin state. But a simple generation of phonon could also give rise to recurrence toward the initial state, which is not observed experimentally. The fast damping of the stretching phonon mode was pointed to as the mechanism suppressing the recurrence toward the initial state.

Our time dependent FFT shows that damping of the breathing mode occurs with a $\approx$ 300-500 fs time scale. It results in energy redistribution at the intramolecular level, with a spectral weight transfer from the 113 cm^{-1} breathing mode to other intra-molecular modes, and especially to the 85 cm^{-1} bending mode (**Fig 3.28**), but also at the inter-molecular level with the activation of lattice phonons, such as the 33 cm^{-1} mode (**Fig 3.30**). This energy transfer to lattice phonon results from the coupling of the molecule with its crystalline environment, and causes lattice expansion on nanosecond timescale (**Lorenc 2012**) which can drive additional switching by elastic coupling, discussed in Chapter 4.

XANES data should also evidence coherent oscillations of the breathing mode as XANES is sensitive to the environment around the Fe. But lack of such in our observation is most likely caused by the fast damping we mention above. **Fig 3.33** shows how XANES should evolve for the activation of a displacive breathing phonon with 113 cm^{-1} (i.e. 300 fs period) for damping constant in the 100-400 fs range and an amplitude equal to 1 (for which the oscillation correspond to the LS-HS displacement). With 300 fs damping, the first oscillation represents 1/3 of the amplitude of the signal between LS and HS states. Such large oscillation is not observed experimentally. But with 100 fs damping, the oscillation is of the order of 3% only and becomes too weak to be observed by XANES. This decay time $2\Gamma_d^{-1}$, where Γ_d is the lifetime broadening associated with the dephasing of phonons, is estimated to be of the order of 25 fs for phonons with 128 fs period. But this cannot explain why the breathing mode is observed during the first ps by optical probe.

Another possibility is that the amplitude of the oscillation is smaller than the difference between LS and HS distance. **Fig 3.33** shows the damping for amplitude of the oscillation corresponding to 1/2 and 1/4 of the distance. In this way, coherent oscillation of the breathing mode can be observed during the first ps even though the first oscillation has small amplitude. It is possible to observe oscillation by optical pump-probe technique because of the very good signal/noise ratio, what is not the case for XANES. Scheme in **Fig 3.33** shows the case with amplitude = 1 and amplitude = 1/4. As very-short lived intermediate states appear (like [3]MLCT) part of the vibrationnal energy is dissipated so that the amplitude of the oscillation once the system reaches the HS potential is smaller than the LS-HS elongation.
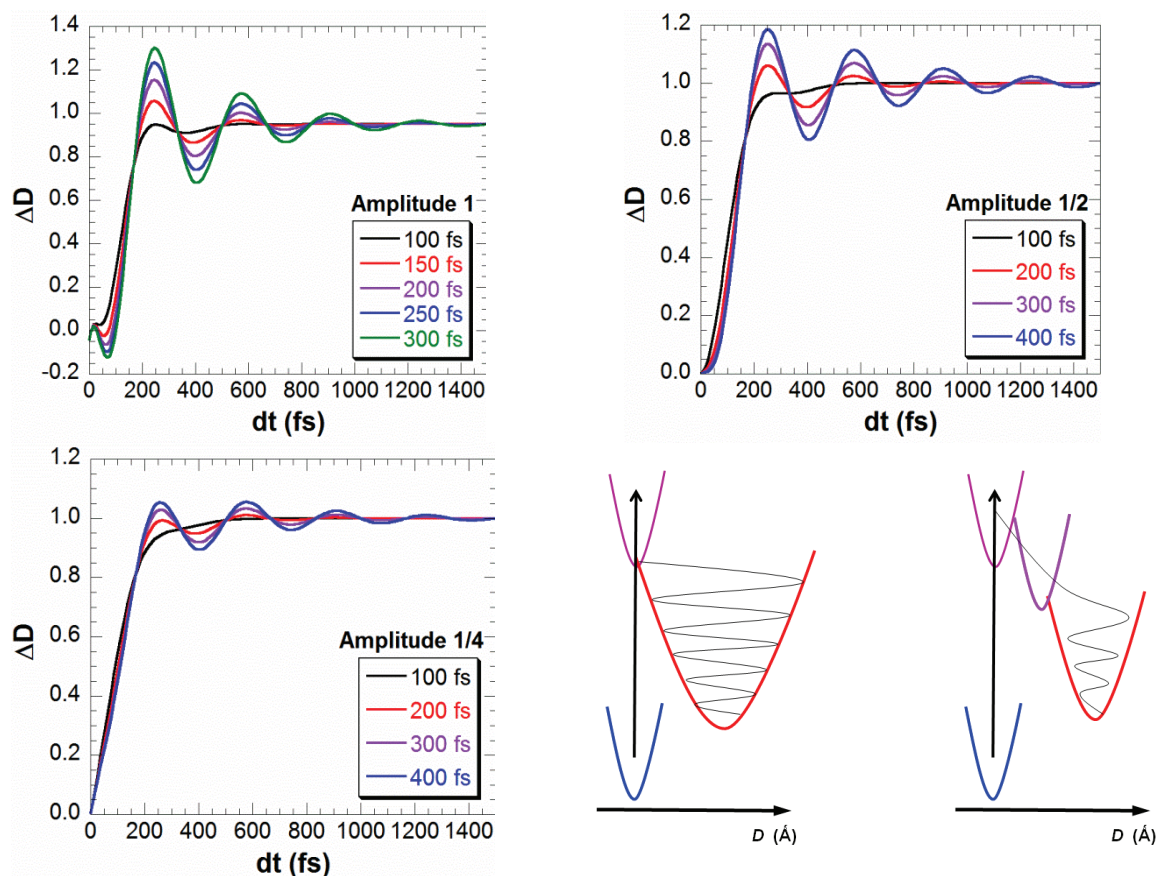
Fig 3.33 *Calculated amplitude of the damped displacive phonon associated with the change of distance ΔD between LS and HS states, for decay times in the 100-300 fs range.*

The above results also evidence that the activation of different structural degrees of freedom allow to reach the final HS structure. The breathing mode (step 1) is activated immediately within our experimental resolution, whereas other structural degrees of freedom such as bending are activated later by energy transfer (step 2) for example. These final structural reorganizations allow to reach the low-lying distorted and elongated equilibrium position in the HS potential. Therefore, a transient high spin state (HS_t) state exists in the 50-2000 fs time window, when the molecule in the HS state as not reached yet the final HS_d structure. This should be also associated with the fact that the breathing mode mainly involves the N atoms from the ligand and not so much those of the NCS groups. XANES spectra were therefore calculated from the structures known at thermal equilibrium: the LS and the HS distorted HS_d structures. In addition, we consider here a transient structure HS_t resulting from the damping of the breathing mode involving the phenantroline ligand motions only. We use a simple molecular structure model for describing the HS_t state, for which only the $Fe-N_{phen}$ distances and the ligand structure are considered to be those of HS_d , whereas the $Fe-N_{NCS}$ retains the LS state structure.

XANES calculations were performed in collaboration with Sergio Di Matteo at IPR, with the FDMNES program (**Joly 2001**) for the LS, the distorted HS_d and the transient HS_t structures shown in **Fig 3.34** and indicate a stronger XANES signal at 7.125 keV between the HS states and the LS state but also a stronger x-ray absorption for HS_d than for HS_t, as the structural change is partial in the transient HS_t state.
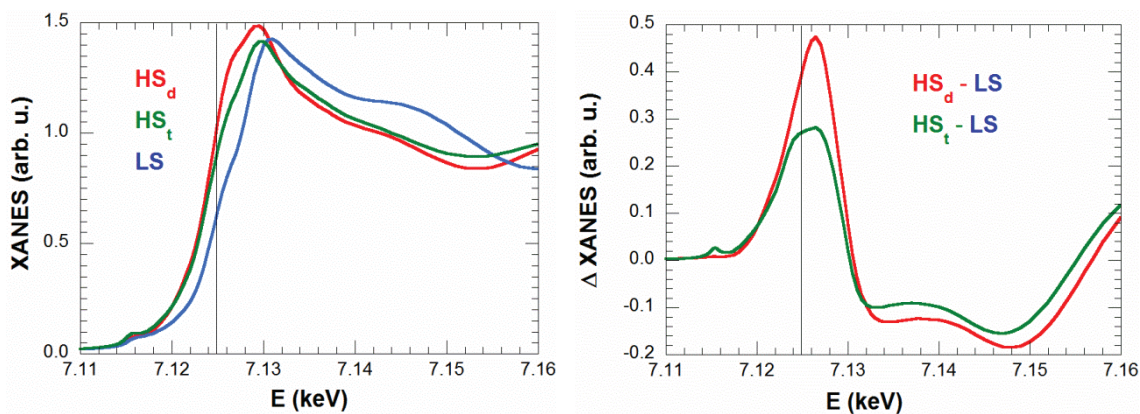
Fig 3.34 *Calculated XANES for LS, HS$_d$ and HS$_t$ structures (left) and variation from LS to HS$_d$ and from LS to HS$_t$ (right).*

The fit of the XANES curve indicates that the population of the HS$_t$ state occurs within 170 fs. The final relaxation towards the HS$_d$ state occurs around $\approx$ 2 ps where the XANES signal increases further. These numbers are also consistent with optical data. In this simple model, the relative change from LS to HS$_t$ should be close to 2/3 of the change from LS to HS$_d$. But here we observe in Fig **3.31** that it is of the order of 0.85. Of course our structural model is very simple and the reality is more complex since Fe-N$_{NCS}$ are slightly involved in the breathing mode too. Nevertheless, combined optical and XANES data show that in this system where the molecular structure is of lower symmetry than the systems studied up-to-now, the structural relaxation towards the final HS state occurs within two steps.

This two steps structural change involving first a structural change around the N atoms of the phenantroline can also be discussed in the frame of DFT calculations (**Cammarata 2013**):

- First, the MLCT process occurs towards orbitals with an electronic density located on the phenantroline ligand only and not involving NCS groups. Two candidates LUMO (lower unoccupied molecular orbitals) lying $\approx$ 2 eV above the LS HOMO (higher occupied molecular orbital) orbitals with paired electrons, are shown in **Fig 3.33**.

- Second, in the HS state, the HOMO with paired electron around the Fe atom shows electron density mainly on the Fe-N$_{NCS}$ atoms. This is due to the fact that the Fe-N$_{NCS}$ bond has an ionic character. They are therefore stronger and correspond to shorter Fe-N bonds (**Fig 3.21**) than the Fe-N$_{phen}$ ones.

This is a significant difference with other molecules of higher symmetry studied by fs XANES in solution, such as [Fe(bpy)$_3$]$^{2+}$ (**Lemke 2012**), for which the 6 N atoms belongs to the bpy ligand. The 170 fs step corresponds therefore to the expansion of the breathing mode coupled directly to the electronic redistribution, which involves mainly bonds with phenantroline groups, as the Fe-NCS bonds are in the lowest energy orbitals. Through phonon-phonon and electron-phonon coupling, the molecule finally reaches the final HS structure within 2 ps. This difference with what is observed for molecules in solution may also be associated with the local structural rearrangement in the solid as expansion and torsion occurs.

LS: LUMO 1 ligand   LS: LUMO 2 ligand   HS: HOMO with paired electrons
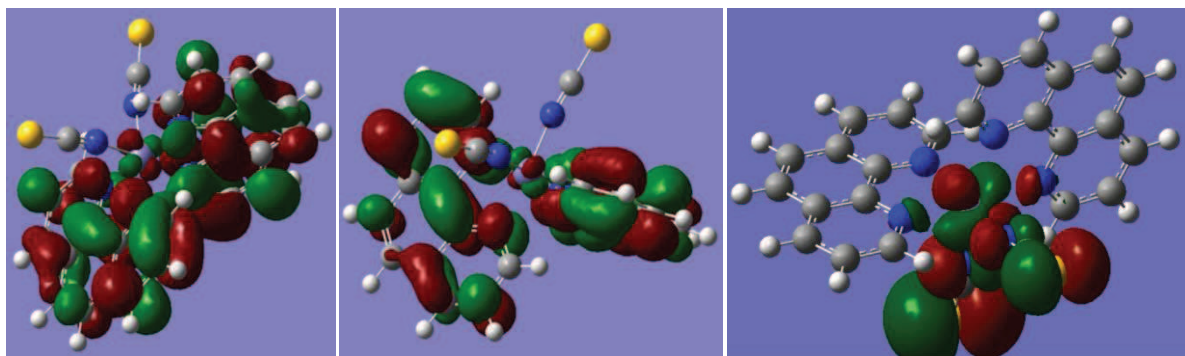
Fig 3.35 *DFT calculation of the LOMO molecular orbitals toward which the CT process can take place.*

This delayed global molecular reorganization, with respect to the displacive breathing, involves for example the distortion Σ , but more generally Σ can represent all other degrees of freedom not directly coupled to the change of electronic distribution around the d orbitals, wheareas *D* represent the coordinate along the breathing mode. Therefore, a kind of curved path in the (D,Σ) PES occurs, as schematically represented in **Fig 3.32**, between the equilibrium position of the LS and HS$_d$ states.

Our results underline the limit in the description of molecular systems with a single coordinate parameter (Fe-N distance) along a potential energy curve considered so far, as other structural degrees of freedom also play their role. In particular, the efficient electron-phonon and phonon-phonon couplings associated with a fast damping are the control parameter in SCO materials, allowing ultrafast photo-switching by moving the system towards the equilibrium position of a new potential. This means that the amplitude of Fe-N stretching become rapidly small after the 0.2 Å elongation, which occurs within 170 fs as observed by XANES. The signal/noise ratio allows estimating a maximum amplitude of 0.02 Å corresponding to the noise limit below which oscillation cannot be observed. This understanding of the crucial initial steps, leading to spin state switching, should help chemical design for efficient trapping of photo-excited states.

3.3 Ultrafast ISC in Spin crossover crystal

One of the most fascinating aspects of the spin state photo-switching is the huge efficiency and speed of this process. In the experiment presented in part 3.1 and 3.2, the number of molecules photo-switched from LS to HS state can be compared to the number of photons in the pump laser pulse. For example, for "[Fe^{III}(3-MeO-SalEen)]PF$_6$ " a typical number of photon in the probe volume is 3 (± 1) photons for 100 molecules whereas the converted fraction is 2.5 (0.5) %. Both values are close to each other suggesting an efficiency close to 1. It was discussed in 3.2 that damping plays a key role, underlying the fact that such phenomenon does not only involve electronic degrees of freedom but also structural ones. Indeed the change from LS to HS leads to an elongation of the <Fe-N> bond length around 0.2 Å for Fe^{II} and 0.15 Å for Fe^{III}. But the bond length is not the only pertinent structural parameter and distortion may play a crucial role on the stabilization of excited state.

This LIESST process was discovered in the middle eighties (**Descurtins 1984, Hauser 1984**). After the pioneer studies investigating photoinduced effect driven by cw excitation, new technologies allowed performing time resolved experiments with nanosecond resolution (**McGravey 1984**) and later with fs resolution (**Monat 2000**). In this way, It has been clearly established that the intersystem crossing from the electronic excited state and the HS state occurs on sup-ps time scale (**Mc Cusker 1992**), and the growing knowledge in fs laser has provided opportunities to watch in real time such ISC (**Damrauer 1997**).

Until now, most of the studies dealt with molecules in solution and Fe^{II} systems, undergoing a MLCT excitation between diamagnetic LS and paramagnetic HS states and the present results are the first detailed analysis of the crystal environment. In addition, different electronic excitation processes, or different electronic states (LS S=1/2 or S=0 to HS S=5/2 or S=2) are of interest and that is the reason why it is crucial to compare the dynamics between Fe^{II} and Fe^{III} systems, since the elementary electronic excitation processes are different.

The two processes can be schematically represented by the energetic diagrams shown in **Fig 3.36 & 3.37**.
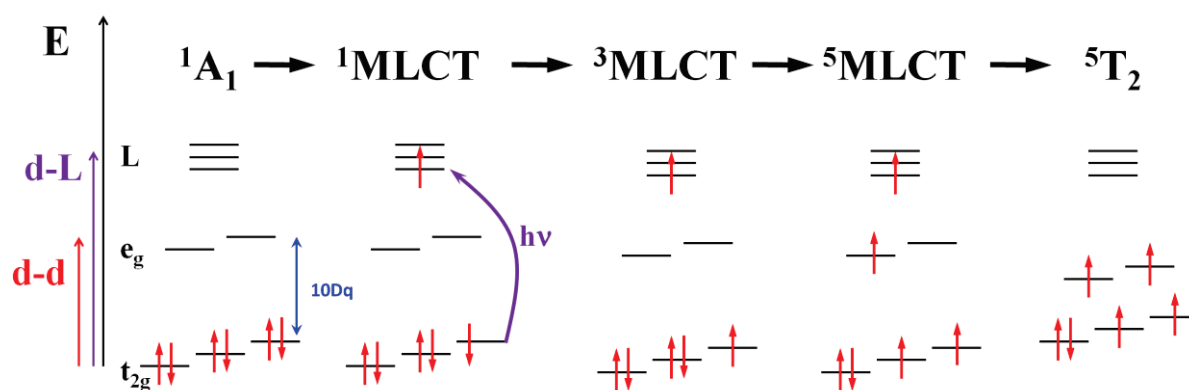
Fig 3.36 *Schematic Drawing of Photo-Switching process in Fe^{II} system.*
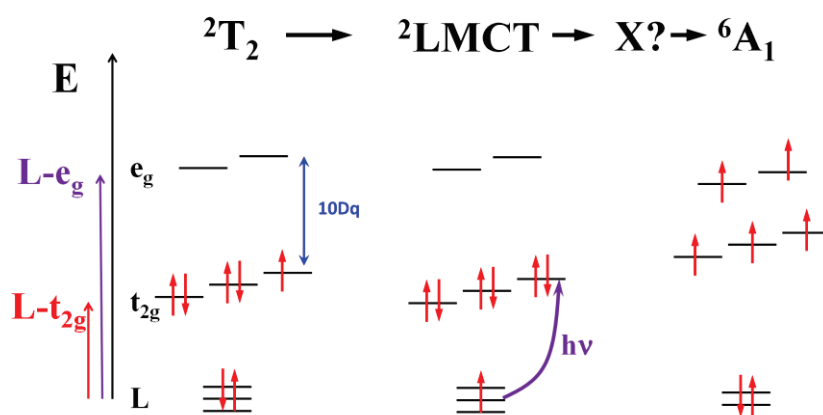
Fig 3.37 *Schematic Drawing of Photo-Switching process in Fe^{III} system.*

In the case of Fe^{II} systems, the electronic excitation of the LS S=0 state promotes an electron from the Fe t$_{2g}$ orbitals to one orbital of the ligand (L), giving rise to a ^{1}MLCT state. Different electronic states of CT character exist such as ^{3}MLCT and possibly ^{5}MLCT, before the final ^{5}T$_2$ state get finally reached, as the electron goes back on Fe and the ligand field decreases. It is experimentally evidenced that the ISC process from the MLCT states to the HS state occurs within less than 50 fs. Of course different ligand orbitals L can be involve in the process, depending on the pump energy. Another possibility is the d-d excitation at lower energy from t$_{2g}$ to e$_g$ (10 Dq), but this process is less efficient due to the forbidden character of this transition. Our studies in [Fe^{II}(phen)$_2$(NCS)$_2$] around this d-d band above 800 nm (**Fig. 3.24** & **Konig 1966**) did not show significant photo-switching and this process was not so investigated here.

In the case of Fe^{III} systems a LMCT excitation process is used and two transition bands exist for promoting an electron from the ligand to the Fe: one towards the t$_{2g}$ orbitals and one towards the e$_g$ orbitals at higher energy. Calculations on Fe^{III} systems indicate that the lowest energy band, referring to an excitation on the t$_{2g}$ orbital is assigned to the absorption band of the LS state observed around 12 000 cm^{-1} (~800 nm, **Fig. 3.2**) (**Dei 1993**). Therefore, during our studies on Fe^{III} systems where the pump wavelength was set to 800-850 nm, it is this LMCT process towards the t$_{2g}$ orbitals which was used. It is difficult to describe more this LMCT process in Fe^{III} system, with a complete nomenclature of excited states since the theorethical pathway from LS to HS since has not been discussed yet in the literature.

Nevertheless, we try here to discuss such a pathway. Once the electron is transferred from the Ligand to the t$_{2g}$ orbitals, the repulsion strength on the new paired electron can be large compared to the ligand field. This will favor another electronic state with electrons dispatched between t$_{2g}$ and e$_g$. This new electronic state with less bonding character will lead to a decrease of the ligand field with structural reorganization and elongation of the Fe-N bonds, equivalent to a gap narrowing in the crystal. This is accompanied by a return of one electron towards the L orbital. These electronic and structural degrees of freedom are coupled and it is difficult for the moment to say in which order they occur after the LMCT process.

Comparing the photo-switching dynamics which have been investigated during this PhD by optical pump-probe spectroscopy resulting from LMCT in Fe^{III} and MLCT in Fe^{II} is interesting. The two Fe^{II} systems are [Fe^{II}(AZA)$_2$(NCS)$_2$] and [Fe^{II}(Phen)$_2$(NCS)$_2$] synthesized by the J.F. Létard group in Bordeaux and the two Fe^{III} systems are [Fe^{III}(3-MeO-SalEen)]PF$_6$ and [(TPA)Fe^{III}(TCC)]PF$_6$ synthesized by the M.L. Boillot group in Orsay. In the data presented in **Fig 3.38**, the pump is set on bands known as LS-MLCT (Fe^{II}) or LS-LMCT (Fe^{III}) and the probe to a wavelength sensitive to ISC. Especially in Fe^{II}(Phen)$_2$(NCS)$_2$, the results shown were probed with 950 nm, where no modulation by the t$_{2g}$-e$_g$ gap exists. In the case of [Fe^{III}(3-MeO-SalEen)]PF$_6$, the probe is set to 625 nm at the isobestic point. Therefore it is mainly the ISC crossing from LS to HS, which is probe for the 4 compounds in such experimental set-up.
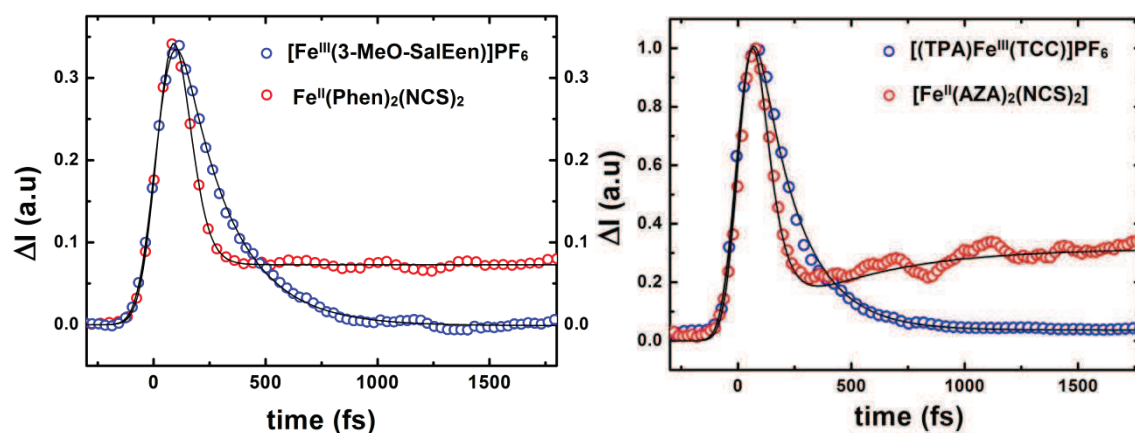
Fig 3.38 *transient absorption during spin state switching*

In blue Fe^{III} system : [Fe^{III}(3-MeO-SalEen)]PF_6 (left) and [(TPA)Fe^{III}(TCC)]PF_6 (right)

In red Fe^{II} system : [Fe^{II}(Phen)$_2$(NCS)$_2$] (left) and [Fe^{II}(AZA)$_2$(NCS)$_2$] (right).

The decay of the INT electronic state, fit here with an exponential dynamics, gives the following time constants for the ISC and the population of the HS state in the four compounds:

[Fe^{II}(Phen)$_2$(NCS)$_2$]	[Fe^{II}(AZA)$_2$(NCS)$_2$]	[Fe^{III}(3-MeO-SalEen)]PF_6	[(TPA)Fe^{III}(TCC)]PF_6
$\tau < 50$ fs	$\tau < 60$ fs	$\tau = 200 \pm 20$ fs	$\tau = 180 \pm 20$ fs

The results tend to indicate a faster ISC in both Fe^{II} cases (~50 fs), for which a MLCT process is used compared to Fe^{III} cases (200 fs), for which a LMCT process is used. But we cannot clear-cut if this is due to the system (Fe^{II} vs Fe^{III}) or to the excitation process used. It would be interesting to compare MLCT vs LMCT processes in Fe^{II} but this uses the higher energy excitation process from the ligand to the e_g band as the t_{2g} states are occupied. In the same way, MLCT processes in Fe^{III} systems are of interest, but band assignment is not clear enough to indicate if the observed band at 400 nm is a MLCT or a LMCT towards the e_g levels.

Regarding the mechanisms involved, in addition to the fastest character of the MLCT ISC, coherent motion is also observed on long time scale until 7 ps in the Fe^{II} systems investigated here (publication 4 and 5). Even if coherent motion is well known in photo excited system (**Iwamura 2010, Van der Veen 2010, Consani 2009**), it often involves wave packet motion on excited state potential energy surface. But in SCO case, the coherent motion play a key role driving the system from the excited to the HS potential.

For sure, the absence of coherence in some SCO systems may be associated with the number of intermediate states crossed on the pathway to the HS potential or by the period of the involved phonons with regard to the ISC time-scale. Some theoretical calculation (**Suaud 2009**) have shown that this ISC can be complex and therefore the pathway from MLCT to HS state may be more or less fast depending on how the PES of the different intermediates cross (**Boilleau 2012**). But another possibility is the effect of the damping, which strongly depends on the ligand, as this process is associated with energy transfer towards the different vibration modes.

Let us mention that we could observe coherent vibrations in the Fe^{III} [Fe^{III}(3-MeO-SalEen)]PF_6 system (**Fig 3.39**), but with weaker signature than in the case of the Fe^{II} systems.
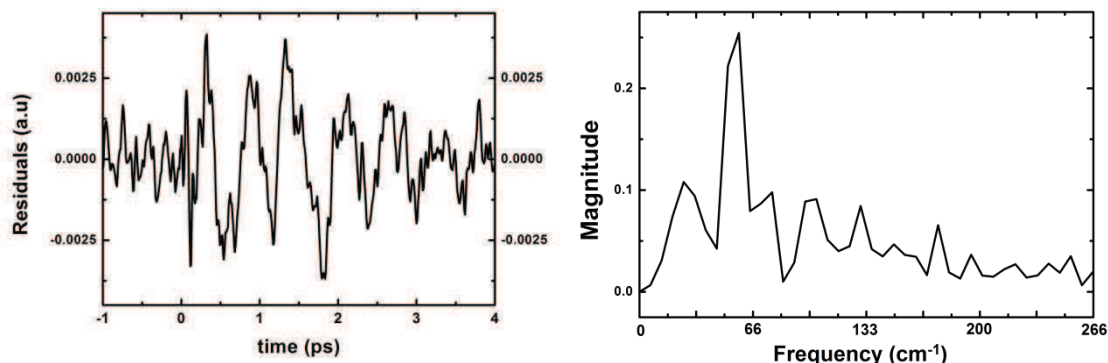
Fig 3.39 *Oscillating part of [Fe^{III}(3-MeO-SalEen)]PF_6 data at 625nm and associated FFT (1.72 THz or 57 cm^{-1}).*

As there is no detailed vibration studies in this compound, we can compare the observed mode to the ones in this frequency range in [Fe^{II}(Phen)$_2$(NCS)$_2$]. The low frequency mainly have a ligand motion character, which is here again activated after the ISC. Compared to our conclusion on the structural dynamics in the [Fe^{II}(Phen)$_2$(NCS)$_2$] compound, what we observe here for [Fe^{III}(3-MeO-SalEen)]PF_6 system is consistent, even though we cannot observe Fe-N elongation modes at higher frequency.

There are two points which can explain this fact. First, the coherence of Fe-N modes may not easily survive to ISC due to the longer character of the ISC (200 fs) compared to the phonon period. Only ligand motions with period longer than 200 fs (frequency below $\approx$ 150 cm^{-1}) can be coherently activated. The other possibility is the high damping of the Fe-N breathing mode. But indeed, these two points have the very same origin : the high damping is nothing else than an efficient transfer towards the other vibration degrees of freedom.

Conclusion

The photoinduced spin-state switching driven by fs laser pulse through LMCT or MLCT processes have demonstrated a high quantum efficiency (close to 1) during the complex pathway towards the HS state on a sub-ps time scale. This change of electronic state is correlated with strong structural rearrangement due to the less bonding character of the HS state.

The experiments performed in different systems (Fe^{II} and Fe^{III}) of different size and environments tend to show the dynamics. It supports the idea of a local molecular process in the spin state trapping. It also explains why the observed dynamics do not differ from previous reports on molecules in solution with a fast ISC (<50 fs) and a slower structural relaxation (with a Fe-N elongation within $\cong$ 200 fs). Another clear fact is the linear response of the ultrafast photoswitching

with the excitation density and more details will be presented at different temperature in chapter 4 on the different compounds studied here. In this process, one photon switches only a single molecule at ps times scale. This is understandable because the cooperativity operates through elastic interaction which manifest at longer time scale and this will be discussed in chapter 4.

One important result presented here is the decoupling of different degrees of freedom during the electronic spin state trapping and the transfer of excess energy to molecular vibration modes. For instance in Fe^{II} system, the intersystem crossing occurs within a 50 fs dynamics. This is followed by the bond length elongation in 170 fs. And finally other structural parameters like distortion are activated at longer time scale (1 ps). The similarity of the dynamics observed in XANES on two Fe^{II} confirms this scenario, where the different degrees of freedom are sequentially activated: first the mode directly coupled to the change of electronic distribution and then the global relaxation towards the final HS state.

The dynamics of ISC between LMCT process in Fe^{III} (200 fs) and MLCT process in Fe^{II} (50 fs) are significantly different. This can be due to a higher number of transient excited states crossed during the LMCT process or to the more difficult evolution of the system during the ISC. And this fact also degrades the coherence of the process because it leads to a higher dephasing between HS molecules. In both cases, coherent molecular structural dynamics is observed, but in Fe^{III} only a low frequency mode with a small amplitude is observed. In Fe^{II} compounds both Fe-N mode and ligand modes are observed, contrary to Fe^{III} where only ligand modes are observed. In any case, the results presented here show that the damping process plays a key role for having an efficient conversion from LS to HS and for avoiding recurrence toward the initial state.

These first studies on ultrafast photo-switching in the solid state need to be applied to other SCO materials, showing other excitation processes but also made of different structure and ligand for underpinning what is general and what is specific. Do all Fe^{II} systems show <50 fs ISC? Do all Fe^{III} systems show 200 fs ISC? Or is this specific to the systems investigated here, as the two Fe^{II} systems have similar structure (4N on aromatic ligand and 2 ionic NCS bonds) and the two Fe^{III} as well (4N and 2O). What is the role of the structure? What is the role of the electronic excitation process? It is therefore necessary to study new materials with different ligand bonding structures and especially without inonic bonds. It is already known that the denticity of the ligand is one of the crucial factors for controlling the stability of metastable photo induced species (**Letard 2005**). Maybe it denticity can play an active role on the ultrafast dynamics during the spin state switching too.
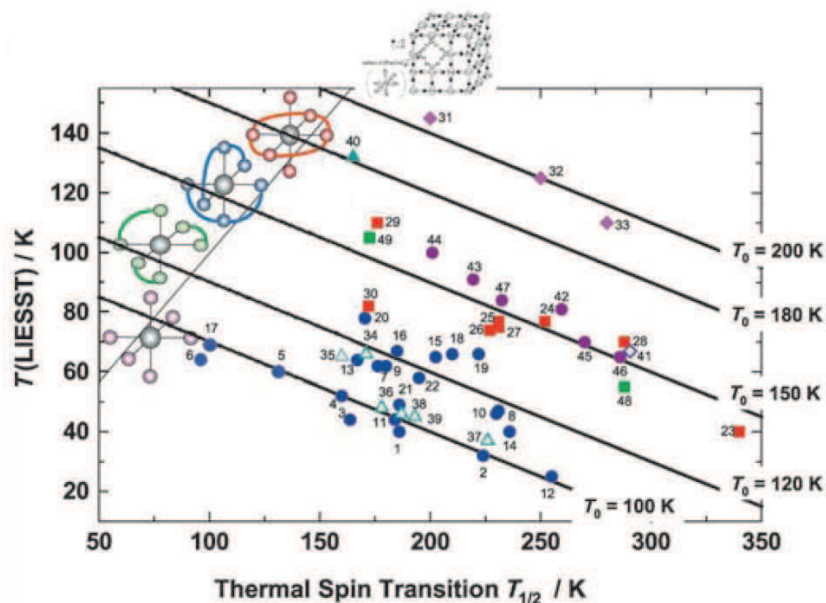
Fig 3.40 *Stability of Photo-trapped state in function of ligand configuration bridge.*

What is obvious now with the present study, in light of theoretical works (**Van Veenendal 2010**), is that generating LIESST requires not only efficient ISC but also important damping as electronic and structural degrees of freedom couple.

This study underlines key aspects of the ultrafast molecular switching, which is the initial step of the photoinduced processes occurring in the active solid. During this molecular photo-switching process, most of the absorbed pump optical energy (1.5 -2 eV) is non radiativelly dissipated, as it is much higher than the energy difference between LS and HS states (tens of meV). This energy redistribution drives on longer time-scales other effects resulting from the local change of the molecular structure (inducing a local stress) and from the dissipation of heating of the lattice, and which will be discussed in chapter 4.

Chapter 4: Out-of-equilibrium dynamics

A new challenge in material science is not only to observe matter at relevant time and length but also to direct the functionality of the system. To achieve this goal, Photo Induced Phase Transitions looks are very promising field with a wealth of interesting systems. Spectacular advances are made in nanoscience with the mastering of energy and information storage on nanometer scale (**Qunitero 2012**). More recently a new field has emerged within material science, whereby an ultra-short laser pulse may induce the collective and cooperative transformation of the material towards another macroscopic state which can be of different electronic and/or structural order (**Buron & Collet 2005 / Tanaka, et al, 2009**). This can trigger spectacular switching of the physical properties of materials, for example from non magnetic to magnetic or from insulator to conductor. The goal is then to realize at the level of a material what femtochemistry has achieved at the level of a single molecule.

Materials with photoactive multi-functional molecules, which can switch between two states or more, are particularly promising to explore. This is especially true for spin-crossover compounds, showing changes in magnetic and optical properties as well as a structural reorganization. The structural investigations of light-driven switching of spin-crossover solids have so far been limited to photo-stationary states at low temperature (**Kusz 2001, Marchivie 2002, Huby 2004, Ichiyanagi 2006, Pillet 2006**). Still, a central question remains on the determination of the dynamics of the photo-switching processes driven by a femtosecond laser in these materials. Most investigations deal mainly with the slow kinetics of recovery to the thermally stable state but not the photo-transformation (**Enachescu 2006**) or to investigate slow kinetics with ns laser inside and outside hysteresis (**Cobo 2008, Fouché 2010**).. In solids, we can expect the photoinduced dynamics to follow a complex pathway from molecular to material scales through a sequence of processes.

The aim of this chapter is to discuss such an out-of-equilibrium dynamics in spin-crossover materials. Indeed, the combination of time resolved X-ray diffraction and femtosecond optical spectroscopy reveals the multi-step aspect of such photo-induced process (**Lorenc 2009**) in the Fe[III] system [(TPA)Fe[III](TCC)]PF$_6$, as introduced in chapter 1. The system will explore different degrees of freedom at different time scales (**Cailleau 2010**). The complete out-of-equilibrium process following an initial femtosecond excitation involves 3 different steps (**Fig 4.1**):

1st step: Local molecular spin state photoswitching at fs time scale,

2nd step: HS conversion associated with volume expansion at ns time scale, propagating effect

3rd step: thermal spin state conversion by heating effect at μs time scale, diffusive process
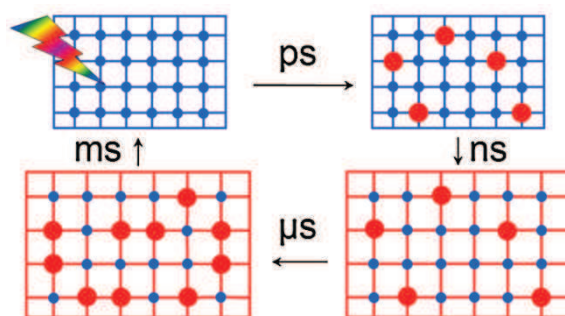
Fig 4.1 *Schematic drawing of the out of equilibrium process (**Lorenc 2009**).*

Before deepening the scientific question associated with the out-of-equilibrium dynamics, I will present first our recent investigations (**Collet 2012**) of the photo-switching process in these non cooperative Fe^{III} materials, which represent the starting point of this project. In this chapter, we will first present the results on different compounds before discussing the physics of the processes involved.

4.1 Starting point of this project

It was recently discovered that this [(TPA)Fe^{III}(TCC)]PF$_6$can crystallize in 2 polymorphs: one monoclinic and one orthorhombic (**Collet 2009**). This first study performed in this project was dealing with the photo-switching dynamics in another polymorph of the molecular system Fe^{III} [(TPA)Fe^{III}(TCC)]PF$_6$. The thermal spin crossover of the two crystalline polymorphs, show similar intramolecular reorganization associated with the change of spin state: the average <Fe-N> bond length changes from 1.96 Å (LS) to 2.13 Å (HS), as the fraction of molecules gradually changes from completely LS to HS. The monoclinic and orthorhombic polymorphs have structures that mainly differ by the layer packing along the crystal **b** axis. These complexes undergo a thermal crossover of spanning over 40 K, which is the sign of weak intermolecular coupling. The complete out of equilibrium process of the monoclinic polymorph has already been investigated (**Lorenc 2009**).

In order to go deeper in the understanding of the out of equilibrium processes, new experiments on time resolved diffraction have been done at APS synchrotron on the Biocars beam line described in chapter 2. This experiment allows 100 ps time resolution like other time resolved beam line over the world. Two polymorphs of the [(TPA)Fe^{III}(TCC)]PF$_6$ were studied on this facility. The difference between this experiment and the previous ones lies in the repetition rate of the pump-probe setup. Typically this rate is 1 kHz rate, whereas the APS experiment runs at 40 Hz which allows the complete recovery of equilibrium.
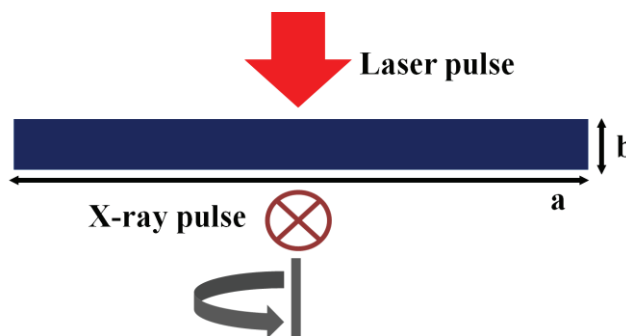
Fig 4.2 *Schema of the APS setup with the crystal orientation.*

Like other time resolved diffraction beam lines, the probe is a 100 ps X-ray pulse and the pump a 1 ps laser pulse. The pump is set here to 800 nm because it involves a LMCT excitation like previously reported (**Lorenc 2009, Moisan 2008**). The typical size of the crystal are 200*100 μm^2 in the (**a**,**c**) plan and 10's μm of thickness (**b** axis). **Fig 4.2** shows a schematic view of the experimental setup where the laser propagates along the crystal thickness, which is the **b** axis. The thickness of the different samples studied was 7μm and 21 μm. In order to explore the reciprocal space, the crystal rotates around the **b** axis. The laser polarization is circular for avoiding polarization effect during the data collection.
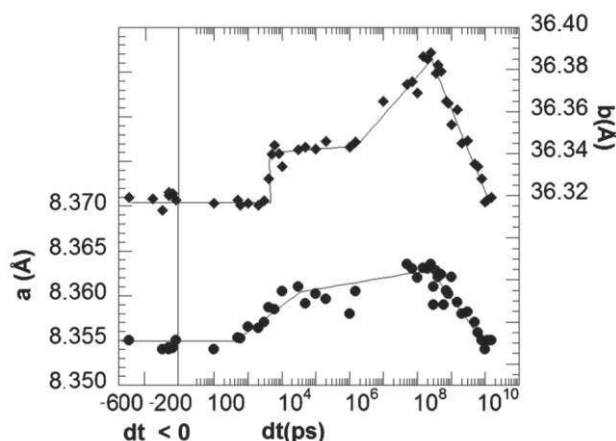
Fig 4.3 *Evolution of **a** and **b** lattice parameter after fs excitation(**Collet 2012**).*

The time evolution of the **a** and **b** cell parameters after photo-excitation is represented in **Fig 4.3.** No change in the lattice cell parameters is observed before 10 ns and it seems that the crystal expands faster along the **b** direction than along **a**. The time of expansion involves elastic deformation, and therefore the speed of sound is a limiting parameter. The difference of expansion time between **a** and **b** underlines the size dependence of the volume expansion. In addition to this elastic step, a second increase is observed around 100 μs, more clearly for the **b** parameter. This second step is identified as resulting from the thermal population of the HS state and previously observed (**Lorenc 2009**).
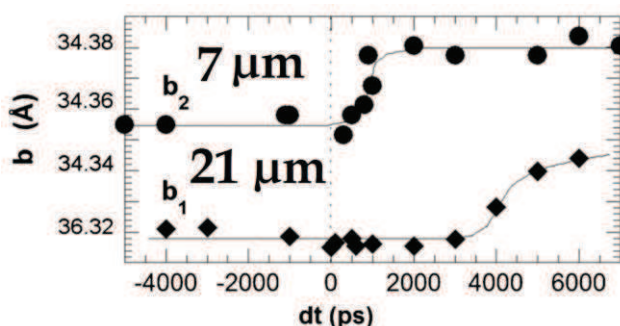
Fig 4.4 *Evolution of b lattice parameter (thickness) for two different sample thicknesses (**Collet 2012**).*

The size effect is also well illustrated in **Fig 4.4**, which compares the lattice expansion of two crystals of the monoclinic polymorph, and shows the time dependence of the lattice parameters b_1 for sample 1 (21 μm thick) and b_2 for sample 2 (7 μm thick). A faster expansion of the lattice parameter **b** (corresponding to the thickness) is observed when the thickness is reduced. It is expected that the expansion time varies linearly with the sample thickness, in good agreement with expansion time of 5 ns (respectively 1.5 ns) for the 21 μm (resp. 7 μm). A kind of time latency is observed since the lattice parameter expansion does not start smoothly after laser excitation but starts only few ns after (Fig. 4.5). This expansion corresponds to a simultaneous increase of the HS fraction observed by fs optical spectroscopy.
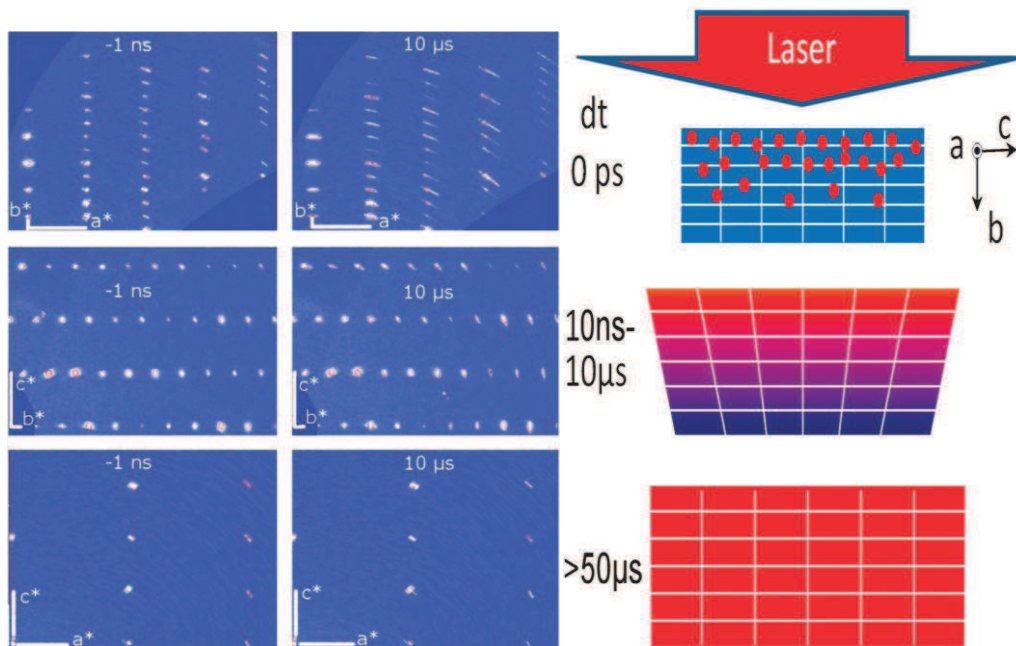
Fig 4.5 *Evolution of the diffracted intensity in the reciprocal planes, showing a deformation of the Bragg peaks between -1 ns and 10 ms(left),*
*Schematic view of the out of equilibrium process illustrating the anisotropic character of transient crystal state between 10ns-10μs (right) (**Collet 2012**).*

Since conversion related to heat diffusion effects is more rapidly activated when the size is small, the excitation of crystals of anisotropic shape induces in the time domain anisotropic deformations. This can be observed by deformation of the Bragg peaks in the reciprocal lattice. **Fig. 4.5** shows reconstruction of different reciprocal planes before laser excitation (-1 ns) and after laser excitation when the effect is maximum (10 μs) measured on a $200×200×7 \ \mu m^3$ single crystal of the orthorhombic form. In the (**a*,c***) plane no significant deformation is observed, whereas in the (**a*,b***) and (**b*,c***) planes an important broadening of the Bragg peaks is observed. Difference in Bragg peak shape according to the desired reciprocal space plan puts under light the strong anisotropic character of the heating effect. Indeed, Bragg peaks are deformed at 10 μs in the (**a*,b***) plan which refers to the thickness but not in the (**a*,c***) plan which refers to the surface. It is explained by the schema shown in **Fig 4.5**. A slice of crystal in the (**a*,c***) plan in the 10 ns-10 μs case looks homogeneous. But in the (**a*,b***) plan, a strong gradient of temperature due to the laser excitation exists and has to be relaxed. After 50 μs, a homogeneous transient state is reached when pressure and temperature gradients are relaxed.

Our new investigation by ultrafast optical spectroscopy and X-ray diffraction in the 100 fs-10 ms time window for both polymorphs shows that the first step is localized at the molecular level, with no indication of a cooperative response. The elastic step is also demonstrated to be sample

dependent in terms of size and shape. The transient state is finally reached within ≈10-100 μs, where heating and elastic effects are relaxed. The results presented above on the first systems studied by combined time-resolved optical spectroscopy and x-ray diffraction gave a similar overview of the entire cascading process to the one provided by the study on the other polymorph (**Lorenc 2009**). But some crucial questions came out from these investigations where elastic and thermal effects compete.

The first point concerns the response of cooperative materials showing sharp thermal transitions from LS to HS state. Some strong effects associated with the cooperative response of SCO materials are well-known during relaxation process from the photoinduced state excited at low temperature. When the system undergoes a weakly intermolecular coupling, molecules behave more or less independently and the relaxation behaviour is described by a mono-exponential curve (**Enachescu 2006, Varret 2004, Hauser 2004**). But in case of strong cooperative materials, the relaxation rate depends on the molecular fraction in the HS state and a self-accelerated process of sigmoid shape is observed (**Enachescu 2009, Hauser 1999**). The response of such materials to a femtosecond laser pulse is therefore of great interest for probing if elastic effects can drive cooperative response or if heating effects can drive complete transition. Time resolved studies open the possibility to study if molecules in cooperative materials behave independently or not and to investigate how the stronger inter-molecular coupling influences the all cascading processes and if it can lead to new behaviours.

The second point is the influence of sample sizes. Would this concept be still valid at nanoscale or with nanosize object? Will confinement of nanocrystals in passive polymeric matrix play a role or not. These two points are discussed in the second part of this chapter.

4.2 The cooperative Fe^{II} [Fe(phen)2(NCS)2] system

A good candidate to quantify/measure the influence of cooperativity in the all out of equilibrium process is the [Fe^{II}(Phen)$_2$(NCS)$_2$] prototype system previously introduced in chapter 3. We have used time-resolved investigations (transient optical absorption and time resolved diffraction) similar to the ones presented above to study the ultra-fast out-of-equilibrium dynamics in this cooperative systems, which presents a 1st order transition around 180 K with as small hysteresis of 2 K width.
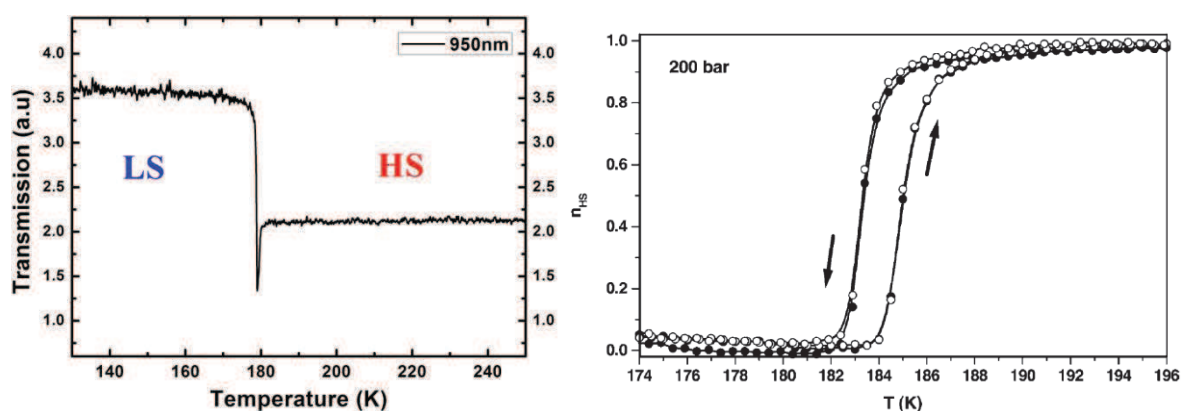
Fig 4.6 *Thermal transition monitored by optical absorption at 950 nm (left) and magnetic susceptibility close to the hysteresis at 200 bar (**Bousseksou 2003**)(right).*

Elastic step is related to pressure effect inside the crystal. Different groups have studied the effect of pressure on this compound, which favors the LS state of smaller volume (**Roux 1996**, **Bousseksou 2003**). The temperature dependence of the magnetic susceptibility measured at 200 bars gives a $T_{1/2}\approx183$ K (**Fig 4.6**), whereas at room temperature the pressure induced transition from HS to LS occurs above 6.5 kbar. As the first order nature of the phase transition from LS to HS is maintained in this pressure range, we can expect some cooperative effects during the photoinduced out-of-equilibrium process. The photoinduced dynamics was studied by an optical pump-probe setup, which allows covering time delays from fs to ms and is described in detail in chapter 2. Furthermore, by synchronizing wisely the two amplifiers, it is possible to get one set of delays where pump and probe are enough close in time to follow the fs spin state switching with mechanical delay line. In this way, the first delay point measured after excitation can be in the 10 ps-1 ns time window.

4.2.1 Results

The optical pump-probe measurements were performed in transmission mode on a single crystal. The crystal has a typical size of 200*200*30 μm^3 and is cooled down to LS state at 140 K. Like ultrafast studies, the pump is set to 650 nm in MLCT band which promote efficiently LS to HS. The probe is set in infrared at 900 nm where a clear signature of the LS→HS transition exists through an increase of optical density. The two colors pump probe (80 fs per pulse) studies are performed in the classical transmission configuration (chapter 2) at 1 kHz. By measuring the change of OD of the probe we can deduce how the HS fraction X_{HS} changes in time. Between the pure HS and LS phase, the change of optical density measured is referred to as OD_{HS-LS}. Our time-resolved set-up give the transmitted light intensity I by the sample and the variation ΔI with respect to the intensity I at a given time delay t. Therefore the fraction of molecules photoswitched to the HS state is deduced from the measured quantity $\Delta I/I$:

$$\Delta OD(t) = -\log\left(\frac{\Delta I}{I}+1\right) \text{ which leads to } \Delta X_{HS}(t) = \frac{\Delta OD(t)}{OD_{HS-LS}}$$

It shows how easy it is to get back to the fraction of HS molecules during the out-of-equilibrium process. All the following results will be expressed in term of ΔX_{HS} which quantifies change of HS fraction at a given delay compared to the fraction at thermal equilibrium
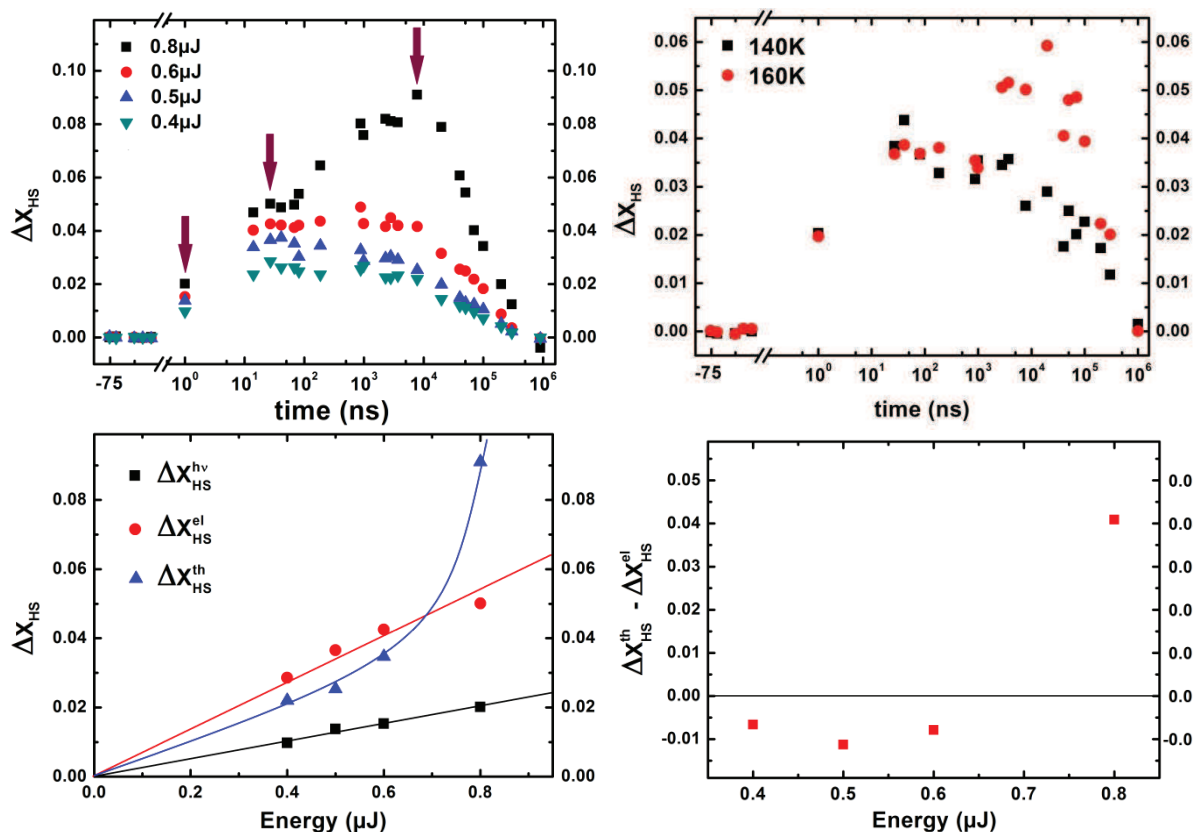
Fig 4.7 *Transient HS fraction of the photo-excited $[Fe^{II}(Phen)_2(NCS)_2]$ in the 1ns-1ms temporal window at 140 K and for different excitation densities (up, left), at 140 K and 160 K for 0.5 µJ ($30mJ/mm^2$) (up, right). Dependence of HS fraction on the photoswitching ($\Delta X_{HS}^{h\nu}$), elastic (ΔX_{HS}^{el}) and thermal (ΔX_{HS}^{th}) steps at 140 K (bottom, left) and difference between ΔX_{HS}^{th} and ΔX_{HS}^{el} with excitation density (bottom, right)*

Fig 4.7 shows the time dependent data in the ns-ms range (the first point at positive delays corresponds to 1 nanosecond in these data). By looking at the curve for the higher energy scan at 0.8 µJ/per pulse (45 µJ/mm^2), it is possible to clearly identify a 3 step process, which is quite similar to the one previously reported (**Lorenc 2012**) for non-cooperative Fe^{III} spin crossover systems :

-The first step $(\Delta X_{HS}^{h\nu})$ corresponds to the ultrafast molecular switching (detailed in chapter 3) which occurs within less than 1 ps and where the HS fraction does not change up to ns.

-The second one (ΔX_{HS}^{el}) is associated with the elastic step, which corresponds to the increase of HS fraction before 13 nanosecond which correspond to the second excited point.

-The third one (ΔX_{HS}^{th}) is due to thermal population of the HS state in the 10 µs range.

The bottom left panel in **Fig 4.7** shows how the signal intensity changes with the pump energy for these three different steps. The photo-switching $\Delta X_{HS}^{h\nu}$ and elastic ΔX_{HS}^{el} steps show a linear response with excitation density, as it is the case for the Fe^{III} compounds presented before. A marked difference with the case of such non cooperative systems, for which the thermal step is always observed in the vicinity of the thermal crossover (**Lorenc 2012, Kaszub 2013**), is that thermal activation is not observed in the data with pump energy ≤ 0.6 µJ (34 µJ/mm^2) . The signal at 10 µs presents a non linear response that refers to the occurrence of the thermal activation only above an excitation density threshold around 45 µJ/mm^2. If the pump energy is not high enough, after the elastic switching, the system starts to relax. For underlying the thermal nature of the 10 µs step, similar measurements were performed at fixed pump energy of 30 µJ/mm^2 (below the 45 µJ/mm^2

thermal threshold observed at 140 K). As presented in **Fig 4.8**, the thermal step is not observed for this excitation density at 140 K, but it appears at 160 K, on approaching the thermal transition (which occurs around 180 K), underlying the thermal nature of this step. It is not only the thermal energy increase due to the laser excitation but the overall temperature of the system which is relevant for this step.
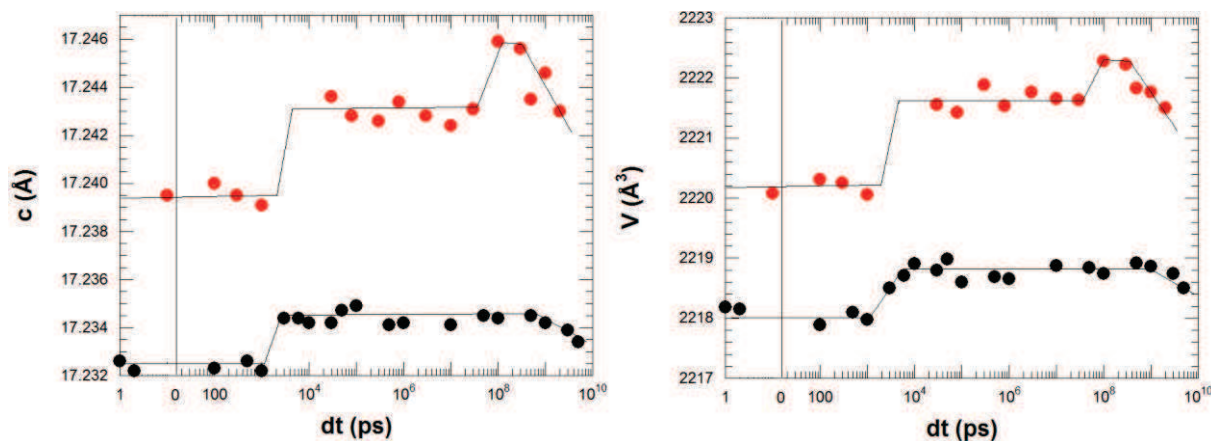
Fig 4.8 *Evolution of the lattice parameter **c** and the volume in time for excitation densities of 30 µJ/mm² (●) dots and 50 µJ/mm² (●).*

These observations are combined to time resolved diffraction studies performed at APS synchrotron on the Biocars beamline. Only the lattice parameters have been measured during this experiment, under similar experimental conditions than for the optical studies: the sample is cool down to 140 K, the pump is set to 650 nm for two excitation density of 30 and 50 µJ/mm**²**.

The time dependence of the lattice parameters data presented in **Fig 4.8** shows that the two excitation densities used correspond well to the two different regimes observed by optical techniques. The lattice expansion corresponds to the elastic step (around 30 ns) and thermal step (10 µs), but this last step is only observed for the highest pump energy (50 µJ/mm²), above the thermal threshold identified by optical measurements. On contrary, in the low energy regime (30 µJ/mm², black dots), the lattice parameters and volume do not change after 10 ns and no significant thermal step is observed.

The very nice correlation between the time-resolved optical and x-ray data show similar conclusions than the ones obtained in previous studies on the [(TPA)Fe^{III}(TCC)]PF$_6$ systems (**Lorenc 2009, Cailleau 2010, Lorenc 2012, Collet 2012**).

4.2.2 Discussion

Femtosecond photo-switching:

The first step associated with the local molecular photo-switching is presented in detail in chapter 3. In our crystals 20 µm thick, we are able to photo-switch $X_{HS}^{h\nu} \approx 2\%$ of the molecules on this time delay. Higher excitation density results in sample damage. The amplitude of the photo-switching step $\Delta X_{HS}^{h\nu}$ shows a linear response to excitation density. This is in agreement with the present

understanding of this process occurring locally at the molecular level. As explained in chapter 3, we could not detect any cooperative response in the 0-1ns range.

Acoustic phonons:

It is well known that the molecular volume changes quite a lot between LS and HS states. The instantaneous molecular switching from LS to HS (within less than 1 ps) should therefore be associated with the generation of elastic strain, as HS molecules newly created can act as source of acoustic waves. By using time-resolved optical reflectivity, we were able to detect the generation of such acoustic phonons, strongly modulating the optical reflectivity and of the transmission as well. **Fig 4.9**, shows such modulations of reflectivity, where clear periodic features are observed. The FFT show that the breathing signal measured at 760 nm involves 2 main frequencies around 12 GHz and 13.5 GHz. In the 20 ps-1.5 ns window range, the modulations oscillate around a constant reflectivity value. The damping of this acoustic phonon is on the order of nanosecond as clearly observed in the result at 950nm.
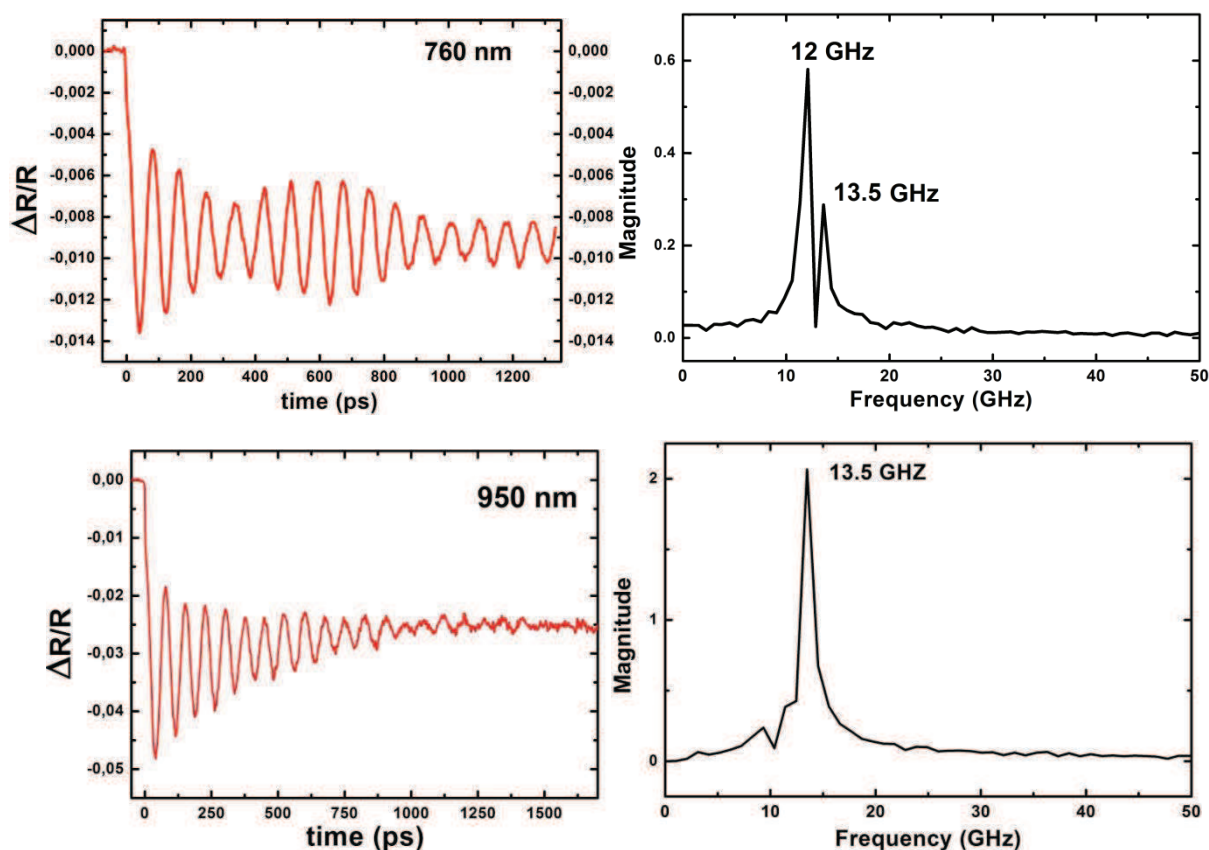
Fig 4.9 *Transient reflectivity in the 1-1000ps range (left), measured at 760nm and 950 nm and corresponding Fourier transform associated to the oscillating component (right).*

As explained in chapter 3, the photo-switching from LS to HS states is associated with a simultaneous decrease of reflectivity and transmission corresponding to an increase of absorption around the optical gap by the HS molecules. It is important to notice that the oscillating parts of transmission and reflectivity are out-of phase (**Fig 4.10**) which means that the oscillating part of optical transmission is high when reflectivity is low. It indicates a constant ΔOD of the crystal in the 10 ps -1ns range, and therefore a constant HS fraction in this time domain. For investigating this point in detail, time resolved XANES has been performed at the XPP beamline of the LCLS X-FEL, as previously mentioned in chapter 3. Due to the local character of the XANES, the amplitude of the

signal is directly related to the HS fraction and is not sensitive to other process that can modulate the dielectric function of the sample.

Fig 4.10 shows the constant time resolved XANES signal during the first 80 ps on contrary to optical transient reflectivity or transmission, which undergo a strong modulation. All the observation put together indicates a constant fraction of HS until the volume expansion around 10 ns. These oscillations are therefore the signature of the modulation of the dielectric function of the medium by the acoustic phonons and not by the HS fraction. Another feature which clearly indicates an acoustic phonon is the difference of frequency measured in function of the probe wavelength (**Fig 4.9**).
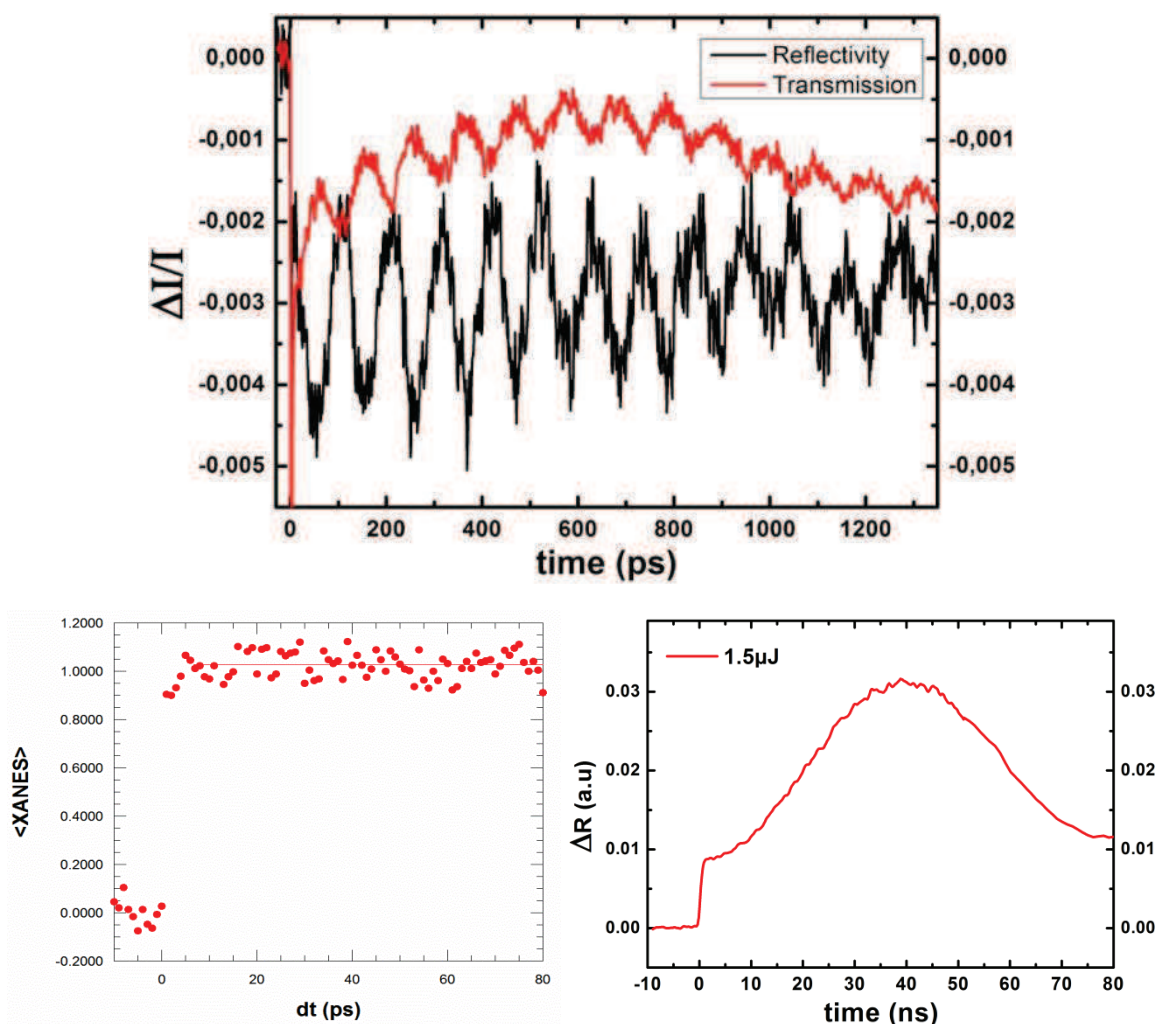
Fig 4.10 *Comparison between transient optical reflectivity and transmission(top) and XANES and reflectivity in the 0-80 ps range (bottom).*

The results on $[Fe^{II}(Phen)_2(NCS)_2]$ presented above show a stepped time evolution of the HS fraction in the crystal resulting from fs laser excitation, represented in **Fig 4.11**, corresponding well with the steps identified by Lorenc et al (**Lorenc 2009**) in non cooperative SCO materials. In the 0-1ns step, the HS fraction does not change. It increases above 1 ns at the elastic step and this is followed by a thermal conversion around 1 µs. These two steps are discussed hereafter.
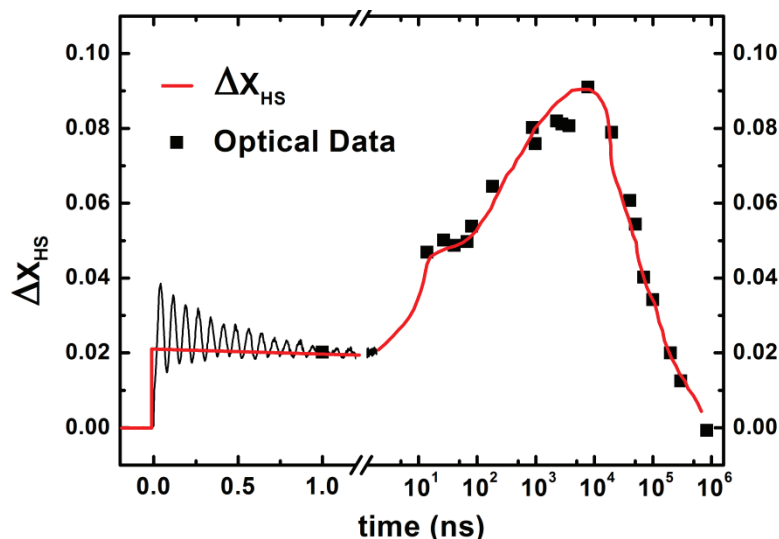
Fig4.11 *Schematic view of out of equilibrium process in Fe^{II}(Phen)$_2$(NCS)$_2$ system.*

Elastic step:

The optical data above show that Δx_{HS} remains constant up to more than 1 ns. With our experimental set-up limiting access to time delays in the 1n-13ns time window (chapter 2), we observe here that Δx_{HS} increases between 1 and 13 ns.
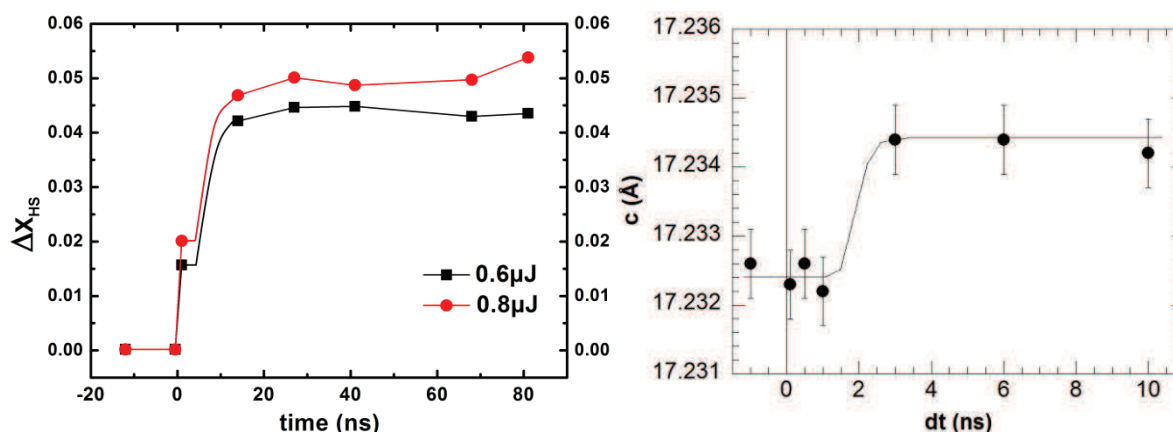
Fig. 4.12 *Elastic step observed by optical techniques (left) and time-resolved x-ray diffraction data (right) Lines are schematic guides for the eyes.*

During this elastic step the lattice parameter and cell volume expend (**Fig 4.8**). **Fig 4.12** shows a zoom on the time resolved x-ray diffraction data around this step, where the volume expansion involves elastic coupling and leads to switch of LS molecules. There is a very good correlation between optical and x-ray data, corresponding well to what is observed for the other compounds studied up to now. During this elastic step, ΔX_{HS} is more than doubled compared to the photoswitching step pointing the importance of such process in solid state.

Thermal step:

Lorenc et al (**Lorenc 2012**) have shown that a significant thermal switching occurs at the microsecond timescale as laser pulse generates a temperature increase ΔT. It is described by the optical energy deposited by the laser flash, which is proportional to the fraction X_{LS} of molecules in the LS state which absorb this energy, and the heat capacity C_p which translate how this optical energy translate in a temperature increase ΔT.
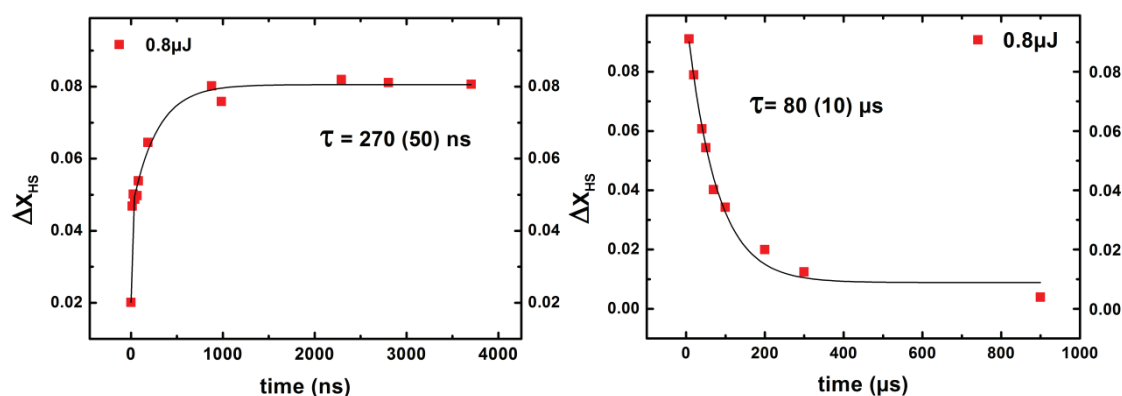
Fig 4.13 Evolution of the HS fraction following a femtosecond laser pulse plot in linear scale,

Thermal population from LS to HS (left) and relaxation from HS to LS (right).

In the present case, the left panel of **Fig 4.13** shows that the thermal population of the HS state in $[Fe^{II}(Phen)_2(NCS)_2]$ follows nearly an exponential law, which is expected for a thermal activation. The continuous line corresponds to the exponential fit, from which a 270 ns time constant is obtained. The right panel shows the relaxation of the photo-excited state in the sub-ms domain, which results from the thermalization of the sample by the cryostream, as the HS fraction recovers the equilibrium value at initial temperature. A cooling time constant of 80 µs is observed, confirming that this system can be investigated with 1 kHz repetition rate of our experimental set-up. This cryostat cooling dynamics was indeed pointed by Enachescu *et al* (**Enachescu 2006**) al as the limiting technical problem for studying fast relaxation in high temperature regime.

It should be underlined that this thermal population may be regarded as a local thermal population and not a macroscopic appearance of the HS phase, because the lattice parameter observed by x-ray diffraction are not the ones of the high temperature HS phase and there is no coexistence of HS and LS domain observed, as it is the case in some compounds in the LITH for example (**Ichiyanagi 2006**).

Before drawing general conclusion from the results presented here, we will present similar studies performed in other compounds, for extracting the general sample dependent aspects of the out-of-equilibrium processes.

4.3 The cooperative Fe^{III} : [Fe^{III}(3-MeO-SalEen)]PF$_6$ complex

In order to investigate in more details the influence of cooperativity and size effects in the out-of-equilibrium process described previously, we have also studied the [Fe^{III}(3-MeO-SalEen)]PF$_6$ complex, which undergoes a first order transition (**Haddad 1981**). As molecular relaxation rates

differ in Fe^{II} and Fe^{III} systems it is interesting to compare both systems. In addition to single crystals, our chemist collaborators involved in the ANR project Antoine Tissot, Jerome Laisney and Marie-Laure Boillot developed thin film in which crystals of this system in different crystal sizes down to nanoscales are available as reported in chapter 3. This concept of nano-sizing goes hand to hand with the goal to get efficient storage device from such photo-switchable systems. Compared to the experiment performed on $[Fe^{II}(phen)_2(NCS)_2]$ only optical transient absorption has been used with the experimental setup described in chapter 2.

4.3.1 Single crystal :

The two colors pump probe (80 fs per pulse) studies are performed in the classical transmission configuration (chapter 2) at 1 kHz. The pump was set to 800 nm and the probe at 550 nm where the thermal ΔOD is maximal. Both pump and probe are polarized following the long axis which refers to the longer dimension. By synchronizing wisely the two amplifiers, like the experiment described before, the first excited point corresponds to a delay of ten picoseconds straight in the plateau.
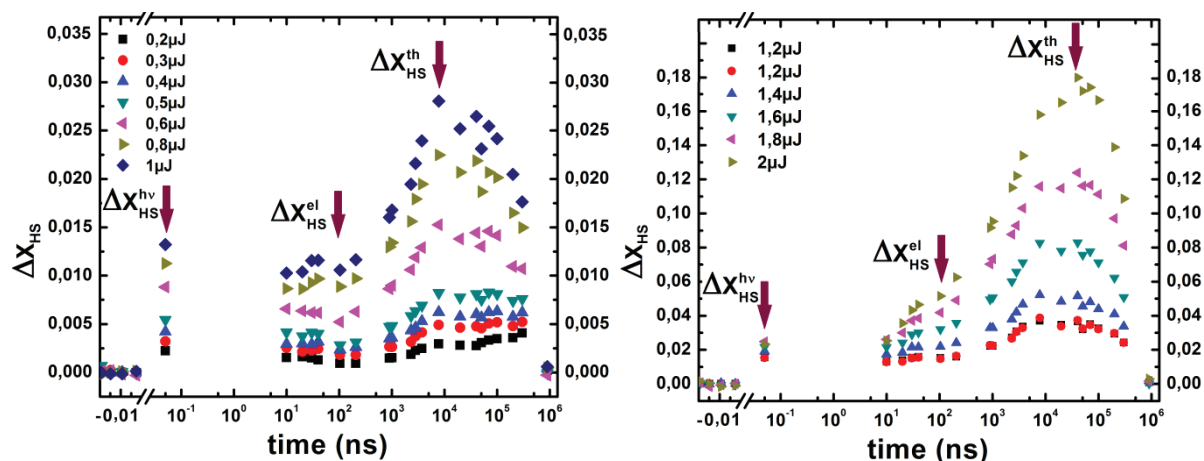
Fig 4.14 *Photo-excited fraction of HS molecules at 140K in function of pump energy.*

Fig 4.14 shows the evolution of HS fraction following fs laser excitation measured in a ≈20 μm thick single crystal. These results are divided into two parts for clarity : low energy (left panel) and high energy (right panel). The pump has a diameter of 150 μm so that a light pulse of 1 μJ corresponds to an excitation density with a fluency of 56 μJ/mm².

Here again, the data clearly indicates a 3 step process like previously observed in the $[(TPA)Fe^{III}(TCC)]$ derivatives (**Kaszub 2013**) and discuss in part 4.1 for the $Fe^{II}(phen)_2(NCS)_2$:

-A first increase $\Delta X_{HS}^{h\nu}$ of the HS fraction of few percents, which occurs within less than 1 ps, corresponds to the local spin state photo-switching.

-A second increase in the 10-100 ns time scale, ΔX_{HS}^{el} is attributed to the elastic switching as it occurs on similar time scale as for the compounds presented is the previous parts.

-A third and larger increase at μs time scale, which corresponds to the thermal population ΔX_{HS}^{th} of the HS state.

The HS fraction generated at 50 μs when pressure and temperature are homogeneous in the sample reaches the high value of 20 %. Compared to weakly cooperative systems introduced in 4.1, this large conversion might be the signature of the cooperative nature of the system studied here. A complete conversion could not be reached by increasing the excitation density since sample damage appears rapidly. For this reason, the maximum conversion on the photo-switching and elastic steps corresponds respectively to 2,5 % and 6 %.
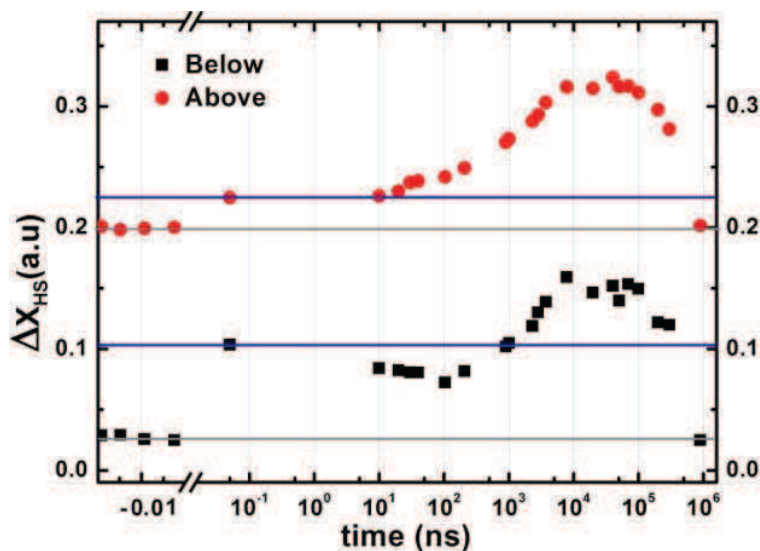
Fig 4.15 *Photo-excitation in the two different regimes.*

Compared to results presented for [$Fe^{II}(phen)_2(NCS)_2$] , a new feature is revealed here in the low energy results only, where ΔX_{HS} decreases after $\Delta X_{HS}^{h\nu}$ in the ps-100 ns time window. These results indicate a threshold excitation density, above which the elastic step around 10-100 ns occurs, characterzied by an increase of X_{HS} compared to ps scales. The curves presented in in **Fig 4.15** show both regimes, for which the fraction of HS molecules always increases during the thermal step around 10 μs, and the amplitude of the μs step increases with excitation density.

Photoswitching step:

The response of the crystal to different excitation density during the photo-switching step is represented in **Fig 4.16**. In this cooperative Fe^{III} system, the photo-switching step shows a linear dependence of $X_{HS}^{h\nu}$ at ps timescale with the excitation density. It proves that each photon transforms a single molecule from the LS to the HS states and confirms the linear character of the ultrafast switching already demonstrated in chapter 3 on nanocrystals and in the other compound [$Fe^{II}(phen)_2(NCS)_2$].
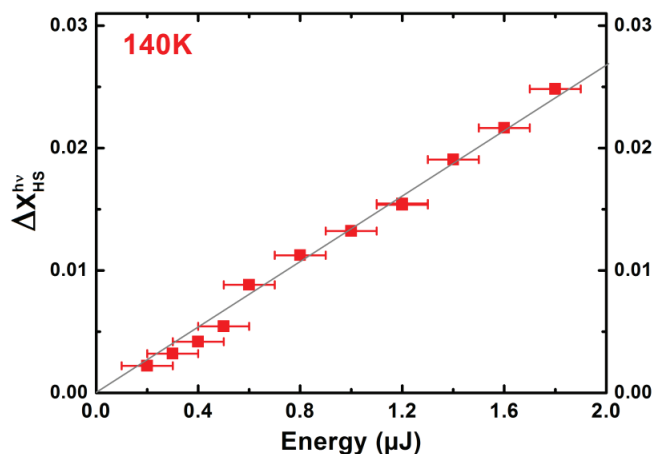
Fig 4.16 Fraction of HS molecules at 10 ps in function of pump energy.

The excitation density is difficult to measure accurately from one experiment to another one because of laser-crystal overlap, energy measurement and profile of the laser beam... Therefore we use this linear dependence for describing the evolution of ΔX_{HS} with respect to the initial fraction of photo-switched molecules on the picosecond step $(\Delta X_{HS}{}^{h\nu})$ instead of the excitation density, since $\Delta X_{HS}{}^{h\nu}$ corresponds roughly to the number of absorbed photon as the quantum efficiency of LIESST is close to 1. This value $\Delta X_{HS}{}^{h\nu}$ refers to the fraction of HS at the first point (10 ps) in **Fig 4.14**. With our experimental set up, the absolute estimation of X_{HS} is much more accurate (10^{-2}) than the one of the pump energy. It is more pertinent and useful to describe the evolution of the system with this parameter for describing the elastic and thermal steps during the out-of-equilibrium dynamics.

Elastic step:

Fig 4.17 shows the difference of the HS fraction $\Delta X_{HS}{}^{el}$ on the elastic step at 100 ns with respect to fraction $\Delta X_{HS}{}^{h\nu}$ on the photoswitching step:

$$\Delta X_{HS}{}^{el} - \Delta X_{HS}{}^{h\nu} = \Delta X_{HS}(100\ ns) - \Delta X_{HS}(10\ ps).$$

Our results indicate a clear threshold effect for the elastic step (**Fig 4.17** left). When the initial fraction of photo-switched molecules is low (below 1.5%) the number of HS molecules decreases up to 100 ns, before heating effects take over. **Fig 4.18** shows this relaxation in linear scale before the elastic step occurs at low excitation densities.
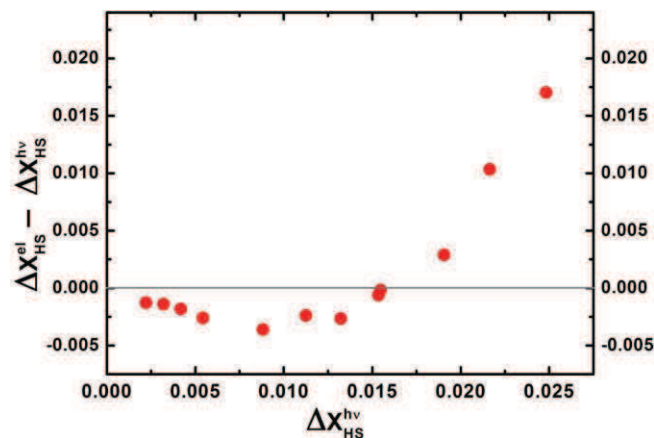
Fig4.17 *Fraction of HS molecules at 100 ns and 10 µs normalized by the fraction at 10 ps*

Fig 4.18 shows how the system behaves around the elastic step for these two regimes. Below the threshold (left panel), a clear relaxation is observed and the exponential fit gives a 30 ns time constant, which is fast for SCO materials but faster are reported for molecules in solution (**Brady 2004**). This means that the photo-switched HS molecules rapidly relax back to the stable LS state. This effect compete with the slower population of the HS state thermally activated discussed hereafter. Above the threshold (right panel), an additional HS fraction is populated at the thermal step, as observed in the compounds presented before. These data show that this step is of complex dynamics with a kind of latency: a significant increase is observed between 26 and 39 ns, whereas at halfway (before 26 ns) no significant increase is observed compared to the photoswitching step.
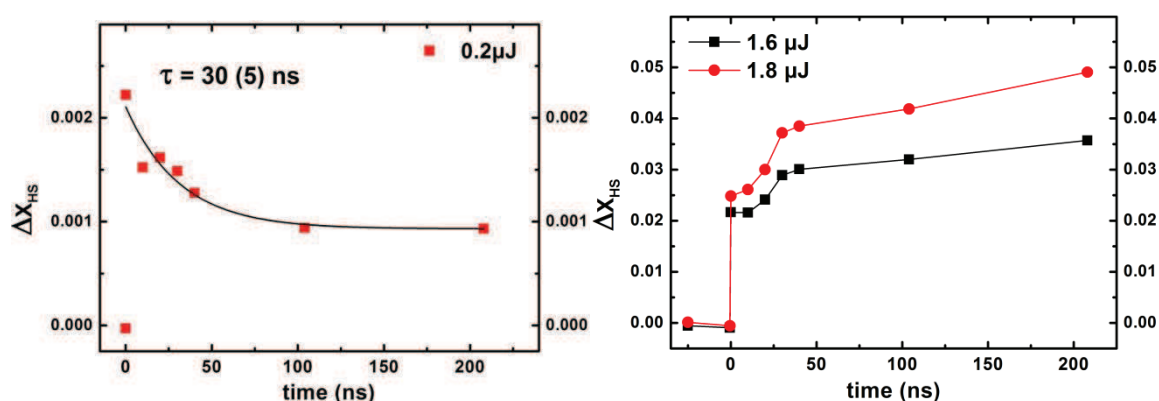
Fig4.18 Switching dynamics around the elastic step below (left) and above (right) elastic threshold.

These data reveal therefore a competition between the elastic switching created at 30 ns and a fast local molecular relaxation. When the initial fraction of photoswitched molecules $\Delta X_{HS}^{h\nu}$ is high, the HS fraction is more than doubled on this step. This is another manifestation of the cooperativity in spin crossover crystal during the out of equilibrium process. On contrary to [Fe^{II}(phen)$_2$(NCS)$_2$] system, the cooperativity can be detected on the elastic effect in [Fe^{III}(3-MeO-SalEen)]PF$_6$ system, probably because in the Fe^{II} system the molecular relaxation is slower than the elastic step itself, as it is known that relaxation from HS state are usually faster in Fe^{III} materials.

Thermal step:

Fig 4.19 shows the normalized plots of the HS fraction on the thermal step at 10 µs and quantifies the relative weight of thermal conversion ΔX_{HS}^{th} as a function of initial fraction of HS $X_{HS}^{h\nu}$:

$$\Delta X_{HS}^{th} - \Delta X_{HS}^{h\nu} = \Delta X_{HS}(100 \ \mu s) - \Delta X_{HS}(10 \ ps)$$

At the µs time scale, the value of HS fraction is always higher than at 10 ps in this compound, what means that a thermal HS population process always exists, contrary to what is observed for [Fe^{II}(phen)$_2$(NCS)$_2$] compound. For low excitation density, the thermal population at µs time scale overcomes the localized fast relaxation anyway. But one interesting features is the non linear character of the thermal switching in function of the pump energy that will be discussed later.
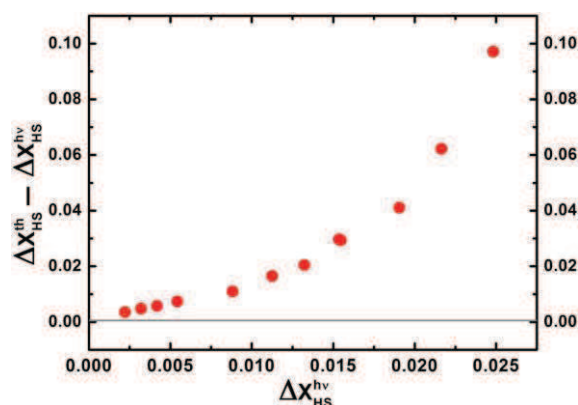
Fig 4.19 *Fraction of HS molecules at 100 ns and 10 µs normalized by the fraction at 10 ps.*
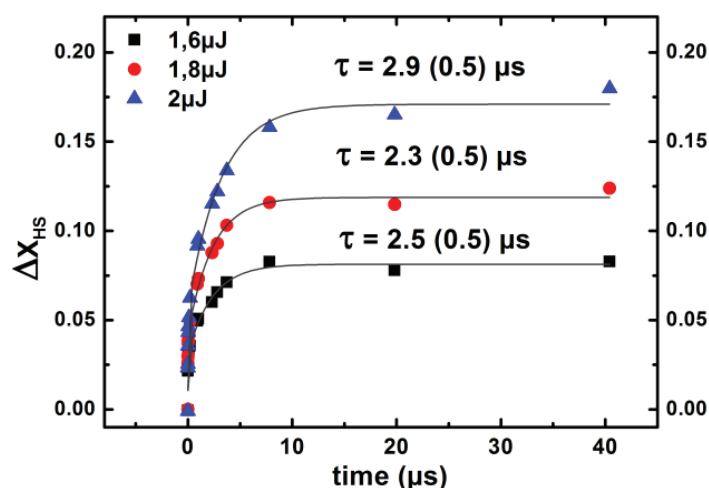
Fig4.20 *Thermal population of the HS state*

Fig 4.20 shows that the population of the HS state also follows nearly an exponential law. The different fits (continuous line) performed for the different excitation densities give an $\approx$ 2 µs time constant. Our data do not allow to extract any excitation density dependence of this time constant. Indeed, the thermal energy (temperature jump ΔT) deposited in the crystal by the laser depends on the excitation density. A transient temperature $T_t = T + \Delta T$ appears in the crystal in the µs range, as confirmed by previous studies on similar materials. The kinetic LS-to-HS population constant $k_{LS\text{-}HS}$ depends on the transient temperature T_t and on the energy barrier E_a between LS and HS potential:

$$k_{LS\text{-}HS} = \exp(-E_a/kT_t)$$

As T=140 K and ΔT is limited to a 20 K range this constant should not change so much for Tt in the 140-160 K range.

4.3.2 Down-sizing effects in [FeIII(3-MeO-SalEen)]PF6

As presented in part 4.1, our time-resolved x-ray diffraction studies revealed a direct relationship between the volume expansion time and the crystal size (**Collet 2012**) which confirms the propagative character of this process. The optical studies above also indicate the stepped evolution of XHS associated with this process. It is therefore relevant to investigate down-sizing effect especially when approaching nanometric scale. A volume ratio of the order of 10^7 exists between single crystal and nanocrystals. Now, it is possible to compare the response of these samples to a femtosecond excitation in function of the sample size. The crystallinity of all the samples has been previously checked by powder diffraction by the groupe of M.-L. Boillot who synthesized these [Fe^{III}(3-MeO-SalEen)]PF$_6$ crystals (**Tissot 2012**). The typical samples dimensions are:

-The single crystal $(200\pm50)\times(300\pm50)\times(10\pm5)$ µm^3
-The so called microcrystals $(7.5\pm2.1)\times(0.64\pm0.15)\times(0.21\pm0.03)$ µm^3
-The so called nanocrystals $(950\pm150)\times(270\pm40)\times(35\pm7)$ nm^3

A single crystal is studied by time resolved spectroscopy in the transmission mode. nanocrystals and microcrystals are also studied in the transmission mode but as we cannot study a single particle, collections of crystals with small size dispersion are embedded in a passive polymer matrics as explained in chapter 3. In order to have an accurate estimation of the down-sizing effects, all the investigations presented here were performed with the same experimental condition as for the single crystal (4.3.1). The temperature is set to 120 K where the system is in the pure LS spin in single crystal and where $X_{HS}<3\%$ for the nano and micro-crystals (**Fig 4.23**). The pump is set to 800 nm and the probe at 550 nm where ΔOD is maximal whatever the size of the sample is. All data are converted in terms of ΔX_{HS} like explained previously.
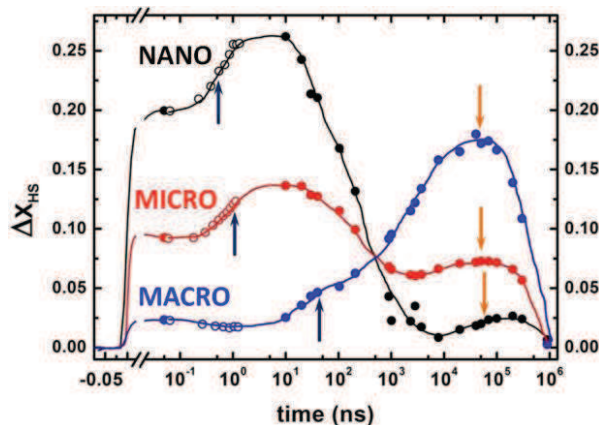
Fig 4.21 Response of the three sizes of crystal at 120 K normalized by the number of incident photons.

Fig 4.21 shows for the 3 sizes of sample the typical response to a femtosecond laser excitation of high energy (120 µJ/mm^2). Due to the wise synchronization of the amplifiers, it is possible to cover the first nanosecond with the delay line (thick line) and to investigate the rest of the time domain with the synchronized setup (full dots), thin lines are guide for the eye. Several informations are provided in this graph.

First the fraction of HS generated at 10 ps is higher with downsizing. It is clearly explained by a better excitation of nanocrystals with regard to the penetration depth at 800 nm (few µm). So microcrystals and even more nanocrsytals are excited in a more homogeneous way, with an overall larger number of photon per molecules in the crystal as the laser penetration depth is around few µm.

Second, a shift of the elastic step by 2-3 decades is observed between single crystal and nanocrystals. It is indicated by the second increase of HS fraction (blue arrow). As observed by x-ray diffraction at the beginning of this chapter, the shift towards shorter time is expected when size of the system decreases. It occurs around 20 ns for the 20 µm thick single crystal, around 1 ns for the microcrystal and around 300 ps for the nanocrystals.

Third, a thermal activation is always observed at around 50 µs and indicated by the orange arrow. Even if this effect is really small in the sample made of nanocrystals, its 50 µs time scale is not affected by the size of the sample. As discussed for the single crystal case, the thermal population of the HS state is driven by barrier energy overcoming between LS and HS states. It follows a kinetic constant that is not affected by the size of the sample but refers to local molecular potential. Even if this process is observable in microcrystals and nanocrystals, it is smaller than in single crystal case.

Single crystal

Nanocrystals in polymer

Heat diffusion

From crystal to polymer

Active medium
In contact with N$_2$
cryostream

Active medium

In a passive polymer

Not absorbing optical energy
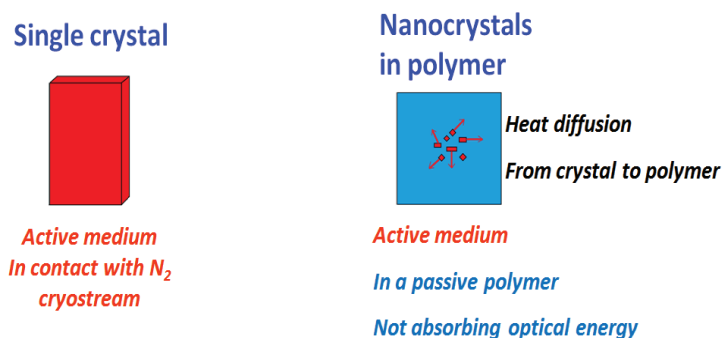
Fig 4.22 *Schema of Single crystal and Nano crystals at time scale when the transient temperature is homogeneous.*

This can be attributed to environment effect. Indeed, for the single crystal, the heating due to laser excitation is relaxed by cooling the crystals with a nitrogen gas flow (**Fig 4.22**). It was underlined that this heat transfer to the cryostat may be too slow to investigate fast relaxation processes (**Enaschescu 2006**) and the sample cooling is the limiting factor for the relaxation of the transient HS state formed. This is the case here for single crystals in the cryostream. On contrary, in nanocrystals and microcrystals the crystals are embedded in a polymer, which is cool down by the cryostat. But this polymer does not absorb the pump pulse at 800 nm and is a passive medium, so there is no laser heating of polymer by the laser pulse. The optical energy, which is only absorbed at the level of the nanocrystals can be rapidly dissipated to the polymer by heat transfer from the crystals to the polymer. This process depends on the surface/volume ratio and is therefore even more efficient in the nanocrystals than in the micro-crystals. The thermally populated HS fraction due to this global warming of the sample relaxes within 300 µs. If the energy is released fast enough like in nanocrystals, this thermal activation can suppressed as no excess energy remains in the 1-10 µs range. Microcrystals show an intermediate behavior where the system starts to relax at ns scale. But this relaxation is not fast enough and some energy remains at µs time scale generating thermal switching.

The more efficient heat transfer from the crystal towards the polymer can be explained the quite different surface/volume ratio as it is 5 times larger for the nano-crystals than for the micro-crystals:

-microcrystals: $V = 1\ \mu m^3$ $S = 13\ \mu m^2$ $S/V = 13\ \mu m^{-1}$

-nanocrystals $V = 0.008\ \mu m^3$ $S = 0.6\ \mu m^2$ $S/V = 75\ \mu m^{-1}$

Therefore the heat transfer is more than more efficient for the nanocrystals than for the microcrystals. The heat diffusivity in such systems corresponds to typical values of $10^{-6} m^2 s^{-1}$ (**Lorenc 2009**). Given the typical 10^{-7} m size here, the heat diffusion time-scale within the micro- or nano-crystals is of the order of 10 ns, but the limiting factor may be the quality of the crystal-polymer interface.

Due to the size, the excitation is almost homogeneous in nano and micro crystals. This result underlines the influence both of the size and the environment in the out of equilibrium cascading process. The first photoswitching process is a local molecular event (chapter 3) and it does not depend of the size or the environment. The second acoustic step involving propagating effects is directly proportional to the size of the crystal and can occurs in 100 ps range for nanometric system. The thermal switching is independent of the size because driven by kinetic constant related to the energy barriers between LS and HS states (1-10 μs), as the optical energy of each photon promoting an electron to the LMCT state is much higher than the energy difference of the HS and LS states. But this step resulting from conversion of optical excess energy to heat in the crystal may be suppressed by environment effect like mentioned in nanocrystals, because an efficient heat transfer may occur on a time-scale shorter than the thermal activation. For going deeper in this investigation we study hereafter how the out-of-equilibrium process depends on temperature.

4.3.3 Temperature and excitation density effects in nano and micro-crystals

For going deeper in the investigation of the out-of-equilibrium process, we present here the response of nano and micro crystals to a femtosecond laser pulse fs promoting LS molecules to the HS state through the LMCT band. The collection of nanocrystals or microcrystals in the polymer film undergoes a similar crossover behavior during the thermal conversion. The temperature dependence of the HS fraction of nanocrystals and microcrystals shown in **Fig 4.23**, which was obtained by measuring the temperature dependence of optical density as explained previously, show that both crossover are slightly shifted by 3 K in the $T_{1/2}$ value.
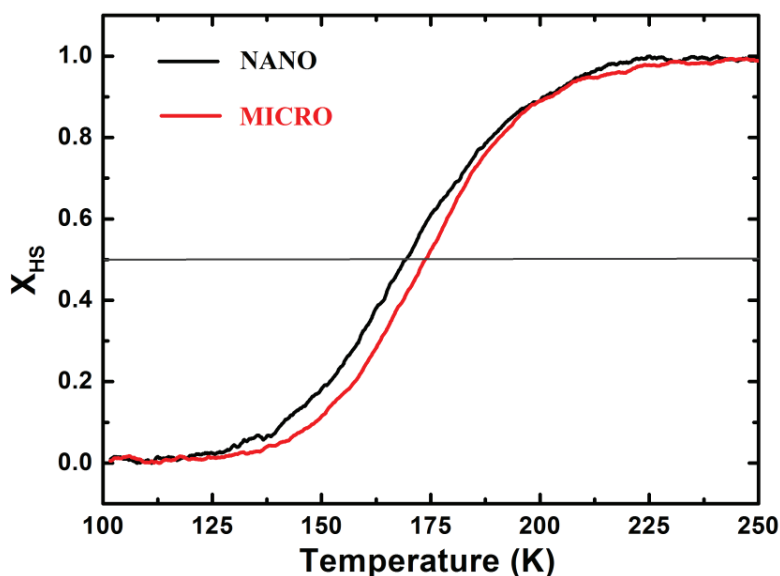
Fig4.23 *HS fraction during thermal conversion for micro and nanocrystals.*

Compared to the single crystals, we observe the loss of 1st order spin transition (**Fig 4.23**). This effect was also reported for another system (**Tissot 2013**) and current investigations tend to incriminate both pressure effect and anchoring process to the polymer.

Fig 4.24 shows the time dependence of the HS fraction after femtosecond laser excitation for microcrystals and nanocrystals, for different temperatures and for different excitation densities. The time dependent data are quite similar for both systems, as introduced in **Fig 4.21**, except that the thermal step resulting from laser heating at µs delays is larger in micro-crystals.

At 100 K, ΔX_{HS} is maximum at 10 ps and relaxes after in the 10 ns-1µs time window.

At 120 K and 140 K, similar behaviors as at 100 K are obtained for low excitation densities. But for high energy, a second increase is observed at ns time scale during the elastic step.

At 160 K and 180 K, this second increase always occurs whatever the pump energy is. Some thermal conversions at µs range are observed in microcrystals especially at 120 K and 140 K. This effect is almost nonexistent in nanocrystals confirming that an efficient heat transfer toward the polymer occurs.

Microcrystals   **Nanocrystals**
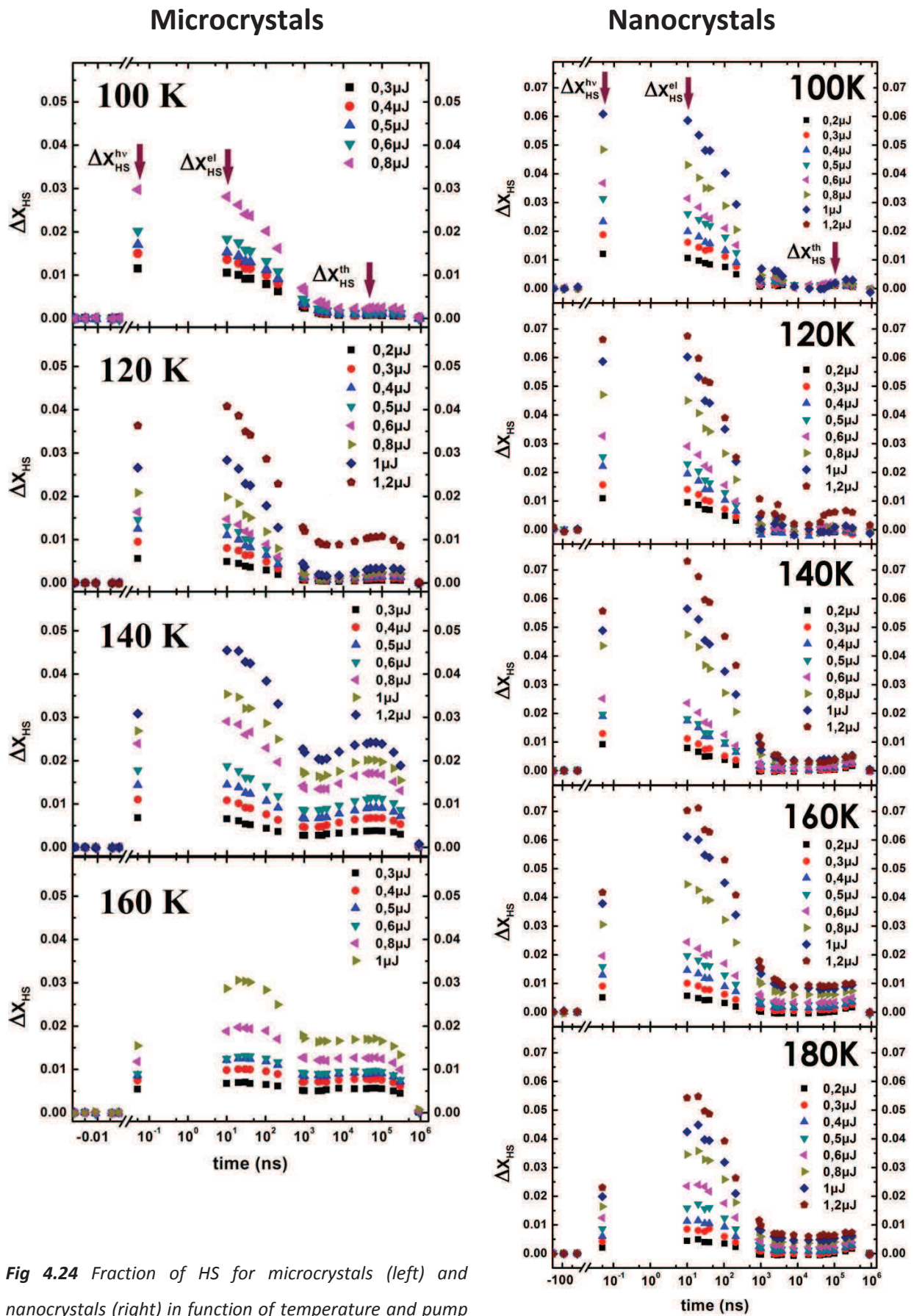
Fig 4.24 *Fraction of HS for microcrystals (left) and nanocrystals (right) in function of temperature and pump energy. 1 µJ per pulse = 56 µJ/mm².*

Femtosecond photo-switching:

The fraction of molecules photoswitched towards the HS state $X_{HS}{}^{h\nu}$ at ps time scale depends on excitation density at any temperature for nano- and micro-crystals. **Fig 4.25** indicates that at a given temperature the response shows a linear dependence with the excitation density, as it is the case for the single crystals (**Fig 4.16**): each photon transforms a single molecule. The main difference is that in the single crystal case, the system is always fully LS at low temperature because of the first-order nature of the thermal transition.
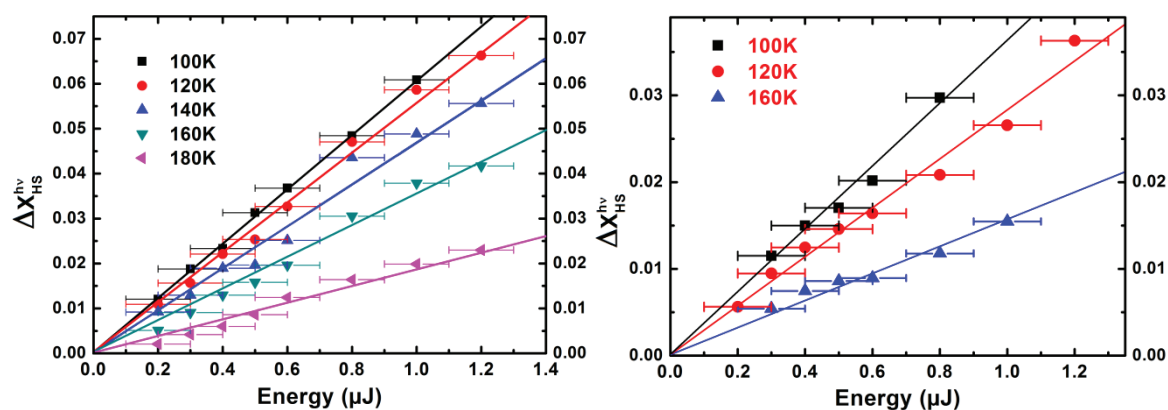
Fig 4.25 *Fraction of HS at 10 ps in function of T and Pump energy for nanocrystals (left) and microcrystals (right)*

In the present case, the initial fraction of molecules in the LS state $X_{LS} = 1 - X_{HS}$ decreases when temperature increases above 120 K (as X_{HS} increases, **Fig 4.23**). Only molecules in the LS state absorb the IR photons in the LMCT bands (chapter 3), driving LS-to-HS switching and that is the reason why response of the systems at any excitation density should be weighted by the initial fraction of molecules in the LS state at a given temperature (**Lorenc 2012**).
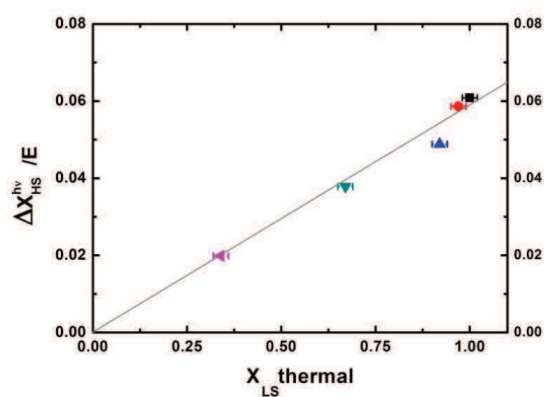
Fig 4.26 *Evolution of the slope of the signal at 10 ps/µJ with the initial LS fraction.*

This is therefore also true for the slope of the photoresponse with excitation density, given here in $X_{HS}{}^{h\nu}$/µJ. **Fig 4.26** indicates that this condition is well fulfilled, with the linear dependence of

these slopes with the initial fraction of LS molecules, as these two parameters are perfectly correlated. Again, this underlines the local nature of the photoswitching response, showing a linear response to excitation density, whatever the initial equilibrium mixture between HS and LS is.

Elastic step:

Fig 4.27 shows the evolution of the fraction of molecules converted during the elastic step elastic step with respect to the fraction of photo-switched molecules, as introduced in **Fig 4.17** and by using the same methods as exposed for single crystal. Here again, the same kind of threshold effect is observed. We notice a strong shift of the threshold value of $X_{HS}{}^{h\nu}$ for having amplification on the elastic step, i.e. a larger HS fraction than after the photo-switching step. It is higher than 6% at low temperature for nanocrystals and the threshold disappears above 140 K. At really low temperature we could not detect an elastic switching with the excitation density used. Higher excitation densities resulted in sample damage.
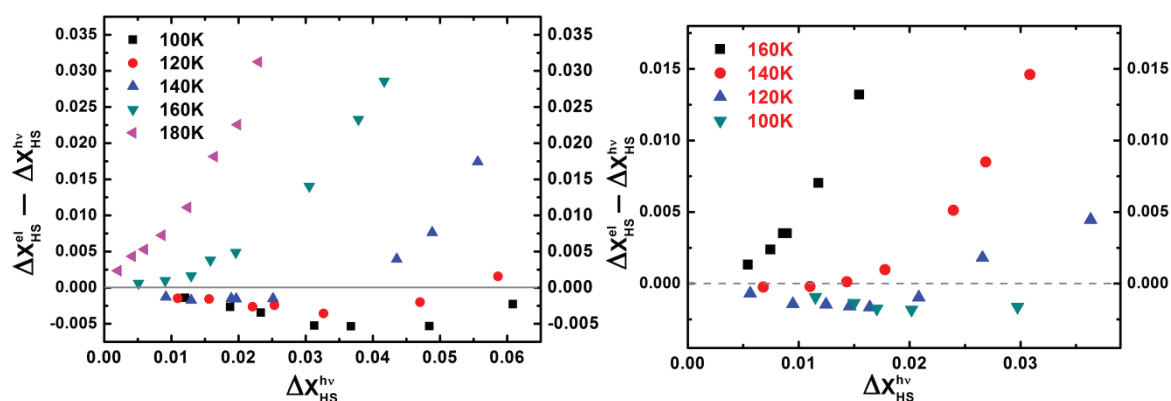
Fig 4.27 Elastic switching in function of pump energy and temperature for nano (left) and micro (right)

One interesting point is the competition between the elastic step and the ns relaxation, better seen in **Fig 4.24** with the measurements in the 1 ns range performed with the delay line and the synchronized amplifiers, in a similar way to what is observed for the single crystal of this compound (**Fig 4.18**). It suggests that for low fraction of photoswitched HS molecules, the relaxation of each molecule is independent and shows the local molecular character of this relaxation. But if the number of HS molecules created in the crystal is high enough, they start to feel the effects induced by the other photo-switched molecules and the elastic step takes over.
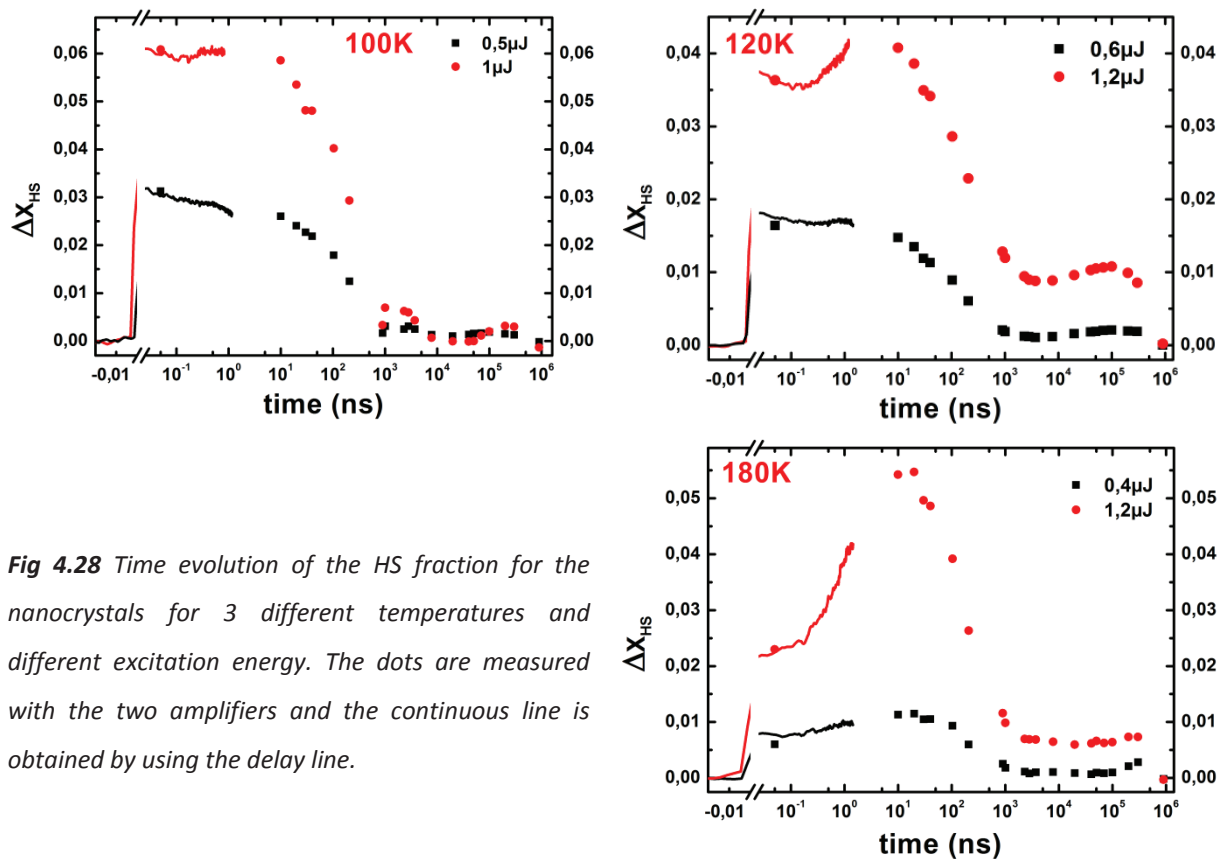
Fig 4.28 *Time evolution of the HS fraction for the nanocrystals for 3 different temperatures and different excitation energy. The dots are measured with the two amplifiers and the continuous line is obtained by using the delay line.*

The 3 graphs in **Fig 4.28** also evidence 3 different cases: At low temperature (100 K), ΔX_{HS} always decreases after photoswitching. An approaching the crossover at 120 K, for low excitation the system relaxes at ns scale like at 100 K, with a 200 ns time constant (**Fig 4.29**) higher than the 30 ns observed in single crystal at 140 K. This is not so surprising as the relaxation kinetic constant of such a thermally activated relaxation process is strongly temperature dependent. For higher excitation density, an elastic switching occurs around 500 ps. At higher temperature the system does relax at ns scale even with a small fraction of HS created at ps scale as the elastic step strongly increases with excitation density, especially around the middle of the crossover ($\approx$180 K).
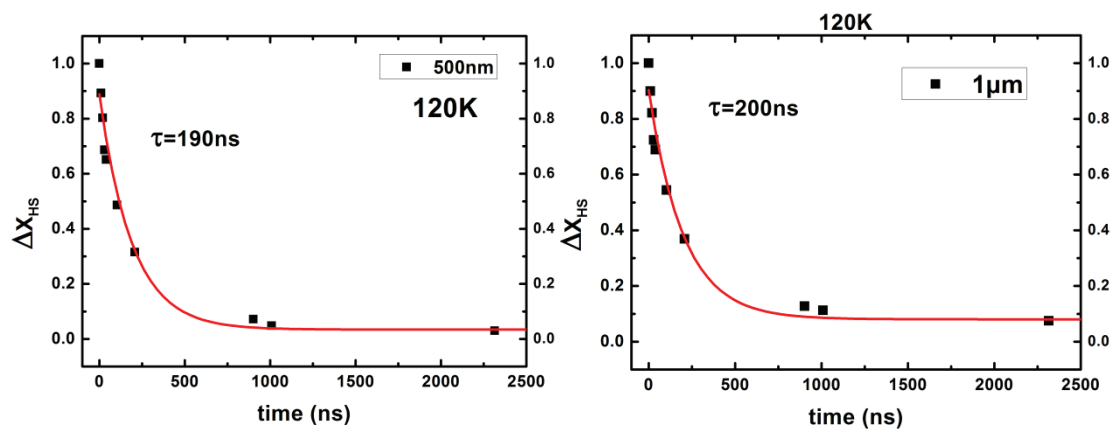
Fig 4.29 *Relaxation of HS fraction to LS at 120K in nano (left) and micro (right).*

4.4 Discussion

The results presented here in the different compounds show consistent results, revealing different steps during the out-of equilibrium process. The combination of time resolved X-ray diffraction, XANES and fs optical spectroscopy gives an overview of the cascading photoswitching, elastic and thermal steps. We can underline here the main conclusions from these comparative studies.

The photo-switching step is a purely local process, not showing any indication of cooperative response, but a simple local photoswitching from LS to HS state, with a linear dependence of the fraction of molecules photoswitched $\Delta X_{HS}^{h\nu}$ with the excitation density and the initial LS population. This process described in detail in chapter 3 shows no difference with the response of independent molecules in solution. The nature of the excitation process used for Fe^{II} or Fe^{III} (LMCT or MLCT) does not affect the local and linear nature of this process.

This local photo-switching induces strain at the local level, but also at the crystal level when the penetration depth is small compared to the crystal size. This results from the larger molecular volume of the photoswitched species (due to Fe-ligand distance elongation). It generates acoustic phonons are but these ones do not switch additional molecules from LS to HS state.

An additional conversion from LS to HS state, mediated by elastic interactions between the molecules in the crystal, is only observed as concomitant with the macroscopic lattice expansion of the crystal, with a kind of latency of the order of 2-20 ns for single crystal (depending on the thickness) and of 400 ps for nanocrystals (**Fig 4.22**). The dynamics of this elastic step is size dependent and the typical time scales correspond to propagation of elastic wave over the typical crystal sizes. This step is mainly observed in the vicinity of the thermal conversion temperature $T_{1/2}$.

The laser heating of the crystal, resulting from the absorbed optical energy, drives a thermal population of the HS state. The time constant of this process is of the order of 300 ns-2 µs depending on the molecular system investigated. But for a same system in the form of single, microcrystals or nanocrystals the kinetic constant for describing the thermal population from LS to HS state remains the same, as the thermal conversion occurs on µs time scale.

The discussion about the photo-switching step being detail in chapter 3, we will discuss hereafter the two other steps involved in the out-of-equilibrium process: the thermal population and the elastic step.

4.4.1 Thermally driven LS-to-HS and HS-to-LS conversion:

There are two processes describing thermally-assisted conversions after the photo-switching step:

- the relaxation of the photoinduced HS molecules to the stable LS potential

- the thermal conversion from LS to HS state.

Such conversions are described by the energy barrier law and as we are dealing with high temperature the main mechanism is a classical process across the LS/HS energy barriers (**Fig. 4.30**). For the Fe^{III} system, a fast HS->LS relaxation at low excitation density is observed with a time constant of 30 ns. This is in the range reported for several systems, often studied in solution (**Gawelda 2006, Brady 2004**). The relaxation is not observed for the Fe^{II} system. It is well known that the molecular distortion is larger in Fe^{II} systems than in Fe^{III} system, and the position of the potential well of the high-spin state relative to the potential well of the low-spin state depends on the metal-ligand bond lengths. Upon spin-state switching it increases by 0.2 Å for Fe^{II} and 0.15 Å for Fe^{III}. Hauser explains this as being due to the Franck-Condon factor (shaded area) increasing exponentially with decreasing bond length difference, strongly increasing the high-spin->low-spin relaxation rate (**Fig 4.31**).
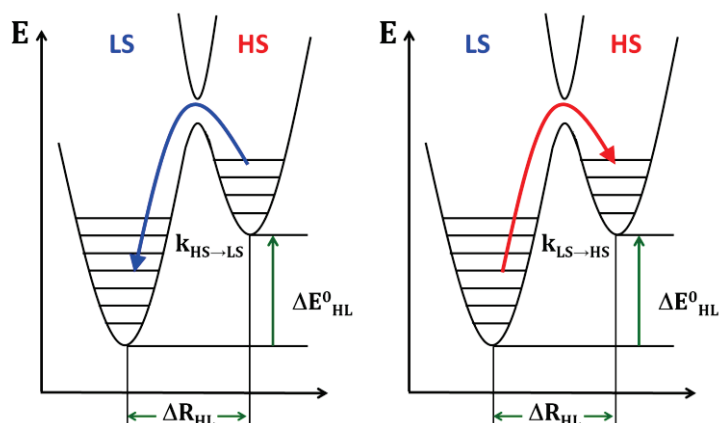
Fig 4.30 Schematic representation of the potential wells of the high-spin and the low-spin state along the normal coordinate, where at elevated temperatures, tunneling occurs as an activated process from thermally populated vibrationnal levels of the spin states.
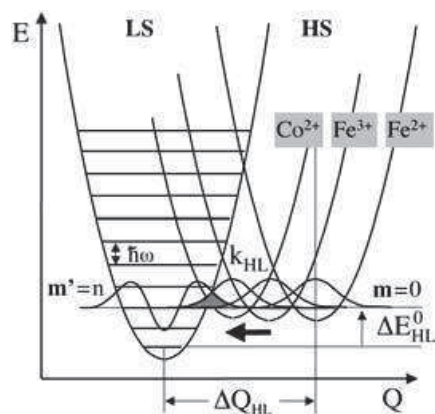
Fig 4.31 *Schematic representation of the potential wells of the high-spin and the low-spin state for Fe^{II} and Fe^{III}*

*system, (**Hauser 2004**).*

In all the system studied here, the observed increase of HS fraction at μs time scale results from the thermal population of the HS state. This effect is directly related to the crystal heating by the dissipation of energy absorbed the molecules. By electron-phonon and phonon-phonon coupling, the lattice becomes hot and the temperature of the crystal increases by ≈ 20 K. In the case of [Fe^{III}(3-MeO-SalEen)]PF$_6$ single crystal at 140 K, this dynamic occurs with a time of constant of τ ≈ 2 μs, or k ≈ 5.10^{-5} s^{-1}. In the case of [Fe^{II}(Phen)$_2$(NCS)$_2$] , this kinetic seems faster (270 ns , or k ≈ 4.10^{-6} s^{-1}) but it is only observed at high temperature or high excitation density, with a clear threshold of excitation density (**Fig 4.21**). This cannot be explained by a global increase of temperature above the transition temperature. Were it the case, the entire sample would switch and the lattice parameters would correspond to the HS phase, which the experiments contradict. We associate this effect with a local thermal population process. The group of E. Freysz reported similar time scales for the thermal population of HS state induced by ns laser in other Fe^{II} SCO solids (**Gallé 2010**).

Another intriguing point is the non-linear character of the thermal population of the HS state in [Fe^{III}(3-MeO-SalEen)]PF$_6$ (**Fig 4.19**), whereby the fraction of HS molecules increases non-linearly with the excitation density. This non-linear response is even more striking in the case of [Fe^{II}(Phen)$_2$(NCS)$_2$], which shows a threshold excitation density for the thermal population (**Fig 4.7**). It has been shown that LS to HS conversion may be regarded as tunneling for thermally populated levels of HS having large Franck Condom factors with the corresponding vibrationnal levels of LS state (**Hauser 2004**). There are two parameters which may explain this non-linear effect. The first one is that the overlap between the vibrationnal level of HS and LS states is higher when temperature is higher (**Fig 4.32**). The other one is that in cooperative systems the relative position in energy of the HS and LS potential depends on the HS fraction. We may therefore consider that when a threshold $\Delta X_{HS}^{h\nu}$ value is reached, the HS potential decreases enough for allowing LS->HS conversion. This increase of tunneling efficiency may be non-linear with the increase of temperature, and this is what we observe in [Fe^{II}(Phen)$_2$(NCS)$_2$]: when thermal switching occurs at 160 K for a low excitation density, it is not observed at 140 K.
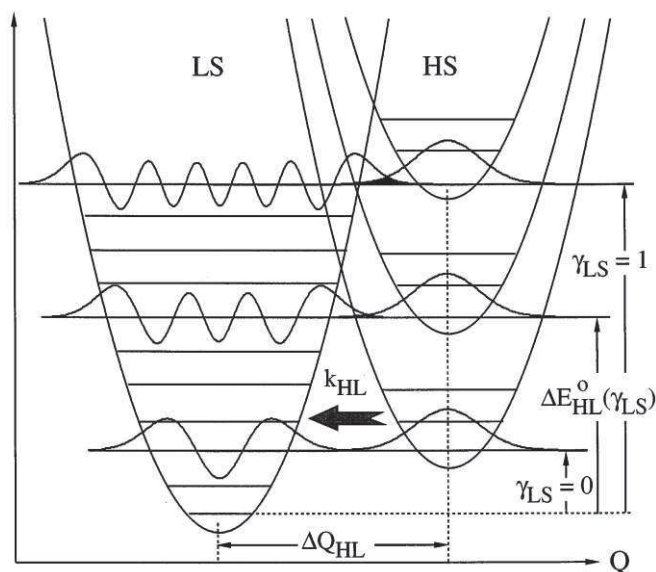
Fig 4.32 Schematic representation of HS and LS potential wells in cooperative spin crossover compounds, for

which the zero-point energy difference $\Delta E°_{HL}$ on the LS fraction.

The experimental set-up used and the compounds investigated do not allow extending these studies over larger temperature range of the thermal conversion. The limited thermalization power of the cryostream and the relaxation rates needed for performing pump-probe measurements limit our investigations to a narrow temperature range. In the case of nanocrystals this thermal conversion is much smaller or suppressed under some conditions.

But, in all this case the pertinent parameter which drives the relaxation is no more the energy of the system E but the free energy G. The representation of this potential is difficult because the degree of freedom activate in the system vary in time so the representation of such thermodynamic quantities is still a challenge. We use the representation of Energy potential well in order to suggest some reflections.

4.4.2 The elastic step:

The volume in the LS state and the photoinduced HS state is different. Since lattice expansion is not instantaneous, this creates a strain field which is defined by the laser penetration depth at the macroscopic scale. This field triggers lattice expansion observed by x-ray diffraction.
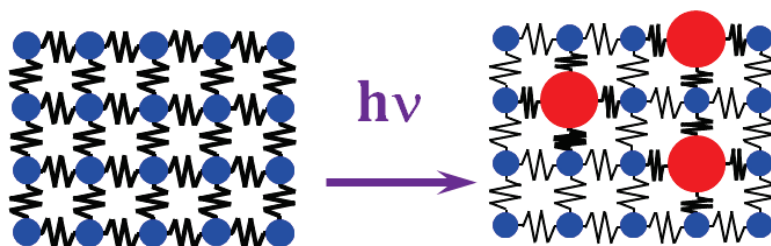
Fig 4.33 Effect of photoswitched HS molecules in a constant LS lattice

At the microscopic scale, the new HS molecules of higher volume interact strongly via elastic coupling with neighboring LS molecules of lower volume, as represented in **Fig 4.33**. The origin of the mechanism driving spin-state switching during elastic step is not well understood. Regarding the relaxation of strain induced by light, we can discuss two limit approaches developed in the literature, depending on the laser penetration depth ξ:

-penetration much smaller than the typical sample size (energy deposited on the surface)

-penetration much larger than the typical sample size (energy homogeneously deposited in volume.

Excitation on the crystal surface:

This case relates the problem to the physics discussed within the picoseconds acoustics. Many simple linear models have been create to solve this problem (**Thomsen 1986, Perrin 2007, Fig 4.34**). They are based on several assumptions:

-The laser pulse duration is shorter than the time needed to observe acoustic transient. It is expressed as $\tau_{laser} \ll \tau_{acoustic} = \dfrac{\xi}{V}$ where ξ is the penetration depth and V the sound velocity in the materials. The system is then described as a 1D problem with an exponential decay of the deposited energy W at the distance z in the material, according to $W(z,t) \propto \xi(1-R)e^{-\xi z}$ with the reflectance R.

Simple models additional assumptions:

-The medium is isotropic and the sample surface stress free.

-The sample is infinitely thick compare to ξ.
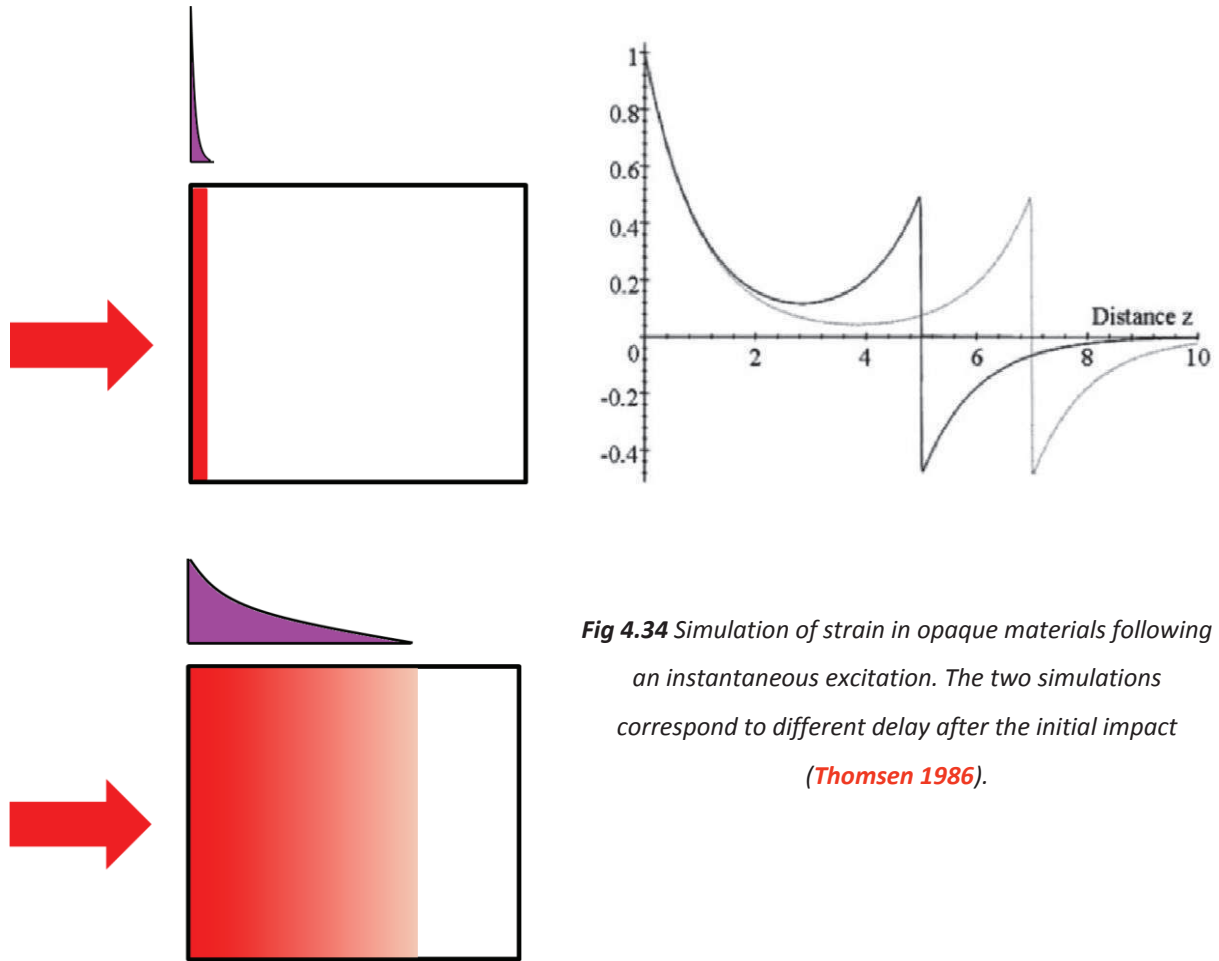
Fig 4.34 *Simulation of strain in opaque materials following an instantaneous excitation. The two simulations correspond to different delay after the initial impact (**Thomsen 1986**).*

In this case a linear approach is possible, so the time and space dependent strain field can be approximated to:

$$\eta(z,t) = \frac{\eta_0}{2}\left[(2 - e^{-KVt})e^{-KV} - \mathrm{sgn}(z - Vt)e^{-K|z-Vt|} \right] \text{(\textbf{Perrin 2007})}$$

Where K is the optical absorption coefficient $K = \frac{1}{\xi}$, η_0 the instantaneous strain created by the laser pulse. In this case shown in **Fig 4.34**, a compression area corresponding to negative value is moving trough z axis following by a dilation zone corresponding to positive value. This acoustic wave propagates at sound velocity in the media. At times long compared to τ_{acoustic}, a static deformation occurs near the surface with a shape defined by the profile of initially deposited energy. Concomitantly, an acoustic wave with compression front followed by decompression moves at sound velocity on the z axis. This model succeeds in reproducing the echo phenomenon observed in opaque system.

In the case of single crystals, 10-20 µm thick with $\xi \approx$ 5-10µm studied here, the model mentioned above is no longer valid. The first static strain field created at t_0 by the photoswitched molecules is more complex to analyze. Still, it will generate acoustic waves propagating at sound velocity. But new problems come into play, as the photoswitched HS molecules relax with typical time constants of the order of nanoseconds. This relaxation is concomitant with a lattice expansion at ns time scale observed by X-ray diffraction. The time of expansion is in agreement with the ratio between the typical dimension of the crystal and the sound velocity in the crystal.

Homogeneous excitation over the crystal volume:

In this second case, a penetration depth ξ much larger than the typical crystals dimension is considered. It is the case for the nano-crystals, for which the excitation may be considered homogeneous throughout the sample. The relaxation of volume induced by a transient internal pressure can therefore be described in a way analogous to the evolution of density of heated liquid. In such a case, the system is homogeneously excited in a volume defined by the laser beam waist and the thickness of the sample (a cylinder defined by the intersection of the beam and sample) (**Wulff 2006, Mirloup 2004**). In our case this volume corresponds to the whole crystal, much smaller than the laser beam waist (**Fig 4.35**).
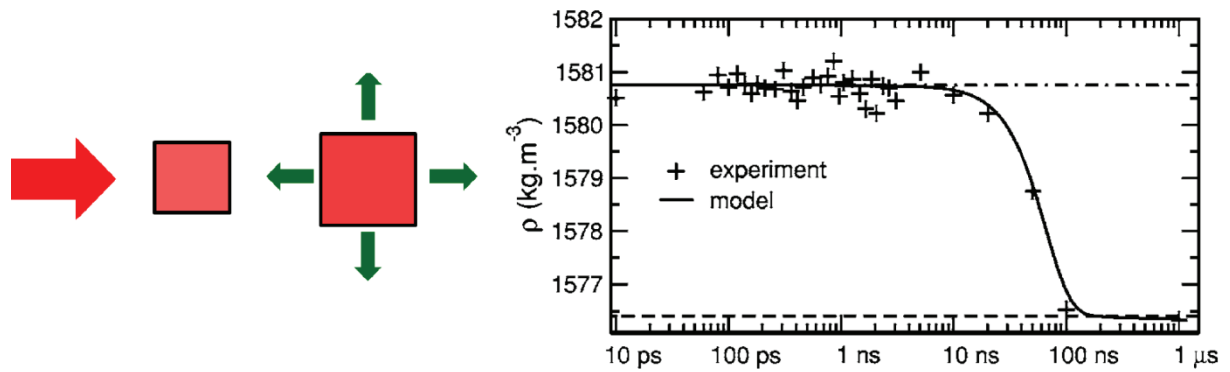
Fig 4.35 *Evolution of the density in a liquid, following fs laser excitation (**Wulff 2006**)*

The classical hydrodynamics under assumption of instantaneous and homogeneous excitation, predict the evolution of the density according to the expression $\Delta\rho(t) \propto \left(e^{-\left(\frac{ct}{L}\right)^2} - 1 \right)$ where ρ is the density, c the sound velocity in the material and L the length of the laser beam waist. This simple model was previously developed by Longaker and Litvak (**Longaker 1969**). If the density is arbitrarily set to 1 before the laser excitation, the volume increases as $\Delta V(t) \propto \frac{1}{\rho} - \frac{1}{\rho_0} \approx \frac{-\Delta\rho}{\rho^2}$. The resulting delay in the expansion has been referred to acoustic horizon, in order to emphasize the fact that dilatation cannot occur faster than at sound velocity (**Fig 4.35**).

By applying this simple formula for different values of L (30µm and 500nm) which correspond to the size of the samples studied here, we can calculate how long the volume takes to expand (**Fig 4.36**). Indeed, in our case the pertinent length L is no more the beam size but the size of the nanocrystallite:
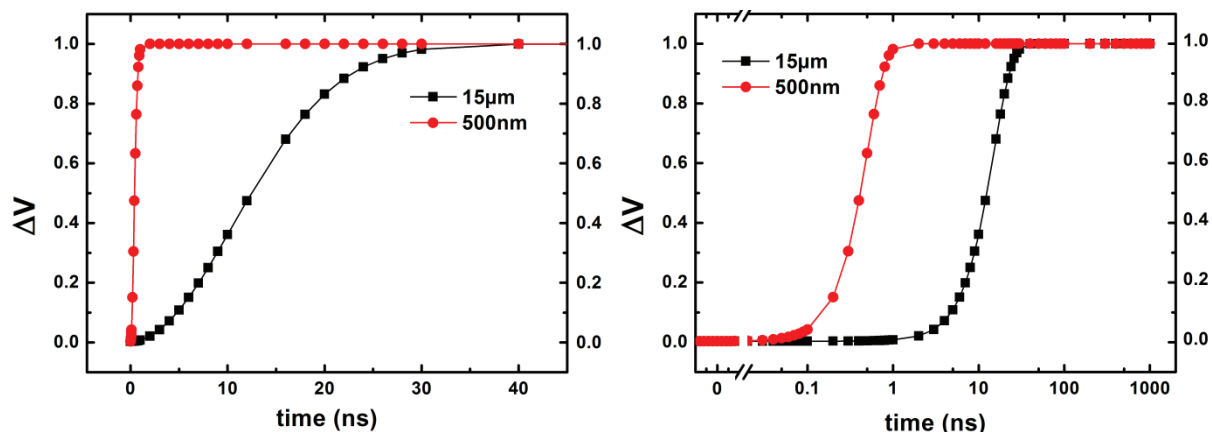
Fig 4.36 Simulation of volume expansion using the homogeneous excitation model

Clearly some time is needed for relaxing the instantaneous and homogenous strain induced by the laser flash in the sample. For instance, the time needed for relaxing the stress should be proportional to the typical dimension of nanocrystals divided by the sound velocity. For nanocrystals of 500 nm and sound velocity of 1 km.s^{-1} , $\tau_{ac} \approx 400$ ps which is in agreement with the expected value (**Fig 4.21 & 4.36**).

All these results indicate that the time scale of this expansion is proportional to the sample size, but it gives no clear answer on the nature of the driving force behind the elastic switching process. We therefore have to discuss in more detail the effect of the internal pressure resulting from the photoswitching of HS molecules with larger molecular volume.

Negative pressure induced by light:

The photo-switching of molecules from LS to HS state in a LS lattice induces at the microscopic scale two effects on the relative stability of HS and LS potentials due to the second coordination sphere:

-the HS molecules feel a positive pressure from the undistorted lattice favoring their relaxation to the LS state.

-the LS molecules feel a negative pressure due to the photoswitched HS molecules, which drive lattice expansion. This internal pressure has two origins: the elastic coupling due to the larger size of the HS state and also the lattice heating as the optical energy is transferred to the lattice after the vibrational cooling.

To some extent, this can be regarded as equivalent to a matrix effect (**Fig 4.37**):

- when SCO molecules are introduced in a lattice made of small passive molecules (top, white circles) the LS state (black) of the switchable molecules is favored (top).

- when SCO molecules are introduced in a lattice made of large passive molecules (bottom, white circles) the HS state (grey) of the switchable molecules is favored (top).

In the present case the new matrix induced by the photoswitched molecules will stabilize the HS state for the molecules which are in the LS state after few ps.
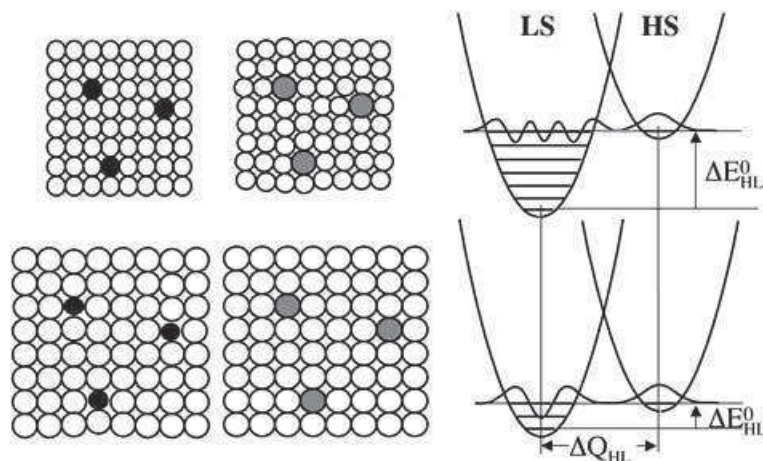
Fig 4.37 Effect of the environment (white) on the HS (grey) and LS (black) potentials. Large molecules in the matrix favor the HS state (bottom).

This microscopic view can be extended to the description of the crossover undergone by the nanocrystals and this will help explaining why the amplitude of the elastic step depends on temperature. It is well-known that SCO can be driven by pressure and temperature and a schematic phase diagram is represented in **Fig 4.38**. At low T, high P the LS state is stable, whereas at high T low P the HS state is favored and at finite temperature, a spin-state crossover can be induced by pressure from HS to LS state. To some extent photoswitching molecules to the HS state in the constant lattice on short time scale corresponds to applying a negative pressure induced by light. Therefore, a system initially in the LS state may switch to the HS state if a negative pressure is applied. The discussion hereafter concerns the molecules which are in the LS state.
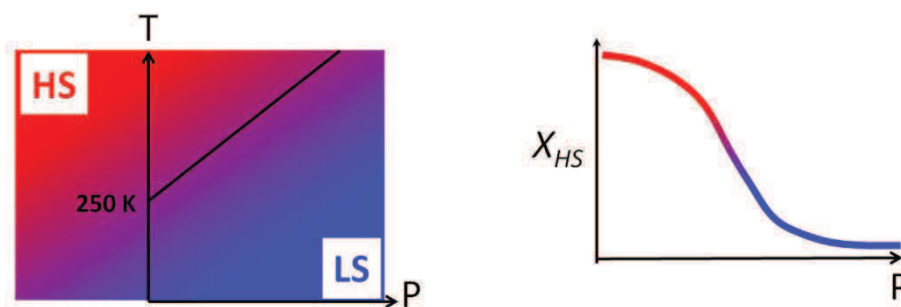
Fig 4.38(P,T) phase diagram and pressure-induced crossover.

The mechanism is schematically described in **Fig 4.37**. A given fraction $\Delta X_{HS}^{h\nu}$ of molecules is photo-switched during the first steps at a given temperature T and ambient pressure (green arrow, A). This generates a negative pressure ΔP in a mainly LS (blue) state, which favors an increase of HS fraction in the elastic step ΔX_{HS}^{el} (red). Therefore ΔX_{HS}^{el} depends on the excitation density: when $\Delta X_{HS}^{h\nu}$ is low ΔX_{HS}^{el} can be lower than $\Delta X_{HS}^{h\nu}$ on the same initial (P_{atm},T) position of the crossover (B). In the case using the same excitation density than in (A), but at a higher temperature T' (P_{atm},T') the position of the pressure-induced crossover is shifted (C) and ΔX_{HS}^{el} can be higher than in (A). The temperature dependence of the elastic step is depicted in **Fig 4.39.** For a constant $\Delta X_{HS}^{h\nu}$, it explains why a threshold exists for the elastic step: if the negative pressure is not strong enough to approach the crossover, the HS fraction on the elastic step decreases, but above a given temperature the negative pressure allows going through the pressure induced crossover. **Fig 4.40** shows in

nanocrystals how the threshold value of $\Delta X_{HS}{}^{h\nu}$ changes with temperature. At low temperature it is necessary to photo-switch $\approx 7\%$ of the molecules for generating a large enough pressure. The threshold disappears between 140 and 160 K, which corresponds to the beginning of the thermal crossover. Any negative pressure above this temperature favors a larger HS fraction. Of course, this relative change due to pressure only is valid when the initial fraction of LS molecules remains close to 1. When the initial temperature is too close to $T_{1/2}$, the limiting effect comes from the lower fraction of LS molecules able to photo-switch.

In the above discussion, we only mention pressure effect and not thermal effect. It is important to underline that the thermal equilibrium (population) of HS fraction only occurs on µs delays. As the elastic step occurs within 500 ps for the nanocrystals (20 ns for the single crystals) the HS fraction has no time to reach its equilibrium value resulting from a transient higher temperature. That is the reason why we slice the (P,T) phase diagram for constant temperature for the HS fraction.

Different steps:

1 the laser creates a fraction $\Delta X_{HS}{}^{h\nu}$ of HS molecules (green arrow)

2 this $\Delta X_{HS}{}^{fs}$ create a negative pressure ΔP
3 the final HS values corresponds to $\Delta X_{HS}{}^{el}$
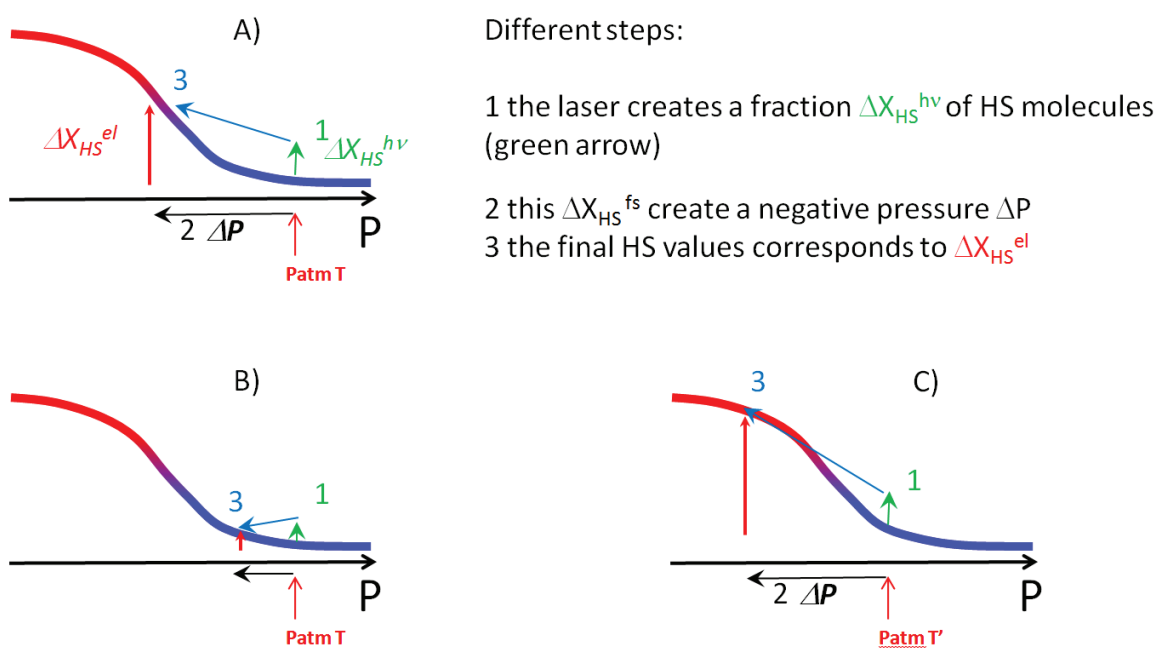
Fig 4.39 *Schematic representation of the negative pressure effect*
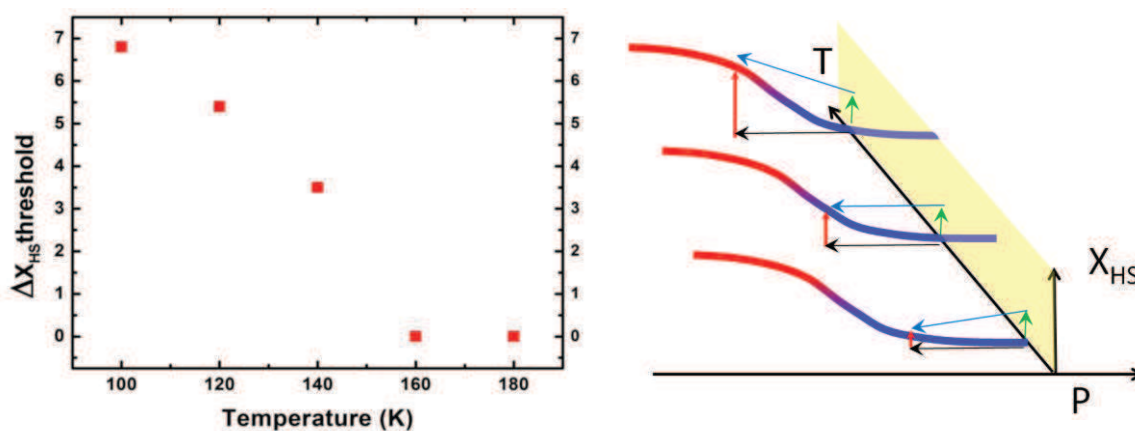
Fig 4.40 *Temperature dependence of the elastic threshold on $\Delta X_{HS}{}^{h\nu}$ (left) and of the negative pressure effect (right).*

130

We can try to roughly estimate the amplitude of this negative pressure induced by light, by comparing our time-resolved x-ray studies to pressure-induced SCO x-ray diffraction studies reported by Granier et al (**Granier 1993**). The lattice parameter in the time domain during the elastic step changes by 0.02%, whereas Granier (1993) reported a 2% change for 5kbars. Therefore in this simple description the elastic step will points to an internal pressure of the order of 50 bars. The (P,T) phase diagram of [Fe^{II}(Phen)$_2$(NCS)$_2$] is reported in **Fig 4.41** from the experimental pressure studies (**Bousseksou 2003, Roux 1996**). At 140 K where our experiment is performed, a negative pressure of 1 kbar is necessary for crossing the equilibrium phase transition line. But we should stress that the present experiments correspond to a highly out of equilibrium processes and on 10 ns timescale many degrees of freedom are not at thermal equilibrium. Therefore describing the out of equilibrium with the phase diagram of thermal equilibrium case does not make sense.

This negative pressure can also be estimated from the structural changes at the microscopic scale. For $\Delta X_{HS}^{h\nu}$ = 4% (value easily reached) one molecule is switched to the HS state in a cubic volume of 3×3×3 molecules. With an intermolecular distance of 10 Å, a 3×3×3 cube has a 20 Å edge. The 0.2 Å molecular expansion in the HS state corresponds therefore locally to a variation of the lattice parameter of 1%. Such a lattice change corresponds to a 2 kbar pressure (**Roux 1996**). We can also notice that whatever the initial value of $\Delta X_{HS}^{h\nu}$, such a structural change with the adjacent molecules always exist. But our data underline that it is mainly the global response of the material that we should consider, because of the latency, rather than the local description.

There is a difference between the 2 kbar estimated from the local structural change and the 50 bar pressure estimated from the lattice expansion measured after the elastic step. But we should not forget that a lot of energy is dissipated during this process for switching LS molecules to HS state, with work or friction. In other words, the elastic step is a non linear process, dissipating energy and the initial internal pressure may be much higher than what is estimated after the elastic step from the lattice expansion.
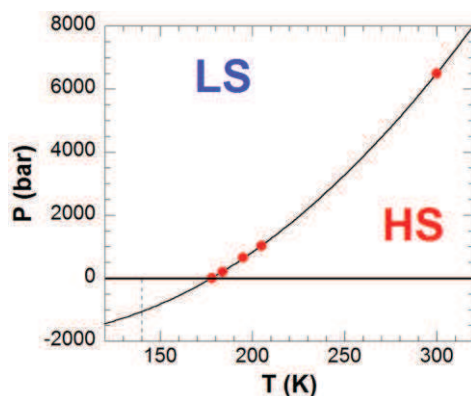
Fig 4.41 (P,T) Phase diagram of [Fe^{II}(Phen)$_2$(NCS)$_2$]

Taking into account internal pressure effect can explain the temperature dependence and the excitation density dependence of the elastic step, as well as the evolution with temperature of the threshold value of $\Delta X_{HS}^{h\nu}$ for generating an elastic step. In order to go further in the understanding of such non trivial effect, the development of new theoretical models is needed.

Collaboration with C. Enaschescu is starting on this topic for applying the mechano-elastic model (**Enachescu 2013**). In this model SCO molecules are considered as sphere and each site is described by the usual energetic and entropy terms. The intermolecular potential is described by springs connecting the molecules on the lattice and a Monte Carlo method is used to determine the switching of the molecules in an open boundary lattice. The idea is to study how an instantaneous

local stress induced by the sudden molecular expansion in a lattice propagates through the crystal and if this can drive molecular switching. A very preliminary result shown in Fig. 4.41 consider an initial state corresponding to our t=1ps state where few molecules (red points) are switched in the initial LS lattice. Each photo-switched molecule is a source of acoustic wave, but the propagation of this wave does not drive molecular switching. The macroscopic rearrangement of the lattice on the timescale of the acoustic propagation over the crystal allows additional switching occurs after this propagation, not during. The results obtained therefore show a latency time between the emission of acoustic wave and switching of LS molecules into HS corresponding well to our experimental observations.
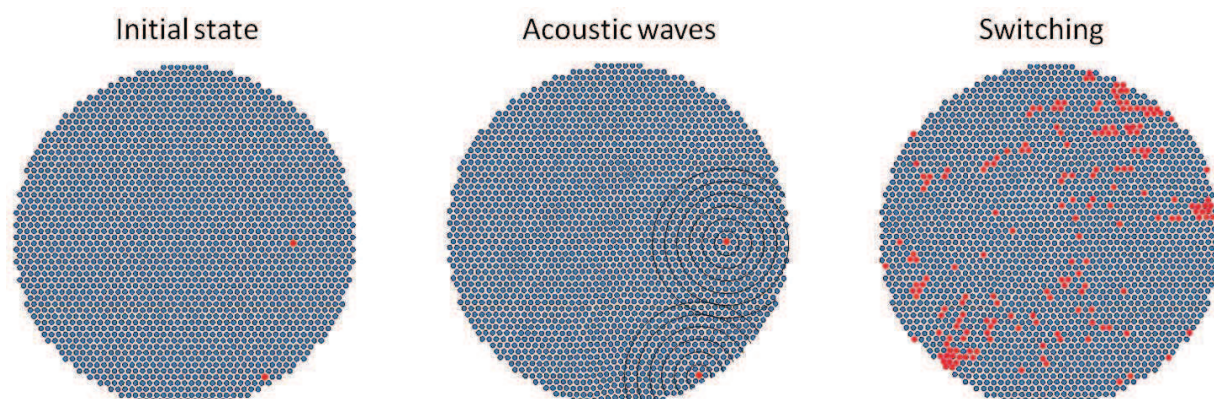
Fig 4.42 Preliminary study on mechano-elastic SCO modelby C. Enachescu et al. .

4.4.3 CONCLUSION

Describing and understanding the complete out of equilibrium process is complex because different types of degrees of freedom of the materials are involved over several decades in space and time: from the ultrafast local molecular switching to the slower macroscopic material response. One of the difficulties we are facing for describing the process is that each degree of freedom has its own time scale corresponding different types of physical processes or to different sub-systems considered (electron, molecule, lattice...). However, the results presented here allow to identify different steps cascading during the out-of-equilibrium process and to underline specific responses, which help understanding the physical processes involved. This is made possible by the use of combined time-resolved techniques: optical spectroscopy, x-ray diffraction and XANES. The first step is the molecular photoswitching, which involves ultrafast ISC, structural reorganization and vibrational cooling. This instantaneous perturbation modifies pressure and temperature in the crystal and leads to lattice dilatation. This expansion is concomitant with a generation of new HS molecules and occurs with time scale proportional to the macroscopic objet. So this elastic step does not correspond to a local switching due to acoustic wave to a macroscopic response (in time and space) of the material.

We should underline that this out-of-equilibrium physics studied in SCO materials showing both photo-induced and thermo-induced switching may be discussed for other types of bi-stable materials. The key difference with regard to out-of-equilibrium dynamics of molecules in solution is that the medium, which the crystal his, plays an active role. The molecules surrounding the photo-switched ones can dissipate energy but can also switch and give rise to the non linear response to excitation density evidenced here for the thermal and elastic steps. This is a perfect illustration of the meaning of what a molecular material is, as in a material molecules do not behave in an independent way. Therefore the response of the material is more than the summation of the individual molecular events.

Conclusion

The results I have obtained during my PhD on the ultrafast photo-switching and out-of-equilibrium dynamics in molecular spin crossover crystals are presented in this manuscript. The general idea behind this work is an attempt to investigate two different aspects related to photo-induced phenomena in material science: the ultrafast molecular switching and the macroscopic out-of-equilibrium dynamics. For performing such investigations, different experimental tools have been used, namely femtosecond optical spectroscopy and ultrafast X-ray diffraction and spectroscopy.

This ultrafast process is the trigger of the overall cascading processes which span over ten decades and involve several degrees of freedom. From the ultrafast dynamics point of view, the investigation of different types of systems (Fe^{II} and Fe^{III}) shed light on the different excitation processes involved. LMCT and MLCT may switch these SCO systems but induce slightly different ISC dynamics. For deepening the understanding of such ISC, a 10 fs setup will be build shortly to investigate in detail the pathway followed by the system from the initial Franck Condom state to the HS state. The better time resolution will allow a better analysis of the coherent structural dynamics both of the <Fe-N> bond length and ligand motion. The tremendous growing of new ultrafast tools for structural science such as femtosecond electron diffraction and the new X-FEL sources will help to investigate such coherent dynamics resulting of the photo-switching. Indeed, some new reports prove the feasibility of ultrafast diffraction in organic system (**Gao 2013**).

The femtosecond XANES experiment also point the direct correlation between the molecular structure and the dynamic of the local molecular trapping. This influence of the structure on such ultrafast dynamics should be explored in the future in order to improve the speed of the ISC and the time need to trap the HS state. Maybe some kind of designing of ligand orbitals may lead to faster process or rigid ligand may avoid fast damping.

The linear response of the femtosecond spin state photo-switching has been clearly evidenced. It results from a local molecular trapping, even in the solid state. The downsizing and the local environment of the crystal do not change the dynamics of this ultrafast process. In addition, the cooperativity relies on 1st order transition do not play a role at this time scale.

But new ways can be explored in order to increase our knowledge on such ISC occurring process. For example the ultrafast dynamic of the opposite process name Reverse-LIESST was not investigated so far and experiments are just starting in the frame of a new collaborating project with A. Hauser and our group. In this case, the photo-switching of HS molecules to the LS state may drive crystal compression if the elastic coupling is strong enough, but this will not be the case if the lattice heating by the excess optical energy takes over.

Now there is plenty of system other than Fe^{II} or Fe^{III} which undergo SCO phenomena like Cu or Co system and very few is known on their ultrafast dynamics. Systems showing stronger structural change with important Jahn Teller distortion should give rise to more important structural dynamics.

Dealing with solid state also raises the question of the (elastic) interaction between the active constituting molecules. The case of SCO is particularly interesting because at each degree of freedom corresponds at typical time scale. So the out-of-equilibrium systems explore different part of the phase space in function of time. The reproduction of the classical 3 steps process in many

different systems confirms the previous mechanism introduced by Lorenc et al (**Lorenc 2009**). But the results presented here are the first attempt of understanding of such out of equilibrium process in strongly cooperative system on timescales spanning from femtosecond to millisecond. These results show that cooperative response emerges on such timescales and give a better understanding of the overall process. In the case of [Fe^{II}(Phen)$_2$(NCS)$_2$], the cooperativity manifests trough a threshold excitation energy in order to observed thermal population. The reflectivity measurement proves the creation of acoustic phonons generated by the freshly created HS molecules. But such an effect is not responsible for the elastic switching as the HS fraction remains constant when acoustic phonons propagate. The elastic switching process is truly scaled on the macroscopic level of the sample, as underlined by the correlation between the size of the sample and the elastic switching dynamics.

In the case of [Fe^{III}(3-MeO-SalEen)]PF$_6$, cooperativity manifest also through elastic interactions at nanosecond time scale and antagonist effects such as the fast molecular relaxation and the elastic switching. The downsizing and confinement of nanocrystals shift the elastic front towards shorter timescales, but their confinement in passive polymer allows a fast dissipation of thermal energy. It opens a new way to study out-of-equilibrium dynamics by suppressing heating effects. The balance between active or passive environment may also be studied by using diluted systems where few SCO molecules are incorporated in neutral matrix. Using matrix made of larger or smaller molecules may enhance or not the cooperativity.

All this work occurs at the interface between chemistry and physics and shows how important it is to work on new systems and try to find new concepts. Thanks to the tremendous growing of ultrafast tools and chemical engineering, a new area where the control, and no longer the observation, is coming.

BIBLIOGRAPHY

A

ALFANO R., « The Supercontinuum Laser Source», Springer, (2006).

ALS-NIELSEN J., McMORROW D., «Elements of Modern X-Ray Physics», Wiley, (2001).

AREZKI B., SCHWARZ G., BODENTIN Y., LUETZENKIRCHEN-HECHT D., MARKERT C., WAGNER R., FRAHM R., KURTH D.G., PIETSCH U., «X-Ray Near-Edge Absorption Study of Temperature-Induced Low-Spin-to-High-Spin Change in Metallo-Supramolecular Assemblies», *ChemPhysChem*, **12**, 2, (2011).

B

BALDE C., « Etude des propriétés optiques, magnétiques et photo-induites dans les matériaux à transition de spin : effets de la dilution de l'ion métallique», (2008).

BAKER S., ROBINSON J.S., HAWORTH C.A., TENG H., SMITH R.A., CHIRILA C.C, LEIN M., TISCH J.W.G., MARANGOS J.P., « Probing Proton Dynamics in Molecules on an Attosecond Time Scale», *Science*, **312**, 5772, p424-427, (2006).

BARANOVIC G., BABIC D., «Vibrational study of the Fe(phen)2(NCS)2 spin-crossover complex by density-functional calculations» *Spectrochimica Acta Part A: Molecular and Biomolecular Spectroscopy*, **60**, 5, p1013-1025, (2004).

BAUM P., YANG D-S, ZEWAIL A.H., «4D Visualization of Transitional Structures in Phase Transformations by Electron Diffraction», *Science*, **318**, 5851, p788-792, (2007).

BECK M., KLAMMER M., LANG S., LEIDERER P., KABANOV V.V., GOLTSMAN G.N., DEMSAR J., «Energy-Gap Dynamics of Superconducting NbN Thin Films Studied by Time-Resolved Terahertz Spectroscopy», *Physical Review Letters*, **107**, 177007, (2011).

BENEDICT J.B., MAKAL A., SOKOLOW J.D., TRZOP E., SCHEINS S., HENNING R., GRABER T., COPPENS P., «Time-resolved Laue diffraction of excited species at atomic resolution : 100 ps single-pulse diffraction of the excited state of the organometalic complex Rh2(μ-PNP)2(PNP)2 BPh4», *Chem. Commun.*, **47**, p1704-1706, (2011).

BERTONI R., LORENC M., TISSOT A., SERVOL M., BOILLOT M.L., COLLET E., « Femtosecond spin-state photo-switching of molecular nanocrystals evidenced by optical spectroscopy », *Angewandte Chemie International Edition*, **51**, p7485-7489 (2012).

BLOEMBERGEN N., «From nanosecond to femtosecond », *Reviews of Modern Physics*, **71**, 2, (1999).

BOILLEAU C., SUAUD N., GUIHERY N., «Ab initio study of the influence of structural parameters on the potential energy surfaces of spin-crossover Fe(II) model compounds », *Journal of Chemical Physics*, **137**, 224304, (2012).

BOILLOT M-L, ZAREMBOWITCH J., ITIE J-P., POLIAN A., BOURDETA E., HAASNOOTD J.G., «Pressure-induced spin-state crossovers at room temperature in iron(II) complexes : comparative analysis; a XANES investigation of some new transitions», *New Journal of Chemistry*, **26**, p313-322, (2002).

BOLDOG I., GASPAR A.B, MARTINEZ V., PARDO-IBANEZ P., KSENOFONTOV V., BHATTACHARJEE A., GUTLICH P., REAL J.A., «Spin-Crossover Nanocrystals with Magnetic, Optical, and Structural Bistability Near Room Temperature», <u>*Angewandte Chemie International Edition*</u>, **47**, p6433-6437, (<u>2008</u>).

BONHOMMEAU S., MOLNAR G., GALET A., ZWICK A., REAL J-S., McGARVEY J., BOUSSEKSOU A., «One Shot Laser Pulse Induced Reversible Spin Transition in the Spin-Crossover Complex [Fe(C4H4N2){Pt(CN)4}] at Room Temperature», *Angewandte Chemie*, **117**, p4137-4141, (2005).

BOSCHETTO D., GAMALY E.G., RODE A.V., LUTHER-DAVIES B., GLIJER D., GARL T., ALBERT O., ROUSSE A., ETCHEPARE J., «Small Atomic Displacements Recorded in Bismuth by the Optical Reflectivity of Femtosecond Laser-Pulse Excitations», *Physical Review Letters*, **100**, 027404, (2008).

BOUKHEDDADEN K., SHTETO I., HOO B., VARRET F., «Dynamical model for spin-crossover solids. I. Relaxation effects in the mean-field approach», *Physical Review B*, **62**, p14796-14805, (2000).

BOUKHEDDADEN K., NISHINO M., MIYASHITA S., «Molecular Dynamics and Transfer Integral Investigations of an Elastic Anharmonic Model for Phonon-Induced Spin Crossover», *Physical Review Letters*, **100**, 177206, (2008).

BOUSSEKSOU A., NASSER J., BOUKHEDDADEN K., VARRET F., «Ising-like model for two-step spin-crossover», *J. Phys.I*, **2**, p1381-1403, (1992).

BOUSSEKSOU A., MOLNAR G., TUCHAGUES J-P., MENENDEZ N., CODJOVI E., VARRET F., «Triggering the spin-crossover of Fe(phen)2(NCS)2 by a pressure pulse. Pressure and magnetic field induce 'mirror effects'», *C. R. Chimie*, **6**, p329–335, (2003).

BRADY C., McGARVEY J., McCUSKER J.K., TOFTLUND H., HENDRICKSON D.N., «Time resolved relaxation studies of spin crossover systems in solutions», Springer, Berlin, **234**, p155-198, (2004).

BRÉFUEL N., <u>WATANABE H.</u>, <u>TOUPET L.</u>, COME J., MATSUMOTO N., <u>COLLET E.</u>, TANAKA K., TUCHAGUES J.P., «Concerted Spin Crossover and Symmetry Breaking Yield Three Thermally and One Light-Induced Crystallographic Phases of a Molecular Material», <u>*Angewandte Chemie International Edition*</u>, **48**, p9304-9307, (<u>2009</u>).

BRESSLER C., MILNE C., PHAM V-T., EL NAHHAS A., VAN DER VEEN R.M., GAWELDA W., JOHNSON S.L., GROLIMUND D., KAISER D., BORCA C.N., INGOLD G., ABELA R., CHERGUI M., «Femtosecond XANES Study of the Light-Induced Spin Crossover Dynamics in an Iron(II) Complex», *Science*, **323**, (5913), p489-492, (2009).

<u>BURON-LE COINTE M.</u>, HEBERT J., BALDE C.H., MOISAN N., <u>TOUPET L.</u>, GUIONNEAU P., LETARD J.F., FREYSZ E., <u>CAILLEAU H.</u>, <u>COLLET E.</u>, «Intermolecular control of thermoswitching and photoswitching phenomena in two spin-crossover polymorphs», <u>*Physical Review B*</u>, **85**, 064114 (<u>2012</u>).

BURON M., COLLET E., «Second International Conference On Photo-Induced Phase Transitions», *Journal of Physics : Conference Series*, **21**, (2005).

C

<u>CAILLEAU H.</u>, <u>LORENC M.</u>, <u>GUÉRIN L.</u>, <u>SERVOL M.</u>, <u>COLLET E.</u>, <u>BURON-LE COINTE M.</u>,«Structural dynamics of photoinduced molecular switching in the solid state», <u>*Acta Crystallographica A*</u>, **66**, p189-197, (<u>2010</u>).

CAMBI L., SZEGO L. , *Ber Deutsch Chem Ges*, 64:167, (1931).

CANIZZO A., MILNE C., CONSANI C., GAWELDA W., BRESSLER C., VAN MOURIK F., CHERGUI M., «Light-induced spin crossover in Fe(II)-based complexes : The full photocycle unraveled by ultrafast optical and X-ray spectroscopies», *Coordination Chemistry Reviews*, **254**, (21-22), p2677-2686, (2010).

CAVALLERI A., TOTH C., SIDERS C.W., SQUIER J.A., RASKI F., FORGET P., KIEFFER J.C., «Femtosecond Structural Dynamics in VO_2 during an Ultrafast Solid-Solid Phase Transition», *Physical Review Letters*, **87**, 237401, (2001).

CAVALLERI A., WALL S., SIMPSON C., STATZ E., WARD D.W., NELSON K.A., RINI M., SCHOENLEIN R.W., «Tracking the motion of charges in a terahertz light field by femtosecond X-ray diffraction», *Nature*, 442, 05041 (2006).

CHERNYSHOV D., HOSTETTLER M., TORNROOS K.W., BURGI H-S., «Ordering Phenomena and Phase Transitions in a Spin-Crossover Compound—Uncovering the Nature of the Intermediate Phase of [Fe(2-pic)3]Cl2·EtOH», *Angewandte Chemie International Edition*, **42**, 32, p3825-3830, (2003).

CHOLLET M., GUERIN L., UNCHIDA N., FUKAYA S., SHIMODA H., ISHIKAWA T., MATSUDA K., HASEGAWA T., OTA A., YAMOCHI H., SAITO G., TAZAKI R., ADACHI S-I., KOSHIHARA S-Y., «Gigantic Photoresponse in 1/4-Filled-Band Organic Salt $(EDO-TTF)_2PF_6$», *Science* , **307**, 86-89, (2005).

COBO S., OSTROVSKII D., BONHOMMEAU S., VENDIER L., MOLNAR G., SALMON L., TANAKA K., BOUSSEKSOU A., «Single-Laser-Shot-Induced Complete Bidirectional Spin Transition at Room Temperature in Single Crystals of (FeII(pyrazine)(Pt(CN)4))», *Journal of the American Chemical Society,* **130** , p9019–9024, (2008).

<u>COLLET E.</u>, LEMÉE-CAILLEAU M.H., <u>BURON-LE COINTE M.</u>, <u>CAILLEAU H.</u>, WULFF M., LUTY T., KOSHIHARA S., MEYER M., <u>TOUPET L.</u>, <u>RABILLER P.</u>, TECHERT S., «Laser-induced ferroelectric structural order in an organic charge-transfer crystal», <u>*Science*</u>, **300**, p612-615, (<u>2003</u>).

COLLET E., BOILLOT M., HEBERT J., MOISAN N., SERVOL M., LORENC M., TOUPET L., BURON-LE COINTE M., TISSOT A., SAINTON J., «Polymorphism in the spin-crossover ferric complexes [(TPA)Fe^{III}(TCC)]PF$_6$ », *Acta Crystallographica Section B*, **65**, p474-480, (2009).

COLLET E., «Dynamical structural science», *Acta Crystallographica A*, **66**, p133-134, (2010).

COLLET E., LORENC M., CAMMARATA M., GUÉRIN L., SERVOL M., TISSOT A., BOILLOT M.L., CAILLEAU H., BURON-LE COINTE M., «100 Picosecond Diffraction Catches Structural Transients of Laser-Pulse Triggered Switching in a Spin-Crossover Crystal», *Chemistry: A European Journal*, **18**, p2051-2055, (2012).

COLLET E., MOISAN N., BALDE C., BERTONI R., TRZOP E., LAULHÉ C., LORENC M., SERVOL M., CAILLEAU H., TISSOT A., BOILLOT M.L., GRABER T., HENNING R., COPPENS P., BURON-LE COINTE M., « Ultrafast spin-state photoswitching in a crystal and slower consecutive processes investigated by femtosecond optical spectroscopy and picosecond X-ray diffraction », *Physical Chemistry Chemical Physics*, **14**, p6192-6199, (2012).

CONSANI C., PREMONT-SCHWARZ M., CANIZZO A., EL NAHHAS A., VAN MOURIK F., BRESSLER C., CHERGUI M., «Vibrational coherences and relaxation in the high-spin state of aqueous [FeII(bpy)3]2», *Angewandte Chemie International Edition*, **48**, 39, (2009).

COPPENS P., BENEDICT J., MESSERSCHMIDT M., NOVOZHILOVA I., GRABER T., CHEN Y-S., VORONTSOV I., SCHEINSA S., ZHENG S-L., «Time-resolved synchrotron diffraction and theoretical studies of very short-lived photo-induced molecular species», *Acta Cryst. A*, **66**, p179-188, (2010).

CORONADO E., GALAN-MASCAROS J.R., MONRABAL-CAPILLA M., GARCIA-MARTINEZ J., PARDO-IBANEZ P., «Bistable Spin-Crossover Nanoparticles Showing Magnetic Thermal Hysteresis near Room Temperature», *Advanced Materials*, **19, 10**, p1359–1361, (2007).

CREUTZ C., CHOU M., NETZEL T.L., OKUMURA M., SUTIN N., «Lifetimes, spectra, and quenching of the excited states of polypyridine complexes of iron(II), ruthenium(II), and osmium(II)», *Journal of the American Chemical Society*, **102** (4), p1309–1319 , (1980).

D

D'AMICO C., LORENC M., COLLET E., GREEN K.A., COSTUAS K., MONGIN O., BLANCHARD-DESCE M., PAUL F., «Probing Charge-Transfer Excited States in a Quasi Non-Luminescent Electron-Rich Fe(II)-Acetylide Complex by Femtosecond Optical Spectroscopy», *Journal of Physical Chemistry C*, **116**, (5), 3719-3727 (2012).

DECURTINS S., GUTLICH P., KOHLER C.P., SPIERING P., HAUSER H., «Light-induced excited spin state trapping in a transition-metal complex : The hexa-1-propyltetrazole-iron (II) tetrafluoroborate spin-crossover system», *Chemical Physics Letters*, **105**, 1, (1984).

DEI A., GATTESCHI D., PARDI L., « Synthesis, characterization, and reactivity of catecholato adducts of iron(III) triaza- and tetraazamacrocyclic complexes: chemical evidence of the role of the metal ion in the oxidative cleavage», *Inorganic Chemistry*, **32**, 8, p1389-1395, (1993).

DIU B., GUTHMANN C., LEDERER D., ROULET B., « Physique Statistique », Hermann, 1989.

E

ENACHESCU C., LINARES J., VARRET F., BOUKHEDDADEN K., CODJOVI E., SALUNKE S.G., MUKHERJEE R., « Nonexponential Relaxation of the Metastable State of the Spin-Crossover System [Fe(L)2](ClO4)2·H2O [L=2,6-Bis(pyrazol-1-ylmethyl)pyridine] »,*Inorganic Chemistry*, **43**, 16, p4880-4888, (2004).

ENACHESCU C., HAUSER A., GIRERD J.-J., BOILLOT M.-L., «Photoexcitation and Relaxation Dynamics of Catecholato–Iron(III) Spin-Crossover Complexes», *ChemPhysChem*, **7**, p1127-1135, (2006).

ENACHESCU C., STOLERIU L., STANCU A., HAUSER A., «Model for Elastic Relaxation Phenomena in Finite 2D Hexagonal Molecular Lattices», *Physical Review Letters*, **102** (25), p257204, (2009).

ERNSTORFER R., HARB M., HEBEISEN C.T, SCIAINI G., DARTIGALONGUE T., MILLER R.J.D., «Experimental Evidence for Electronic Bond Hardening of Gold», *Science,* **323**, (5917), p1033 -1037, (2009).

F

FREYER B, ZAMPONI F., JUVE V., STINGL J., WOERNER M., ELSAESSER T., CHERGUI M., « Ultrafast inter-ionic charge transfer of transition-metal complexes mapped by femtosecond X-ray powder diffraction», *The Journal of Chemical Physics*, **138**, 144504, (2013).

FRITZ D.M., REIS D.A., ADAMS B., AKRE R.A, ARTHUR J., BLOME J., BUCKSBAUM P.H., CAVALIERI A.L., ENGEMANN S., FAHY S., FALCONE R.W., FUOSS P.H., GAFFNEY K.J., GEORGE M.J., HADJU J., HERTLEIN M.P., HILLYARD P.B., HORN-VON-HOEGEN M., KAMMLER M., KASPAR J., KIENBERGER R., KREJCIK P., LEE S.H., LINDENBERG A.M., McFARLAND B., MEYERS D., MONTAGNE T., MURRAY E.D., NELSON A.J., NICOUL M., PAHL R., RUDATI J., SCHLARB H., SIDDONS D.P., SOKOLOWSKI-TINTEN K., TSCHENTSCHER T., VON DER LINDE D., HASTINGS J.B., «Ultrafast Bond Softening in Bismuth : Mapping a Solid's Interatomic Potential with X-rays», *Science*, **315**, p633-636, (2007).

FOUCHE O., DEGERT J., JONUSKAUSKAS G., DARO N., LETARD J-F., FREYSZ E., « Mechanism for optical switching of the spin crossover [Fe(NH2-trz)3](Br)2•3H2O compound at room temperature», *Physical Chemistry Chemical Physics*, **12**, (12)p 3044-3052, (2010).

G

GALLE G., DEGERT J.,MAURIAC C. ,ETRILLARD C., LETARD J-F., FREYSZ E., «Nanosecond study of spin state transition induced by a single nanosecond laser shot on [Fe(NH2 trz)3] compounds inside and outside their thermal hysteresis loops» , *Chem. Phys. Lett.*, **18**, 500 ,(2010).

GALLOIS B., REAL J.A., HAUW C., ZAREMBOWITCH, «Structural changes associated with the spin transition in bis(isothiocyanato)bis(1,10-phenanthroline)iron : a single-crystal x-ray investigation», *Inorganic Chemistry*, **29**, (6), p1152–1158, (1990).

GAO M., LU C., HUBERT J-R., LIU C.L., MARX A., ONDA K., KOSHIHARA S-Y., NAKANO Y., SHAO X., HIRAMATSU T., SAITO G., YAMOCHI H., COONEY R.R., MORIENA G., SCIAINI G., MILLER D.R.J, «Mapping molecular motions leading to charge delocalization with ultrabright electrons», *Nature*, **496**, p343-346, (2013).

GAWELDA W., PHAM V.-T., BENFATTO M., ZAUSHITSYN Y., KAISER M., GROLIMUND D., JOHNSON S.L., ABELA R., HAUSER A., BRESSLER C., CHERGUI M., «Structural Determination of a Short-lived Iron(II) Complex by Picosecond X-ray Absorption Spectroscopy», *Physical Review Letters*, **98**, p57401, (2007).

GAWELDA W., CANIZZO A., PHAM V-T., VAN MOURIK F., BRESSLER C., CHERGUI M., «Ultrafast Nonadiabatic Dynamics of [FeII(bpy)3]2+ in Solution», *Journal of the American Chemical Society*, **129**, (26), p8199-8206 (2007).

GOULIELMAKIS E., UIBERACKER M., KIENBERGER R., BALTUSKA A., YAKOVLEV V., SCRINZI A., WESTERWALBESLOH T., KLEINEBERG U., HEINZMANN U., DRESCHER M., «Direct Measurement of Light Waves», *Science*, **305**, 5688, p1267-1269, (2004).

GRANIER T., GALLOIS B., GAULTIER J., REAL J.A., «High-pressure single-crystal x-ray diffraction study of two spin-crossover iron(II) complexes : Fe(Phen)2(NCS)2 and Fe(Btz)2(NCS)2», *Inorganic Chemistry*, **32**, (23), p5305-5312, (1993).

GUIONNEAU P., MARVICHIE M., BRAVIC G., LETARD J-F., CHASSEAU D., «Structural Aspects of Spin Crossover. Example of the [Fe(II)Ln(NCS)2] Complexes», Springer, Berlin, (2004).

GUTLICH P., HAUSER A., SPIERING H., «Thermal and Optical Switching of Iron(II) Complexes», *Angewandte Chemie International Edition*, **33** , (20), p2024-2054, (1994).

GUTLICH P., GOODWIN H.A, «Topics in Current Chemistry, Spin crossover in Transition Metal Compounds, Vol I», Springer, Berlin, **234**, (2004).

GUTLICH P., GOODWIN H.A, «Topics in Current Chemistry, Spin crossover in Transition Metal Compounds, Vol II», Springer, Berlin, **234**, (2004).

GUTLICH P., GOODWIN H.A, «Topics in Current Chemistry, Spin crossover in Transition Metal Compounds, Vol III», Springer, Berlin, **234**, (2004).

H

HADDAD M.S., LYNCH M.W., FEDERER W.D., HENDRICKSON D.N., «Spin-crossover ferric complexes : curiosities observed for unperturbed solids», *Inorganic Chemistry*, **20**, (1), p123-131, (1981).

HARMAND M., COFFEE R., BIONTA M.R., CHOLLET M., FRITZ D.M., LEMKE H.M., MEDVEDEV N., ZIAJA B., TOLEIKIS S., <u>CAMMARATA M.</u>, «Achieving few-femtosecond time-sorting at Hard X-ray Free Electron Lasers», <u>*Nature Photonics*</u>, **7**, (3), p215-218, (<u>2013</u>).

HAUSER A., «Reversibility of light-induced excited spin state trapping in the $Fe(ptz)_6(BF_4)_2$, and the $Zn_{1-x}Fe_x(ptz)_6(BF_4)_2$ spin-crossover systems», *Chemical Physics Letters*, **124** (6), p543-548, (1986).

HAUSER A., «Cooperative Effects on the HS -> LS Relaxation in the $[Fe(ptz)_6](BF_4)_2$ Spin-Crossover System», *Chemical Physics Letters*, **192** (1), p65-70, (1992).

HAUSER A., JEFTIC J., ROMSTEDT H., HINEK R., SPIERING H., «Cooperative phenomena and light-induced bistability in iron(II) spin-crossover compounds», *Coordination Chemistry Reviews*, **190-192**, p471-491, (1999).

HAUSER A., «Light induced spin crossover and the high spin→ low spin relaxation», Springer, Berlin, **234**, p155-198, (2004).

HAYAMI S., MIYAZAKI S., YAMAMOTO M., HIKI K., MOTOKAWA N., SHUTO A., INOUE K., SHINMYOZU T., MAEDA Y., «Spin-Crossover Behaviors of Iron(III) Compounds with Strong Intermolecular Interactions», *Bull. Chem. Soc. Jpn.*, **79**, 3, p442–450, (2006).

HERCULES (High European Research Course for Users of Large Facilities Systems), « Neutron and Synchrotron Radiation for condensed matter studies», Springer,(1993).

HIRORI H., SHINOKITA K., SHIRAI M., TANI S., KADOYA Y., TANAKA K., «Extraordinary carrier multiplication gated by a picosecond electric field pulse», *Nature Communications*, **2**, 594, (2011).

HUBY N., GUÉRIN L., COLLET E., TOUPET L., AMELINE J.C., CAILLEAU H., ROISNEL T., TAYAGAKI T., TANAKA K.,« Photoinduced Spin Transition Probed by X-ray Diffraction »,*Physical Review B*, **69**, 020101 (2004).

HUSE N., CHO H., HONG K., JAMULA L., DE GROOT F.M.F., KIM T.K., McCUSKER J.K., SCHOENLEIN R.W., «Femtosecond Soft X-ray Spectroscopy of Solvated Transition-Metal Complexes : Deciphering the Interplay of Electronic and Structural Dynamics», *Phys. Chem. Lett.* , **2,** (8), p880-884, (2011).

I

ICHIYANAGI K., HEBERT J., TOUPET L., CAILLEAU H., GUIONNEAU P., LETARD J.F., COLLET E.« Nature and mechanism of photoinduced spin transition in the [Fe(PM-BiA)2(NCS)2] Rapid com », *Physical Review B*, **73**, 060408, (2006).

IHEE H., LORENC M., KIM T.K., KONG Q.Y., CAMMARATA M., LEE J.H., BRATOS S., WULFF M., « Ultrafast X-ray Diffraction of Transient Molecular Structures in Solution», *Science*, **309**, 5738, p1223-1227, (2005).

IWAI S., ISHIGE Y., TANAKA Y., OKIMOTO Y., TOKURA Y., OKAMOTO H., «Coherent Control of Charge and Lattice Dynamics in a Photoinduced Neutral-to-Ionic Transition of a Charge-Transfer Compound», *Physical Review Letters*, **96**, 057403, (2006).

IWAMURA M., WATANABE H., ISHII K., TAKEUCHI S., TAHARA T., «Coherent Nuclear Dynamics in Ultrafast Photoinduced Structural Change of Bis(diimine)copper(I) Complex», *Journal of the American Chemical Society*, **133**, (20), p7728–7736, (2011).

J

JOHNSON S.L., BEAUD P., VOROBEVA E., MILNE C., MURRAY E.D., FAHY S., INGOLD G., «Directly Observing Squeezed Phonon States with Femtosecond X-Ray Diffraction», *Physical Review Letters*, **102**, (2009).

JOHNSON S.L., VOROBEVA E., BEAUD P., MILNE C., INGOLD G., «Full Reconstruction of a Crystal Unit Cell Structure during Coherent Femtosecond Motion», *Physical Review Letters*, **103**, (2009).

JOLY Y., «X-ray absorption near-edge structure calculations beyond the muffin-tin approximation», *Physical Review B*, **63**, 125120, (2001).

JUBAN E.A., SMEIGH A.L., MONAT J.E., McCUSKER J.K., «Ultrafast dynamics of ligand-field excited states», *Coordination Chemistry Reviews*, **250**, p1783-1791, (2006).

JUNG Y.O., LEE J.H., KIM J., SCHMIDT M., MOFFAT K., SRAJER V., IHEE H., «Volume-conserving trans-cis isomerization pathways in photoactive yellow protein visualized by picosecond X-ray crystallography», *Nature Chemistry*, **5**, 212, (2013).

K

KHALIL M., MARCUS M.A., SMEIGH A.L., McCUSKER J.K., CHONG H.H.W., SCHOENLEIN R.W., « Picosecond X-ray Absorption Spectroscopy of a Photoinduced Iron(II) Spin Crossover Reaction in Solution», *Journal of Chemical Physics A*, **110**, p38-44, (2006).

KASZUB W., « Photo-induced phase transitions in molecular materials », (2012).

KASZUB W., BURON-LE COINTE M., LORENC M., BOILLOT M.L., SERVOL M., TISSOT A., GUÉRIN L., CAILLEAU H., COLLET E.,« Spin-State Photoswitching Dynamics of the [(TPA)Fe^{III}(TCC)]SbF$_6$ Complex», *European Journal of Inorganic Chemistry*, **5-6**, p992-1000, (2013).

KASZUB W., et al, *in preparation*.

KIM J-W., VOMIR M., BIGOT J-Y., «Ultrafast Magnetoacoustics in Nickel Films», *Physical Review Letters*, **109**, 166601, (2012).

KOENIG E., MADEJA K, «T$_2$-^{1}A$_1$ Equilibriums in some iron(II)-bis(1,10-phenanthroline) complexes», Inorganic Chemistry, 6, (1), p48-55, (1967).

KOSHIHARA S-Y., TAKAHASHI Y., SAKAI H., TOKURA Y., LUTY T., S "Photo-induced Cooperative Charge Transfer in Low Dimensional Organic Crystals", *The Journal of Physical Chemistry B*, **103**, 14, p2592, (1999).

KSENOFONTOV V., GASPARD A.B., GUTLICH P., «Pressure effect studies on spin crossover and valence tautomeric systems», Springer, Berlin, **234**, p155-198, (2004).

KRIVOKAPIC I., CHAKRABORTY P., BRONISZ R., ENASCHESCU C., «Significant variation of the singlet-quintet intersystem crossing rate constant in an iron(II) high-spin complex as a function of temperature», *Angewandte Chemie*, **49**, p8509-8512, (2010).

KUBICKI J., ZHANG Y., WANG J., LING LUK H., PENG H-L, VYAS S., PLATZ M.S., «Direct Observation of Acyl Azide Excited States and Their Decay Processes by Ultrafast Time Resolved Infrared Spectroscopy», *Journal of the American Chemical Society,* **131** , p4212–4213, (2009).

KUBICKI J., LING LUK H., ZHANG Y., VYAS S., WANG J., PENG H-L., HADDAD M.C., PLATZ M.S., «Direct Observation of a Sulfonyl Azide Excited State and Its Decay Processes by Ultrafast Time-Resolved IR Spectroscopy», *Journal of the American Chemical Society,* **134** , p7036–7044, (2012).

KUSZ J., SPIERING H., GUTTLICH P., « X-ray structure study of the light-induced meta-stable states of the spin crossover compound [Fe(mtz)6](BF4)2», *Journal of Appl. Crystallography*, **34**, p229-238, (2001).

L

LANDAU L.D., LIFSHITZ E.M., «Statiscical Physics Part 1», *Elsevier*, (1980).

LARIONOVA J., SALMON L., GUARI Y., TOKAREV A., MOLVINGER K., MOLNAR G., BOUSSEKSOU A., «Towards the Ultimate Size Limit of the Memory Effect in Spin-Crossover Solids», *Angewandte Chemie International Edition*, **47**, (43), p8236-8240, (2008).

LAWTHERS I., McGARVEY J., «Spin-State Relaxation Dynamics in Iron(Il) Complexes: Photochemical Perturbation of the ^{2}T ^{6}A Spin Equilibrium by Pulsed-Laser Irradiation in the Ligand-to-Metal Charge-Transfer Absorption Band», *Journal of the American Chemical Society*, **15**, 106, (1984).

LEMKE H.T., BRESSLER C., CHEN L.X., FRITZ D.M., GAFFNEY K.J., GALLER A., GAWELDA W., HALDRUP K., HARTSOCK R.W., IHEE H., KIM J., KIM K.H., LEE J.H., NIELSEN M.N., STICKRATH A.B., ZHANG W., ZHU D., CAMMARATA M., «Femtosecond X-ray Absorption Spectroscopy at a Hard X-ray Free Electron Laser : Application to Spin Crossover Dynamics», *Journal of Physical Chemistry* A, **117**, p735-740, (2013).

LETARD J-F., «Photomagnetism of iron(II) spin crossover complexes—the T(LIESST) approach», *J. Mater. Chem ,* **16**, p2550-2559, (2006).

LE COINTE M.,LEMEE-CAILLEAU M.H., CAILLEAU H., TOUDIC B., TOUPET L., HEGER G., MOUSSA F, SCHWEISS P., KRAFT K.H., KARL N., «Symmetry breaking and structural changes at the neutral-to-ionic transition in tetrathiafulvalene-p-chloranil», *Physical Review B*, **51**, 3374, (1995).

LINDENBERG A.M., KANG I., JOHNSON S.L., MISSALLA T., HEIMANN P.A., CHANG Z., LARSSON J., BUCHSBAUM P.H., KAPTEYN H.C., PAYDMORE H.A., LEE R.W., WARK J.S., FALCONE R.W., «Time-Resolved X-Ray Diffraction from Coherent Phonons during a Laser-Induced Phase Transition», *Physical Review Letters*, **84**, 111, (2000).

LONGAKER P.R., LITVAK M.M., «Perturbation of the Refractive Index of Absorbing Media by a Pulsed Laser Beam*», Journal of Applied Physics*, **40**, 4033, (1969).

LORENC M., HEBERT J., MOISAN N., TRZOP E., SERVOL M., BURON-LE COINTE M., CAILLEAU H., BOILLOT M., PONTECORVO E., WULFF M., KOSHIHARA S., COLLET E., «Successive Dynamical Steps of Photoinduced Switching of a Molecular Fe(III) Spin-Crossover Material by Time-Resolved X-Ray Diffraction», *Physical Review Letters*, **103**, 028301, (2009).

LORENC M., BALDE C.H., KASZUB W., TISSOT A., MOISAN N., SERVOL M., BURON-LE COINTE M., CAILLEAU H., CHASLE P., CZARNECKI P., BOILLOT M., COLLET E., «Cascading photoinduced, elastic, and thermal switching of spin states triggered by a femtosecond laser pulse in an Fe(III) molecular crystal», *Physical Review B*, **85**, 054302, (2012).

M

MARGARITONDO G., RIBICA P.R., « A simplified description of X-ray free-electron lasers», *Journal of Synchrotron Radiation*, **18**, p101-108, (2011).

MATAR S., LETARS J-F., «Ab initio Molecular and Solid-state Studies of the Spin Crossover System [Fe(phen)2(NCS)2]», *ZEITSCHRIFT FÜR NATURFORSCHUNG SECTION B - A JOURNAL OF CHEMICAL SCIENCES*, **65b**, p565-570, (2010).

MARCHIVIE M., GUIONNEAU P., HOWARD J.A.K., CHASTANET G., LETARD J-F., GOETA A.E., CHASSEAU D., «Structural Characterization of a Photoinduced Molecular Switch», *Journal of the American Chemical Society*, **124**,(124), p194–195 , (2002).

McCUSKER J.K, WALDA K.N., DUNN R.C, SIMON J.D., MADGE D., HENDRICKSON D.N. , «Sub-Picosecond ΔS = 2 Intersystem Crossing in Low-Spin Ferrous Complexes», *Journal of the American Chemical Society*, **114**, p6919-6921, (1992).

McWHAN D.B., MENTH A., REMEIKA J.P., BRINLMAN W.F., RICE T.M., «Metal insulator transition in pure and V_2O_3», *Physical Review B*, **7**, 1920, (1973).

MIRLOUP F., « Diffraction des rayons X résolues en temps, dissociation et recombinaison de l'iode en solutions», 2004.

MIYASHITA S., KONISHI Y., NISHINO M., TOKORO H., RIKVOLD P.A., «Realization of the mean-field universality class in spin-crossover materials», *Physical Review B*, **77**, 014105, (2008).

MIYASHITA S., «Phase transition in spin systems with various types of fluctuations», *Proc. Jpn. Acad. Ser. B,* **86**, (2010).

MOISAN N., SERVOL M., LORENC M., TISSOT A., BOILLOT M., CAILLEAU H., KOSHIHARA S., COLLET E., « Towards ultrafast photoinduced spin state switching in molecular solids », *Comptes Rendus Chimie*, **1-6,** (2008).

MOLNAR G., COBO S., REAJ J.A., CARCENAC F., DARAN E., VIEU C., BOUSSEKSOU A., «A Combined Top-Down/Bottom-Up Approach for the Nanoscale Patterning of Spin Crossover Coordination Polymers», *Advanced Materials*, **19**, p2163-2167, (2007).

MONAT J.E, McCUSKER J.K., «Femtosecond Excited-State Dynamics of an Iron(II) Polypyridyl Solar Cell Sensitizer Model», *Journal of the American Chemical Society,* **122**, (17), p4092-4097, (2000).

N

NASU K., «Relaxations of Excited States and Photo-Induced Structural Phase Transitions», *Springer Series in Solid-State Science*, (1997).

NASU K., «Photo-Induced Phase Transition», ed NASU K., World Scientific Publishing, Singapore , (2004).

NISHINO M., BOUKHEDDADEN K., MIYASHITA S., VARRET F., « Arrhenius Monte Carlo study of two-step spin crossover: Equilibrium and relaxation paths», *Physical Review B*, **68**, 224402, (2003).

NISHINO M., BOUKHEDDADEN K., KONISHI Y., MIYASHITA S., «Simple Two-Dimensional Model for the Elastic Origin of Cooperativity among Spin States of Spin-Crossover Complexes», *Physical Review Letters*, **98**, 247203, (2007).

NISHINO M., BOUKHEDDADEN K., MIYASHITA S., « Molecular dynamics study of thermal expansion and compression in spin-crossover solids using a microscopic model of elastic interactions», *Physical Review B*, **79**, 012409, (2009).

O

P

PAPALAZAROU E., FAURE J., MAUCHAIN J., MARSI M., TALEB-IBRAHIMI A., RESHETNYAK I., VAN ROEKEGHEM A., TIMROV A., VAST N., ARNAUD B., PERFETTI L., «Coherent Phonon Coupling to Individual Bloch States in Photoexcited Bismuth», *Physical Review Letters*, **108**, 256808, (2012).

PERFETTI L., KAMPFRATH T., SCHAPPER F., HAGEN A., HERTEL T., AGUIRRE C.M., DESJARDINS P., MARTEL R., FRISCHKORN C., WOLF M., «Ultrafast Dynamics of Delocalized and Localized Electrons in Carbon Nanotubes», *Physical Review Letters*, **96**, 027401, (2006).

PERMAN B., SRAJER V., REN Z., PRADERVAND C., URSBT T., BOURGEOIS D., SCHOTTE F., WULFF M., KORT R., HELLINGWERF K., MOFFAT K., « Energy Transduction on the Nanosecond Time Scale: Early Structural Events in a Xanthopsin Photocycle», *Science*, **279**, 5328, p1946-1950, (1998).

PERRIN B., « Investigation of short-time heat transfer effects by an optical pump-probe method», *Topics Applied Physics*, **107**, p333-359, (2007).

PEZERIL T., KLIEBER C., ANDRIEU S., NELSON K.A., «Optical Generation of Gigahertz-Frequency Shear Acoustic Waves in Liquid Glycerol», *Physical Review Letters*, **102**, 107402 (2009).

PILLET S., HUBSCH J., LECOMTE C., «Single crystal diffraction analysis of the thermal spin conversion in [Fe(btr)2(NCS)2] (H2O): evidence for spin-like domain formation», *Eur. Phys. J. B*,**38**, p541-552, (2004).

PILLET S., LECOMTE C., SHEU C. F., LIN Y. C., HSU I. J. AND WANG Y. - "Light induced modulated structure of the spin crossover compound {Fe(abpt)2[N(CN)2]2}" - Accounts of Chemical Research 21 (2005) 221-226.

POLLI D., ALTOE P., WEINGART O., SPILLANE K.M., MANZONI C., BRIDA D., TOMASELLO G., ORLANDI G., KUKURA P., MATHIES R.A., GARAVELLI M., CERULLO G., «Conical intersection dynamics of the primary photoisomerization event in vision», *Nature*, **467**, p440-443, (2010).

POLLI D., BRIDA D., MUKAMEL S., LANZANI G., CERULLO G., « Effective temporal resolution in pump-probe spectroscopy with strongly chirped pulses», *Physical Review A*, **82**, 053809 (2010).

POULIN P.R., NELSON K.A., «Irreversible Organic Crystalline Chemistry Monitored in Real Time», *Science*, **291**, (5509), p1756-1760, (2006).

Q

QUINTERO C.M., GURALSKIY I.A., SALMON L., BERGAUD C., MOLNAR G., BOUSSEKSOU A., « Soft Lithographic Patterning of Spin Crossover Complexes. Part 1: Fluorescent Detection of the Spin Transition in Single Nano-Objects », *Journal of material Chemistry* , **22**, p3745-3751, (2012).

R

RINI M., TOBEY R., DEAN N., ITATANI J., TOMIOKA Y., TOKURA Y., SCHOENLEIN R.W., CAVALLERI A., «Control of the electronic phase of a manganite by mode-selective vibrational excitation», *Nature*, **449**, p72-74 (2007).

RONAYNE K.L., PAULSEN H., HOFER A., DENNIS A.C., WOLNY J.A., CHUMAKOV A.I., SCHUNEMANN V., WINKLER H., SPIERING H., BOUSSEKSOU A., GUTLICH P., TRAUTWEIN A.X., McGARVEY J, «Vibrational spectrum of the spin crossover complex

[Fe(phen)2(NCS)2] studied by IR and Raman spectroscopy, nuclear inelastic scattering and DFT calculations», *Physical Chemistry Chemical Physic*, **8**, p4685-4693, (2006).

ROUSSE A., RISCHEL C., FOURMAUX S., USCHMANN I., SEBBAN S., GRILLON G., BALCOU P., FORSTER E., GEINDRE J.P., AUDEBERT P., GAUTHIER J.C., HULIN D., «Non-thermal melting in semiconductors measured at femtosecond resolution», *Nature*, **410**, p65-68, (2001).

ROUX C., ZAREMBOWITCH J., ITIE J-P., POLIAN A, VERDAGUER M., «Pressure-Induced Spin-State Crossovers in Six-Coordinate FeIILnL'm(NCS)2 Complexes with L = L' and L ≠ L': A XANES Investigation», *Inorganic Chemistry*, **35**, (3), p574-580, (1996).

S

SCHMITT F., KIRCHMANN P.S., BOVENSIEPEN U., MOORE R.G., RETTIG L., KRENZ M., CHU J-H., RU N., PERFETTI L., LU D.H., WOLF M., FISCHER I.R., SHEN Z-X., « Transient Electronic Structure and Melting of a Charge Density Wave in TbTe3», *Science*, **321**, 5896, p1649-1652, (2008).

SCHOENLEIN R.W., CHATTOPADHYAY S., CHONG H.H.W., GLOVER T.E., HEIMANN P.A., SHANK C.V., ZHOLENTS A.A., ZOLOTOREV M.S., «Generation of Femtosecond Pulses of Synchrotron Radiation», *Science*, **287**, 5461, p2237-2240, (2000).

SCHOTTE F., LIM M., JACKSON T.A., SMIRNOV A., SOMAN J., OLSON J.S., PHILIPS G.N., WULFF M., ANFINRUD P.A., «Watching a Protein as it Functions with 150-ps Time-Resolved X-ray Crystallography», *Science*, **300**, 5627, p1944-1947, (2003).

SCIAINI G., HARB M., KRUGLIK S.G., PAYER T., HEBEISEN C.T, ZU HERINGDORF F.J.M., YAMAGUCHI M., HORN-VON HOEGEN M., ERNSTORFER R., MILLER R.J.D., «Electronic Acceleration of Atomic Motions and Disordering in Bismuth», *Nature,* **458**, (7234), (2009).

SLITCHER C., DRICKAMER H.G., « Pressure-induced electronic changes in compounds of iron », *The Journal of Chemical Physics*, **56**, p2142-2160, (1972).

SIM P.G., SINN E., PETTY R.H., MERRILL C.L., WILSON L.J., «Electronic and molecular structure of variable-spin metal complexes. Spin state dependent crystal and molecular structures of [FeIII(5-OCH3Salmeen)2]PF6 (S = 5/2), [FeIII(3-OCH3Salmeen)2]PF6 (S = 1/2), and [FeIII(5-NO2Salmeen)2]PF6 (S = 1/2) », *Inorganic Chemistry*, **20**, 4, p1213-1222, (1981).

SIWICK B.J., DWYER J.R, JORDAN R.E., MILLER R.J.D., «An Atomic-Level View of Melting Using Femtosecond Electron Diffraction», *Science,* **302***, (5649)*, p1382-1385, (2003).

SMEIGH A.L., CREELMAN M., MATHIES R.A., McCUSKER J.K., «Femtosecond Time-Resolved Optical and Raman Spectroscopy of Photoinduced Spin Crossover: Temporal Resolution of Low-to-High Spin Optical Switching», *Journal of the American Chemical Society*, **130,** (43), p14105-14107, (2008).

SOKOLOWSKI-TINTEN K., BLOME C., BLUMS J., CAVALLERI A., DIETRICH C., TARASEVITCH A., USCHMANN I., FORSTER E., KAMMLER M., HORN-VON-HOEGEN M., VON DER LINDE D., «Femtosecond X-ray measurement of coherent lattice vibrations near the Lindemann stability limit», *Nature*, **422**, p287-289, (2003).

SONG K.S., WILLIANS R.T., «Self-Trapped Excitons», *Springer Series in Solid-State Sciences*, **105, (1993).**

SORAI M., SEKI S., «Phonon coupled cooperative low-spin $^1A_1$ high spin $^5T_2$ transition in [Fe(phen)$_2$(NCS)$_2$] and [Fe(phen)$_2$(NCSe)$_2$] crystals», J. Phys. Chem. Solids, **35**, p555-570, (1974).

SORAI M., « Heat capacity studies of spin crossover compounds», Springer, Berlin, **234**, p155-198, (2004).

SPIERING H., WILLENBACHER N., «Elastic interaction of high-spin and low-spin complex molecules in spin-crossover compound», *J. Phys. Condens. Matter* , p10089-10105,(1989).

SPIERING H., BOUKHEDDADEN K., LINARES J., VARRET F., «Total free energy of a spin-crossover molecular system», *Physical Review B*, **70**, 184106, (2004).

STOLERIU L., ENACHESCU C., STANCU A., HAUSER A., « Elastic Model for Complex Hysteretic Processes in Molecular Magnets», *Magnetics, IEEE Transactions*, **44**, 11, p3052-3055, (2008).

STRICKLAND D., MOUROU G., « Compression of amplified chirped optical pulses», *Opt. Commun.*, **56**, 219, (1985).

SUAUD N., BONNET M-L., BOILLEAU C., LABEGUERIE P., GUIHERY N., «Light-Induced Excited Spin State Trapping: Ab Initio Study of the Physics at the Molecular Level», *Journal of the American Chemical Society*, **131,** (2), p715-722, (2009).

SUMMERTOM A.P., DIAMANTIS A.A., SNOW M.R, «The crystal structure of bis[N-(2-aminoethyl)salicylaldiminato] iron (III) chloride monohydrate, a low spin oron(III) complex stabilized by lattice water», *Inorganica Chimica Acta*, **27**, p123-128, (1978).

T

TANAKA K., OGAWA T., HASHIMOTO H., KOSHIHARA S-Y., «The LXIII Yamada Conference on Photo-Induced Phase Transition and Cooperative Phenomena (PIPT3)», *Journal of Physics: Conference Series*, **148**, (2009).

TANI S., BLANCHARD F., TANAKA K., «Ultrafast Carrier Dynamics in Graphene under a High Electric Field», *Physical Review Letters* ,**109**, 166603, (2012).

TEMNOV V., KLIEBER C., NELSON K.A., THOMAY T., KNITTEL V., TEITENSTORFER A., MAKAROV D., ALBRECHT M., BRATSCHITSCH R., «Femtosecond nonlinear ultrasonics in gold probed with ultrashort surface plasmons», *Nature Communications*, **4**, 1468, (2013).

TECHERT S., SCHOTTE F., WULLF M., « Picosecond X-Ray Diffraction Probed Transient Structural Changes in Organic Solids», *Physical Review Letters* ,**86**, 2030 (2001).

THOMSEN C., GRAHN H.T., MARIS H.J., TAUC J., « Surface generation and detection of phonons by picosecond light pulses», *Physical Review B*, **34**, 4129, (1986).

TISSOT A., BERTONI R., COLLET E., TOUPET L., BOILLOT M-L., «The cooperative spin-state transition of an iron(III) compound [FeIII(3-MeO-SalEen)2]PF6 : thermal- vs. ultra-fast photo-switching», *Journal of Material Chemistry*, **21**, p18347-18353, (2011).

TISSOT A., RECHIGNAT L., BOUSSEKSOU A., BOILLOT M-L., «Micro- and nanocrystals of the iron(III) spin-transition material [FeIII(3-MeO-SalEen)2]PF6», *Journal of Material Chemistry*, **22**, p3411-3419, (2012).

TISSOT A., ENACHESCU C., BOILLOT M-L., «Control of the thermal hysteresis of the prototypal spin-transition FeII(phen)2(NCS)2 compound via the microcrystallites environment: experiments and mechanoelastic model», *Journal of Material Chemistry*, **22**, p20451-20457, (2012).

TOKORO H., MIYASHITA S., HASHIMOTO K., OKHOSHI S-I., «Huge thermal hysteresis loop and hidden stable phase in a charge-transfer phase transition of $Rb_{0.64}MN[Fe(CN)_6]_{0.88}.1.7H2O$», *Physical Review B*, **73**, 172415, (2006).

TRIBOLLET J., GALLE G., JONUSAUKAS G., DELDICQUE D., TONDUSSON M., LETARD J-F., FREYSZ E., et al, «Transient absorption spectroscopy of the iron(II) [Fe(phen)3]2+ complex : Study of the non-radiative relaxation of an isolated iron(II) complex» *Chem. Phys. Lett.* , **513**, 42, (2011).

TRZOP E., BURON-LE COINTE M., CAILLEAU H., TOUPET L., MOLNAR G., BOUSSEKSOU A., GASPAR A.B., REAL J.A., COLLET E.« Structural Investigation of the Photoinduced Spin Conversion in the Binuclear Compound {[Fe(bt)(NCS)2](bpm)}:Toward Multi-stepped Molecular Switches », *Journal of Applied Crystallography*, **40**, p158-164, (2007).

U

UEMURA H., OKAMOTO H., «Direct Detection of the Ultrafast Response of Charges and Molecules in the Photoinduced Neutral-to-Ionic Transition of the Organic Tetrathiafulvalene-p-Chloranil Solid», *Physical Review Letters*, **105**, 258302, (2010).

V

VANKO G., RENZ F., MOLNAR G., NEISIUS T., KARPATI S., « Hard-X-ray-Induced Excited-Spin-State Trapping», *Angewandte Chemie International Edition*, **46**, 28, p5306-5309, (2007).

VAN KONINGSBRUGGEN P.J., MAEDA Y., OSHIO H., «Iron(III) Spin Crossover Compounds», Springer, Berlin, **234**, p155-198, (2004).

VAN VEENENDAAL M., CHANG J., FEDRO A.J., «Model of Ultrafast Intersystem Crossing in Photoexcited Transition-Metal Organic Compounds», *Physical Review Letters*, **104** (25), 061401, (2010).

VAN DER VEEN R.M., CANIZZO A., VAN MOURIK F., VLCEK A., CHERGUI M., «Vibrational Relaxation and Intersystem Crossing of Binuclear Metal Complexes in Solution», *Journal Of The American Chemical Society*, **133**, p305-315, (2011).

VAN DER VEEN R.M., KWON O-H., TISSOT A., HAUSER A., ZEWAIL A.H., «Single-nanoparticle phase transitions visualized by four-dimensional electron microscopy», *Nature Chemistry*, **5**, (5), p395-402, (2013).

VARRET F., SLIMANI A., BOUKHEDDADEN K., CHONG C., MISHRA H., COLLET E., HAASNOOT J., PILLET S.,«The propagation of the thermal spin transition of [Fe(btr)2(NCS)2].H2Osingle crystals, observed by optical microscopy», *New Journal of Chemistry*, **35**, p2333-2340, (2011).

W

WAJNFLASZ J., PICK R., «Low-spin-high-spin transitions in Fe^{2+} complexes», *J.Phys.Coll*, (1971).

WALL S., PRABAKHARAN R., BOOTHROYD A.T.J., CAVALLERI A., «Ultrafast Coupling between Light, Coherent Lattice Vibrations, and the Magnetic Structure of Semicovalent $LaMnO_3$», *Physical Review Letters*,**103**, 097402 (2009).

WALL S., WEGKAMP D., FOGLIA L., APPAVOO K., NAG J., HAGLUND R.F., STAHLER J., WOLF M., «Ultrafast changes in lattice symmetry probed by coherent phonons», *Nature Communications*, **3**, 721, (2012).

M.N. WOLF M., GROSS R., SCHUMANN C., WOLNY J.A., SCHUNEMANN V., DOSSING A., PAULSEN H., McGARVEY J., DILLER R., «Sub-picosecond time resolved infrared spectroscopy of high-spin state formation in Fe(II) spin crossover complexes», *Physical Chemistry Chemical Physic*, **10**, p4264-4273, (2008).

WULLF M., BRATOS S., PLECH A., VUILLEUMIER R., MIRLOUP F., LORENC M., KONG Q., IHEE H., «Recombination of photodissociated iodine: A time-resolved x-ray-diffraction study», *The Journal Of Chemical Physics*, **124**, 034501, (2006).

X

Y

YEH A.T., SHANK C.V., McCUSKER J.K., « Ultrafast Electron Localization Dynamics Following Photo-Induced Charge Transfer», *Science*, **289**, 5481, p935-938, (2000).

Z

ZEIGER H.J, VIDAL T., CHENG T.K., IPPEN E.P., DRESSLHAUS G., DRESSELHAUS M.S., «Theory for displacive excitation of coherent phonons», *Physical Review B*, **45**, 768, (1992).

ZEWAIL A.H, « Femtochemistry : Atomic-Scale Dynamics of the Chemical Bond Using Ultrafast Lasers» , *Angewandte Chemie International Edition*, **39**, 15, p2586-2631, (2000).

ZHANG Y., BURDZINSKI G., KUBICKI J., PLATZ S.M, «Ultrafast Time-Resolved Infrared Spectroscopy Study of the Photochemistry of N,N-Diethyldiazoacetamide : Rearrangement in the Excited State», *Journal of the American Chemical Society,* **131** , p9646–9647, (2009).

ANNEXE 1 : PUBLICATIONS

1- TISSOT A., BERTONI R., COLLET E., TOUPET L., BOILLOT M.
   « The cooperative spin-state transition of an iron(III) compound [Fe^{III}(3-MeO-SalEen)$_2$]PF$_6$: thermal- *vs*. ultra-fast photo-switching »
   Journal of Materials Chemistry, **21** , 18347-18353 (2011).

2- COLLET E., MOISAN N., BALDE C., BERTONI R., TRZOP E., LAULHÉ C., LORENC M., SERVOL M., CAILLEAU H., TISSOT A., BOILLOT M.L., GRABER T., HENNING R., COPPENS P., BURON-LE COINTE M.
   « Ultrafast spin-state photoswitching in a crystal and slower consecutive processes investigated by femtosecond optical spectroscopy and picosecond X-ray diffraction »
   Physical Chemistry Chemical Physics, **14**, 6192-6199 (2012).

3- BERTONI R., LORENC M., TISSOT A., SERVOL M., BOILLOT M.L., COLLET E.
   « Femtosecond spin-state photo-switching of molecular nanocrystals evidenced by optical spectroscopy »
   Angewandte Chemie International Edition, **51**, 7485-7489 (2012).

4- MARINO A., SERVOL M., BERTONI R., LORENC M., MAURIAC C., LETARD J.F., COLLET E.
   « Femtosecond optical pump-probe reflectivity studies of spin-state photo-switching in the spin-crossover molecular crystals [Fe(PM-AzA)2(NCS)2] »
   Polyhedron (2013), http://dx.doi.org/10.1016/j.poly.2013.03.009 .

PAPER

The cooperative spin-state transition of an iron(III) compound [Fe^{III}(3-MeO-SalEen)$_2$]PF$_6$: thermal- *vs.* ultra-fast photo-switching†

Antoine Tissot,[a] Roman Bertoni,[b] Eric Collet,[b] Loic Toupet[b] and Marie-Laure Boillot[*a]

The switching properties of the spin-transition solid [Fe^{III}(3-MeO-SalEen)$_2$]PF$_6$ (H-3-MeO-SalEen resulting from the condensation of 3-methoxy-substituted salicylaldehyde and *N*-ethylethylenediamine), exhibiting a first-order transition, were investigated by using temperature and light as stimulation. The structural analysis reveals a first-order isostructural transition occurring with a 3 K width thermal hysteresis ($T\downarrow$ = 162.5 K, $T\uparrow$ = 165.5 K) coupled to the magnetic transition. The microscopic origin of this bistable behavior derives from strong coupling between pairs of complexes and the molecular packing. An extensive 3D network of intermolecular interactions, reinforced near the transition temperature, appears as a key feature for the cooperativity. The LMCT (ligand-to-metal charge transfer) transitions, detected by single-crystal transmission measurements, were selected for analyzing the photoswitching process of this cooperative solid. Only optical pump-probe experiments could detect photoinduced low-spin to high-spin conversion because of the too short lived excited state. The spin-state transformation induced by the femtosecond laser flash is very fast: electronic excitation corresponding to the low-spin LMCT transition relaxes toward the transient photoexcited high-spin state within 170 ± 50 fs.

Introduction

Optical switching of bistable molecular materials is an active and challenging area of research explored both for addressing fundamental issues and exploiting technological potentialities in information storage or signal processing. A major interest derives from the possibility to manipulate small collections of photo-active bistable objects and to rapidly switch their physical (or chemical) state. Systems showing a molecular bistability evolve between two stable states in a controllable and detectable manner when applying a given perturbation.[1] Spin-crossover compounds, whose behavior depends on the interaction between molecules and their environments, provide good examples of bistable materials.[2,3] Since the first report by Cambi and Szergö concerning Fe^{III} ions,[4] the spin-crossover phenomenon has been established for complexes of transition-metal ions with 3d^4–3d^7

[a]ICMMO-ECI, UMR CNRS 8182, Univ. Paris-Sud 11, 91405 Orsay, France. E-mail: marie-laure.boillot@u-psud.fr; Fax: +33 1 6915 4754; Tel: +33 1 6915 4755
[b]IPR, UMR UR1-CNRS, Campus de Beaulieu, University Rennes 1, Rennes, France

electronic configurations.[3] In suitable octahedral environments of donor atoms, the metal ions adopt two low-spin (LS) and high-spin (HS) states in close energy proximity, which are easily interconverted under external perturbations (temperature, pressure or light irradiation). In the spin-crossover process, the electron transfer is coupled to a sizeable structural reorganization of the inner- and outer-sphere of coordination. Typical changes in the metal–ligand donor atom bonds of iron(III) complexes average from 0.12 to 0.15 Å,[5] whereas those of Fe^{II} are larger (*ca.* 0.20–0.24 Å).[6] These differences, due to their respective ionic radii and LS electronic configurations, are associated to distinctive spin-crossover characteristics. At solid state, the changes of the molecular volume are responsible for intermolecular interactions of elastic nature. Moderate variations of the molecular volume are easily accommodated by Fe^{III} solids and thus, progressive HS $\leftrightarrow$ LS transitions are the rule.[7] In the case of Fe^{II} compounds, large volume changes may produce strong cooperative effects, which may result in very abrupt transitions and hysteretic behaviors.[3]

Obviously, the structural reorganization influences the kinetic of the spin-state interconversions. The HS $\leftrightarrow$ LS transition of Fe^{III} is much more rapid than the Fe^{II} one (*ca.* one order of magnitude at room temperature),[8,9] yielding to dynamic effects in Mössbauer spectra (line-width broadening). Concerning the photoexcitation of Fe^{II} spin-transition solids, the so-called LIESST (Light-induced excited spin state trapping) effect[10] induces the quantitative LS- to HS- conversion and the trapping

This journal is © The Royal Society of Chemistry 2011

J. Mater. Chem., 2011, **21**, 18347–18353 | 18347

of HS metastable species. The LIESST observation requires cryogenic temperatures as the HS-to-LS relaxation through a tunneling effect is thermally activated at high temperature.[11] Consistent with the structural and kinetic characteristics of Fe[III] spin-crossover compounds, their LIESST effect, *i.e.* the trapping of HS species, is hardly detected. A quasi-unique example of photoinduced transition was described for the very cooperative [Fe[III](pap)$_2$]ClO$_4$ compound. The effect was accounted for by the particular distortion of the coordination sphere and the especially strong π–π stacking interactions.[12]

Very recent achievements concern the photoexcitation and the dynamic of the spin-state conversion. Non-interacting Fe[II] or Fe[III] complexes in solution have been selected for examining the ultra-fast reorganization of the first coordination sphere driven by a LS-to-HS switching process.[9,13] At solid state, the coupling between photoactive centers and their environment has been probed with single crystals of a spin-crossover Fe[III] complex by both ultra-fast X-ray diffraction and optical spectroscopy.[14] The electronic switching of the spin-state (on the sub-picosecond time scale) is the first stage of a complex sequence, which links the localized excitation to the solid evolution up to the equilibrium state. For this poorly cooperative system, one photon triggers the initial conversion of one molecule, although later the energy excess dissipated within the crystalline solid yields to additional spin conversions. Accordingly, an important issue concerns the role of elastic interactions in the photoswitching process, which starts to be investigated in the ns time-scale.[14–17]

Aiming at investigating the photoinduced transition of a cooperative solid, we focus here on a Fe[III] prototype, [Fe[III](3-MeO-SalEen)$_2$]PF$_6$, exhibiting a rather unique first-order spin transition centered at *ca.* 162 K.[18] It is characterized by

a discontinuous evolution of the magnetic susceptibility (Fig. 1b and S2 in the ESI†) with a thermal hysteresis indicative of a strong cooperativity of this material in relation with the $S = 1/2 \leftrightarrow S = 5/2$ spin-state switching. Weak pretransitional spin conversion is observed on both sides of the hysteresis. A first question concerns the origin of this cooperative transformation associated with the thermal hysteresis, while progressive transitions have been reported for numerous Fe[III](R^1-Salen R$_2$)$_2$X analogues.[19] From a single-crystal X-ray diffraction study achieved at variable temperatures, we have analyzed the structural evolutions (space group, unit-cell, packing, and coordination sphere) in relation with the cooperative spin-state switching, the interacting centers and their general organizations. Herein, we report the structural analysis and then the optical properties of crystalline solids measured by variable-temperature optical microscopy and UV-vis absorption. Finally, we examine the photoswitching of the single crystal.

Experimental section

Synthesis

The molecular compound [Fe(3-MeO-SalEen)$_2$]PF$_6$ was prepared as previously described in the literature.[18] Dark brown single crystals were obtained by slow evaporation of a methanolic solution of the compound. Elemental analysis: formula C$_{26}$H$_{40}$F$_6$FeN$_4$O$_4$P (%); Calcd: C 44.80, H 5.33, N 8.71; found: C 44.76, H 5.29, N 8.71%.

Details of the X-ray crystallography studies

Single crystal data collections were performed at 120, 200 and 300 K with an Xcalibur Oxford Diffraction diffractometer (Institut de Physique, Université de Rennes 1, France) with Mo-Kα radiation ($\lambda = 0.71069$ Å). To ensure the thermal equilibrium of the single-crystal, a sweeping rate of 1 K h^{-1} was selected for the data collection within the hysteretic range, while 10 min per measurement were used for unit-cell determinations. The low temperature device is a Cryostream 700 from Oxford Cryosystems. Reflections were indexed, Lorentz-polarization corrected and integrated by the *Crysalis* package.[20] Structure determinations were performed by direct methods with the solving program SIR97[21] that revealed all the non-hydrogen atoms. SHELXL program[22] was used to refine the structures by full-matrix least-squares based on F^2. All non-hydrogen atoms were refined with anisotropic displacement parameters. Hydrogen atoms were included in idealised positions and refined with isotropic displacement parameters. Atomic scattering factors for all atoms were taken from International Tables for X-ray Crystallography.†

Magnetic measurements

Magnetic measurements were carried out using a Quantum Design SQUID magnetometer (MPMS5S Model) calibrated against a standard palladium sample. The data were collected between 300 and 10 K at a rate of 0.5 K min^{-1}.

Fig. 1 (a) Plot of the relative unit-cell volume variation $(V_T - V_{120K})/(V_{300K} - V_{120K})$ as a function of temperature (T) with an expanded view in the inset. △ and ▼ characters refer to increasing and decreasing values of T. The lines indicate the hysteresis domain. (b) $\chi_M T$ *versus* T plot of the microcrystalline powder, χ_M being the molar magnetic susceptibility.

Optical microscopy measurements

Photographs of an ~50 μm thick single crystal were taken in transmission mode on a standard optical microscope Laborlux 12 pol from Leica equipped with a CCD camera Sony Digital Hyper HAD SSC-DC38P.

UV-vis measurements

The UV-vis-NIR spectra were collected using a Varian Cary 5000 double-beam spectrophotometer, equipped with an ADP Cryogenics closed-cycle Helium cryogenic system including a DMX-1E cryostat and a DE-202 expander. Transparent pellets were prepared with a few % of Fe(III) complex dispersed into KBr powder. The mixture of KBr and coordination compound was not ground in order to minimize the physical alteration of the spin-transition solid.

Femtosecond photo-excitation measurements

Femtosecond optical pump-probe measurements were performed for time-resolved photo-excitation measurements. In this experience, the probe wavelength was 750 nm demonstrated to be sensitive to the change of the spin state (see below), and the pump wavelength was 880 nm. The measurement was performed on a 50 μm thick single crystal, cooled down to 140 K in order to be in completely LS state. Data were accumulated in a stroboscopic way for increasing the signal/noise ratio through locking amplifier detection.[23] All laser beams used during this measurement were polarized along the a axis of the crystal for which the penetration depth is maximum. The pump energy of the laser beam focussed on 300 μm was of the order of 1 μJ per pulse.

Results and discussion

Structural properties

[Fe^{III}(3-MeO-SalEen)$_2$]PF$_6$ crystallizes in the triclinic $P\bar{1}$ space group and no symmetry change occurs upon cooling from 300 to 120 K. This $S = 1/2 \leftrightarrow S = 5/2$ spin-transition is thus an example of isostructural spin transition, as it is often the case in spin-transition systems.[6,24] Relevant crystallographic parameters are given in Tables 1 and 2 (see also Tables ST2–ST3 in the ESI†). Both the spin transition and the thermal contraction of solid give rise to 7.9% decrease of the unit-cell volume in the whole range of temperature and only 3.3% between 200 and 120 K.

The volume and unit-cell parameters, recorded at 300 K and between 200 and 120 K, are shown in Fig. 1a and S1 (in the ESI†). Consistent with the ref. 18, these data show the first-order nature of the transition that is observed here on a single-crystal.

The down- and up-conversion temperature corresponding to the half-conversion of the single-crystal can be estimated at $T\uparrow$ = 165.5 K, $T\downarrow$ = 162.5 K in the warming and cooling modes, respectively; the hysteresis loop being equal to ~3 K. Despite small changes deriving from the comparison between averaged (magnetic data in Fig. 1b and S2†) and single-crystal (structural data in Fig. 1a) measurements performed with different cryocooling devices, both measurements evidence the hysteretic behavior and the concomitant change of the electronic state and structural reorganization. In contrast to the β parameter of the

triclinic unit-cell, which decreases by increasing the temperature, the other parameters increase (Fig. S1†). Notice that in the hysteresis loop the accuracy of the measurement is limited by the change of sample quality as important strains appear.

Molecular structures

The unique independent cation observed in the asymmetric unit is a six-coordinated Fe^{III} ion with tridentate Schiff-Base ligands (Fig. 2). At 300 K, the bond lengths to the Fe^{III} atom (mean value $\langle$Fe–L$\rangle$ = 2.094 Å) and bond angles measured fall within the range of expected values for a high-spin [FeN$_4$O$_2$] complex with this type of ligand (Table 2 and ST1†).[19,25,26] The coordination sphere of Fe^{III} ions, which is characterized by the Σ and ζ parameters (Table 2), roughly compares to those of spin-crossover analogues [Fe(R′-SalRen)$_2$]X (R = H, Me, Et, Pr, Bu; R′ = H, 3- or 5-MeO; X = PF$_6^-$, ClO$_4^-$), Σ = 95.7–108.7 and 50.08–61.91°, ζ = 0.590–0.650 and 0.334–0.418 Å for HS and LS species, respectively, except the fact that its 300 K ζ parameter (at 0.692 Å) is slightly higher than reported values.

While the unit-cell is compressed by 4.2% at 200 K, pre-transitional reorganization is found at the intra-molecular level as the structure adopted by cationic species corresponds to intermediate distances and ζ parameters (Table 2). In the same temperature range, the fraction of HS species determined from magnetic measurements changes from 0.96 (300 K) to 0.93 (200 K). The reduction of the HS content is consistent with a decrease of the averaged metal–ligand distance and ζ values. In comparison to room temperature, the change in the coordination core is asymmetric as it mainly concerns the 5-membered chelate ring (N(1)–Fe–N(2)–C(9)–C(8)) of one ligand. In the second ligand, the Fe–O(21) bond is elongated and the O(21)–Fe–N(21) and N(21)–C(27)–C(26) angles are closed. The adjacent 5-membered chelate ring is essentially preserved.

On cooling down the crystal to 120 K, the data collected in Table 2 (including the Σ and ζ structural parameters) show the formation of LS species with reduced asymmetry. The relative disposition of phenyl rings and torsion angles (Fe–O(1)–C(1)–C(6), Fe–O(21)–C(21)–C(26)) are essentially unchanged during the transition.[27,28] Between 300 and 120 K, the average metal–ligand bond distance is shortened by 0.144 Å, a variation which can be related to the observation at 300 K of structurally relaxed HS Fe^{III} species in the expanded unit-cell.

Crystal packing and intermolecular interactions

The crystal packing consists in cationic layers separated by anionic layers of PF$_6^-$. Within the cationic plane (see Fig. 3) ferric complexes are arranged in a dimeric fashion *via* face-to-face π–π interactions and C–H edge-to-face···π contacts (in Table ST2†). Pairs of anions (P···P distances equal to 5.012 Å at 300 K) interact with 8 distinct ferric complexes, each of them being involved in π-stacking interactions with neighboring molecules. The structure cohesion is achieved by numerous intermolecular contacts (C–H···F, C–H···O) or hydrogen bonding (N–H···F) between neighboring cations and anions (in Table ST3†).

At 300 K, rather weak contacts are essentially observed between one tridentate ligand and the PF$_6^-$ anion. Their number and strength markedly increase at 200 K under the

This journal is © The Royal Society of Chemistry 2011

J. Mater. Chem., 2011, **21**, 18347–18353 | 18349

Table 1 Crystal data and structure refinement for $[Fe^{III}(3\text{-MeO-SalEen})_2]PF_6$ at 300, 200 and 120 K

Crystal phase, temperature	HS, 300 K	HS, 200 K	LS, 120 K
Empirical formula	$C_{24}H_{34}F_6FeN_4O_4P$		
Formula weight/g.mol^{-1}	643.37		
Crystal system	Triclinic		
Space group	$P\bar{1}$		
a/Å	10.4850(10)	10.3140(10)	10.2970(10)
b/Å	11.015(9)	10.8755(8)	10.716(2)
c/Å	14.280(10)	14.0270(10)	13.955(2)
α/°	74.61(9)	74.896(6)	72.220(10)
β/°	69.29(9)	69.384(8)	70.450(10)
γ/°	75.29(7)	75.921(7)	74.130(10)
V/Å^3	1463.7(16)	1401.6(2)	1356.4(3)
Z	2	2	2
Density (calc.)/g cm^{-3}	1.460	1.524	1.575
$F(000)$	666	666	666
θ Range/°	2.61 → 26.99	2.65 → 27	2.65 → 27
Collected data	10 607	9674	17 727
Unique data	3589	5823	5416
R_{int}	0.1557	0.0550	0.0671
Data/restraints/parameters	3589/0/361	5823/0/361	5416/0/361
Goodness-of-fit on F^2	0.674	0.722	0.781
$R1\ [I > 2\sigma(I)]$	0.0620	0.0414	0.0384
$wR1[I > 2\sigma(I)]$	0.0576	0.0834	0.0679
$R2$ (all data)	0.3536	0.1168	0.0925
$wR2$ (all data)	0.0802	0.0941	0.0770

effect of the unit-cell contraction and the PF_6^- reorientation (for example, strengthening of C(27)–H(27)···F(1), N(22)–H(22)···F(2) or appearance of N(2)–H(2)···F(4), N(2)–H(2)···F(6), C(12)–H(12C)···F(1) strong contacts). Note that at this stage, direct contacts appear between adjacent cations (C(7)–H(7)···O(22) and C(23)–H(23)···O(2)), which mediate efficient paths for cooperative interactions between the spin-transition centers. At 120 K, all these tendencies are reinforced in the LS phase.

Therefore, dense and strong intermolecular contacts organized in a 3D extended network of interacting complexes contribute to the cooperative transformation of this solid. This feature combined with a transition temperature at 164 K gives rise to the occurrence of a small hysteresis loop. Finally, we note that significant σ–π or π–π type intermolecular interactions have been pointed out for analogues in the literature, but their organization in a 2D network corresponds to a weaker cooperative character of the transition.[19]

**Table 2** The geometry of the Fe site surroundings

	HS 300 K	HS 200 K	LS 120 K
Fe–N bonds/Å			
Fe–N1	2.118(10)	2.095(3)	1.925(2)
Fe–N2	2.223(7)	2.200(2)	2.045(2)
Fe–N21	2.138(11)	2.074(3)	1.921(2)
Fe–N22	2.239(9)	2.242(3)	2.057(2)
⟨Fe–N⟩	2.180(10)	2.153(3)	1.987(2)
Fe–O bonds/Å			
Fe–O1	1.936(8)	1.921(2)	1.8718(17)
Fe–O21	1.904(9)	1.924(4)	1.8718(19)
⟨Fe–O⟩	1.921(9)	1.923(3)	1.8718(18)
ζ/Å^a	0.692	0.618	0.410
Σ/°^{a}	100.1	106.41	58.87

$$^a\ \zeta = \sum_{i=1}^{6} |Fe - L_i - <Fe - L>| \quad \text{and} \quad \sum = \sum_{i=1}^{12} |90 - \phi_i|.$$

Optical properties

In Fig. 4, the photographs recorded with the microscope in transmission mode show a parallelogram-shaped crystal, whose color in polarized light (along the *a* axis) turns from orange at 285 K to dark green at 90 K. The change of color is a direct consequence of the spin-state switching, a thermochromism that is well-known in spin-crossover materials.[29]

The evolution of the optical transmission at 750 nm measured on a single crystal as a function of temperature is also presented in Fig. 4. It suddenly decreases with lowering temperatures ($T\downarrow$ = 160 K), or conversely increases with raising temperatures ($T\uparrow$ = 164 K). Both the transition temperatures and the hysteresis loop compare well to the data extracted from the single-crystal structure. Some pretransitional variations are
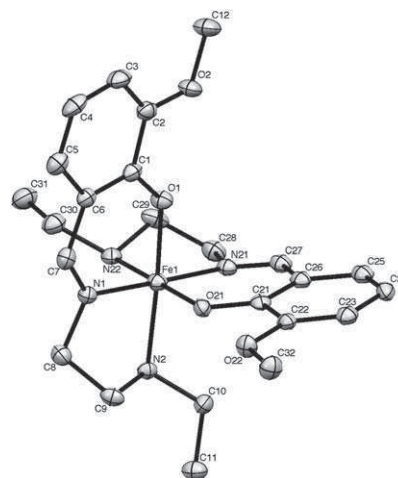
Fig. 2 ORTEP view of $[Fe(3\text{-MeO-SalEen})_2]PF_6$ at 120 K showing 50% probability displacement ellipsoids. Hydrogen atoms are omitted for clarity.
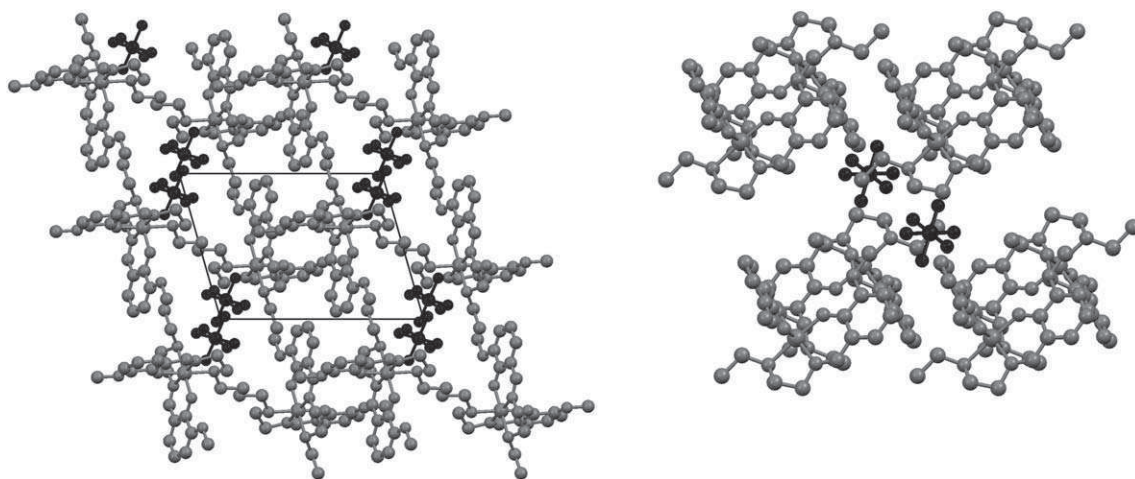
Fig. 3 (Left) View of 120 K crystal packing showing the π–π stacking interactions in the (*a*,*c*) plane; (right) view of 120 K packing along *c**, showing the PF$_6^-$ pair (in black) interacting with 8 cationic centers (in grey).
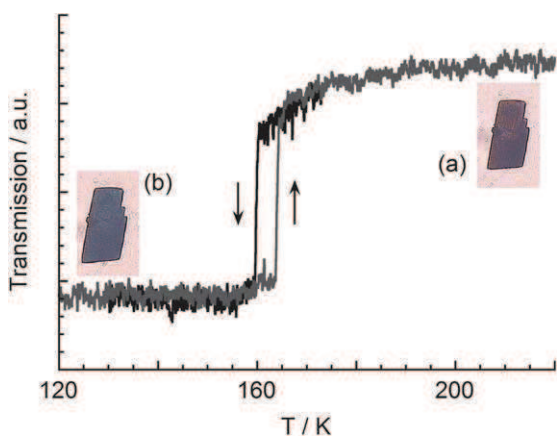
Fig. 4 Temperature dependence of the optical transmission measured at 750 nm on a single crystal. Photographs of the single crystal showing thermochromism from orange (a,285 K) to dark green (b,90 K). Light is polarized along the long crystal axis corresponding to the *a* unit-cell parameter, for which the penetration depth is larger.

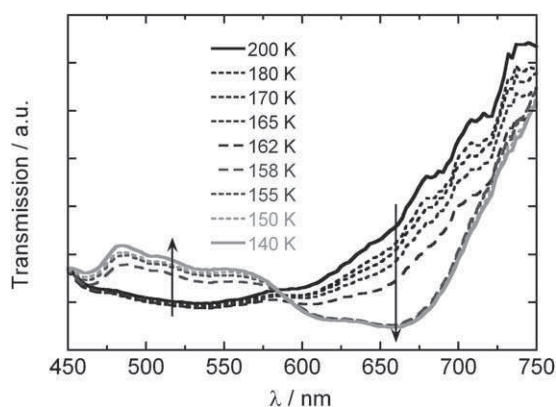**Fig. 5** Variable temperature single-crystal transmission spectra of [Fe^{III}(3-MeO-SalEen)$_2$]PF$_6$.

observed on both sides of the hysteresis, in good agreement with the magnetic response (Fig. 1b). Here again, this measurement indicates the first-order nature of the phase transition, which contrasts with the continuous evolution reported with similar measurements on less cooperative Fe(III) materials.[30] The wavelength of 750 nm, less efficiently transmitted by LS species than HS ones, is thus suitable for analyzing the single-crystal's optical properties and detecting the generation of HS molecular states.

In Fig. 5, the temperature dependence of transmission spectra measured on a single crystal with light polarized along the *a* axis is more informative. Absorptions typical for phenolate-to-iron(III) charge transfer transitions appear in the vis-NIR range, while intraligand absorptions occur in UV. The intensities of these former data strongly depend on the temperature. As the HS-to-LS conversion takes place (see also in Fig. S3†, the absorption spectra of the microcrystalline solid dispersed in KBr), the LMCT band of LS species, centered at *ca.* 660 nm, increases in intensity at the expense of the LMCT band of HS species observed at higher energy (*ca.* 535 nm). The

variation observed in the transmission spectra is consistent with the single-crystal transmission curve shown in Fig. 4. In KBr pellet, the spin transition observed between *ca.* 150 and 100 K corresponds to a slightly lowered transition temperature with respect to magnetic measurement. This feature very likely derives from mechanochemical effects associated to the in-KBr incorporation of the solid and/or to a rough thermalization in KBr. Indeed, this molecular material presents remarkable sensitivity to mechanical perturbation resulting in the variation of transition thermodynamical parameters, a weaker transition temperature and the formation of residual HS species.[31] From the above data, a low-energy excitation of [Fe^{III}(3-MeO-SalEen)$_2$]PF$_6$ (*i.e.* wavelengths corresponding to the LS LMCT transitions, here 880 nm) should be convenient for inducing a LS-to-HS state conversion.

It has been checked first that magnetic measurements carried out at 10 K in the presence of a weak *cw* (continuous-wave) NIR light (800–1000 nm) fail to detect any photoinduced change of magnetization of the solid sample. This result was not unexpected as the LIESST relaxation of Fe(III) molecular compounds is known to be rapid.[32,33] Therefore a weak *cw* irradiation cannot populate a detectable fraction of the HS state. Accordingly, only time-resolved optical techniques can allow to characterize

transient population of the HS state in single-crystals of [Fe^{III}(3-MeO-SalEen)$_2$]PF$_6$, and we consider here femtosecond pump-probe spectroscopy.

Photo-excitation properties

The photoswitching dynamic was studied by using a femtosecond optical pump-probe experiment, which was previously applied to evidence the ultra-fast LS-to-HS photo-conversion in non-cooperative Fe(III) materials.[14,23] For the first time, we investigate the femtosecond dynamic of the photo-induced process in the present highly cooperative material undergoing a first-order thermal transition. This measurement has been achieved by the use of femtosecond laser pulses in classical transmission setup as previously described in ref. 14 and 23.

As observed in Fig. 6, the crystal exhibits a small but clear response to fs laser excitation, which can be attributed to the photoswitching of a small amount of molecules from the LS to the HS states. First, a sub-picosecond peak appears, which can be attributed to the electronic excitation during the LMCT process. By taking into account the experimental time resolution of 150 fs, it decays within a time scale of 170 ± 50 fs, which corresponds to typical timescales reported for this type of molecules in solution,[13] as well as in the solid state[14,23] for reaching the photoinduced HS state. From the variation of the optical transmission between negative delays (before laser excitation) and ps delays (on the plateau where the HS state is partially populated), we can estimate the percentage of photo-converted molecules to be around 0.2%. Even though this value is small, it is larger than the experimental detection limit.

The attempt to increase the fraction of photo-converted molecules resulted in sample damage, which may be associated with the important cooperative nature of the spin transition in this compound. Indeed, sample cracking is already observed with optics and X-ray diffraction during thermal cycling between LS and HS phases. In the femtosecond pump-probe experimental set-up, a large excitation density may induce too large transformation of the crystal; and the relaxation of the mechanical stress in the 1 kHz excitation mode rapidly decreases sample quality, thereby limiting the achievable transformation rate in the stroboscopic set-up. This unfortunately precludes deeper
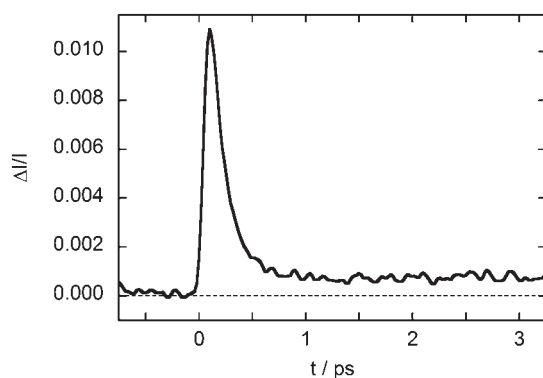
Fig. 6 Relative variation of the transmitted intensity measured at 750 nm. The single-crystal is photoexcited at 880 nm with a 100 fs laser pulse (polarization along *a* axis). The experiment was performed in the LS phase at 140 K.

investigations in this material by this technique, but demonstrates however that it is possible to drive ultra-fast molecular switching in highly cooperative systems, which is of importance for the development of applications.

Conclusions

The investigation of a spin-transition prototype [Fe^{III}(3-MeO-SalEen)$_2$]PF$_6$ in the form of single-crystals has allowed us first to establish the structure–property relationship for a cooperative compound exhibiting a first-order transition, a rather uncommon property of Fe(III) ions. The crystal packing consists of a 3D extended network of interconnected molecules *via* strong intermolecular interactions. It gives rise to an isostructural phase transition coupled to the electronic spin-state switching and a 3 K hysteresis. With respect to room temperature, a unit-cell compression larger than *ca.* 4% precedes the transition around 162 K. At this stage, the quality of single-crystals may be altered as strains due to the first-order thermal transition produce cracks and crystalline defects. Despite a pronounced color due to LMCT transitions in the vis-NIR range typical for Schiff-base complexes, the analysis of single-crystal thermochromism has provided the LS and HS transmission spectra, and thus conditions required for a selective excitation and detection of these species.

Because of the too short lived excited state in the material, we had to use time-resolved optical techniques to demonstrate the possibility to switch by light between LS and HS states. We have also demonstrated the ultra-fast nature of the first events produced by single-crystal photo-excitation, this feature being for the very first time observed in a strongly cooperative spin-transition material. At 140 K, the LS-to-HS conversion is shown to occur within a 170 fs time-scale in agreement with recent works on spin-crossover systems reported in the solid state and in solution.

In cooperative materials, the role of the active environment is a key question. A small fraction of photo-excited HS species may rapidly recover the LS state as a result of the mean-field effect of the majority of neighboring molecules remaining in the LS state,[34] therefore applying an important lattice pressure on converted HS species. Therefore, the next step will be to analyze the response of the solid in the time scale for which the lattice expansion and collective effects of elastic nature are expected to take place. As mentioned before, the low threshold of damage observed under fs laser irradiation precludes a more quantitative transformation of solids and thus, such an analysis. The alternative approach, that we are presently exploring, consists of elaborate size-reduced particles for optimizing both the penetration-depth of light and the conversion. Crystalline μm to nm sized objects have been synthesized and the relationship between photoswitching properties, time-scale and size effects is under investigation.

18352 | *J. Mater. Chem.*, 2011, **21**, 18347–18353

This journal is © The Royal Society of Chemistry 2011

Notes and references

1 O. Kahn and J.-P. Launay, *Chemtronics*, 1988, **3**, 140.
2 O. Kahn, *Molecular Magnetism*, VCH, New-York, 1993.
3 P. Gütlich and H. A. Goodwin, *Topics in Current Chemistry*, Springer-Verlag, Heidelberg, 2004, pp. 233–235.
4 L. Cambi and L. Szegö, *Ber.*, 1931, **10**, 2591.
5 E. König, *Prog. Inorg. Chem.*, 1987, **35**, 527.
6 P. Guionneau, M. Marchivie, G. Bravic, J.-F. Létard and D. Chasseau, *Topics in Current Chemistry*, Springer-Verlag, Heidelberg, 2004, vol. 234, p. 97.
7 M. Nihei, T. Shiga, Y. Maeda and H. Oshio, *Coord. Chem. Rev.*, 2007, **251**, 2606.
8 E. König, *Struct. Bonding (Berlin, Ger.)*, 1991, **76**, 51.
9 C. Brady, J. J. McGarvey, J. K. McCusker, H. Toftlund and D. N. Hendrickson, *Topics in Current Chemistry*, Springer-Verlag, Heidelberg, 2004, vol. 235, p. 1.
10 S. Decurtins, P. Gütlich, C. P. Köhler, H. Spiering and A. Hauser, *Chem. Phys. Lett.*, 1984, **13**, 1.
11 A. Hauser, *Topics in Current Chemistry*, Springer-Verlag, Heidelberg, 2004, vol. 234, p. 155.
12 S. Hayami, K. Hiki, T. Kawahara, Y. Maeda, D. Urakami, K. Inoue, M. Ohama, S. Kawata and O. Sato, *Chem.–Eur. J.*, 2009, **15**, 3497.
13 A. Cannizzo, C. J. Milne, C. Consani, W. Gawelda, C. Bressler, F. van Mourik and M. Chergui, *Coord. Chem. Rev.*, 2010, **254**, 2677.
14 M. Lorenc, J. Hebert, N. Moisan, E. Trzop, M. Servol, M. Buron-Le Cointe, H. Cailleau, M.-L. Boillot, E. Pontecorvo, M. Wulff, S. Koshihara and E. Collet, *Phys. Rev. Lett.*, 2009, **103**, 028301.
15 M. Lorenc, C. Balde, W. Kaszub, A. Tissot, N. Moisan, M. Servol, M. Buron-Le-Cointe, H. Cailleau, P. Chasle, P. Czarnecki, M.-L. Boillot and E. Collet, submitted.
16 O. Fouché, J. Degert, G. Jonusauskas, N. Daro, J.-F. Létard and E. Freysz, *Phys. Chem. Chem. Phys.*, 2010, **12**, 3044.
17 G. Galle, J. Degert, C. Mauriac, C. Etrillard, J.-F. Létard and E. Freysz, *Chem. Phys. Lett.*, 2010, **500**, 18.
18 (*a*) M. S. Haddad, M. W. Lynch, W. D. Federer and D. N. Hendrickson, *Inorg. Chem.*, 1981, **20**, 123; (*b*) M. S. Haddad, W. D. Federer, M. W. Lynch and D. N. Hendrickson, *Inorg. Chem.*, 1981, **20**, 131.
19 S. Hayami, S. Miyazaki, M. Yamamoto, K. Hiki, N. Motokawa, A. Shuto, K. Inoue, T. Shinmyozu and Y. Maeda, *Bull. Chem. Soc. Jpn.*, 2006, **79**, 442.
20 Oxford Diffraction Poland Sp. CCD data reduction Version 1.171.33.5. Copyright 1995–2006.
21 A. Altomare, M. C. Burla, M. Camalli, G. Cascarano, C. Giacovazzo, A. Guagliardi, A. G. G. Moliterni, G. Polidori and R. Spagna, *J. Appl. Crystallogr.*, 1999, **32**, 115.
22 G. M. Sheldrick, *SHELX97, Program for the Refinement of Crystal Structures*, University of Göttingen, Germany, 1997.
23 N. Moisan, M. Servol, M. Lorenc, A. Tissot, M.-L. Boillot, H. Cailleau, S.-Y. Koshihara and E. Collet, *C. R. Chim.*, 2008, **11**, 1235.
24 E. Collet, M. Buron-Le Cointe and H. Cailleau, *J. Phys. Soc. Jpn.*, 2006, **75**, 011002.
25 A. P. Summerton, A. A. Diamantis and M. R. Snow, *Inorg. Chim. Acta*, 1978, **27**, 123.
26 P. G. Sim, E. Sinn, R. H. Petty, C. L. Merrill and L. J. Wilson, *Inorg. Chem.*, 1981, **20**, 1213.
27 R. Pritchard, S. A. Barrett, C. A. Kilner and M. A. Halcrow, *Dalton Trans.*, 2008, 3159.
28 S. Dorbes, L. Valade, J. A. Real and C. Faulmann, *Chem. Commun.*, 2005, 69.
29 A. Goujon, F. Varret, K. Boukheddaden, C. Chong, J. Jeftic, Y. Garcia, A. D. Naik, J. C. Ameline and E. Collet, *Inorg. Chim. Acta*, 2008, **361**, 4055.
30 E. Collet, M.-L. Boillot, J. Hebert, N. Moisan, M. Servol, M. Lorenc, L. Toupet, M. Buron-Le Cointe, A. Tissot and J. Sainton, *Acta Crystallogr., Sect. B: Struct. Sci.*, 2009, **65**, 474.
31 M. Sorai, R. Burriel, E. F. Westrum, Jr and D. N. Hendrickson, *J. Phys. Chem. B*, 2008, **112**, 4344.
32 S. Schenker and A. Hauser, *J. Am. Chem. Soc.*, 1994, **116**, 5497; S. Schenker, A. Hauser and R. M. Dyson, *Inorg. Chem.*, 1996, **35**, 4676.
33 C. Enachescu, A. Hauser, J.-J. Girerd and M.-L. Boillot, *ChemPhysChem*, 2006, **7**, 1127.
34 A. Hauser, C. Enachescu, L. M. Lawson Daku, A. Vargas and N. Amstutz, *Coord. Chem. Rev.*, 2006, **250**, 1642.

This journal is © The Royal Society of Chemistry 2011

J. Mater. Chem., 2011, **21**, 18347–18353 | 18353

PAPER

Ultrafast spin-state photoswitching in a crystal and slower consecutive processes investigated by femtosecond optical spectroscopy and picosecond X-ray diffraction†

Eric Collet,*[a] Nicolas Moisan,[a] Chérif Baldé,[a] Roman Bertoni,[a] Elzbieta Trzop,[b] Claire Laulhé,[c] Maciej Lorenc,[a] Marina Servol,[a] Hervé Cailleau,[a] Antoine Tissot,[d] Marie-Laure Boillot,[d] Timothy Graber,[e] Robert Henning,[e] Philip Coppens[c] and Marylise Buron-Le Cointe[a]

We report the spin state photo-switching dynamics in two polymorphs of a spin-crossover molecular complex triggered by a femtosecond laser flash, as determined by combining femtosecond optical pump–probe spectroscopy and picosecond X-ray diffraction techniques. The light-driven transformations in the two polymorphs are compared. Combining both techniques and tracking how the X-ray data correlate with optical signals allow understanding of how electronic and structural degrees of freedom couple and play their role when the switchable molecules interact in the active crystalline medium. The study sheds light on crossing the border between femtochemistry at the molecular scale and femtoswitching at the material scale.

1 Introduction

With the advent of control science the current challenge is not only to observe matter on an ever smaller scale but also to direct its functionality at the relevant length, time and energy scales. It is the aim of light-driven transformations, either under continuous light flux or a brief light pulse, to force the matter towards a new state far from thermal equilibrium for generating a photoinduced phase transition.[1] This opportunity to direct material properties by light promises impacting future technologies. Thus, spectacular switching of the macroscopic physical properties of materials resulting from an ultrafast light excitation was reported in different systems for switching from insulator to conductor,[2–4] from paraelectric to ferroelectric,[5,6] or between magnetic states.[7–11] Nevertheless, the understanding of physical mechanisms involved in the transformation induced by an ultra-short femtosecond laser pulse is only emerging.

Understanding and tracking of how materials work, during elementary dynamical processes, has to face with several new and challenging basic questions. For instance, ultrafast information processing based on the control of light-driven switching of the physical properties of materials requires mastering how to direct the system through a complex pathway from atomic to material scales and what fundamentally limits the transformation speed. This feat can be accomplished thanks to the increase of sophisticated instrumentation in ultrafast science. In addition to femtosecond optical pump–probe studies in solids or in solution, recent advances in time-resolved X-ray diffraction[12] make it now possible to probe structural processes at a much finer level than the time average studies allowed before.

More recently, the field of ultrafast photoinduced phase transitions has emerged within material science. If we attempt simple parallels here, the goal is then to realize at the level of a material what has been achieved at the level of a molecule in femtochemistry.[13] The photo-induced transformation pathway in a material is complex,[14] as it is underlined here in spin-crossover materials, for which a magnetic molecular state may be photo-activated in a transient state. In the active crystalline medium other effects of elastic or thermal nature should be considered for describing the macroscopic response, as different processes spanning from molecular to material scales are linked together.

2 Spin-state photoswitching in a crystal

Crystals made of bistable magnetic molecules may be switched from Low Spin (LS) to High Spin (HS) states under the

[a] *Institut de Physique de Rennes, UMR 6251 UR1-CNRS, Bat 11A Campus de Beaulieu, University Rennes 1, Rennes, France. E-mail: eric.collet@univ-rennes1.fr; Fax: +33 223236717; Tel: +33 223236532*
[b] *Chemistry Department, University at Buffalo, State University of New York, Buffalo, NY 14260-3000, USA*
[c] *Synchrotron SOLEIL, L'Orme des Merisiers, Saint Aubin B.P. 48, 91192 Gif-sur-Yvette, France*
[d] *Institut de Chimie Moléculaire et Matériaux d'Orsay, UMR-CNRS 8182, Université Paris-Sud 11, Orsay, France*
[e] *The Consortium for Advanced Radiation Sources, University of Chicago, Chicago, IL 60637, USA*
† Electronic supplementary information (ESI) available. See DOI: 10.1039/c2cp23587k

6192 | *Phys. Chem. Chem. Phys.*, 2012, **14**, 6192–6199

This journal is © the Owner Societies 2012

influence of various external perturbations, including laser excitation.[7–11,15–20] In these systems, the electronic distribution around the metal ion, with $3d^4$–$3d^7$ electronic configurations, of the constituting molecules can change from LS to HS when the octahedral environment of the ion is suitable, that is when the energies of LS and HS states are closely spaced. Then molecules can be easily inter-converted under external perturbations (temperature, pressure or light irradiation). In the spin-crossover process, the electron transfer is coupled to a sizeable structural reorganization of the inner and outer-sphere of coordination, accompanied by large changes in crystal volume.[21–26]

Here we compare the photoresponse of two crystalline polymorphs of the molecular complex [(TPA)Fe(III)(TCC)]PF$_6$ [TPA = tris(2-pyridylmethyl)amine and TCC = 3,4,5,6-tetra-chlorocatecholate dianion]. One crystalline polymorph is monoclinic and the other orthorhombic and their structures, consisting of similar cation layers alternating with PF$_6^-$ anion layers, mainly differ by the layer packing[27] along the crystal axis *b*. In addition to X-ray diffraction, optical identification of the two polymorphs is easy, since at room temperature the crystal colour is purple for the orthorhombic polymorph and orange for the monoclinic one, as illustrated in Fig. 1. The UV-vis-NIR spectra of the monoclinic and orthorhombic polymorphs recorded in the LS and HS phases are presented in Fig. S1 (ESI†) and indicate the iron(III) charge transfer absorption band (LMCT) of LS species centered at 890 nm.

To characterize the thermal spin conversion of both compounds, optical transmission measurements were performed at 480 and 600 nm with light polarized parallel to the long crystal axis (the crystallographic axis **a** for both polymorphs), which yields maximum transmission. By lowering the temperature both undergo a thermal spin-crossover between a high spin ($S = 5/2$) and a low spin ($S = 1/2$) state[27] with the thermal crossover only slightly shifted between the polymorphs: the characteristic temperatures $T_{1/2}$ corresponding to 50% conversion of the metal ions are 214 K for the monoclinic system and 203 K
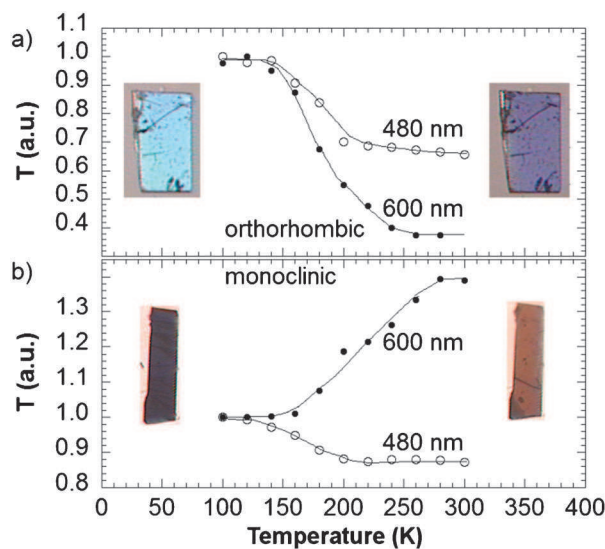
for the orthorhombic one. Fig. 1 shows the temperature dependences of the optical properties when the HS molecular fraction changes from 0 to 1 as temperature increases are different for the polymorphs. In agreement with the change of colour, the optical transmission (T) decreases for both at 480 nm, whereas at 600 nm it decreases for the orthorhombic form and increases for the monoclinic form. These optical changes are commonly used for monitoring the evolution of HS population at thermal equilibrium or under weak *cw* laser excitation.[9,15,20,28] Here we use it for probing ultrafast photo-switching dynamics in the solid state.

The intramolecular reorganization associated with the change of the spin state occurs mainly around the central Fe ion (Fig. 2), and is characterized by the evolution of the bonds between the ion and the ligand.[27] For both polymorphs, the average ⟨Fe–N⟩ bond length changes from 1.96 Å (LS) to 2.13 Å (HS). As the fraction of molecules gradually changes from completely LS to HS, the above mentioned intramolecular structural change induces a gradual evolution of the lattice parameters. We recently demonstrated the possibility to generate in these materials a transient molecular and material transformation towards high spin multiplicity by using femtosecond laser irradiation of the LS phase.[10,11]

In the monoclinic polymorph, a sequence of physical processes was evidenced by using ultrafast optical and X-ray techniques,[10] otherwise hidden in the time domain. In a first step occurring at the molecular level, the LMCT to HS relaxation cascade occurs within 300 fs. In a second step, unit cell expansion occurs within 100 ns. In a third step, heating effects generate an additional thermal population of the HS state. Finally, the recovery to the thermal equilibrium occurs within few ms.[28]

Here we present new results of ultrafast optical spectroscopy and X-ray diffraction in the 100 fs–10 ms time window for both polymorphs. Our results show that the first step is localized at the molecular level, with no indication of a cooperative
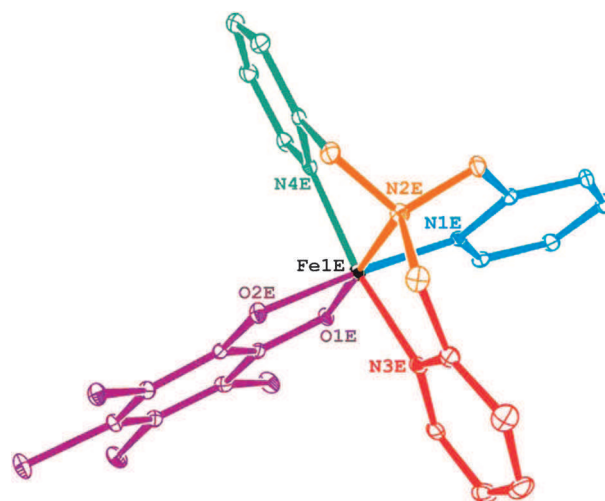

Fig. 1 Temperature dependence of the optical transmission at 480 and 600 nm normalized to values at 100 K for the orthorhombic (a) and monoclinic (b) polymorphs. Measurements were performed with light polarized parallel to the long crystal axis **a**. Photographs were obtained at 50 and 350 K.

Fig. 2 Structure of the [(TPA)Fe(III)(TCC)] cation of both polymorphs and the rigid bodies' model used for refining the structure of the excited state with the LASER refinement. The TCC ligand was treated as one rigid body (violet lines) whereas the TPA ligand was split into 4 parts (orange, red, blue and green lines represent each of the rigid fragments). The PF$_6^-$ counter ion and hydrogen atoms are omitted for clarity.

This journal is © the Owner Societies 2012

Phys. Chem. Chem. Phys., 2012, **14**, 6192–6199 | 6193

response. The elastic step is also demonstrated to be sample dependent in terms of size and shape. The transient state is finally reached within ~ 10–100 µs, where heating and elastic effects are relaxed. The present comparison of both polymorphs shows at a quantitative level that the main molecular LS to HS transformation effect resulting from the laser irradiation is not the purely photoinduced contribution which takes place at the early stage. A complex dynamics results from the energy deposition in the crystal, driving its macroscopic scale response within an out-of-equilibrium process that extends up to tenths of µs. It is this out-of-equilibrium dynamics which induces the most important molecular conversion from LS to HS states.

3 Methods

3.1 Ultrafast optical spectroscopy

The ultrafast dynamics of the photo-response of the [(TPA)-Fe(TCC)]PF$_6$ polymorphs to 45 fs laser excitation were investigated by time-resolved optical experiments. We used typical photon densities up to 100 µJ mm^{-2}, i.e. below the damage value found to be around 300 µJ mm^{-2}. Experiments were performed by using a stroboscopic pump–probe method.[10] The light pulses generated by an amplifier at 1 kHz were split in pump and probe beams. Crystals were excited with near IR pulses (800 nm) in the vicinity of the absorption band (LMCT) of LS species. An optical parametric amplifier (OPA) was used for generating the 600 nm probing light, the wavelength we identified as most sensitive to the spin crossover for both polymorphs in the VIS range (Fig. 1). Pump and probe light used were polarized along the long crystal axis a. We used transmission geometry for probing the response of crystals of typically 200×100 µm^2 size. The pump–probe time resolution was ~ 80 fs. Light was propagating along the b crystal axis, corresponding to the thickness of the crystals, which was in the 5–15 µm range.

This thickness is approaching the laser penetration depth of the pump light for both polymorphs (3–5 µm @ 800 nm) and strikes a good compromise for maximizing the number of photo-excited molecules in the probed bulk. A phase sensitive detection set-up (lock-in amplifier Stanford) was used, in which the pumping rate is halved to 500 Hz with an optical chopper also phase-locked to the reference laser frequency. The earliest steps of the process, from 100 femtoseconds to 1 nanosecond, were monitored using a delay line. Longer delays between the pump and probe were generated electronically by using a second amplifier seeded by the same oscillator. Pump and probe pulses were then delayed by triggering the Pockels cells of the second amplifier, and its Q-switch if necessary so that the pulses from the RF train are trapped and amplified later than those trapped in the first amplifier. By coupling this method in the same experiment with the femtosecond-resolved one, we can track the dynamical response to a laser excitation pump from 10s fs to ms by keeping the time resolution to ~ 100 fs.

3.2 100 ps resolved X-ray diffraction

Time-resolved X-ray diffraction experiments were performed at the Biocars beamline at the APS synchrotron.[29] It is one of the beamlines[5,30–32] at synchrotrons allowing time-resolved diffraction studies at 100 ps resolution. X-Ray pulses were selected by a fast chopper. X-Ray diffraction data were collected for both polymorphs at 15 keV with a MAR-CCD detector and varying delays dt between the laser pump and the probe. For measuring the time dependence of the lattice parameters, partial data were collected for each delay with 60 frames with 10 s of exposure for every 1° step of the diffractometer φ axis. The plate shaped crystals were aligned perpendicular to this axis. The laser beam was incident along the φ rotation axis, and was circularly polarized to avoid any laser polarization dependence with respect to crystal rotation. We used typical excitation densities of 150 µJ mm^{-2}, with a laser beam diameter of ~ 500 µm (FWHM), i.e. more than twice the sample size for a homogeneous excitation. The unit cell parameters and data reduction were obtained with CrysAlis software.[33]

To evaluate the structural reorganization on spin cross-over, more complete data were accumulated for the monoclinic polymorph in a sequence consisting in measuring the diffraction pattern at every 1° oscillation for each time delay (−1 ns, 500 ps and 50 µs). We could only use the 220 first frames of these data collections because of subsequent deterioration of the crystal. The resulting intensities were averaged over repeated and symmetry-equivalent measurements with SORTAV.[34] Details of SORTAV merging and data filtering are listed in Table S1 of the ESI.† The structural changes were analysed with the LASER program.[35]

Least-squares analysis was only performed for data collected in the monoclinic form at the 50 µs time delay, since the number of reflections at the 500 ps time point was insufficient for this procedure. However, both the 500 ps and the 50 µs data were used for the calculation of photodifference maps using the −1 ns dataset as reference state as described further below.

At 50 µs, the structure of the excited state[36,37] was refined based on the response ratios $\eta(hkl)$, defined as:

$$\eta(hkl) = (I_{50\ \mu s}(hkl) - I_{-1\ ns}(hkl))/I_{-1\ ns}(hkl) = R(hkl) - 1,$$

where $I_{50\ \mu s}(hkl)$ represents the intensities of the data collected 50 µs after laser excitation, and $I_{-1\ ns}(hkl)$ the intensities of the data at the negative time delay −1 ns, i.e. with X-ray pulses probing the sample 1 ns before the laser pulse excitation. $R(hkl)$ is the ratio $I_{50\ \mu s}(hkl)/I_{-1\ ns}(hkl)$. LASER assumes a random spatial distribution of the excited state species with the corresponding structure factor expression:[38]

$$F_{50\ \mu s}(hkl) = (1 - P) \times F_{50\ \mu s,\ GS}(hkl) + P \times F_{50\ \mu s,\ ES}(hkl)$$

where GS and ES refer to the ground and excited states and P is the fraction of photo-converted molecules. In the refinement procedure the structure factor of the ground state was taken as the one measured at negative delays:

$$F_{-1\ ns}(hkl) = F_{50\ \mu s,\ GS}(hkl).$$

The ground state position of the Fe1 atom was used as the starting point of the excited state Fe1E atom. The excited state was defined as 5 rigid bodies, as further described in Fig. 2. Rigid bodies were allowed to rotate on their anchor atom, Fe1E and translate independent of the anchor atom. The positions of the ground state molecule and the PF$_6^-$ ion were kept fixed. The starting value of the thermal factor, k_B, was estimated from the photo-Wilson plot. The ratio-agreement

6194 | Phys. Chem. Chem. Phys., 2012, **14**, 6192–6199

This journal is © the Owner Societies 2012

factor R_R[39] was used to compare observed and calculated ratios:

$$R_R = \frac{\sum_{hkl} |R_{obs}(hkl) - R_{calc}(hkl)|}{\sum_{hkl} R_{obs}(hkl)}$$

The final agreement obtained for the 50 µs data set is $R_R = 9.63\%$. A list of refinement details is given in Table S2 of the ESI.† The molecular geometry from this LASER refinement was also used to estimate the excited state population of the 500 ps data, based on the 500 ps R_R factor changes on varying the population, as shown in Fig. S2 of the ESI.†
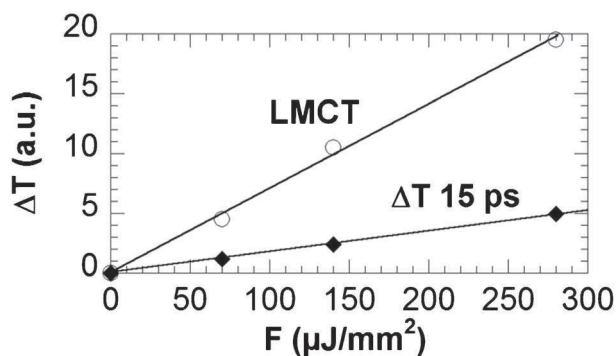
4 Results

4.1 Ultrafast dynamics studied by optical spectroscopy

The time dependent variation of optical transmission (ΔT) at 600 nm between negative and positive delays following fs laser excitation at 800 nm is shown in Fig. 3 for each polymorph. As the transmission varies in opposite directions for the two polymorphs between LS and HS states, $-\Delta T$ is plotted for the orthorhombic form in such a way that the positive signal at long delay corresponds to the formation of HS states. In this way it is easier to compare both polymorphs. Data were measured in the LS phase at 180 K for 40 µJ mm^{-2} excitation density (~ 2 photons/100 molecules). A transient absorption peak appears for both polymorphs as transmission decreases within the 80 fs time resolution. This is due to a Ligand-to-Metal Charge-Transfer state (LMCT state). It is followed by a variation of ΔT characteristic of an exponential-like population of the HS state, which is fed from the LMCT state with $\tau \approx 300$ fs time constant. The initial step of LS–HS conversion in solids is therefore as fast as the one observed for similar spin-crossover molecules in solution.[40–45] The evolution of the response with laser fluence measured on the monoclinic polymorph is presented in Fig. 4. It only shows a linear response and therefore
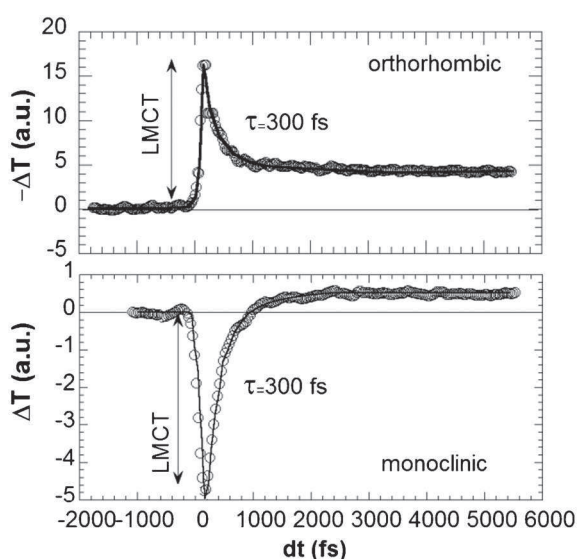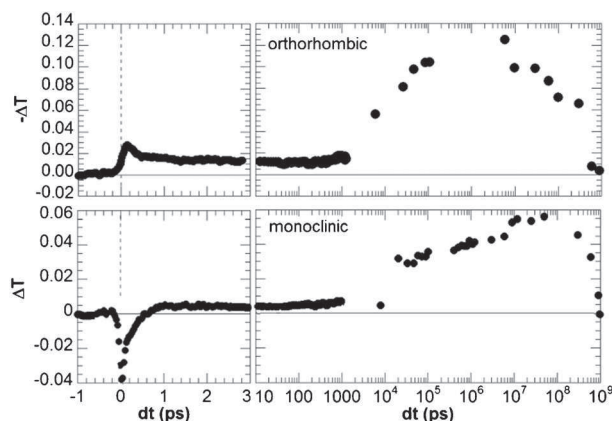

Fig. 4 Fluence dependence of the photo-response on the LMCT peak and transmission variation at 15 ps (monoclinic polymorph).

no threshold or cooperative effect is detected here. This linear response on an ultrashort time scale is also a clear indication that the early events in the photoinduced spin-state switching occur locally at the molecular level in this non-cooperative sample.

4.2 Optical spectroscopy studies of ns–ms dynamics

The photoconverted HS fraction on the picosecond plateau is estimated to be ~ 0.5–1%, and it extends as such up to a few ns as observed in Fig. 5. The main difference between this study and the case of photoinduced spin-crossover dynamics for molecules in solution is that in the latter case the relaxation of photo-excited molecules occurs within ns as the molecules cool down by heat exchange with the solvent.[40–45] In the present case, we do not observe relaxation of photoinduced molecular switching but an additional conversion in the active crystal medium. An abrupt increase of the response occurs after a few ns, and continues until ~ 1 µs. After that, a third step is observed, especially in the data for the monoclinic polymorph, around 10 µs after laser excitation. This last stage was clearly demonstrated to be associated with a thermal heating effect in previous picosecond X-ray diffraction studies.[10] These previous studies on the monoclinic polymorph could however only show a change on the a unit-cell parameter in the 50 ns time delay.

This ns step is more extensively investigated in the present experiments performed at BIOCARS, making it possible to

Fig. 3 Time dependence of the variation of transmission in ultra-short scale $-\Delta T$ (orthorhombic) and ΔT (monoclinic) at 600 nm following femtosecond laser excitation at 800 nm.

Fig. 5 Time dependence of the variation of transmission over several temporal scales $-\Delta T$ (orthorhombic) and ΔT (monoclinic) at 600 nm following femtosecond laser excitation at 800 nm.

assign this ns step to elastic effects as lattice expansion occurs at this time. The transmission changes plotted in Fig. 5 were compared and normalized to values measured during the thermal conversion (Fig. 1), so that the scales correspond approximately to the HS fraction X_{HS}. We estimate from optical data that this jump corresponds to an increase of the fraction of HS molecules by a factor of $\sim$5–10 compared to the intramolecular step which occurs within 300 fs, as the converted fraction of HS molecules approaches 5–10% on µs delays.

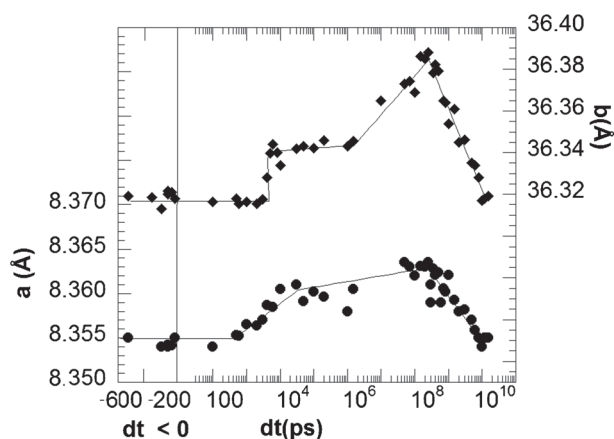This higher conversion rate for the orthorhombic polymorph might be related to the smaller thickness of the sample used ($\sim$7 µm) compared to the monoclinic one ($\sim$15 µm), making it possible to have a better matching between the sample thickness and the laser penetration depth (reaching for both polymorphs 3–5 µm).

Finally, both polymorphs recover the initial state existing prior to laser excitation at a ms time scale, in good agreement with time-resolved studies of the lifetime of the transient photoexcited state.[30]
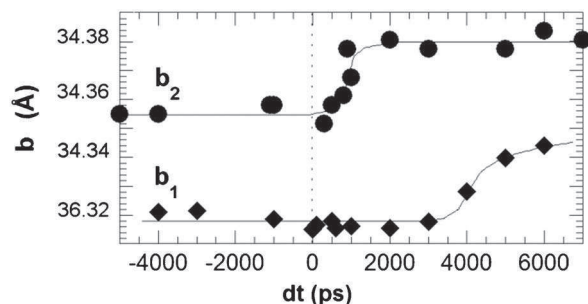
4.3 Elastic and heating effects probed by X-ray diffraction

The structural reorganization associated with the swelling of the molecules and lattice heating induces expansion of the crystal volume. It can be easily detected by time-resolved X-ray diffraction, as shown in Fig. 6 for the monoclinic polymorph. From these results, we observe that the first stage of the transformation detected by femtosecond optical spectroscopy takes place in a crystal with a constant lattice. Indeed, it takes time for cell deformation to propagate and these elastic effects therefore occur at the speed of sound. We observe an abrupt increase of the lattice parameter b around 4 ns, as indicated in Fig. 6 and 7 and a second slower step in the 1 µs–100 µs range.

This response is anisotropic since the increase of the lattice parameter a is slower and takes few tenths of ns. It is followed by a slower heating effect in the 100 ns–100 µs range.[10,14] The earlier investigations provided a more accurate evolution of a than the current study, because a different diffraction geometry was used. The lattice expansion is clearly governed by propagating effects and the timescale is therefore sample dependent. This is illustrated in Fig. 7, which compares the lattice expansion of
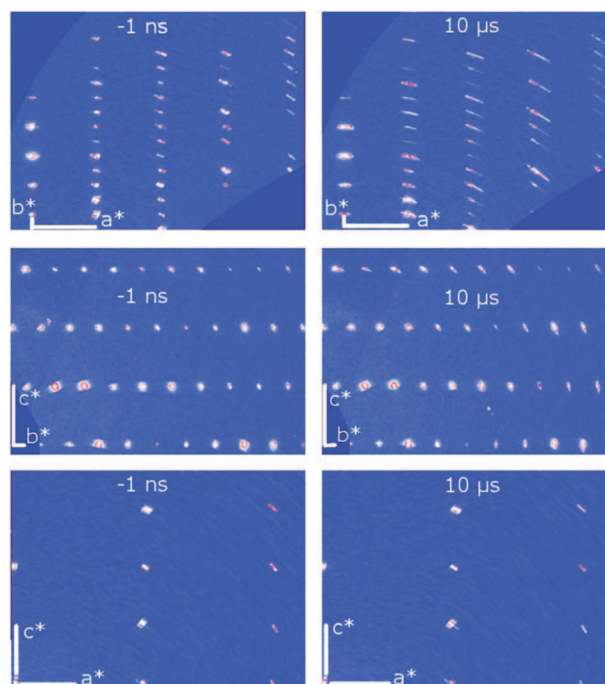

Fig. 7 Time dependence of the lattice parameters b of 2 crystals of the monoclinic polymorph with 20 µm (b_1 ◆) and 7 µm (b_2 ●) thickness. b_2 values are shifted for clarity.
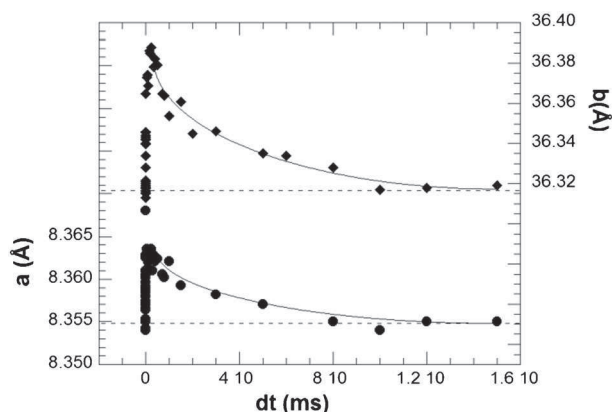
two crystals of the monoclinic polymorph, and shows the time dependence of the lattice parameters b_1 for sample 1 ($\sim$20 µm thick) and b_2 for sample 2 ($\sim$7 µm thick). A faster expansion of the lattice parameter b is observed when the thickness (corresponding to b axis) of the crystal plate is reduced. It is expected that the expansion time varies linearly with the sample thickness, in good agreement with the expansion time of 5 ns (respectively 1.5 ns) for the 20 µm (resp. 7 µm) thick crystal presented in Fig. 7. Similar responses were observed for the orthorhombic polymorph but with a too limited number of data to allow detailed conclusions.

Since conversion related to heat diffusion effects is more rapidly activated when the size is small, the excitation of crystals of anisotropic shape induces in the time domain anisotropic deformations. This can be observed by deformation of the Bragg peaks in the reciprocal lattice. Fig. 8 shows reconstruction of different reciprocal planes before laser excitation (-1 ns) and after laser excitation when the effect is maximum (10 µs) measured on a

Fig. 8 Evolution of the diffracted intensity on the orthorhombic polymorph in the (a^*,c^*), (b^*,c^*) and (a^*,b^*) reciprocal planes, showing a deformation of the Bragg peaks between -1 ns and 10 µs.

Fig. 6 Time dependence of the lattice parameters a (●) and b (◆ sample thickness) measured on the monoclinic polymorph.

6196 | *Phys. Chem. Chem. Phys.*, 2012, **14**, 6192–6199

This journal is © the Owner Societies 2012

Fig. 9 Time dependence of the lattice parameters *a* (●) and *b* (◆) in the ms window measured on the monoclinic polymorph.

$200 \times 200 \times 7\ \mu m^3$ single crystal of the orthorhombic form. In the (a^*,c^*) plane no significant deformation is observed, whereas in the (a^*,b^*) and (b^*,c^*) planes an important broadening of the Bragg peaks is observed in the 10 ns–10 μs time domain.

With the present X-ray diffraction measurements, this recovery to equilibrium can be observed by the relaxation of the lattice parameters *a* and *b* plotted in Fig. 9 for the monoclinic polymorph. This kinetics is governed by heat exchange with the sample environment. Compared to previous studies performed at 1 kHz repetition rate, the present study, performed at 40 Hz, allows precise determination of the recovery time of ~ 8 ms.

4.4 Structural analysis of the molecular reorganization

The photodifference maps[46] of type II ($F_{obs}^{dt\ >\ 0} - F_{obs}^{-1\ ns}$) based on independent reflections with $I/\sigma(I) > 4$, calculated at isosurfaces of ± 0.14 e $Å^{-3}$ and 0.46 e $Å^{-3}$, respectively, for $dt = 500$ ps and 50 μs are shown in Fig. 10. These two maps show significant changes in the electron density on excitation. The molecular response on excitation at 500 ps is illustrated by the sideward shift of the electron density of the Fe1 atom towards O2 (Fig. 10a). This shift is even more pronounced at 50 μs time delay (Fig. 10b). At this delay, the excited state population should be significantly higher in view of the optical data presented in Fig. 5. Additionally an increase of the Fe–N distances is observed (Table 1).

The estimated population of the excited state at 500 ps is in the 1.5%–2% range. LASER refinement of 50 μs data indicates a much larger excitation percentage of 10.5 (16)%. The increase of excited state population with longer time delay due to the temperature increase agrees also well with the signal seen in photodifference maps, associated with a larger change of the average structure. The molecular geometry of the excited state at 50 μs is compared in Table 1 with the one of the ground state measured at -1 ns delay. Although the standard deviations are large, all changes in the Fe–N bond lengths are positive, as expected. This is a result of significant shifts of the iron by 0.17(2) Å and of the two oxygen atoms.

5 Discussion

The photoinduced switching dynamics in both spin-crossover materials can present different consecutive steps. Just after the
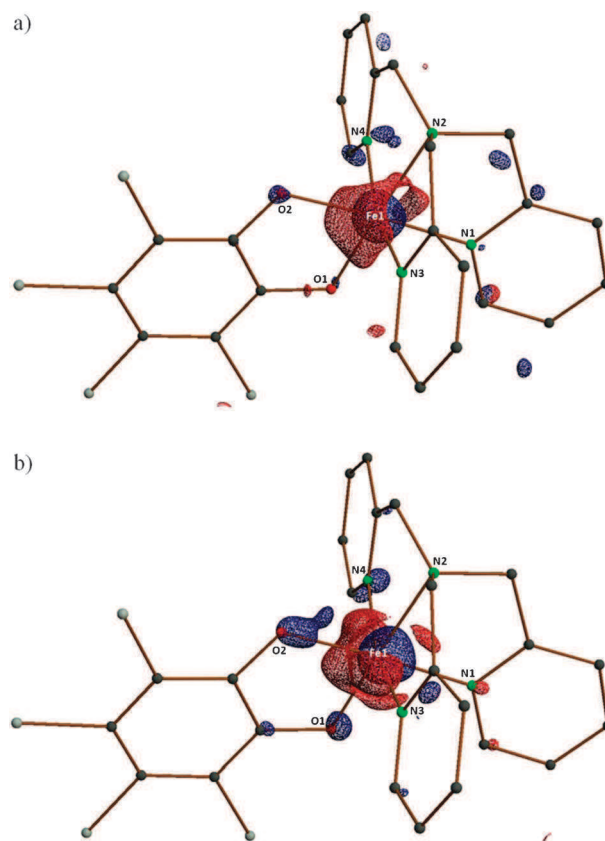

Fig. 10 Photodifference maps obtained for the monoclinic polymorph with isosurfaces (red positive, blue negative) of (a) ± 0.14 e $Å^{-3}$ for the 500 ps data and (b) ± 0.46 e $Å^{-3}$ for the 50 μs data calculated with XDGRAPH of the XD program set.[46] The PF_6^- counter ion and hydrogen atoms are omitted for clarity.

Table 1 Geometry changes for the monoclinic polymorph on excitation based on the LASER refinement of the 50 μs data. The accuracy of the excited state molecular distances was estimated by error propagation

| | Bond length/Å | |
Contact	GS	ES
Fe1–O1	1.866(2)	1.92(2)
Fe1–O2	1.915(2)	1.83(3)
Fe1–N1	1.977(3)	2.03(6)
Fe1–N2	2.031(3)	2.13(3)
Fe1–N3	1.982(3)	2.02(3)
Fe1–N4	1.989(3)	2.04(3)

	Shift/Å
Fe1–Fe1E	0.17(2)
N1–N1E	0.11(5)
N2–N2E	0.05(5)
N3–N3E	0.07(3)
N4–N4E	0.08(4)
O1–O1E	0.14(2)
O2–O2E	0.12(2)

femtosecond laser excitation, the LMCT state generated at the molecular level relaxes towards the metastable HS molecular state, illustrated by dots at $dt = 0$ ps in Scheme 1.

This process occurs with a typical 300 fs time-constant corresponding well to time scales reported for spin crossover

This journal is © the Owner Societies 2012

Phys. Chem. Chem. Phys., 2012, **14**, 6192–6199 | **6197**
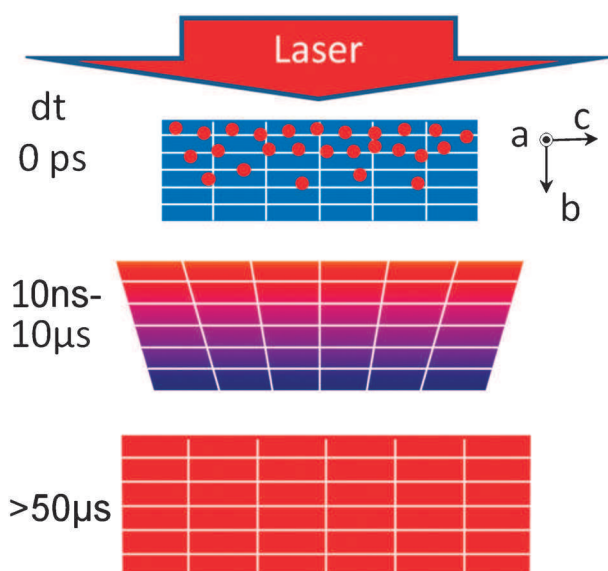
Scheme 1 Schematic drawing of the dynamics. The laser deposits energy on photo-excited molecules (dots) of the crystal at $dt = 0$ ps. The gradient of deposited energy results in an inhomogeneous lattice expansion over the b axis (sample thickness) in the 10 ns–10 μs time window. At 50 μs the temperature is homogenized over the crystal and the heating effect results in thermal population of the HS state.

molecules in solution.[40–45] The related molecular swelling and the lattice heating induce an internal pressure and generate a propagating nonlinear wave resulting in crystal expansion during the next step. Since the crystals used have anisotropic shapes, the elastic stress propagation takes less time along the thickness ($\sim$20 μm within a few ns) than along the perpendicular directions (200 μm within $\sim$50 ns). Such a pressure front induces an over-compressed region followed by a depression, which will favour switching from LS to HS states. During this elastic expansion in the 2 ns–100 ns time window, the fraction of HS molecules increases.

The optical energy absorbed at the molecular level is much higher than the thermal energy difference between LS and HS states. This energy is mainly redistributed as heat in the crystal, resulting in global warming. The temperature homogenization is reached within 10 μs at the macroscopic level, leading to an increase of the average temperature. This heating and the associated additional conversion to HS states result both in another lattice expansion within 100 ns–100 μs.

However, the gradient of deposited optical energy over the sample thickness (b axis in Scheme 1) induces a temperature gradient in the crystal thickness. This gradient of temperature gives rise to an inhomogeneous distribution of unit cell volume over the sample thickness. This gradient of unit cell parameter over the b axis induces a deformation of the Bragg reflections in the (b^*,a^*) and (b^*,c^*) reciprocal planes, but not in the (a^*,c^*) planes (Fig. 9). The unit cell gradient of lattice parameters a or c over the thickness corresponding to the b axis should give rise to a radial broadening of the peaks in the (a^*,c^*) plane. But this expected broadening, which can be estimated by the corresponding variation of lattice parameters in Fig. 6, is smaller than the HWHM of the Bragg peaks and therefore difficult to observe. The deformation of the peaks is therefore

very likely associated with the inhomogeneous distribution of the lattice parameters over the sample thickness, as the crystal is not equilibrated, which should induce a crystal deformation.

Within 50 μs, temperature is homogeneous in the sample and the reciprocal lattice recovers its initial shape. This increase of temperature results in a higher population of the HS fraction (thermally activated) in the transient equilibrated state.

The elastic and thermal steps clearly underline the active role of the crystal medium, made of switchable molecules, mediating a self-amplification process. This type of phenomena cannot exist for molecules in solution, as the solvent is mainly passive. The interaction of the photo-excited molecule with the surrounding media only results in transfer of excess energy. In the active crystalline medium studied here, this energy transfer, which takes different forms (elastic and thermal), is at the origin of additional switching activation across the crystal.

6 Conclusions

The present results underline the very good correlation between time-resolved optical data (mainly sensitive to the electronic molecular state) and X-ray data (sensitive to structural deformation) in systems where electronic and structural degrees of freedom are strongly coupled. Our data show that a macroscopic system made of bistable molecules can be switched on an ultra-short time scale, and as so represents a first test for crossing the border between femtochemistry at the molecular scale and femtoswitching at the material scale.

However, in the present systems, our data also clearly give evidence that macroscopic descriptions are required in fast transformation of matter driven by light irradiation. It is necessary here to take into account the shock-wave driven transformation or the heating effect for example. By comparing two solids made of the same molecules, we can draw a general conclusion on the occurrence of different steps, resulting from different stimuli driven by light: photo-switching, elasto-switching and thermo-switching. These last two effects, which finally prevail over the purely photoinduced effect observed on the femtosecond time scale, may be limited by chemical engineering if in future material the elastic effects can be diminished, with less deformable molecules or by introducing absorbers in the crystal, or/and reducing the heating effects with HS states unreachable at high temperature. The detailed crystallography analysis presented here and elsewhere also opens the way towards femtosecond crystallography,[47] which will hopefully be performed on the new generation of femtosecond X-ray sources.[48]

6198 | *Phys. Chem. Chem. Phys.*, 2012, **14**, 6192–6199

This journal is © the Owner Societies 2012

Notes and references

1 S. Koshihara and M. Kuwata-Gonokami, ed., *J. Phys. Soc. Jpn.*, 2006, **75**, 011001.

2 M. Chollet, L. Guerin, N. Uchida, S. Fuhaya, H. Shimoda, T. Ishikawa, K. Matsuda, T. Hasegawa, A. Ota, H. Yamochi, G. Saito, R. Tazaki, S. Adachi and S. Koshihara, *Science*, 2005, **307**, 86.

3 Y. Okimoto, T. Miyata, M. S. Endo, M. Kurashima, K. Onda, T. Ishikawa, S. Koshihara, M. Lorenc, E. Collet, H. Cailleau and T. Arima, *Phys. Rev. B: Condens. Matter Mater. Phys.*, 2011, **84**, 121102.

4 T. Ishikawa, N. Fukazawa, Y. Matsubara, R. Nakajima, K. Onda, Y. Okimoto, S. Koshihara, M. Lorenc, E. Collet, M. Tamura and R. Kato, *Phys. Rev. B: Condens. Matter Mater. Phys.*, 2009, **80**, 115108.

5 E. Collet, M.-H. Lemée-Cailleau, M. Buron-Le Cointe, H. Cailleau, M. Wulff, T. Luty, S.-Y. Koshihara, M. Meyer, L. Toupet, P. Rabiller and S. Techert, *Science*, 2003, **300**, 612–615.

6 L. Guérin, E. Collet, M. H. Lemée-Cailleau, M. Buron, H. Cailleau, A. Plech, M. Wulff, S. Koshihara and T. Luty, *Chem. Phys.*, 2004, **299**, 163.

7 S. Bonhommeau, G. Molnar, A. Galet, A. Zwick, J.-A. Real, J. J. McGarvey and A. Bousseksou, *Angew. Chem., Int. Ed.*, 2005, **44**, 4069.

8 O. Fouché, J. Degert, G. Jonusauskas, N. Daro, J.-F. Létard and E. Freysz, *Phys. Chem. Chem. Phys.*, 2010, **12**, 3044.

9 G. Galle, J. Degert, C. Mauriac, C. Etrillard, J. F. Letard and E. Freysz, *Chem. Phys. Lett.*, 2010, **500**, 18–22.

10 M. Lorenc, J. Hébert, N. Moisan, E. Trzop, M. Servol, M. Buron-Le Cointe, H. Cailleau, M.-L. Boillot, E. Pontecorvo, M. Wulff, S. Koshihara and E. Collet, *Phys. Rev. Lett.*, 2009, **103**, 028301.

11 N. Moisan, M. Servol, M. Lorenc, A. Tissot, M.-L. Boillot, H. Cailleau, S. Koshihara and E. Collet, *C. R. Chim.*, 2008, **11**, 1235.

12 E. Collet, *Acta Crystallogr., Sect. A: Found. Crystallogr.*, 2010, **66**, 133.

13 A. H. Zewail, *Angew. Chem., Int. Ed.*, 2000, **39**, 2586–2631.

14 H. Cailleau, M. Lorenc, L. Guérin, M. Servol, E. Collet and M. Buron-Le Cointe, *Acta Crystallogr., Sect. A: Found. Crystallogr.*, 2010, **66**, 189.

15 A. Goujon, F. Varret, K. Boukheddaden, C. Chong, J. Jeftic, Y. Garcia, A. D. Naik, J. C. Ameline and E. Collet, *Inorg. Chim. Acta*, 2008, **361**, 4055–4064.

16 N. Bréfuel, H. Watanabe, L. Toupet, J. Come, N. Matsumoto, E. Collet, K. Tanaka and J.-P. Tuchagues, *Angew. Chem., Int. Ed.*, 2009, **48**, 9304–9307.

17 S. Decurtins, P. Gütlich, C. P. Köhler, H. Spiering and A. Hauser, *Chem. Phys. Lett.*, 1984, **105**, 1.

18 J. F. Létard, L. Capes, G. Chastanet, N. Moliner, S. Létard, J. A. Real and O. Kahn, *Chem. Phys. Lett.*, 1999, **313**, 115.

19 J. F. Létard, P. Guionneau, L. Rabardel, J. A. K. Howard, A. E. Goeta, D. Chasseau and O. Kahn, *Inorg. Chem.*, 1998, **37**, 4432.

20 P. Gütlich and H. A. Goodwin, ed. *Top. Curr. Chem.*, 2004, **233**, **234** and **235**.

21 E. Collet, M. Lorenc, M. Buron-Le Cointe and H. Cailleau, *Z. Kristallogr.*, 2008, **223**, 272–282.

22 (a) C.-F. Sheu, S.-M. Chen, S.-C. Wang, G.-H. Lee, Y.-H. Liu and Y. Wang, *Chem. Commun.*, 2009, 7512–7514; (b) C. H. Shih, C. F. Cheu, K. Kato, K. Sugimoto, J. Kim, Y. Wang and M. Takata, *Dalton Trans.*, 2010, **39**, 9794–9800.

23 M. Marchivie, P. Guionneau, J. F. Létard and D. Chasseau, *Acta Crystallogr., Sect. B: Struct. Sci.*, 2003, **59**, 479.

24 V. Legrand, S. Pillet, M. Souhassou, N. Lugan and C. Lecomte, *J. Am. Chem. Soc.*, 2006, **128**, 13921–13931.

25 S. Pillet, V. Legrand, M. Souhassou and C. Lecomte, *Phys. Rev. B: Condens. Matter Mater. Phys.*, 2006, **74**, 140101.

26 E. Collet, M. Buron-Le Cointe and H. Cailleau, *J. Phys. Soc. Jpn.*, 2006, **75**, 011002.

27 E. Collet, M.-L. Boillot, J. Hébert, N. Moisan, M. Servol, M. Lorenc, L. Toupet, M. Buron-Le Cointe, A. Tissot and J. Sainton, *Acta Crystallogr., Sect. B: Struct. Sci.*, 2009, **65**, 474.

28 C. Enachescu, A. Hauser, J.-J. Girerd and M.-L. Boillot, *ChemPhysChem*, 2006, **7**, 1127.

29 T. Graber, P. Anfinrud, H. Brewer, Y.-S. Chen, H.-S. Cho, N. Dashdorj, R. W. Henning, I. Kosheleva, G. Macha, M. Meron, R. Pahl, Z. Ren, S. Ruan, F. Schotte, V. Šrajer, P. J. Viccaro, F. Westferro and K. Moffat, *J. Synchrotron Radiat.*, 2011, **18**, 658–670.

30 S. Nozawa, S. Adachi, J. Takahashi, R. Tazaki, L. Guérin, M. Daimon, A. Tomita, T. Sato, M. Chollet, E. Collet, H. Cailleau, S. Yamamoto, K. Tsuchiya, T. Shioya, H. Sasaki, T. Mori, K. Ichiyanagi, H. Sawa, H. Kawata and S. Koshihara, *J. Synchrotron Radiat.*, 2007, **14**, 313–319.

31 S. L. Johnson, P. Beaud, C. J. Milne, F. S. Krasniqi, E. S. Zijlstra, M. E. Garcia, M. Kaiser, D. Grolimund, R. Abela and G. Ingold, *Phys. Rev. Lett.*, 2008, **100**, 155501.

32 L. Guérin, J. Hebert, M. Buron-Le Cointe, S. Adachi, S. Koshihara, H. Cailleau and E. Collet, *Phys. Rev. Lett.*, 2010, **105**, 246101.

33 CrysAlis RED, Version 1.171.26. Oxford Diffraction Ltd, Abingdon, Oxfordshire, England.

34 R. H. Blessing, *J. Appl. Crystallogr.*, 1997, **30**, 421–426.

35 I. Vorontsov, S. Pillet, R. Kaminski, M. S. Schmøkel and P. Coppens, *J. Appl. Crystallogr.*, 2010, **43**, 1129–1130.

36 A. Makal, E. Trzop, J. Sokolow, J. Kalinowski, J. Benedict and P. Coppens, *Acta Crystallogr., Sect. A: Found. Crystallogr.*, 2011, **67**, 319–326.

37 P. Coppens, J. Benedict, M. Messerschmidt, I. Novozhilova, T. Graber, Y.-S. Chen, I. Vorontov, S. Scheins and S.-L. Zheng, *Acta Crystallogr., Sect. A: Found. Crystallogr.*, 2010, **66**, 179–188.

38 I. I. Vorontsov and P. Coppens, *J. Synchrotron Radiat.*, 2005, **12**, 488–493.

39 P. Coppens, R. Kamiński and M. S. Schmøkel, *Acta Crystallogr., Sect. A: Found. Crystallogr.*, 2010, **66**, 626–628.

40 W. Gawelda, V.-T. Pham, M. Benfatto, Y. Zaushitsyn, M. Kaiser, D. Grolimund, S. L. Johnson, R. Abela, A. Hauser, C. Bressler and M. Chergui, *Phys. Rev. Lett.*, 2007, **98**, 057401.

41 C. Bressler, C. Milne, V.-T. Pham, A. El Nahhas, R. M. van der Veen, W. Gawelda, S. Johnson, P. Beaud, D. Grolimund, M. Kaiser, C. N. Borca, G. Ingold, R. Abela and M. Chergui, *Science*, 2009, **323**, 489.

42 M. Khalil, M. M. Marcus, A. L. Smeigh, J. K. McCusker, H. H. W. Chong and R. W. Schoenlein, *J. Phys. Chem. A*, 2006, **110**, 38.

43 C. Brady, J. J. McGarvey, J. K. McCusker, H. Toftlund and D. N. Hendrickson, *Top. Curr. Chem.*, 2004, **235**, 1.

44 A. Cannizzo, F. van Mourik, W. Gawelda, G. Zgrablic, C. Bressler and M. Chergui, *Angew. Chem., Int. Ed.*, 2006, **45**, 3174.

45 J. Tribollet, G. Galle, G. Jonusauskas, D. Deldicque, M. Tondusson, J. F. Letard and E. Freysz, *Chem. Phys. Lett.*, 2011, **513**, 42–47.

46 A. Volkov, P. Macchi, L. J. Farrugia, C. Gatti, P. R. Mallinson, T. Richter, T. Koritsanszky, (2006). XD2006. Middle Tennessee State University, USA, Università di Milano and CNR-ISTM Milano, Italy, University of Glasgow, Scotland, State University of New York at Buffalo, USA, and Freie Universität Berlin, Germany).

47 E. Collet, M. Lorenc, M. Cammarata, L. Guérin, M. Servol, A. Tissot, M. L. Boillot, H. Cailleau and M. Buron-Le Cointe, *Chem.–Eur. J.*, DOI: 10.1002/chem.201103048.

48 R. A. Kirian, T. A. White, J. M. Holton, H. N. Chapman, P. Fromme, A. Barty, L. Lomb, A. Aquila, F. R. Maia, A. V. Martin, R. Fromme, X. Wang, M. S. Hunter, K. E. Schmidt and J. C. Spence, *Acta Crystallogr., Sect. A: Found. Crystallogr.*, 2011, **67**, 131–140.

Ultrafast Photoswitching

Femtosecond Spin-State Photoswitching of Molecular Nanocrystals Evidenced by Optical Spectroscopy**

Roman Bertoni, Maciej Lorenc,* Antoine Tissot, Marina Servol, Marie-Laure Boillot, and Eric Collet*

In the field of control science, which aims at switching the physical properties of materials, photoinduced phase transitions[1] open fascinating perspectives for driving a material towards a new state, far from thermal equilibrium. Such photoswitching will impact future technologies as it provides doorways to the light-control of various photoswitchable functions (for example, magnetic, optical, conducting, and ferroelectric).[2] In control science, tailored laser pulses are widely regarded as the most likely source for achieving that goal.[3] In that respect, the great challenge for molecular-based materials is directing the functionality, both at the relevant size and time scales. If we attempt simple parallels here, the goal is to achieve at the level of a material what femtochemistry has accomplished at the level of a molecule.[4] In observing and understanding how materials work during elementary dynamical processes, several challenging basic questions are confronted. For instance, ultrafast information processing based on the control of light-driven switching of the physical properties of materials requires that such systems be directed through a complex pathway from atomic to material scales, and that the fundamental limits of trans-formation speed be overcome, or circumvented. Molecular magnets,[5] and especially the spin-crossover compounds (SCO),[6] are ideal candidates for photo-active prototypes, which show photomagnetic and photochromic properties driven by the switching of the constituent molecules between their electronic low spin (LS) and high spin (HS) states. Herein we report the ultrafast spin state photoswitching of a spin-crossover nanocrystal of an Fe^{III} complex, [Fe(3-MeO-SalEen)$_2$]PF$_6$ (Figure 1), as studied through femtosecond optical spectroscopy (H-3-MeO-SalEen being the condensa-tion product of 3-methoxy-substituted salicylaldehyde and *N*-ethyl-ethylenediamine). This result provides proof-of-prin-ciple for femtosecond switching at the nanoscale in SCO materials showing photomagnetic and photochromic responses.
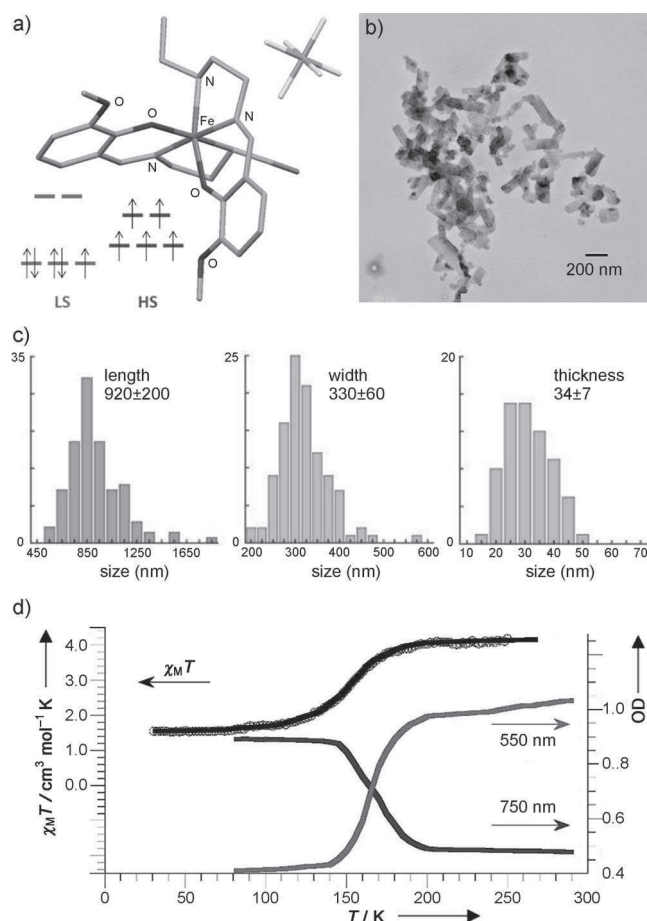
Figure 1. Fe^{III} spin-crossover nanocrystals. a) The [Fe(3-MeO-SalEen)$_2$] cation and PF$_6$ anion with the LS and HS electronic configurations. b) TEM image of the nanocrystals. c) Size distribution of the nano-crystals. d) $\chi_M T$ vs. T plot of the nanocrystal film and OD versus T at 550 and 750 nm.

[*] R. Bertoni, Dr. M. Lorenc, Dr. M. Servol, Prof. E. Collet
Institut de Physique de Rennes, UMR CNRS 6251
Université Rennes 1, 35042 Rennes cedex (France)
E-mail: maciej.lorenc@univ-rennes1.fr
          eric.collet@univ-rennes1.fr

Dr. A. Tissot, Dr. M.-L. Boillot
Institut de Chimie Moléculaire et Matériaux d'Orsay
UMR-CNRS 8182, Université Paris-Sud 11 (France)

Supporting information for this article is available on the WWW under http://dx.doi.org/10.1002/anie.201202215.

SCO materials are bistable systems, for which nanosecond laser excitation within the range of thermal hysteresis can generate LS to HS transition.[7] Ultrafast investigations of similar photo-transformations have been mainly limited to single molecules in solution,[8] and only recently also carried out on crystals.[9] Despite formidable progress in the chemis-try and engineering of spin-crossover nanoparticles,[10] as well as their nano-patterning and nanoscale assembling[6b, 11] while preserving their switchable properties, the ultrafast switching of such materials has not yet been observed. Herein we study the ultrafast LS-to-HS spin-state photoswitching pathway of nanocrystals (Figure 1), taking advantage of growing knowl-edge in the field of ultrafast chemical physics.[12]

Hendrickson and co-workers were the first to synthesize the Fe^{III} complex [Fe(3-MeO-SalEen)$_2$] PF$_6$ (Figure 1 a).[13] Its crystalline form undergoes a first-order phase transition between LS ($S = 1/2$) and HS ($S = 5/2$) states around 162 K, where it also exhibits a narrow hysteresis.[9b] Nanoparticles of this compound were obtained by a precipitation method and were previously characterized with magnetic, Raman, EPR, and X-ray analysis[10e] to confirm their crystalline nature. For the investigation of ultrafast photoswitching dynamics, new nanocrystals were synthesized. These needle-shaped crystals have typical dimensions of $(34 \pm 7) \times (330 \pm 60) \times (920 \pm 200)$ nm^3 with a satisfactory size dispersion, when observed by TEM (Figure 1 b,c). The nanocrystals were embedded in a thin polymer film, which had been spin-coated on a glass substrate. These robust films allow for easy manipulation of nanocrystals and thus envisioning unrestricted scaffolding for nanocrystal-based devices.

The film of nanocrystals appears homogeneous at the sub-millimetric scale. The SCO properties of nanocrystals embedded in polyvinylpyrrolidone (PVP) thin films were investigated by magnetic and optical measurements, as shown in Figure 1. They undergo a thermal spin-crossover between LS and HS states centered at $T_{1/2} =$ ca. 156 K, characterized by a change in color (Figure 2 a&b) accompanying the change in magnetic susceptibility (Figure 1 d). Below about 100 K the SCO system remains fully LS, whereas it is fully HS above about 200 K. In comparison with macroscopic single crystals,[9b] the thermal conversion of the nanocrystals has somewhat lost its first-order character. For the nanocrystals embedded in the PVP film, the evolution of the fraction of the HS species appears even more gradual, and we are currently investigating whether this effect can be attributed to chemical and/or physical factors.[6b, 14]

A detailed optical absorption spectroscopy study was performed to characterize the thermal LS-to-HS conversion of the nanocrystals. The variation in the optical density (ΔOD) is gradual during the thermal crossover (Figure 2 c). Figure 2 d, showing ΔOD between 90 K (pure LS state) and 230 K (pure HS state), reveals phenolate-to-iron charge-transfer (CT) bands with the distinct features of LS and HS states. The OD of the HS state, with respect to that of the LS state, is higher in the visible (VIS) and lower in the near-infrared (NIR) parts of the spectra, an observation which is in agreement with the change of color pictured in Figure 2 a,b. The evolution is marked by a well-defined isosbestic point at ca. 670 nm (Figure 2 c,d), as the HS and LS species interchange their relative concentrations during the thermal conversion. Figure 1 d, showing the temperature dependence of the OD for selected wavelengths (550 and 750 nm) on either side of the isosbestic point, marks the LS-to-HS conversion and shows a very good correlation between magnetic measurements and optical markers. All observed features were attributed to the nanocrystals, as the optical transparency of the polymer was experimentally verified in the temperature and spectral ranges considered here. We would like to emphasize a unique advantage offered here by the solid state: the molecules can be thermally switched between LS and HS states without otherwise resorting to
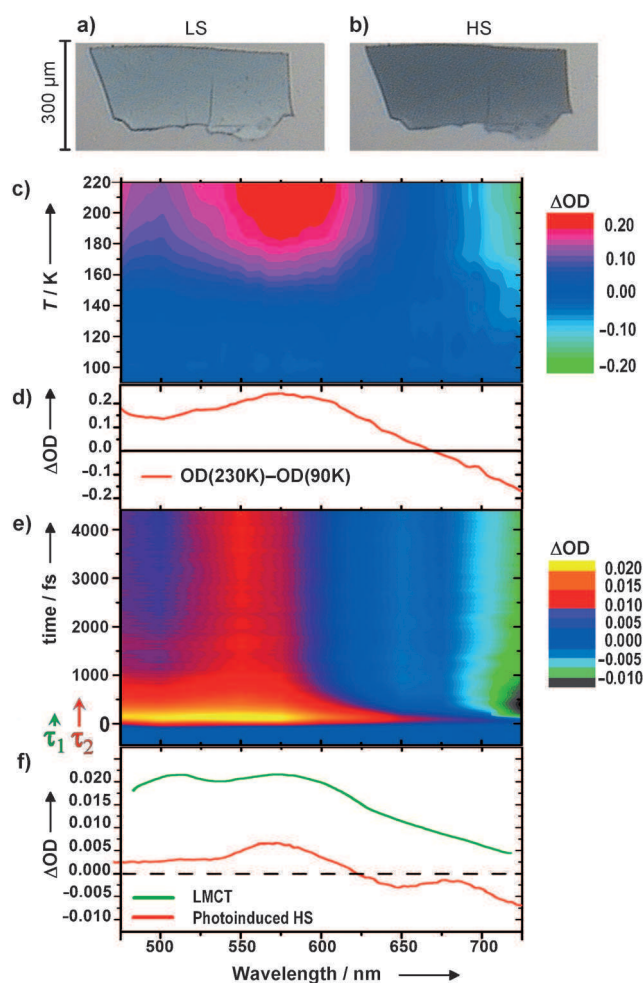

Figure 2. Optical analysis. a,b) Microscope photographs obtained by back illumination of a slice of PVP polymer film containing homogeneously dispersed nanocrystals, changing color between LS (80 K) and HS (280 K) states. c) Thermal variation of the optical density (ΔOD) recorded with a white-light spectrometer during LS to HS conversion. d) ΔOD between the complete HS (230 K) and LS (90 K) states. e) 2D time–wavelength plot of ΔOD after femtosecond laser excitation obtained by a two-color pump–probe experiment; the color coded change follows the characteristic τ_1 and τ_2 time constants. f) ΔOD spectra obtained by white-light spectroscopy at time 0 (——, LMCT and INT states) and at 15 ps (——, photoinduced HS).

chemical substitution. It is then straightforward to obtain spectroscopic fingerprints of the two spin states.

We exploit these spectroscopic fingerprints to study the ultrafast dynamics of nanoscaled SCO crystals at far from thermal equilibrium. To track the photoinduced spin-state switching dynamics in real time, we employed two different transient absorption experiments, one kinetically resolved and the other spectrally resolved (see the Supporting Information). The pump wavelength was set to 850 nm, where it efficiently induces LS-to-HS transition at 90 K from the pure LS state. Single-wavelength measurements probed the resulting dynamics through OD change in the identified spectral zones (475–725 nm). The overall instantaneous response function (IRF) of this experiment, conducted with a fine time step of 10 fs, is ca. 140 fs.

Selected time traces are shown in Figure 3a,b. The two dimensional time–wavelength plot of ΔOD following femtosecond laser excitation is shown in Figure 2e. These figures
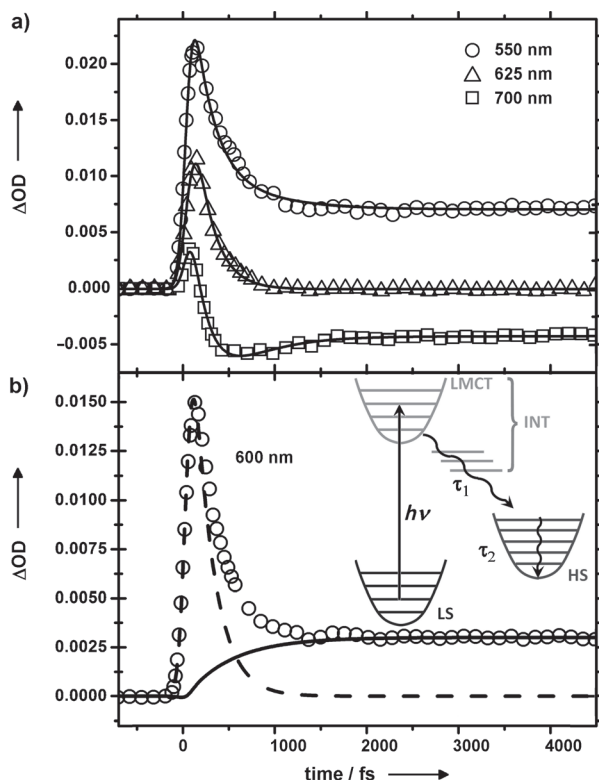
Figure 3. Kinetic traces of ΔOD at selected wavelengths obtained by a two-color pump–probe experiment at $T = 90$ K. a) Raw data (○,△,□) and fits with the biexponential model (——). b) Deconvolution of raw data (○) for the 600 nm probe into the relaxation kinetic of the intermediate electronic states (– – –) and the population kinetic of the HS state (——). The inset shows a schematic representation of the photoswitching pathway with time constants τ_1 for the relaxation of short-lived intermediate states (INT), and τ_2 for the vibrational cooling of the photoinduced HS state.

indicate two main steps, a transient peak appearing immediately after laser excitation and a plateau reached with a time constant shorter than one picosecond. ΔOD recorded on this plateau, positive in VIS and negative in NIR, reveals the formation of a HS state less than 1 ps after laser excitation of the nanocrystals. The transient response recorded during the first 100 fs differs significantly, showing a broad and strong absorption band dominating the VIS–NIR spectrum, indicating that the observed transient species are neither LS nor HS. These findings suggest that the HS formation mechanism involves a short-lived intermediate step resulting from the population of the ligand-to-metal charge-transfer (LMCT) state, as is similarly proposed for the macroscopic single crystal,[9] and for molecules in solution.[8]

For more detailed characterization through ΔOD of the transient LMCT and the photoinduced HS states, we performed time-resolved broad band spectroscopy at 90 K (see

the Supporting Information). The transient LMCT spectrum around time zero is compared in Figure 2f to the spectrum of the photoinduced HS state taken at 15 ps, which does not change on the plateau (at least up to 100 ps). Here again the observed photoinduced absorption in the VIS range and bleaching in the NIR obey the spectral behavior expected for LS-to-HS switching. The spectrum at time zero differs significantly from that of the LS ground state and that of the HS photoinduced state; the VIS part (Figure 2) shows neither a bleach signal nor an isosbestic point, which prevents assignment of the species to LS or HS.

Spin state photoswitching dynamics are known to proceed through transient states, as the direct low energy excitation from a LS to a HS state is forbidden by spin parity. Photoswitching is now understood at the molecular level[8] to a degree that allows the following description: the femtosecond pump pulse promotes the d electrons of the metal ion in the LS state into a Franck-Condon state (charge-transfer state). This electronic excited state relaxes through intersystem crossing[15] and through different intermediate states to a state with higher parity (HS). Our time-resolved data lead us to a similar description of the LS-to-HS transformation pathway of the Fe^{III} complex in nanocrystals. Specifically, the simple model used here for reproducing the kinetics of this photoswitching is biexponential (inset Figure 3b). The shorter time constant (τ_1) describes the population of the HS state by the depopulation of intermediate (INT) electronic states (including LMCT and other possible intermediates) before the final electronic HS state is reached. The longer time constant (τ_2) describes the vibrational cooling of the HS state, which is populated with excess vibrational energy as most of the absorbed energy is still localized at the molecular level on this time scale.

Figure 2e and Figure 3 show that the contributions from HS or LS states to ΔOD cancel out around 625 nm on the picosecond plateau. Therefore, the corresponding kinetic trace (Figure 3a) can be used to track the INT electronic states, which are expected to have distinct absorption spectra.

This kinetic trace, which shows a rapid rise followed by a rapid drop in ΔOD was deconvoluted from the IRF by a single exponential model and gave a decay time constant for the INT state of 200 ± 20 fs. This is in excellent agreement with earlier reports on the SCO of metal complexes both in solution[8] and in macroscopic crystals,[9] as well as a femtosecond Raman experiment,[8c] which probed the charge density shift timescale within a Fe^{II} complex upon Franck–Condon excitation.

As the photoinduced HS state is OD silent only around this isosbestic point, the variation of OD at other wavelengths involves both INT and HS states. Thus, INT states are the bottleneck for the relaxation process. Therefore, τ_1 should not vary with wavelength and was fixed in the model to 200 fs, whereas τ_2 was left as a free parameter. The fitting (lines in Figure 3a) yields a τ_2 in the 500–800 fs range, depending on the probe wavelength. The existence of two time constants is clearly seen on the 2D map in Figure 2e. The strong absorption in the VIS range (yellow), vanishing within the first 200 fs, marks the very short INT states. The slower increase of bleaching in the NIR, as well as the global spectral

narrowing, which is easily visualized by band narrowing around 575 nm and 725 nm, all occur within less than 1 ps. Spectral narrowing is a well-known marker of vibrational cooling[8c, 16] and is associated here with a downslide of the vibrationally hot HS molecules to the bottom of the HS potential (inset Figure 3 b). Compared to the cooling constants reported for such molecules in solution in the 1–10 ps range,[8] the process reported here is faster. Vibrational cooling dissipates excess energy to the environment, on which the efficiency of this process will depend. Thus, the same molecules in different solvents cool down differently.[8d] In the case of crystalline solids, additional cooling channels may exist. Namely, lattice phonons, which allow efficient coupling of the locally photoexcited molecules with the environment.[9a, 17] The direct comparison of the optical signatures of LS-to-HS switching driven by temperature with those driven by the laser pulse (Figure 2) provides clear-cut evidence of a photoinduced HS state. However, a more detailed description of the ultrafast relaxation to this state is difficult, as theoretical studies have shown that the intersystem crossing is complex;[15] several pathways involving different excited spin states and different crossing between the potential energy curves of the states exist and are hidden here in the INT state (or manyfold state). The physical mechanism underlying the inter-system crossing dynamics is poorly understood and awaits the development of theoretical studies and simulations, including spin-orbit coupling of the excited states. Unlike cooperative materials,[1,2d] where the electronic excitation can be delocalized, thus allowing one photon to transform several molecules,[18] in SCO materials the excitation is localized at the intramolecular scale. Therefore, one photon transforms a single molecule on the femtosecond timescale, even though the cooperative elastic effect and thermal activation may exist on significantly longer time scales.[9, 17]

The fraction of molecules photoswitched from LS to HS states can be reliably estimated by a comparison of the OD change resulting from photoexcitation to that of the OD change from a complete thermal conversion. Compared to macroscopic crystals under similar excitation,[9b] we find an intriguing difference in the case of nanocrystals studied here. The fraction of photoconverted molecules on the picosecond plateau in these nanocrystals is 50 times higher and reaches 10%. Such an improvement in the switched fraction can be put down to a very good penetration of the pump laser through minute nanocrystals.

In conclusion, femtosecond laser pulses should ultimately allow for control over molecules, and open new perspectives for nanoscale molecular materials. Downsizing SCO materials is a very encouraging route to efficient photoswitchable solids. Our main motivation was to study the possibility of photoswitching a SCO system whose volume size is nine orders of magnitude smaller than common molecular crystals, and unveiling the associated photoswitching pathway. Herein, we have demonstrated a one-way laser pulse switching between LS and HS states in a solid compound of nanometric size embedded in a PVP film. This morphological modification does not deteriorate the ultrafast photoswitching ability of the SCO material in the optically silent polymer. Appli-

cation prospects have already been recognized for SCO materials, and seem even more appealing in the case of nanocrystals. They should be downsizeable at will, and switchable with relatively low laser power. Despite their minute size, the nanocrystals studied here are still far above the infinite system size limit, precluding first-order phase transition and thereby prompting finite size scaling as an interesting aspect for device design.[19] Now that ultrafast switching of SCO nanoparticles has been demonstrated, the next challenge is to control a single nanoparticle on a femtosecond timescale.

[1] K. Nasu in *Photoinduced phase transitions*, World Scientist, Singapore, **2004**.

[2] a) H. Ichikawa, S. Nozawa, T. Sato, A. Tomita, K. Ichiyanagi, M. Chollet, L. Guérin, N. Dean, A. Cavalleri, S. Adachi, T. Arima, H. Sawa, Y. Ogimoto, M. Nakamura, R. Tamaki, K. Miyano, S. Koshihara, *Nat. Mater.* **2011**, *10*, 101–105; b) M. Rini, R. Tobey, N. Dean, J. Itatani, Y. Tomioka, Y. Tokura, R. W. Schoenlein, A. Cavalleri, *Nature* **2007**, *449*, 72–74; c) S. Kobatake, S. Takami, H. Muto, T. Ishikawa, M. Irie, *Nature* **2007**, *446*, 778–781; d) E. Collet, M.-H. Lemée-Cailleau, M. Buron-Le Cointe, H. Cailleau, M. Wulff, T. Luty, S.-Y. Koshihara, M. Meyer, L. Toupet, P. Rabiller, S. Techert, *Science* **2003**, *300*, 612–615.

[3] a) K. Moore, H. Rabitz, *Nat. Chem.* **2012**, *4*, 72–73; b) I. S. Ulusoy, M. Nest, *J. Am. Chem. Soc.* **2011**, *133*, 20230–20236; c) D. Polli, P. Altoè, O. Weingart, K. M. Spillane, C. Manzoni, D. Brida, G. Tomasello, G. Orlandi, P. Kukura, R. A. Mathies, M. Garavelli, G. Cerullo, *Nature* **2010**, *467*, 440–443.

[4] A. H. Zewail, *Angew. Chem.* **2000**, *112*, 2688–2738; *Angew. Chem. Int. Ed.* **2000**, *39*, 2586–2631.

[5] a) M. Verdaguer, *Science* **1996**, *272*, 698–699.

[6] a) A. Hauser, *Top. Curr. Chem.* **2004**, *234*, 155–198; b) A. Bousseksou, G. Molnar, L. Salmon, W. Nicolazzi, *Chem. Soc. Rev.* **2011**, *40*, 3313–3335; c) Y. Sunatsuki, Y. Ikuta, N. Matsumoto, H. Ohta, M. Kojima, S. Iijima, S. Hayami, Y. Maeda, S. Kaizaki, F. Dahan, J.-P. Tuchagues, *Angew. Chem.* **2003**, *115*, 1652–1656; *Angew. Chem. Int. Ed.* **2003**, *42*, 1614–1618; d) N. Bréfuel, H. Watanabe, L. Toupet, J. Come, N. Matsumoto, E. Collet, K. Tanaka, J.-P. Tuchagues, *Angew. Chem.* **2009**, *121*, 9468–9471; *Angew. Chem. Int. Ed.* **2009**, *48*, 9304–9307; e) J. F. Létard, P. Guionneau, E. Codjovi, O. Lavastre, G. Bravic, D. Chasseau, O. Kahn, *J. Am. Chem. Soc.* **1999**, *121*, 10630–10631; f) S. Ohkoshi, K. Imoto, Y. Tsunobuchi, S. Takano, H. Tokoro, *Nat. Chem.* **2011**, *3*, 564–569.

[7] a) G. Galle, J. Degert, C. Mauriac, C. Etrillard, J. F. Létard, E. Freysz, *Chem. Phys. Lett.* **2010**, *500*, 18–22; b) S. Cobo, D. Ostrovskii, S. Bonhommeau, L. Vendier, G. Molnar, L. Salmon, K. Tanaka, A. Bousseksou, *J. Am. Chem. Soc.* **2008**, *130*, 9019–9024.

[8] a) C. Bressler, C. Milne, V.-T. Pham, A. El Nahhas, R. M. van der Veen, W. Gawelda, S. Johnson, P. Beaud, D. Grolimund, M. Kaiser, C. Borca, G. Ingold, R. Abela, M. Chergui, *Science* **2009**, *323*, 489–492; b) M. Khalil, M. M. Marcus, A. L. Smeigh, J. K. McCusker, H. H. W. Chong, R. W. Schoenlein, *J. Phys. Chem. A* **2006**, *110*, 38–44; c) A. L. Smeigh, M. Creelman, R. A. Mathies, J. K. McCusker, *J. Am. Chem. Soc.* **2008**, *130*, 14105–14107; d) J. Tribollet, G. Galle, G. Jonusauskas, D. Deldicque, M.

Tondusson, J. F. Létard, E. Freysz, *Chem. Phys. Lett.* **2011**, *513*, 42 – 47; e) W. Gawelda, A. Cannizzo, V. T. Pham, F. van Mourik, C. Bressler, M. Chergui, *J. Am. Chem. Soc.* **2007**, *129*, 8199 – 8206; f) M. M. N. Wolf, R. Groß, C. Schumann, J. A. Wolny, V. Schünemann, A. Døssing, H. Paulsen, J. J. McGarvey, R. Diller, *Phys. Chem. Chem. Phys.* **2008**, *10*, 4264 – 4273.

[9] a) M. Lorenc, C. Baldé, W. Kaszub, A. Tissot, N. Moisan, M. Servol, M. Buron-Le Cointe, H. Cailleau, P. Chasle, P. Czarnecki, E. Collet, *Phys. Rev. B* **2012**, *85*, 054302; b) A. Tissot, R. Bertoni, E. Collet, L. Toupet, M.- L. Boillot, *J. Mater. Chem.* **2011**, *21*, 18347 – 18353; c) E. Collet, M. Lorenc, M. Cammarata, L. Guérin, M. Servol, A. Tissot, M.-L. Boillot, H. Cailleau, M. Buron-Le Cointe, *Chem. Eur. J.* **2012**, *18*, 2051 – 2055.

[10] a) T. Forestier, A. Kaiba, S. Pechev, D. Denux, Ph. Guionneau, C. Etrillard, N. Daro, E. Freysz, J. F. Létard, *Chem. Eur. J.* **2009**, *15*, 6122 – 6130; b) J. R. Galán-Mascarós, E. Coronado, A. Forment-Aliaga, M. Monrabal-Capilla, E. Pinilla-Cienfuegos, M. Ceolín, *Inorg. Chem.* **2010**, *49*, 5706 – 5714; c) T. Forestier, S. Mornet, N. Daro, T. Nishihara, S. Mouri, K. Tanaka, O. Fouché, E. Freysz, J.-F. Létard, *Chem. Commun.* **2008**, 4327 – 4329; d) I. Boldog, A. B. Gaspar, V. Martínez, P. Pardo-Ibañez, V. Ksenofontov, A. Bhattacharjee, P. Gütlich, J. A. Real, *Angew. Chem.* **2008**, *120*, 6533 – 6537; *Angew. Chem. Int. Ed.* **2008**, *47*, 6433 – 6437; e) A. Tissot, L. Rechignat, A. Bousseksou, M.-L. Boillot, *J. Mater. Chem.* **2012**, *22*, 3411 – 3419; f) F. Volatron, L. Catala, E. Rivière, A. Gloter, O. Stéphan, T. Mallah, *Inorg. Chem.* **2008**, *47*, 6584 – 6586.

[11] a) G. Molnár, S. Cobo, J. A. Real, F. Carcenac, E. Daran, C. Vieu, A. Bousseksou, *Adv. Mater.* **2007**, *19*, 2163 – 2167; b) M. Cavallini, I. Bergenti, S. Milita, G. Ruani, I. Salitros, Z.-R. Qu, R. Chandrasekhar, M. Ruben, *Angew. Chem.* **2008**, *120*, 8724 – 8728; *Angew. Chem. Int. Ed.* **2008**, *47*, 8596 – 8600; c) C. Bartual-Murgui, L. Salmon, A. Akou, C. Thibault, G. Molnar, T. Mahfoud, Z. Sekkat, J. A. Real, A. Bousseksou, *New J. Chem.* **2011**, *35*, 2089 – 2094; d) A. Tissot, J.-F. Bardeau, E. Rivière, F. Brisset, M.-L. Boillot, *Dalton Trans.* **2010**, *39*, 7806 – 7812.

[12] J. A. Weinstein, N. T. Hunt, *Nat. Chem.* **2012**, *4*, 157 – 158.

[13] M. S. Haddad, M. W. Lunch, W. D. Federer, D. N. Hendrickson, *Inorg. Chem.* **1981**, *20*, 123 – 131.

[14] A. Hauser, J. Adler, P. Gütlich, *Chem. Phys. Lett.* **1988**, *152*, 468.

[15] a) N. Suaud, M. L. Bonnet, C. Boilleau, P. Labèguerie, N. Guihéry, *J. Am. Chem. Soc.* **2009**, *131*, 715 – 722; b) M. van Veenendaal, J. Chang, A. J. Fedro, *Phys. Rev. Lett.* **2010**, *104*, 067401.

[16] E. A. Juban, J. K. McCusker, *J. Am. Chem. Soc.* **2005**, *127*, 6857 – 6865.

[17] E. Collet, N. Moisan, C. Baldé, R. Bertoni, E. Trzop, C. Laulhé, M. Lorenc, M. Servol, H. Cailleau, A. Tissot, M.-L. Boillot, T. Graber, R. Henning, P. Coppens, M. Buron-Le Cointe, *Phys. Chem. Chem. Phys.* **2012**, *14*, 6192 – 6199.

[18] L. Guérin, J. Hebert, M. Buron-Le Cointe, S. Adachi, S. Koshihara, H. Cailleau, E. Collet, *Phys. Rev. Lett.* **2010**, *105*, 246101.

[19] K. Binder, D. P. Landau, *Phys. Rev. B* **1984**, *30*, 1477.

Femtosecond Spin-State Photoswitching of Molecular Nanocrystals Evidenced by Optical Spectroscopy**

Roman Bertoni, Maciej Lorenc,* Antoine Tissot, Marina Servol, Marie-Laure Boillot, and Eric Collet*

anie_201202215_sm_miscellaneous_information.pdf

Supplementary information

Synthesis and embedding of the nanocrystals:

Nanoparticles of the [Fe(3-MeO-SalEen)$_2$]PF$_6$ compound were obtained by precipitation method described in ref [10e], except that the 50 mg of Fe(III) complex were dissolved in 5 mL of acetone and the subsequent precipitation was carried out in butan-1-ol (100 mL) at –60°C. The needle-shaped crystals thus obtained observed by TEM have typical dimension of 34(7)×330(60)×900(200) nm^3 with satisfactory size dispersion (Fig. 1b & 1c), in good accordance with 35(7)×270(40)×950(150) nm^3 previously reported from the first synthesis method[10e]. These nanocrystals were then dispersed in a viscous solution of 100 mg of PVP (polyvinylpyrrolidone, M~ 40000 g.mol-1) with 500 μL of butan-1-ol. After sonication (2 min), 150 μL of the mixture were spin-coated on a glass substrate (1000 rpm) and dried under vacuum. Fig. S1 shows photographs of the film with homogeneously dispersed nanocrystals in the PVP polymer.
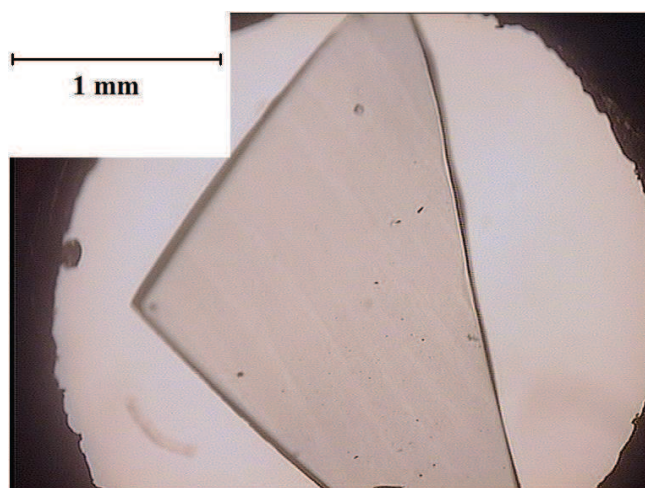

Fig. S1. Microscope photographs of the film showing homogeneous dispersion of nanocrystals in the PVP polymer.

The χ_MT vs. T curve observed for the nanocrystals in the form of a powder is displayed in figure S2. The process centred at 158 K occurs between 120 and 190 K. For the nanocrystals embedded in the PVP film, the evolution of the fraction of HS species appears even more gradual (from 95 to 205 K, T1/2 = 155 K, Fig. 1). This can be attributed to coating effect of the polymer - here PVP - a capping agent with high adherence properties. This effect known to affect SCO conversion can be attributed to chemical/physical factors[14] that are currently under investigation (A. Tissot, C. Enachescu, M.-L. Boillot, submitted).
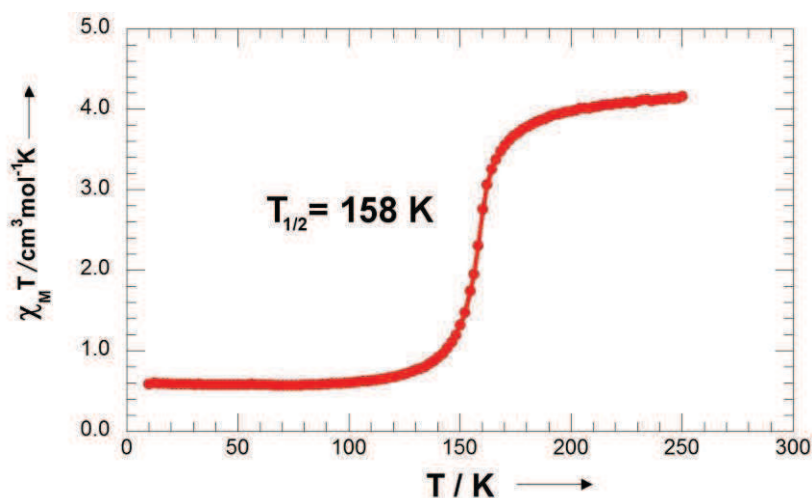

Fig. S2. χ_MT versus T plot of the powder of nanocrystals.

Optical pump-probe spectroscopy studies.

Time-resolved variations of optical density were investigated by using an ultrafast pump-probe setup. The sample was irradiated by a 70 fs laser pulse (the pump) and probed by a second fs laser pulse (the probe). A time delay between the pump and the probe pulses is introduced, which can be adjusted by controlling an optical delay-line. By monitoring the transmitted probe signal as a function of the time delay, it is possible to follow in real-time the photo-switching dynamics. For two-color pump-probe spectroscopy, we used wavelength tunable femtosecond laser operating at 1 kHz and delivering 80 fs pulses. These measurements performed by heterodyning transient signal in a lock-in amplifier[9a] provide high sensitivity. We used typical excitation density of $45\mu J/mm^2$/pulse. The recovery time of the photo-excited HS state to the ground LS state was measured to be of the order of 1μs (Fig. S3). The lasers hit the same spot of the sample with 1 kHz repetition rate, without causing any measurable damage at the excitation density used. Above $150\mu J/mm^2$/pulse sample damage was observed, precluding stroboscopic measurements. For sample cooling, we used an Oxford Cryosystems nitrogen-flow cryostat for measurements down to 80 K.
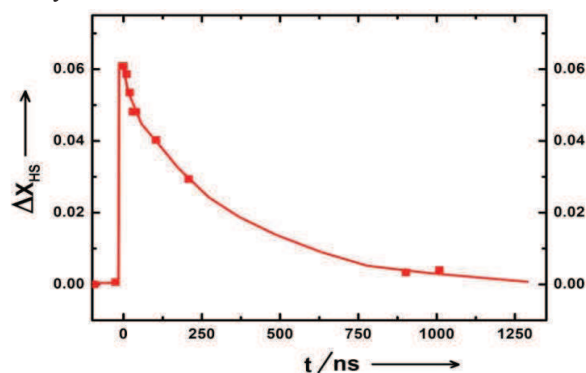

Fig. S3. Relaxation from the photoexcited HS state towards the LS states.

For white-light spectroscopy, the probe pulse, centered at 800 nm, was focused onto a fused silica (or CaF_2) window, in order to generate a white light supercontinuum. This supercontinuum was used to study the change of OD in the visible region. A spectrometer is used to disperse different wavelengths of supercontinuum on a CCD camera, which reads out the ratio R(λ) between the transmitted signal in the presence of the pump and that transmitted in the absence of the pump. By scanning the delay time of the pump pulse within probe's temporal envelope, that is from the coincidence with the blue (475 nm) edge of white light until the coincidence with its red edge (725 nm), the onset of spectral amplitude at each wavelength can be well resolved. Indeed, the wavelength concomitant with the pump at any given time shows up sharply (grey curves in the figure below). By connecting these sharp features an outline of transient LMCT spectrum around time zero can be drawn (Fig. S4). The spectrum of the photoinduced HS state was taken at 15 ps, when 2 ps chirp is negligible, and ΔOD does not change any longer (at least up to 100 ps).
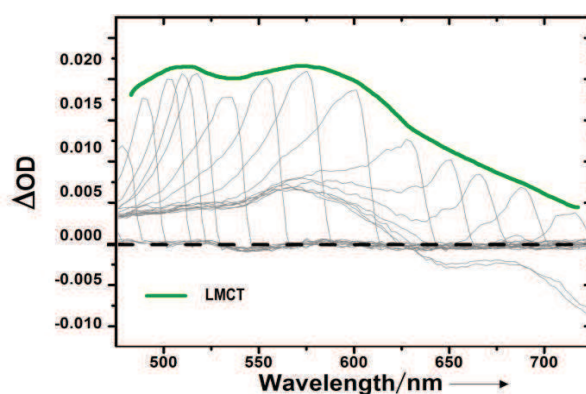

Fig. S4. ΔOD spectra obtained by white-light spectroscopy at time 0.

References

[9] a) M. Lorenc, J. Hébert, N. Moisan, E. Trzop, M. Servol, M. Buron-Le Cointe, H. Cailleau, M.-L. Boillot, E. Pontecorvo, M. Wulff, S. Koshihara, E. Collet, *Phys. Rev. Lett.* **2009**, *103*, 028301;

[10] e)A. Tissot, L. Rechignat, A. Bousseksou, M.-L. Boillot, J. Mater. Chem., **2012**, *22*, 3411–3419.

[14] A. Hauser, J. Adler, P. Gütlich, Chem. Phys. Lett., **1988**, *152*, 468.

Femtosecond optical pump–probe reflectivity studies of spin-state photo-switching in the spin-crossover molecular crystals [Fe(PM-AzA)$_2$(NCS)$_2$]

Andrea Marino [a], Marina Servol [a], Roman Bertoni [a], Maciej Lorenc [a], Cindy Mauriac [b], Jean-François Létard [b], Eric Collet [a,*]

[a] Institut de Physique de Rennes, UMR 6251 University Rennes 1-CNRS, 35042 Rennes, France
[b] CNRS, Université de Bordeaux, ICMCB, 87 avenue du Dr A. Schweitzer, Pessac, F-33608, France

ABSTRACT

We report here on the ultrafast photo-switching dynamics of a Fe(II) molecular material [Fe(PM-AzA)$_2$(NCS)$_2$]. It undergoes a thermal spin-crossover which can be detected by magnetic measurements or by optical reflectivity. We use here femtosecond optical reflectivity to study the ultrafast photo-switching dynamics. Our results indicate that the HS state is reached from the LS state within less than 100 fs, through an intermediate MLCT state. This ultrafast relaxation from the electronic excited state towards the structurally relaxed HS state is followed by a vibrational cooling of the hot HS molecules within ≈1 ps timescale.

© 2013 Elsevier Ltd. All rights reserved.

1. Introduction

Photoinduced phase transitions [1] open fascinating perspectives for controlling with light the physical properties of materials and especially molecule-based magnets. A well-known example is the Light-Induced Excited Spin State Trapping (LIESST) phenomenon [2] undergone by numerous spin-crossover (SC) compounds [3,4]. These prototype photo-active materials show photomagnetic and photochromic properties. Weak continuous wave (cw) laser irradiation at low temperature is known as an efficient way for controlling SC materials by light. By choosing the appropriate excitation wavelength, one can selectively populate the high spin (HS) state (LIESST [2a]) or low spin (LS) state (reverse LIESST [2b]), which are long-lived at low temperature. Usually, the photoinduced HS phase is similar to the HS phase observed at thermal equilibrium with similar structural reorganization, especially at the intra-molecular level [5]. More recently, light-induced symmetry breaking in the photoinduced HS phase [6] as well as transition from incommensurate HS/LS order to commensurate HS phase [7] have been also reported, illustrating that light allows access to new phases, which sometime cannot be reached at thermal equilibrium. When LIESST effect is driven by weak cw laser irradiation, the switching dynamics at the macroscopic scale in crystals is limited by the photons flux: it typically occurs within few hours or minutes at low temperature. Nanosecond laser irradiation has been used on

solids for driving photoinduced spin-crossover [8]. The observations of photo-switching inside thermal hysteresis represent important progress toward molecular memory devices, especially with bi-directional switching properties [3]. But despite these reports on relaxation mechanisms after nanosecond laser excitation, little has been known about the molecular transformation dynamics. Ultrafast studies of the photo-switching dynamics of single molecule in solution as shown that LS-to-HS photo-switching occurs on the sub-picosecond time scale [9]. We recently performed several studies of the ultrafast spin-state photo-switching dynamics in the Fe(III) solids, by using femtosecond optical spectroscopy [10] and time-resolved X-ray diffraction [11]. These studies have shown that the macroscopic transformation of the material driven by an intense laser pulse involves several processes driving HS conversion. In addition to the ultrafast photo-switching at the molecular scale cascading shock-wave and heating effects take place. However, the very first process involved in the photo-switching dynamics is the local trapping of the electronic excited state at the molecular level. It is now quite well established that the femtosecond pump pulse promotes instantaneously d electrons of the metal ion in the LS state to a Franck–Condon state (charge-transfer state). Transient optical absorption studies performed on molecules in solution, in solids and in nano-crystals [9,10] have concluded that this electronic excited state relaxes through the intersystem crossing via different intermediate states (INT) to a state with higher parity (HS). But in the solid state, the large optical density of some SC materials does not allow using transient absorption spectroscopy for studying the photo-switching. It is the case for the dark

---

* Corresponding author. Tel.: +33 223236532.
E-mail address: eric.collet@univ-rennes1.fr (E. Collet).

single crystals studied here of the SC Fe(II) molecular material [Fe(PM-AzA)$_2$(NCS)$_2$] (i.e. cis-bis(thiocyanato)-bis(N-2′-pyridyl methylene)-4-(phenylazo) aniline iron(II) [12]). We propose therefore to use femtosecond optical reflectivity to study this photoswitching dynamics. In the first part of this paper, we demonstrate the correlation between optical reflectivity and spin-crossover observed at thermal equilibrium and in the second part we use time-resolved optical reflectivity to study the ultrafast dynamics.

2. Thermal crossover of [Fe(PM-AzA)$_2$(NCS)$_2$] studied by polarized optical reflectivity

The [Fe(PM-AzA)$_2$(NCS)$_2$] single crystals have been characterized by magnetic measurements (Fig. 1) through the evolution of the $\chi_M T$ product (χ_M being the magnetic susceptibility and T the temperature). The compound undergoes a thermal spin crossover centered at $T_{1/2}$ = 189 K between a LS ($S = 0$) diamagnetic state and a HS ($S = 2$) paramagnetic state where the relative population of HS and LS states gradually changes with temperature from a mainly HS phase above 270 K to a mainly LS phase below 130 K [12]. As usual for SC compounds a structural reorganization is coupled to the spin conversion, characterized at the molecular level by changes of bond lengths and angles. Guionneau et al. have shown that the most important changes involve the active $Fe^{II}N_6$ core with a contraction of ≈10% of the average ⟨Fe–N⟩ bond length during the HS-to-LS switching [12b].

We used optical reflectivity to figure out the fingerprints of the spin-state change at thermal equilibrium. The experiments were performed on typically $4 \times 1 \times 1$ mm^3 [Fe(PM-AzA)$_2$(NCS)$_2$] single crystals. These ones have a typical parallelepiped shape represented in Fig. 2 with two different crystallographic faces ([1 1 0] and [1 −1 0]). The long crystal axis, which is the edge common to both faces, corresponds to the crystallographic axis $\vec{c}$. The crystal is monoclinic but these faces are almost perpendicular to each other. Reflectivity spectra were accumulated in [450–750] nm range at different temperatures by using a white-light spectrometer and a nitrogen gas flow cryostat. The thermal conversion was characterized on both crystal faces under linearly polarized light illumination. Parallel and perpendicular light polarization axes were defined with respect to the long crystal axis $\vec{c}$ (scheme in Fig. 2). Reflectivity spectra of the LS and HS state, taken under perpendicular polarization, are reported in Fig. 3a. An important change of optical reflectivity spectra is observed between 130 K (LS state) and 270 K (HS state), with a well marked isosbestic point around 685 nm. We plot in Fig. 3b the ratio of the reflected spectra between HS and LS states. It clearly underlines that for both faces, the reflectivity of the HS state with respect to that of LS state is higher in the visible (VIS) region and lower in the near-infrared
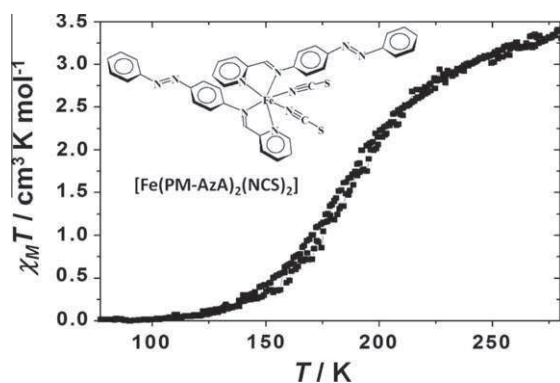
(NIR) region, with a large difference around 660 nm. The temperature dependence of $\Delta R/R$ at 660 nm is plotted in Fig. 3c. It corresponds to the relative difference between $R(T)$, the reflectivity at a given temperature, and R(LS) the reflectivity in the LS state:

$$\frac{\Delta R}{R} = \frac{R(T) - R(LS)}{R(LS)}$$

There is a good correlation between $\Delta R/R$ and the change of $\chi_M T$ product, making reflectivity change a good optical marker of the spin-state. The quality of the optical reflectivity of the large faces of the single crystals is maintained under cycling between LS and HS states. The reflectivity change are very similar for both faces and hereafter we will refer only to the analysis of the [1 1 0] face under perpendicular light irradiation for a detailed discussion. Because the crystal is monoclinic, reflectivity of light parallel or perpendicular to $\vec{c}$ axis are not equivalent by symmetry and therefore the polarization most sensitive to the change of spin state has to be identified. We found that the relative change of the reflectivity spectra measured with parallel light polarization (not shown here) shows less marked changes during the crossover. Therefore, in the following we exploit these spectroscopic fingerprints measured with perpendicular polarization, to study in real time the ultrafast photoinduced spin state switching dynamics by using femtosecond optical reflectivity.

3. Femtosecond optical reflectivity study of the photo-switching dynamics

3.1. Experimental set-up

Optical pump–probe studies are appropriate techniques to follow ultrafast dynamical process in real time. Its key point is to control the time delay Δt between a pump pulse, which triggers the transformation, and a probe pulse, which images the photo-induced changes at different Δt (Fig. 4). In such a way, snapshot by snapshot, a "movie" of the system evolution is obtained by monitoring the change of probe signal.

For this project, we employed two different transient absorption experiments: one kinetically resolved and the other spectrally resolved. The pump wavelength chosen here (850 nm), was shown to efficiently photoswitch from LS to HS states the [Fe(PM-AzA)$_2$(-NCS)$_2$] compound, as well as different [Fe(PM-L)$_2$(NCS)$_2$] derivatives, where L refers to different ligands [5]. This excitation corresponds to the metal-to-ligand charge transfer (MLCT). Since the coupled molecular reorganization involves molecular and atomic motion like Fe–N stretching, with typical time scale of ≈130 fs, femtosecond time resolution is required to study these dynamics. In our experimental set up, the delay between the pump and probe pulses is controlled by a delay line changing the optical path length of the pump with regard to the one of the probe, with a fine time-step of 10 fs. The time resolution is then mainly limited by the laser pulse duration, and more precisely by the cross-correlation between pump and probe temporal width. The time resolution $P(t)$ of our experiment is the convolution between the Gaussian temporal dispersion of the pump (σ_{pump}) and probe (σ_{probe}) laser pulses and corresponds to:

$$P(t) = \sqrt{\sigma^2_{pump} + \sigma^2_{probe}}$$

By using a regenerative amplifier with a Gaussian temporal distribution of ≈90 fs FWHM, we are able to reach a temporal resolution with an overall instantaneous response function of 140 fs. Because we are using a stroboscopic technique with 1 kHz repetition rate, the relaxation time of the photoinduced HS state towards the LS state should be shorter than 1 ms to avoid accumulating effects. This condition is fulfilled above 110 K, where the relaxation is
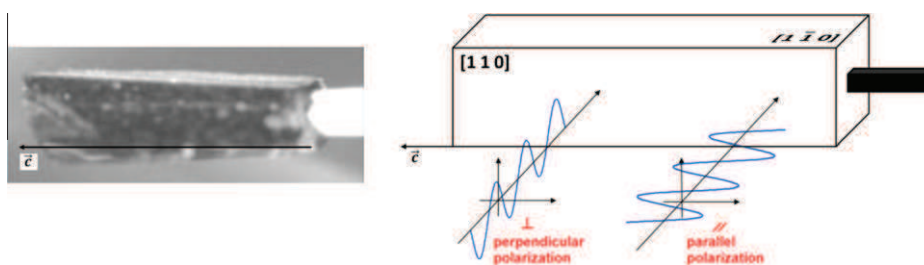

Fig. 1. The [Fe(PM-AzA)$_2$(NCS)$_2$] compound and its thermal spin-crossover characterized by magnetic susceptibility.

Fig. 2. Photograph of the crystal (left) and schematic drawn of the two indexed faces and light polarization direction.
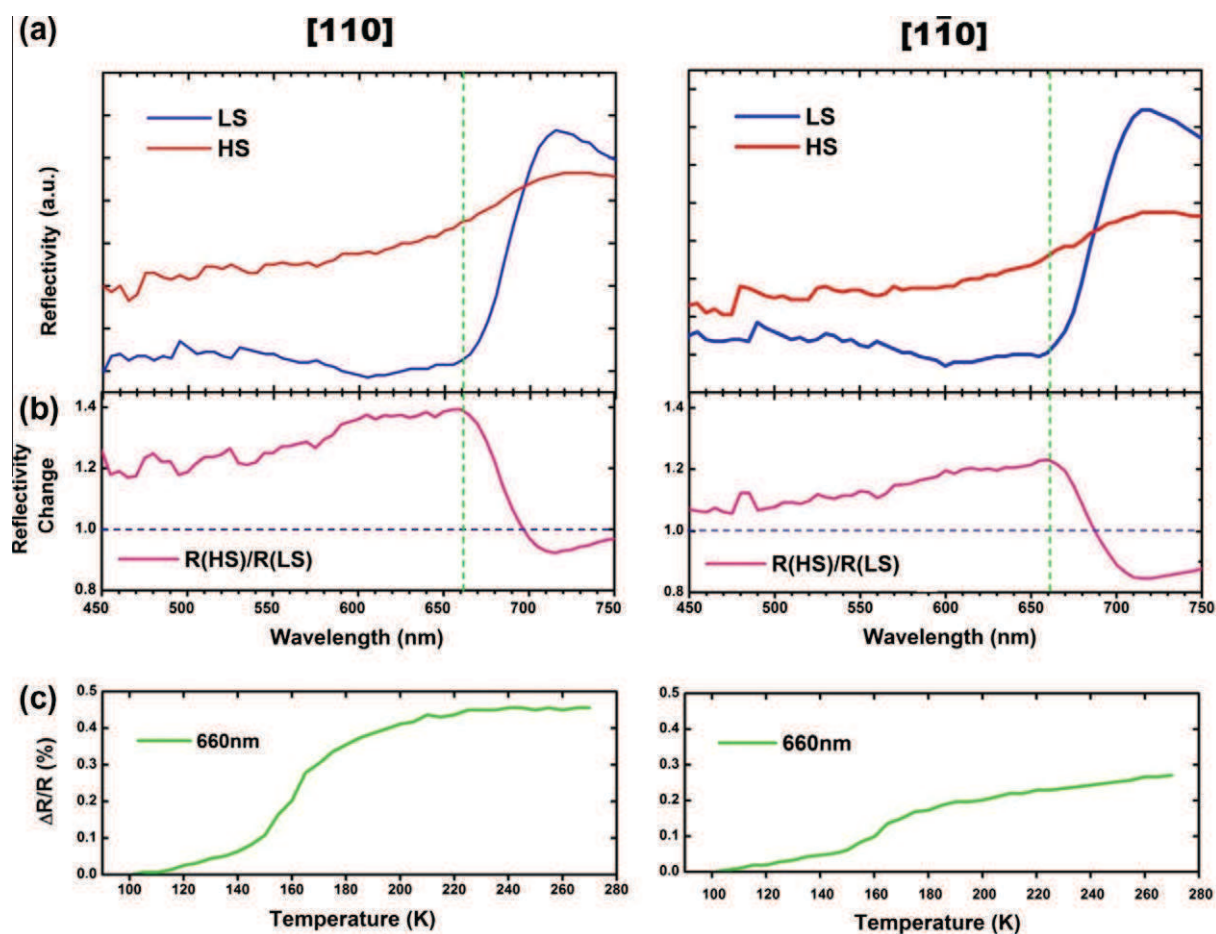

Fig. 3. (a) Thermal variation of the optical reflectivity during the LS (130 K) to HS (270 K) thermal conversion, measured with light polarization perpendicular to the long crystal axis *c* for [1 1 0] (left) and [1 –1 0] (right) faces. (b) Ratio of the reflectivity spectra of HS and LS states. (c) Temperature dependence of the relative reflectivity change with respect to the LS state at 100 K at 660 nm for both faces.
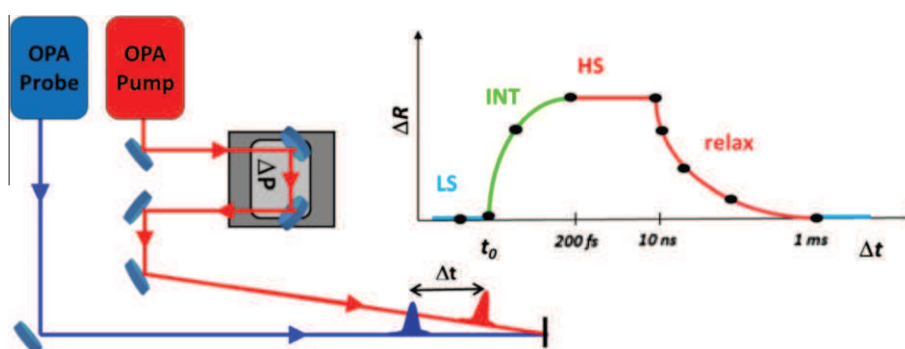

Fig. 4. Schematic pump–probe set-up consisting in monitoring the change of reflectivity ΔR with a probe pulse delayed by Δt from the pump pulse.
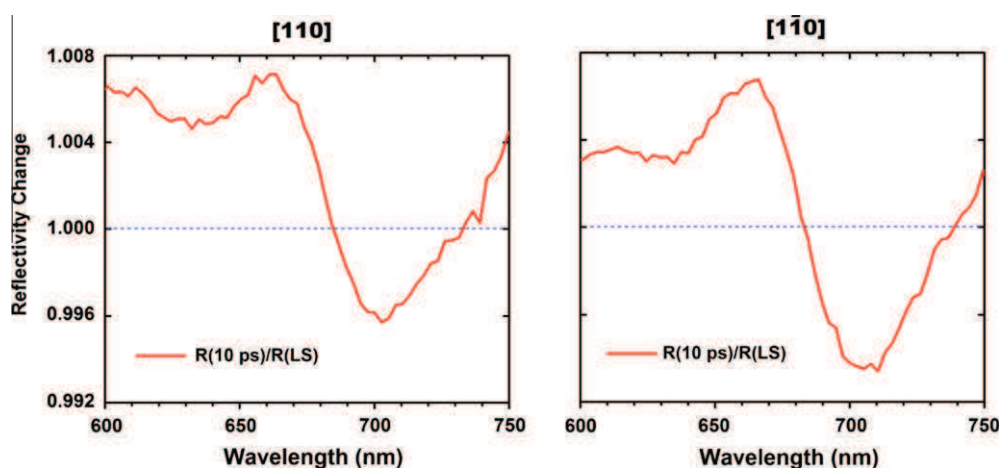
Fig. 5. Relative change of reflectivity between the LS and photoinduced HS states measured 10 ps after laser excitation by white-light spectroscopy for face [1 1 0] and [1 −1 0].
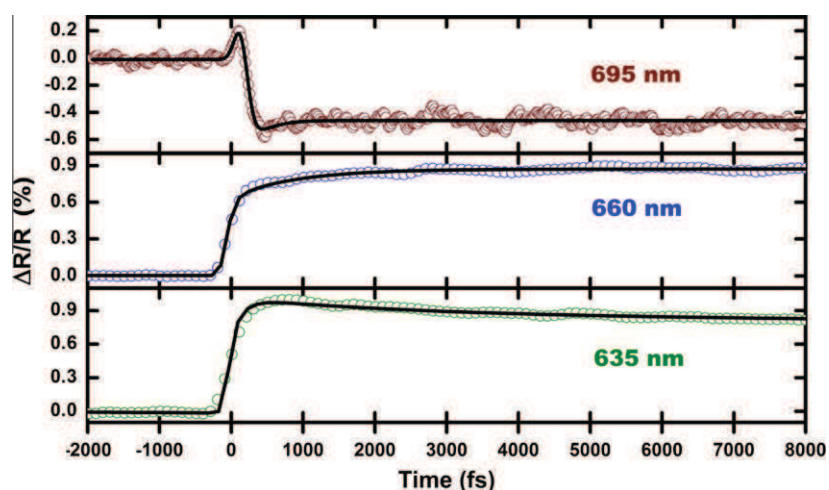

Fig. 6. Raw data (symbols) of the kinetic traces of relative reflectivity at 635, 660 and 695 nm following fs laser excitation. Solid lines show the results of the fitting procedure taking into account a time constants τ_1 for the ISC and τ_2 for the vibrational cooling of the photoinduced HS state.

faster and for this reason the experiment was performed at 130 K, where the crystal is in the mainly LS state (the HS fraction is around 2%). The reflectivity change around the isosbestic point was measured by white-light spectroscopy at a time delay 10 ps after laser excitation (Fig. 5). We used then single-wavelength probe to measure the time course of the photoinduced LS-to-HS transformation, through the relative reflectivity change ($\Delta R/R$) in identified spectral zones (Fig. 6) around the isobestic point, where reflectivity is expected to increase below 685 nm and decrease above as HS state is formed (Fig. 3).

3.2. Results

The reflectivity change spectra of the photoinduced state measured 10 ps after laser excitation are shown for both faces in Fig. 5. In each of them it is observed that reflectivity increases in VIS part and a decreases in the NIR parts, with an isosbestic point found around 685 nm. This is a direct signature of the photoinduced HS state as the changes observed obey the spectral behavior resulting from LS-to-HS switching observed at thermal equilibrium (Fig. 3). We now discuss how the clear optical fingerprint of the photoswitching from LS to HS states evolves in the time domain and on which time scale the HS state is formed.

For studying this photo-switching dynamics, additional measurements were performed in the time domain by using different monochromatic probes. Selected time traces are plotted in Fig. 6, indicating two main steps:

– a very short transient peak (<100 fs, observed at 695 nm) and associated with fast changes of reflectivity immediately after laser excitation
– a slower ($\approx$1 ps) relaxation towards a plateau (observed at 635 and 660 nm).

This two-step photo-switching process is very similar to the studies reported by transient absorption spectroscopy for SC molecules in solution or in nano-crystals [9,10a].

We can use here the same simple model to take into account the two different dynamics. The increase of reflectivity at 695 nm, just after laser excitation, is not an optical fingerprint of the HS state as this wavelength corresponds to the isosbestic point of LS and HS species. This peak characterizes therefore the intermediate (INT) electronic excited state (including MLCT and other possible intermediates).

The population of the MLCT state is too fast to be observed here and therefore the first dynamics we observe is the population of HS
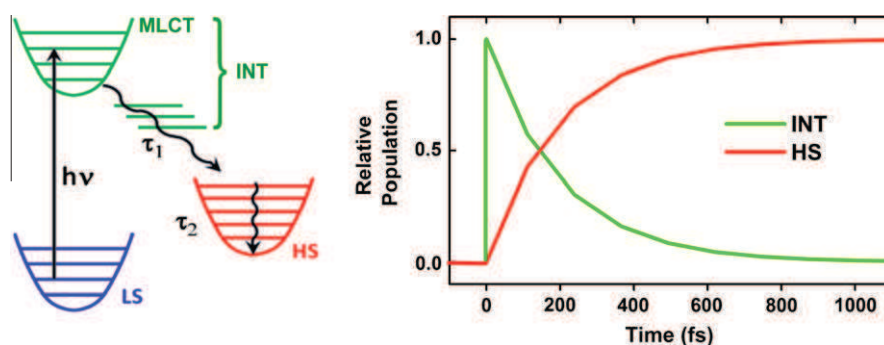
Fig. 7. (left) Schematic photo-switching pathway (left) with time constants τ_1 for the relaxation of short-lived intermediate states (INT), and τ_2 for the vibrational cooling of the photoinduced HS state. (right) Kinetic relative population of the INT (green) and HS (red) states (solid line) of photo-excited molecules deconvoluted from experimental data in Fig. 6. (Color online.)

state by depopulation of the INT electronic states. This inter-system crossing (ISC) process is associated with a time constant τ_1 (which is less than 100 fs), as schematically shown in Fig. 7. The second process involved is the vibrational cooling of the HS state, associated with a longer time constant τ_2 (of the order of 1 ps). Indeed, a huge excess of energy is deposited on the molecule by the absorbed photon (1.46 eV), since the energy difference between the LS and HS states is of the order of the thermal energy (20 meV). After 100 s fs, most of the absorbed energy is still localized at the molecular level.

For obtaining accurate time constants, fits of the time traces were performed with the bi-exponential model (solid lines in Fig. 6), by taking into account the 140 fs instantaneous response function of our experimental set-up. As a result, it is possible to deconvoluate these time traces and obtain the time dependence of the photoinduced INT (green line) and HS species (red line) as shown in Fig. 7. The different fits gave ISC dynamics $\tau_1 < 100$ fs, in agreement with earlier reports on SC metal complex in solution [9] or in crystals [10]. It was underlined that the relaxation from the INT states towards the HS state is the bottleneck for the relaxation process and that τ_1 does not vary with the probe wavelength. This is not the case for τ_2, which is observed here to be in the [500–2000 fs] range for the different probe wavelengths used. Vibrational cooling corresponds to the slower increase of reflectivity at 660 nm and decrease at 635 nm after the stepped-like change following the photo-excitation. This slower change of optical properties results from optical band narrowing ([10a] and references therein), a well-known marker of vibrational cooling. The probe wavelength dependence of the time-scale of this second process is therefore only apparent.

4. Conclusion

Light-control over molecular systems and especially molecular magnet is a key topics of interest. Up to now, studies have been mainly limited to slow kinetics, induced by weak *cw* laser excitation. Ultrafast transient absorption spectroscopy was used to study molecules in solution or (nano) crystals by transient absorption spectroscopy [9,10]. Here we demonstrate that transient optical reflectivity can also be used on single crystals for revealing the ultra-fast photoinduced processes, as clear optical markers of the different spin states can be obtained.

Our conclusion on the LS-to-HS photoswitching dynamics is that it takes less than 100 fs for populating the HS potential. For moving from the LS potential to the HS potential, Fe–N bond lengths have to expand. This dynamics is limited by the intrinsic time-scale of Fe–N expansion, which occurs when d electrons are removed from the t_{2g} orbitals in the LS state. The time-scale can

be estimated from the Fe–N stretching mode in the HS state, which is observed at 255 cm^{-1} in [Fe(PM-AzA)$_2$(NCS)$_2$] [13] and corresponds to a period of 130 fs. This time-scale is of the same order as what we found here and indicates that it is the structural molecular reorganization inside the potential energy surface which limits the LS-to-HS transformation. The vibrational cooling, which we found here to occur within ≈ 1 ps corresponds well to the process discussed in the literature of SC systems, being molecules in crystals or in solution. The only difference is that vibrational cooling is slower in solution. This is very likely due to the less efficient dissipation of the excess energy to the environment: in solids lattice phonons allow an efficient coupling of the locally excited molecules with the environment, whereas in solution molecule has to transfer the excess energy to the solvent.

It should be underlined that in addition to Fe-based SC materials studied here, optical reflectivity or absorption can be used to study the photo-switching process involved in other types of photo-active molecule-based magnets. Of course, ultrafast spectroscopy can be applied to study LIESST effect in SC materials based on other metal ions, like Cu [14], Mn [15] or others. But ultrafast studies are also of interest for other types of photomagnetic materials where electronic and structural degrees of freedom are strongly coupled. Among them, we can mention charge-transfer (CT) systems like Fe–Co molecular materials [16] or Prussian Blue analogues [17], whose photo-switching process is associated with different types of dynamics. In addition to understanding the photoswitching pathway were different types of electronic and structural degrees of freedom will be involved, one of the fundamental points of interest is to know if (and how) the localized CT process can drive switching of adjacent active sites. This is also an open question for bi-nuclear or multi-nuclear SC systems.

References

[1] A. Lewanowicz, T. Luty, Acta Phys. Pol., A 121 (2012) 291.
[2] (a) S. Decurtins, P. Gütlich, C.P. Köhler, H. Spiering, A. Hauser, Chem. Phys. Lett. 105 (1984) 1;
    (b) A. Hauser, Chem. Phys. Lett. 124 (1986) 543;
    (c) A. Bousseksou, G. Molnar, L. Salmon, W. Nicolazzi, Chem. Soc. Rev. 40 (2011) 3313.
[3] (a) J.-F. Létard, P. Guionneau, O. Nguyen, J.S. Costa, S. Marcén, G. Chastanet, M. Marchivie, L. Capes, Chem. Eur. J. 11 (2005) 4582;
    (b) J.-F. Létard, J. Mater. Chem. 16 (2006) 2550.
[4] (a) A. Hauser, J. Jeftic, H. Romstedt, R. Hinek, H. Spiering, Coord. Chem. Reviews 190–192 (1999) 471;

(b) E. Trzop, M.B.L. Cointe, H. Cailleau, L. Toupet, G. Molnar, A. Bousseksou, A.B. Gaspar, J.A. Real, E. Collet, J. Appl. Crystallogr. 40 (2007) 158;
(c) J.-F. Létard, P. Guionneau, L. Rabardel, J.A.K. Howard, A.E. Goeta, D. Chasseau, O. Kahn, Inorg. Chem. 37 (1998) 4432;
(d) J.-F. Létard, L. Capes, G. Chastanet, N. Moliner, S. Létard, J.A. Real, O. Kahn, Chem. Phys. Lett. 313 (1999) 115;
(e) S. Marcén, L. Lecren, L. Capes, H.A. Goodwin, J.-F. Létard, Chem. Phys. Lett. 358 (2002) 87;
(f) S. Ohkoshi, K. Imoto, Y. Tsunobuchi, S. Takano, H. Tokoro, Nature Chem. 3 (2011) 564;
(g) M. Griffin, S. Shakespeare, H.J. Shepherd, C.J. Harding, J.-F. Létard, C. Desplanches, A.E. Goeta, J.A.K. Howard, A.K. Powell, V. Mereacre, Y. Garcia, A.D. Naik, H. Müller-Bunz, G.G. Morgan, Angew. Chem., Int. Ed. 50 (2011) 896;
(h) C. Chong, M. Haritosh, K. Boukheddaden, S. Denise, G. Bouchez, E. Collet, J.C. Ameiline, A. Naik, Y. Garcia, F. Varret, J. Phys. Chem. B 114 (2010) 1975.
[5] (a) M. Marchivie, P. Guionneau, J.A.K. Howard, G. Chastanet, J.-F. Létard, A.E. Goeta, D. Chasseau, J. Amer. Chem. Soc. 124 (2002) 194;
(b) M. Marchivie, P. Guionneau, J.-F. Létard, D. Chasseau, Acta Crystallogr., Sect. B 61 (2005) 25;
M. Buron-Le Cointe, J. Hébert, Phys. Rev. B 85 (2012) 064114.
[6] (a) N. Bréfuel, H. Watanabe, L. Toupet, J. Come, N. Matsumoto, E. Collet, K. Tanaka, J.-P. Tuchagues, Angew. Chem., Int. Ed. 48 (2009) 9304;
(b) N. Bréfuel, E. Collet, H. Watanabe, M. Kojima, N. Matsumoto, L. Toupet, K. Tanaka, J.P. Tuchagues, Chem. Eur. J. 16 (2010) 14060;
(c) H. Watanabe, N. Bréfuel, E. Collet, L. Toupet, K. Tanaka, J.-P. Tuchagues, Eur. J. Inorg. Chem. 5–6 (2013) 710.
[7] E. Collet, H. Watanabe, N. Bréfuel, L. Palatinus, L. Roudaut, L. Toupet, K. Tanaka, J.-P. Tuchagues, P. Fertey, S. Ravy, B. Toudic, H. Cailleau, Phys. Rev. Lett. 109 (2012) 257206.
[8] (a) J. Degert, N. Lascoux, S. Montant, S. Létard, E. Freysz, G. Chastanet, J.-F. Létard, Chem. Phys. Lett. 415 (2005) 206;
(b) E. Freysz, S. Montant, S. Létard, J.-F. Létard, Chem. Phys. Lett. 394 (2004) 318;
(c) S. Cobo, D. Ostrovskii, S. Bonhommeau, L. Vendier, G. Molnar, L. Salmon, K. Tanaka, A. Bousseksou, J. Am. Chem. Soc. 130 (2008) 9019;
(d) S. Bedoui, M. Lopes, W. Nicolazzi, S. Bonnet, S. Zheng, G. Molnár, A. Bousseksou, Phys. Rev. Lett. 109 (2012) 135702;
(e) G. Galle, J. Degert, C. Mauriac, C. Etrillard, J.F. Letard, E. Freysz, Chem. Phys. Lett. 500 (2010) 18.
[9] (a) C. Consani, M. Prmont-Schwarz, A. ElNahhas, C. Bressler, F. van Mourik, A. Cannizzo, M. Chergui, Angew. Chem., Int. Ed. 48 (2009) 7184;
(b) W. Gawelda, A. Cannizzo, V.T. Pham, F. van Mourik, C. Bressler, M. Chergui, J. Am. Chem. Soc. 129 (2007) 8199;

(c) A.L. Smeigh, M. Creelman, R.A. Mathies, J.K. McCusker, J. Am. Chem. Soc. 130 (2008) 14105;
(d) J. Tribollet, G. Galle, G. Jonusauskas, D. Deldicque, M. Tondusson, J.F. Letard, E. Freysz, Chem. Phys. Lett. 513 (2011) 42;
(e) M.M.N. Wolf, R. Groß, C. Schumann, J.A. Wolny, V. Schünemann, A. Døssing, H. Paulsen, J.J. McGarvey, R. Diller, Phys. Chem. Chem. Phys. 10 (2008) 4264;
(f) M. Chergui, Dalton Trans. 41 (2012) 13022;
(g) E.A. Juban, J.K. McCusker, J. Am. Chem. Soc. 127 (2005). 6857-6855.
[10] (a) R. Bertoni, M. Lorenc, A. Tissot, M. Servol, M.-L. Boillot, E. Collet, Angew. Chem., Int. Ed. 51 (2012) 7485;
(b) W. Kaszub, M. Buron-Le Cointe, M. Lorenc, M.-L. Boillot, M. Servol, A. Tissot, E. Collet, Eur. J. Inorg. Chem. 5–6 (2013) 992;
(c) A. Tissot, R. Bertoni, E. Collet, L. Toupet, M.L. Boillot, J. Mater. Chem. 21 (2011) 18347;
N. Moisan, M. Servol, C. R. Chim. 11 (2008) 1235;
M. Lorenc, Phys. Rev. B. 85 (2012) 054302.
[11] (a) M. Lorenc, J. Hébert, N. Moisan, E. Trzop, M. Servol, M. Buron-Le Cointe, H. Cailleau, M.L. Boillot, E. Pontecorvo, M. Wulff, S. Koshihara, E. Collet, Phys. Rev. Lett. 103 (2009) 028301;
(b) H. Cailleau, M. Lorenc, L. Guérin, M. Servol, E. Collet, M. Buron-Le Cointe, Acta Crystallogr., Sect. A 66 (2010) 133;
(c) E. Collet, M. Lorenc, M. Cammarata, L. Guérin, M. Servol, A. Tissot, M.-L. Boillot, H. Cailleau, M. Buron-Le Cointe, Chem. Eur. J. 18 (2012) 2051;
(d) E. Collet, N. Moisan, C. Baldé, R. Bertoni, E. Trzop, C. Laulhé, M. Lorenc, M. Servol, H. Cailleau, A. Tissot, M.-L. Boillot, T. Graber, R. Henning, P. Coppens, M. Buron-Le Cointe, Phys. Chem. Chem. Phys. 14 (2012) 6192.
[12] (a) P. Guionneau, J.F. Létard, D. Yufit, D. Chasseau, G. Bravic, A.E. Goeta, J.A. Howard, O. Kahn, J. Matter. Chem. 9 (1999) 985;
(b) P. Guionneau, M. Marchivie, G. Bravic, J.-F. Létard, D. Chasseau, Structural aspects of spin crossover, in: P. Gütlich, H.A. Goodwin (Eds.), Spin Crossover in Transition Metal Compounds Topics in Current Chemistry, vol. 234, Springer WienNewYork, 2004, p. 97.
[13] A. Hoefer, PhD Thesis, University of Mainz, 2000.
[14] M.V. Fedin, E.G. Bagryanskaya, H. Matsuoka, S. Yamauchi, S.L. Veber, K.Yu. Maryunina, E.V. Tretyakov, V.I. Ovcharenko, R.Z. Sagdeev, J. Am. Chem. Soc. 134 (2012) 16319.
[15] G.G. Morgan, K.D. Murnaghan, H. Müller-Bunz, V. McKee, C.J. Harding, Angew. Chem., Int. Ed. 45 (2006) 7192.
[16] (a) Y. Zhang et al., Angew. Chem., Int. Ed. 49 (2010) 3752;
(b) D. Siretanu et al., Chem. Eur. J. 17 (2011) 11704.
[17] M. Clemente-Leon, E. Coronado, A. Lopez-Munoz, D. Repetto, C. Laure, Mallah Talal, Langmuir 28 (2012) 4525.

Curved trajectory on the potential energy surface
in a spin-crossover material

Marco Cammarata,[1] Roman Bertoni,[1] Maciej Lorenc,[1] Hervé Cailleau,[1] Sergio Di Matteo,[1] Cindy Auriac,[2] Jean-François Létard,[2] Samir Matar,[2] Henrik Lemke,[3] Matthieu Chollet,[3] Sylvain Ravy,[4] Claire Laulhé,[4,5] Eric Collet[*,1].

* To whom correspondence should be addressed. E-mail: Eric.Collet@univ-rennes1.fr

[1]Institut de Physique de Rennes, UMR CNRS 6251, Université Rennes 1, 35042 Rennes, France,
[2] CNRS-Université de Bordeaux, ICMCB, 87 Av. du Doc. A. Schweitzer, F-33608 Pessac,
[3]LCLS, SLAC National Laboratory, Menlo Park, CA, USA,
[4]Synchrotron SOLEIL, L'Orme des Merisiers, Saint Aubin, F-91 192 Gif-sur-Yvette Soleil.
[5]Université Paris-Sud, 91405 Orsay Cedex France

We study how electronic excitation by light drives ultrafast photoswitching in a bistable spin-crossover molecular solid. It is of fundamental interest to understand the basic mechanisms allowing light to switch the molecular state with high efficiency, here from low spin (LS) to high spin (HS). Combined femtosecond x-ray absorption performed at LCLS X-FEL and optical spectroscopy reveal that the stabilization of the photoinduced HS state results from self-trapping of the electronic excited state, driven by the generation and damping of coherent phonons. The stabilization of the newly formed electronic state results from a two steps relaxation sequentially involving molecular breathing and torsion. We draw a complete scenario of the photoswitching pathway where the system is "bobsledding" across a potential energy surface along identified coordinates, which opens the way for optimizing molecular design for highly efficient photo-active systems.

A wide range of phenomena in nature are driven by changes that occur after illumination with light *(1)*, including chemical, bio-chemical or isomerization reactions *(2-4)*. In technology and material science, photo-driven functions related to magnetism *(5)* or conductivity *(6)* for example are of great interest for technological development. The field of photoinduced phase transition is at the heart of light-control science *(1)* inspiring light-based devices. The coupling between electronic and structural degrees of freedom of constituents of matter is the key parameter that determines the primary events at the onset of light-activated functions *(1,7,8)*. However, their development is limited by our understanding of these primary events occurring within less than a billionth of a second, when the out-of-equilibrium electronic excited state drives the change of structure for giving rise to a new function. Here we investigate the basic mechanisms leading to photo-switching between low spin (LS) and high spin (HS) states in a prototype spin-crossover (SCO) material *(9)*. By combining femtosecond x-ray absorption and optical spectroscopy we show that the ultrafast switching is driven by the generation and damping of coherent molecular breathing phonons, a phenomena recently proposed theoretically as the mechanism limiting conversion speed *(7)* and explaining the high efficiency of the process as it precludes recovery towards the initial state. We extract the main parameters sequentially involved describing the evolution of the system across the potential energy surface towards the HS state for describing the photoswitching pathway where different electronic and structural sub-systems are involved.

$[Fe(phen)_2(NCS)_2]$ (phen=1,10-phenanthroline, Fig. 1) is one of the prototypes systems of SCO family showing photo-magnetic and photo-chromic properties related to bi-stability between two electronic configurations of the Fe ion: the diamagnetic LS (S=0, $t_{2g}^6 e_g^0$) and paramagnetic HS (S=2, $t_{2g}^4 e_g^2$) states. It undergoes a first-order phase transition, where all the constituting molecules of the crystal simultaneously switch from LS to HS states above 176 K *(10,11)*. The strong coupling between electronic and structural degrees of freedom drives important structural reorganization of the constituting molecules (Fig. 1a), mainly around the central FeN_6 octahedron. The Fe atom is bonded by 2 N to each phen group and by 1 N to each NCS *(12)*, with $Fe-N_{NCS}$ bonds shorter than $Fe-N_{phen}$ because of their ionic character. As observed for many Fe^{II} complexes, the average Fe-N bond distance expands between LS and HS states (Fig. S1) from $<Fe-N>_{LS}$= 1.97 Å to $<Fe-N>_{HS}$=2.16 Å, because of the less bonding character of the HS electronic distribution. This change is associated with important modifications of the x-ray absorption near edge structure (XANES) spectra around the Fe K edge (Fig 1b). The measured increase at 7.125 keV and decrease at 7.148 keV, agree with the well documented XAS literature on this compound *(13)*.

Even though $[Fe(phen)_2(NCS)_2]$ is amongst the most widely investigated SCO solids, nothing is known on its ultrafast photo-switching dynamics. It is investigated here in the LS phase at 140 K. We used two complementary pump-probe methods where a fs laser pulse (650 nm) photo-excite molecules from LS to HS state via a metal-to-ligand charge-transfer process (MLCT, *10*). On the one hand, fs x-ray pulses were used as probe for measuring XANES at the XPP station of the LCLS x-ray free electron laser (X-FEL) *(14)*. On the other hand, fs laser pulses were used for measuring transient optical reflectivity (OR) and transmission (OT). Experimental details are given in supplementary information.
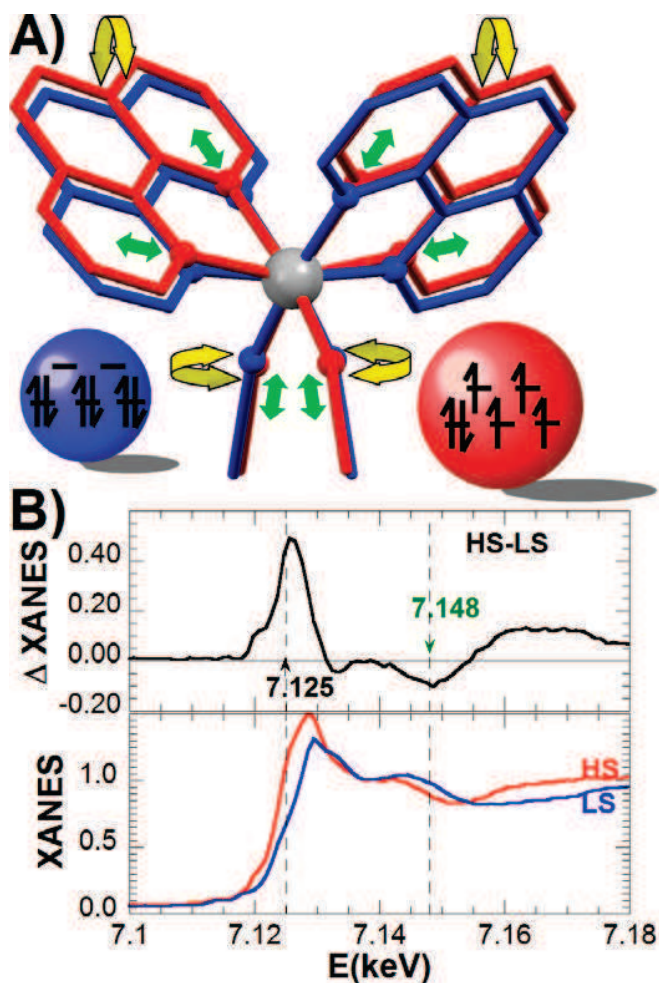
Fig. 1: (A) LS (140 K, blue) and HS (200 K, red) structures of the [Fe(phen)$_2$(NCS)$_2$] compound. The central Fe atom (grey) is bonded to the ligand by 6 N atoms (balls). The green and yellow arrows represent Fe-N stretching and ligand bending mode and respectively. (B) XANES spectra and variation ΔXANES measured between the LS and HS states.

The time course of the XANES signal (Fig. 2) was measured at two energies, identified as most sensitive to the change of spin state (Fig. 1), by varying the time delay between the laser pump and the x-ray probe pulses. A timing tool (14) was used for synchronizing the optical and x-ray laser pulses. The increase (respectively decrease) of XANES at 7.125 keV (resp. 7.148) are clear fingerprints of the photo-switching dynamics between LS and HS states. The rising time trace was fitted by convolving a Gaussian temporal Instrument Response Function (IRF) with an exponential rise mainly associated with Fe-N elongation (with a time constant τ_{Fe-N}). The results give a 110 (10) fs FWHM IRF allowing an accurate determination of τ_{Fe-N} = 170 (10) fs. OT and OR measurements were performed at different probe wavelengths (Fig. 3), also with a 110 fs IRF. Selected time traces in identified spectral zones are shown in Fig. 3A-C & S3.
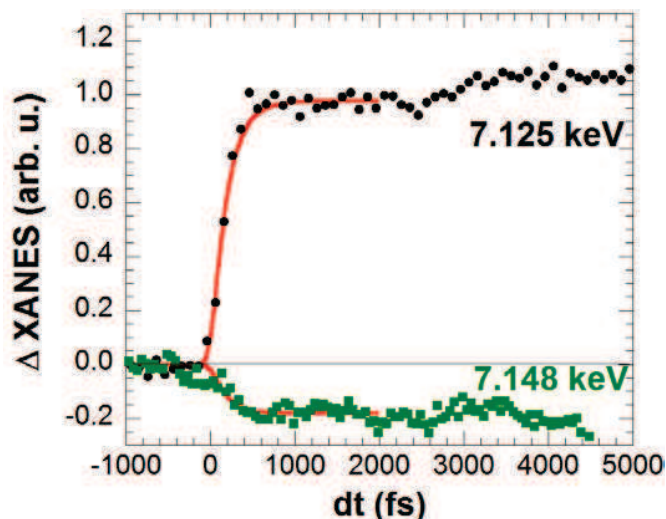
Fig. 2: Kinetic traces of XANES at 7.125 (●) and 7.148 (■) keV and fit with a single-exponential function of the rising edge (τ_1=170 (10) fs) represented by red solid lines.

Two main steps are revealed in the variation of optical transmission ΔOT: a transient peak appearing at 950, 850 and 760 nm immediately after laser excitation, followed by a relaxation towards a plateau during the first 100's fs.

The increase of optical absorption on the plateau, which translates into a simultaneous decrease of OT and OR at 760 nm, is another fingerprint of LS-to-HS conversion observed during the thermal conversion (10). It is explained by density of state calculations (Fig. S5), showing a decrease of the optical gap between t_{2g} and e_g bands from ≈ 1.9 eV (LS) to ≈1.6 eV (HS). The stronger absorption of the HS state at 760 nm (*i.e.* 1.6 eV) results from the gap narrowing, as the ligand field (t_{2g}-e_g splitting) decreases when <*Fe-N*> increases and optical data at 760 nm point to a ≈140 (20) fs time constant (Fig. 3 & S3). This optical signature of the Fe-N elongation dynamics through optical gap narrowing correlates well with the elongation time τ_{Fe-N}=170 (10) fs obtained by XANES.

The transient peak is the signature of electronic states different from LS and HS including the photo-excited [1]MLCT state and other possible intermediates (INT) such as [3]MLCT (7,8) which are difficult to identify because they are short-lived and have weak distinctive fingerprints. The transient peak of OT at 950 nm (Fig. 3C) indicates that the intersystem crossing (ISC) between MLCTs and HS potential corresponds to a time constant (τ_{ISC}) shorter than 50 fs, too short to be accurately determined with our IRF. These results in the solid state showing an ultrafast ISC (τ_{ISC} < 50 fs) followed by a structural elongation of Fe-N (τ_{Fe-N} ≈ 170 fs) are in good agreement with previous reports for similar Fe[II] molecules in solution (15-19) or Fe[III] nanocrystals (20). The analysis presented hereafter allow learning more about the basic mechanisms that allow efficient trapping of the photo-excited HS state.

An important feature is the observation of oscillating components in our data. Fig. 3D-F show the difference between time-dependent data and their single exponential fit. The corresponding Fourier transforms are
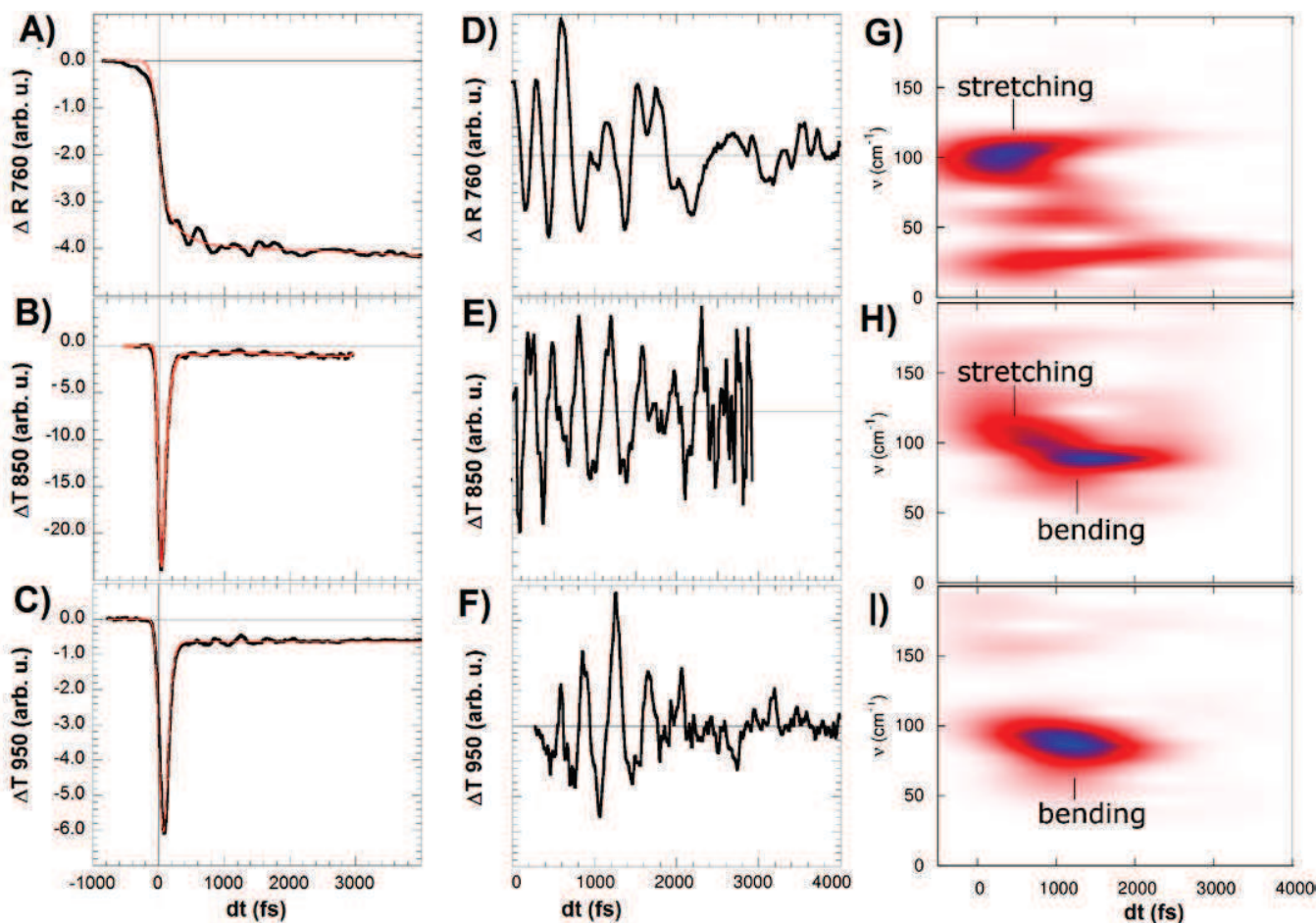
Fig. 3: Kinetic traces of optical reflectivity at 760 nm (A), transmission at 850 nm (B) and transmission at 950 nm (C). Fits with a single-exponential function (solid lines) are represented by red solid lines. The corresponding oscillating component of optical data are given in Fig 2D-F. Time dependent FFT of optical data (G-I) show activation of the stretching mode and delayed activation of the bending mode.

presented in Fig. G-I&S3-S4. OT and OR data at 760 nm, sensitive to the amplitude of the ligand field, evidence the excitation of a coherent mode around 113 cm^{-1}. This mode is identified in the literature as the breathing mode of the octahedron, involving mainly a stretching of the Fe-N$_{phen}$ bonds *(21,22,23)*. It is schematically represented by green arrows in Fig. 1 and shown in video S1 as obtained from molecular dynamics calculation (supp. Mat.). It is the strong modulation of the t_{2g}-e_g gap by the Fe-N$_{phen}$ elongation that makes it possible to observe this breathing mode in optical data at 760 nm and 850 nm. It is important to underline that the rich literature on [Fe(phen)$_2$(NCS)$_2$] *(21,22 and references therein)* allows assigning the 113 cm^{-1} frequency to the breathing mode of the HS state, as the frequency of this mode in the LS state is significantly higher ($\approx$150 cm^{-1}). This breathing mode is activated immediately after photo-excitation and corresponds to the first oscillations in Fig. 3D & 3E. The OT data below the gap (950 nm) are not so modulated by the ligand field and better probe the ISC

dynamics (τ_0<50 fs), and are later modulated by another coherent vibration around 85 cm^{-1} (Fig. 3F), identified in the literature as the ''butterfly'' mode *(21,22)*. It involves a bending of all the N-Fe-N angles with rigid phen groups without significant change of Fe-N distances, as shown in video S2 and schematically represented by yellow arrows in Fig. 1. Such a coherent ligand vibration was also observed for another Fe^{II} SCO molecular system in solution *(18)*, but here we should underline that, contrary to breathing, bending rises only after $\approx$ 500 fs and is maximum around 1300 fs (Fig. 3F&I).

A recent theoretical work *(7)* underlined that an ISC of tens of femtoseconds is compatible with a structural elongation of the order of 100–200 fs and that this is made possible by dephasing of MLCT state into HS phonon states. This is what we observe here, with the activation of breathing mode of the HS state within our experimental time resolution. But a simple generation of phonon could also give rise to recurrence toward the initial state, which is not observed. The fast damping of the stretching phonon was pointed as the mechanism suppressing the recurrence toward the initial state *(7)*. Our time dependent FFT show that coherent breathing has a spectral weight during the first ps only. Its damping occurs via energy redistribution and spectral weight transfer to other intra-molecular modes such as bending (85 cm^{-1}), but also at the inter-molecular level with the activation of lattice phonons (33 cm^{-1}, Fig. 3 H&I). This energy transfer to lattice phonon results from the coupling of the molecule with its crystalline environment,
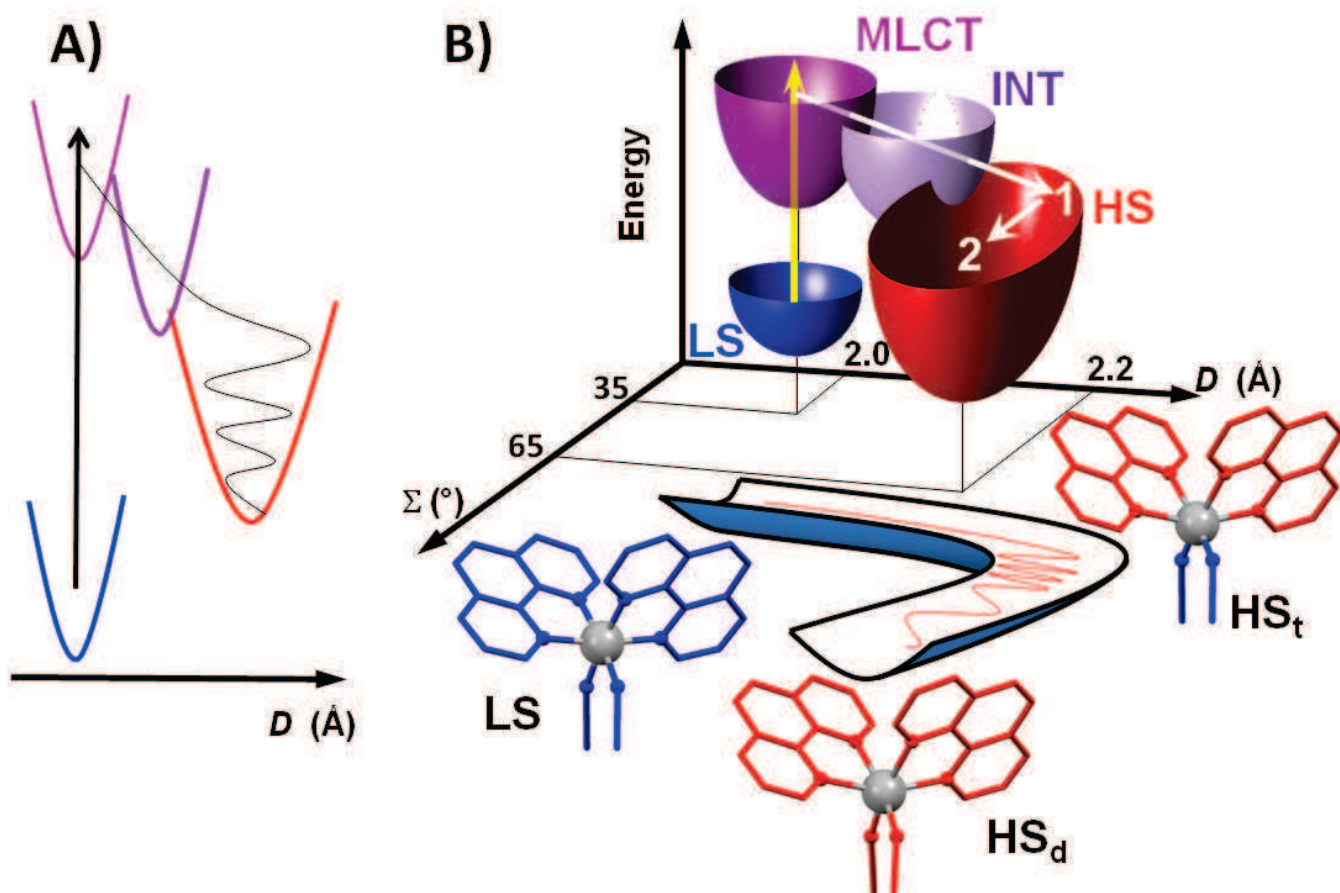
Fig. 4: (A) Schematic representation of the elongation and damping of the breathing mode along D. (B) Classical trajectory in the (D,Σ) space. Molecules in the LS potential reach MLCT state by light excitation. Fast ISC through possible INT states drive D elongation during step 1 with the generation and damping of breathing phonon involving mainly Fe-N$_{phen}$ bonds and giving rise to the HS$_t$ structure. The final equilibrium position in the HS potential is reached by activating additional phonons, as distortion Σ, during step 2.

and causes lattice expansion on nanosecond timescale which can drive additional switching by elastic coupling *(26)*. Our XANES data (Fig. 2) indicate that after the ≈ 0.2 Å elongation occurring within 170 fs the breathing amplitude is rapidly small. The signal/noise ratio allows estimating a maximum amplitude of 0.02 Å corresponding to the noise limit below which oscillation cannot be observed in our experiment. It indicates an important damping during the ISC (Fig. 4A), resulting from the cascading decay from MLCTs to HS state.

In SCO materials the elongation of $<Fe-N>$ during LS-to-HS conversion are very similar. But it is now established that the relative stability of LS and HS states is governed by the torsion Σ of the ligand *(12,24,25, supp. mat.)*. We draw a scenario of the ultrafast photoswitching pathway, by taking into account these two relevant structural changes associated with the sequential activation of the breathing (step 1) and bending (step 2) modes. Fig. 4B represents the trajectory across the potential energy surface (PES) in the (D,Σ) space, where D is the breathing

coordinate (mainly Fe-N$_{phen}$ elongation). The structural analysis at thermal equilibrium (Fig. S1) indicates that the potential of the LS ground state is centered at ($D_{LS} \approx 2$ Å, $\Sigma_{LS} = 35°$), whereas the one of the HS state is centered at ($D_{HS} \approx 2.2$ Å, $\Sigma_{HS} = 65°$). The photo-excitation of the initial $^1A_1$ ground LS state, with initial electronic configuration $t_{2g}^6 e_g^0 L^0$, where t_{2g} and e_g are the metal orbitals and L is the one of the ligand conserves spin, so that the photoexcited state is a ^{1}MLCT associated with an electron transfer from the metal to the ligand ($t_{2g}^5 e_g^0 L^1$). This transient CT step, which may involve other INT states *(7,8,14)*, is characterized by the transient absorption peak (Fig. 3) and the ISC for reaching the $t_{2g}^4 e_g^2 L^0$ HS potential is very fast (<50 fs).

In step 1 Fe-N elongates within 170 fs towards a new equilibrium distance, as the electronic distribution in the HS state corresponds to a less bonding state. This occurs through the activation and damping of the breathing mode, which involves mainly the Fe-N$_{phen}$ bonds *(21 & video S1)*. Indeed, the t_{2g} orbital of lower energy (of ionic character) shows electron density mainly on the Fe-N$_{NCS}$ bonds (Fig. S7). As the paired electrons always lie on this orbital in the LS and HS states, these stronger bonds are not directly affected by the electron redistribution on the other orbitals. In addition, the L orbitals toward which the metal is transferred, and lying ≈ 2 eV above the LS HOMO orbitals, show electronic densities located on the phen groups only, and do not involve NCS groups.

In step 2, the dephasing of the breathing mode is associated with the activation of other modes (such as bending), which allow reaching the low-lying equilibrium position in the HS potential. The activation and damping of

these other modes occur within $\approx$ 2ps. Around this delay, a small change of OT at 760 nm (Fig. S3) and a small increase of XANES at 7.125 keV (Fig. 2) are observed and the signal remains constant up to 80 ps (Fig. S6). This can be interpreted as the signature of a transient HS_t state in the 170-2000 fs time window resulting from the Fe-N_{phen} bonds elongation with the breathing mode, as this one does not involve so much the Fe-N_{NCS} (Fig. 4). These last may elongate when the complete molecular relaxation towards the HS structure occurs within $\approx$ 2 ps, as bending also involves NCS groups too. XANES spectra were calculated for the LS and HS structures and for a transient structure HS_t (Fig. S6), confirling an increase of XANES at 7.125 keV from LS to HS_t states and a weaker increase from HS_t to HS states. The delayed distortion activation of molecular modes, such as Σ, with respect to the elongation D of the Fe-N_{phen} indicates a curved path in the (D,Σ) PES, schematically represented in Fig. 4B, between the equilibrium position of the LS and HS states. It is known that molecular reactions or collisions often proceed not monotonically but oscillatory, since along the trajectory from the initial to final state the geometrical path can be complicated. Reactions often vibrate strongly but perpendicularly to the most probable classical path, whose energy is always the lowest at each step of this reaction process. This is the so-called "bobsled" effect *(27,28)*. In the present case, the photoinduced transformation occurring in a multi-dimensional coordinate space can be regarded as another king bobsled effect, as the system evolves in the PES along a curved trajectory with a spectral weight transfer from the breathing mode to others such as bending.

Our results underline the limit in the description of molecular systems with a single coordinate parameter (Fe-N) along a potential energy curve considered so far, as other structural degrees of freedom also play their role. In particular, the efficient electron-phonon and phonon-phonon couplings associated with a fast damping (Fig. 4B) are the control parameter of the photo-switching process. In the present case, the Fe-N_{NCS} are not directly involved in the early stage and this is a significant difference with molecules of higher symmetry, such as $[Fe(bpy)_3]^{2+}$ with 6 equivalent N atoms on the bpy *(15,17)* showing a single structural step. The structure of the FeN_6 coordination sphere and its denticity are indeed known as playing a key role in the thermal stabilization of the HS state *(29)*. This should also be true in the basic mechanism trapping the photo-excited states studied here. Investigating molecular systems with different types of coordination sphere, with different breathing, bending and damping, will help optimizing the crucial initial steps, for a rational design of materials with ultrafast and efficient photo-switching properties.

References and Notes

1. K. Nasu, Ed., Photoinduced phase transitions (World Scientist, Singapore, 2004).
2. Schotte et al, *Science* **300**, 1944 (2003)
3. D. Polli, et al *Nature* **467**, 440–443 (2010)
4. A.B. Wohri, *et al. Science* **328**, 630-633 (2010).
5. M. Verdaguer, *Science* **272**, 698 (272).
6. M. Gao, et al *Nature* **496**, 343-346 (2013)
7. M. van Veenendaal, J. Chang, A.J. Fedro, *Phys. Rev. Lett.* **104**, 067401 (2010).
8. J. Chuang, A.J. Fedro, M. van Veenendaal, *Phys. Rev. B* **82**, 075124 (2010)
9. M. Halcrow, Ed., Spin-crossover materials (Wiley, West Sussex, 2013) ISBN 9781119998679.
10. E.König and K. Madeja, *Inorg. Chem.* **6**, 48 (1967)
11. E. W. Müller, H. Spiering and P. Ganutlich, *Chem. Phys. Lett.,* **93,** 567 (1982)
12. M. Marchivie *et al, J. Am. Chem. Soc.* **124** 195 (2002)
13. B. Arezki *et al, Chem. Phys. Chem.* **12**, 405 – 410 (2011)
14. M. Harmand, *et al, Nature Photonics*, **7** 215-218 (2013)
15. C. Bressler, et al, *Science* **323**, 489-492 (2009)
16. N. Huse, et al, *J. Phys. Chem. Lett.* **2**, 880, (2011)
17. H. Lemke et al, *J. Phys. Chem. A* **117**, 735-740 (2013)
18. C. Consani, et al, *Angew. Chem.* **121**, 7320 (2009)
19. W. Gawelda, et al *J. Am. Chem. Soc.* **129**, 8199–8206 (2007)
20. R. Bertoni et al, *Angew. Chem Int. Ed.* **51**, 7485 (2012)
21. K.L. Ronayne et al, *Phys. Chem. Chem. Phys.* **8**, 4685 (2006)
22. G. Baranovic, D. Babic, *Spectrochem. Acta A* **60**, 1013 (2004)
23 S. Matar, J.F. Létard, *Z. Naturforsch* **65b**, 565 (2010)
24. M. Buron-Le Cointe et al, *Phys. Rev. B* **85**, 064114 (2012)
25. A. Hauser et al, *Chem. Rev.* **250**, 1642 (2006).
26. E. Collet et al, *Phys. Chem. Chem. Phys.* **14**, 6192-6199 (2012).
27. J. Polanyi, W.H. Wong, *J. Chem. Phys.* **51**, 1439 (1969).
28. K. Nasu, *Eur. Phys. J. B* **75**, 415–430 (2010)
29. J. F. Létard, *J. Mater. Chem.* **16**, 2550 (2006).

30 P. Ganguli, P. Gütlich, E. W. M Wuller, Inorg. Chem. 21, 3429 (1982)

31 M. J. Frisch, et al, GAUSSIAN03 (revision C.02), Gaussian, Inc., Wallingford CT, 2004.

32 Y. Joly, Phys. Rev. B 63 125120 (2001)

Curved trajectory on the potential energy surface in a spin-crossover material

Marco Cammarata, Roman Bertoni, Maciej Lorenc, Hervé Cailleau, Sergio Di Matteo,

Cindy Auriac, Jean-François Létard, Samir Matar, Henrik Lemke, Matthieu Chollet,

Sylvain Ravy, Claire Laulhé, Eric Collet[*].

* To whom correspondence should be addressed. E-mail: Eric.Collet@univ-rennes1.fr

Movies: 2 movies are attached as supplementary material.

Video S1: the breathing mode of $[Fe(phen)_2(NCS)_2]$

Video S2: the ligand torsion mode of $[Fe(phen)_2(NCS)_2]$.

Samples:

Single crystals of $[Fe(phen)_2(NCS)_2]$ compound were obtained by slow diffusion as indicated in reference *(11)*. The powder films of $[Fe(phen)_2(NCS)_2]$ compound has been prepared according to the description of Gütlich and co-workers *(30)*; i.e. i) by reacting 0.77 g (2.77 mmol) of $FeSO4 \cdot 7H2O$ and 0.539 g (5.55 mmol) of KSCN in dry and freshly distilled methanol (6 ml), ii) by filtered off the K2SO4 precipitated, and iii) by adding the solution to 1 g (5.55 mmol) of 1,10-phenanthroline in 3 ml of methanol. The Red precipitated was filtered off, washed with methanol and diethyl ether and further purified by the Soxhlet technique during 48 hours. The powder film consists in µm size crystals in a polymeric matrix. XANES spectra measured on single crystal or on powder film are very similar. Fig. 1B shows the XANES spectra for the LS (140 K) and HS (200 K) states measured on the powder film.

X-ray structure analysis of thermal LS to HS phase transition.

Structural investigations at thermal equilibrium in the 100-250 K range were performed by X-ray diffraction on single crystals. Data were collected on a four-circle Oxford Diffraction Xcalibur 3 diffractometer (MoK_α radiation) with a 2D Sapphire 3 CCD detector, on samples with typical sizes around $200 \times 150 \times 50$ μm^3. The single crystals were mounted in an Oxford Cryosystems nitrogen-flow cryostat. The structural refinements gave similar results as the ones already reported in the literature *(12)*, allowing to follow the evolution of the main structural changes around the coordination sphere of the Fe atom:

- the distances between the Fe and the bonded N atoms (there are 2 Fe-Nphen and 1 Fe-N_{NCS} independent bonds) and the average: $<Fe-N> = \frac{1}{6} \sum_{i=1}^{6} Fe-N_i$

- the distortion Σ of the FeN_6 octahedron measuring by the sum of the deviation from 90° of the 12 N-Fe-N cis ϕ angles in the coordination sphere: $\Sigma = \sum_{i=1}^{12} |90 - \phi_i|$

In the LS phase $<Fe-N>_{LS} \approx 1.97$ Å and $\Sigma_{LS} \approx 35°$ and these parameters discontinuously change in the HS phase to $<Fe-N>_{HS} \approx 2.17$ Å and $\Sigma_{HS} \approx 65°$. This discontinuous change of the structure is related to the discontinuous change of the spin state of $[Fe(phen)_2(NCS)_2]$ *(10,12)* and illustrate that structure and electronic states are strongly coupled.

Figure S1. Temperature dependence of Fe-N bonds and Σ parameter, showing the first-order phase transition around 176 K between LS and HS states.
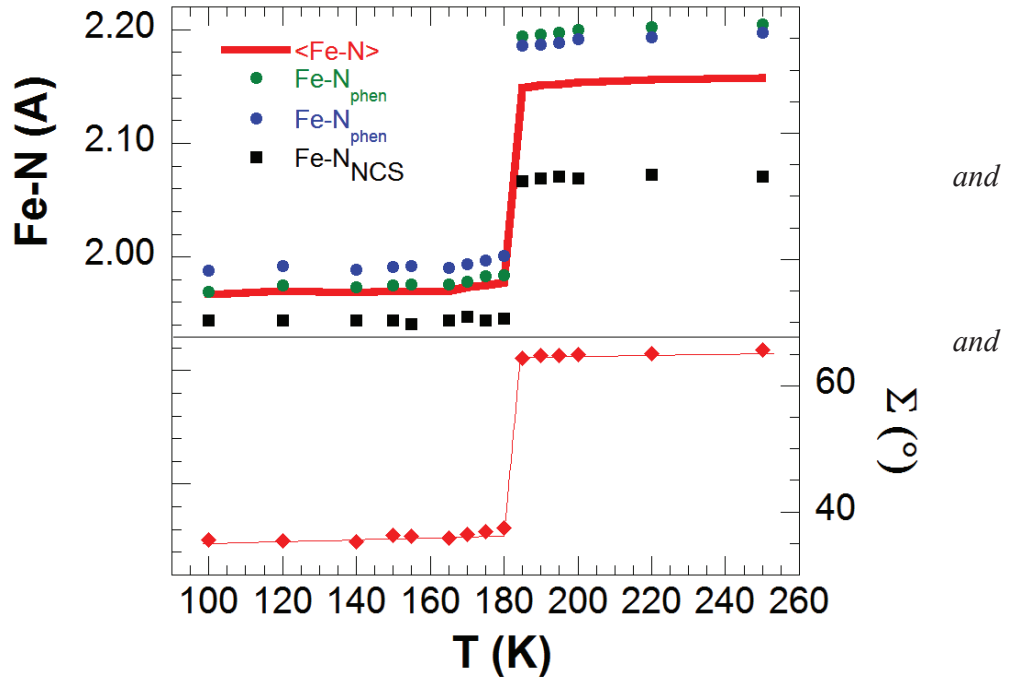
Experimental details of femtosecond pump-probe studies

We have investigated the LS-to-HS photoswitching dynamics by performing pump-probe measurements at 140 K, where [Fe(phen)2(NCS)2] compound is in the pure LS state. The sample was cooled by a nitrogen cryostream. For x-ray and optical studies, the pump wavelength was set to 650 nm where it efficiently induces LS-to-HS transition.

x-ray absorption probe:

Optical pump and x-ray probe studies were performed at the XPP beamline of the LCLS X-FEL. A femtosecond laser operating at 100 Hz delivered 40 fs pump pulses at 650 nm focused to 200x200 μm on the sample, with intensities of the order of 2-5 mJ. The x-ray beam was monochromatised using the XPP double Si(111) crystal monochromator and focused to about 100x100 mm on the sample. To ensure pulse durations limited time resolution and avoid thermal drifts of the timing, the recently developed "timing tool" has been used. This has the capability of measuring the shot to shot relative arrival time between x-ray and infrared laser pulses with few tens of femtoseconds resolution *(14)*. The x-ray fluorescence was collected using a Si diode (Canberra FD450-18-300RM) positioned at a 90° angle with respect to the x-ray beam propagation direction. The incoming intensity was measured using two noninvasive diagnostics (one before and one after the x-ray monochromator) developed for pulsed x-ray radiation *(14)*. We detected the total x-ray fluorescence yield to obtain the XANES spectra in the vicinity of the Fe K-edge (7.112 keV). Optical pump - XANES probe studies on single crystal gave weak signal because of the limited matching of the penetration depths of optical pump and x-ray probe. Therefore, we used the powder films (~few centimeters square) and yet thin (5 μm) samples for increasing the signal/noise ratio. Fig. S2 show the constant XANES signal after few ps.

*Figure S2. XANES at 7.125 keV* *in the [-2 ,80] ps range.*
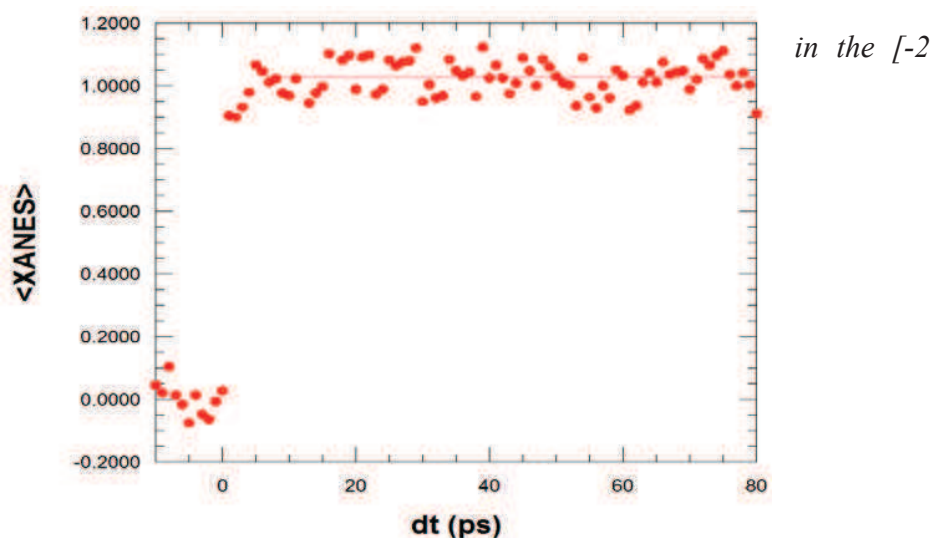
Optical probe:

Optical pump-probe studies were performed in Rennes, with a wavelength tunable femtosecond laser operating at 1 kHz and delivering 80 fs pump and probe pulses. Two-colour pump-probe spectroscopy studies were performed on single crystals (10-20μm thick). Single-wavelength measurements probed the resulting dynamics through optical reflectivity (OR) change at 760 nm and optical transmission (OT) at 760, 850 and 950 nm, as the absorption is too high in the visible range. Measurements presented here were performed on single crystal. In addition to data presented in Fig. 2 we show in Fig. S2 OT data at 760 nm, where the Fe-N stretching mode is observed. FFT of the oscillating component of time-dependent optical spectroscopy are presented in Fig. S3.
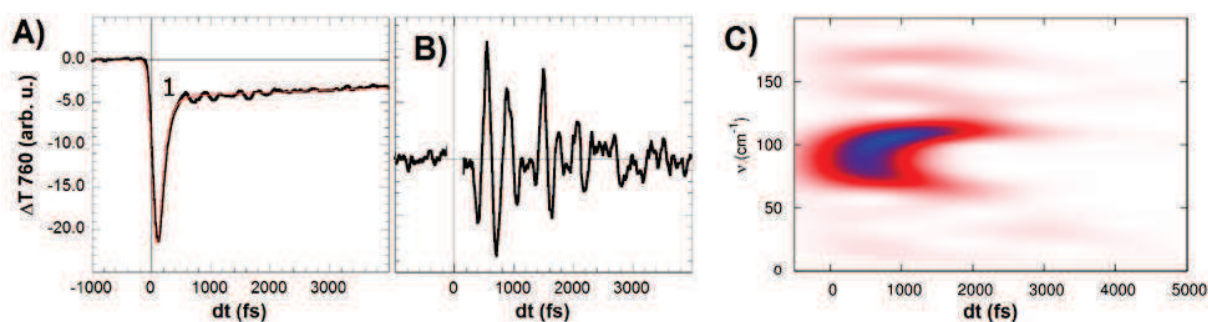
Figure S3. OT at 760 nm (A), oscillating component (B) and time-dependent FFT showing the 113 cm^{-1} mode (C).
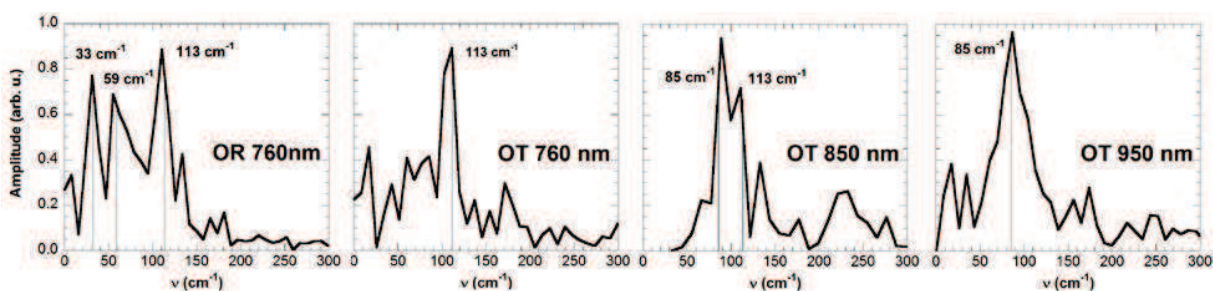
Figure S4. FFT of OR at 760 nm and OT at 760, 850 and 950 nm indicating the two main modes at 113 cm^{-1} (stretching) and 85 cm^{-1} (bending).

**Solid-state Computations of the density of state and molecular dynamics:**

Density Of State (DOS) calculations were already performed for in the LS phase of [Fe(phen)$_2$(NCS)$_2$] and detailed presentation is given in ref (23). The same method was used here for comparing the change of DOS

in the HS phase. Results are given in Fig. S5. The major feature is the low dispersion of the peaks which is descriptive of a molecular system, *i.e.* in opposition to a metal or an intermetallic system where the DOS are broadened. Somehow, even in the organized periodic solid state, [Fe(phen)$_2$(NCS)$_2$] exhibits molecular behavior. The key information regarding the time-resolved optical studies presented here is that on both sides of the gap the DOS correspond the Fe d states which are respectively t_{2g} and e_g like.

The DOS calculations indicate that
- in the LS state the t_{2g}-e_g gap is around 1.9 eV
- in the HS state the t_{2g}-e_g gap is around 1.6 eV
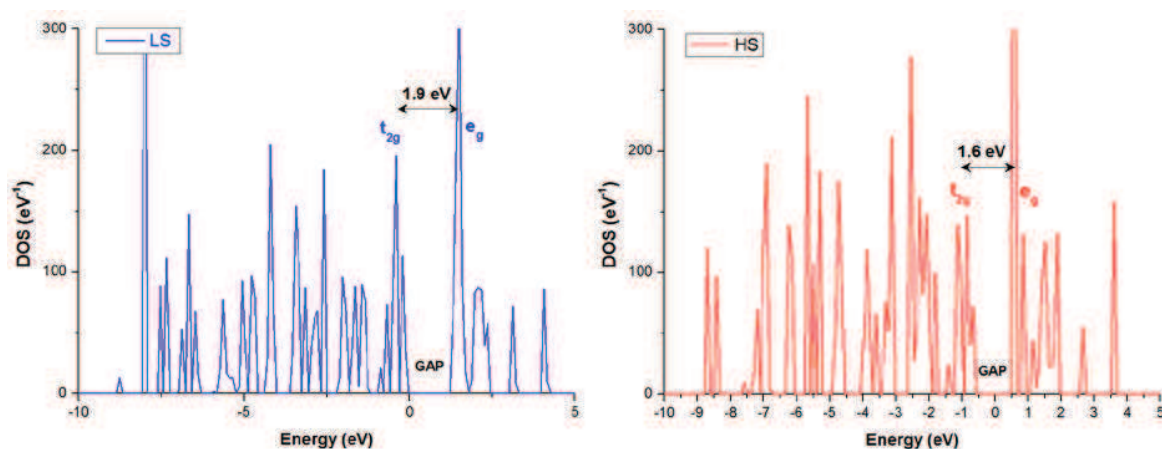
Figure S5. Total DOS for [Fe(phen)$_2$(NCS)$_2$] in its LS (blue) and HS (red) states.

The LUMO (lower unoccupied molecular orbitals) lying $\approx$ 2 eV above the LS HOMO (higher occupied molecular orbital) orbitals with paired electrons, are shown in Fig. S6 and have electron density on the phen groups only. The t_{2g} orbital of lower energy is of ionic character and shows electron density mainly on the Fe-N$_{NCS}$ bonds.
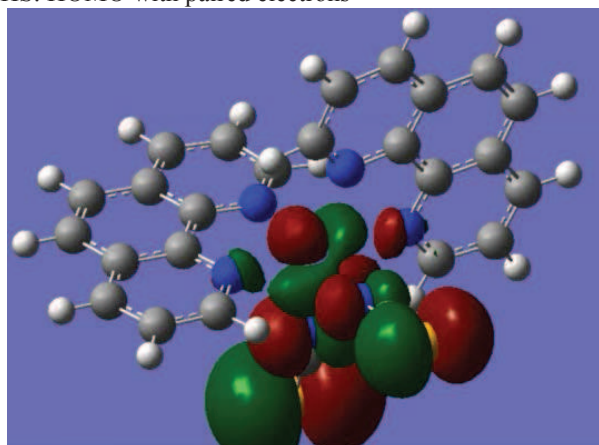
LS: LUMO 1 ligand
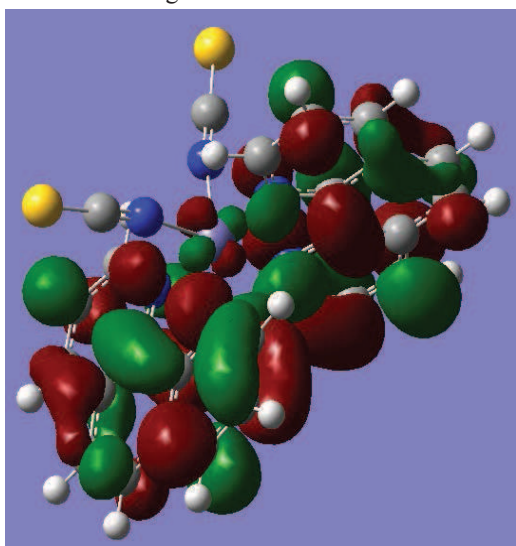
LS: LUMO 2 ligand
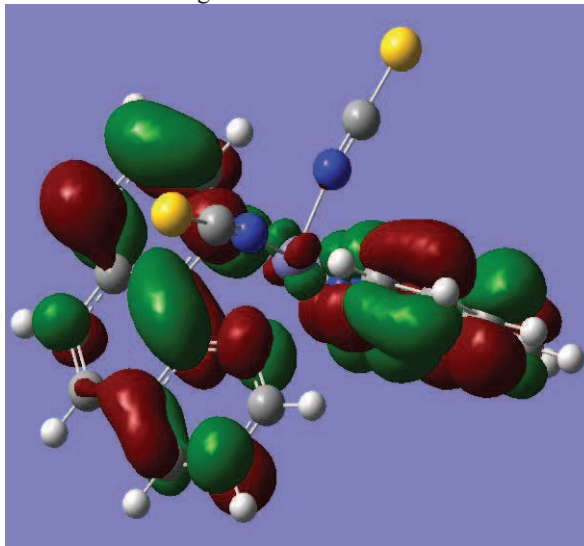
HS: HOMO with paired electrons

Figure S6. DFT calculation of the LS LUMO molecular orbitals, indicating that the CT process occurs on the phen groups, and HS HOMO with paired electron on the Fe-N_{NCS} bonds. Fe is in the center, N atoms are blue, C atoms are grey, S atoms are yellow, H atoms are white.

Molecular vibration frequencies calculations were carried out for [Fe(phen)$_2$(NCS)$_2$] after geometry optimization, by using hybrid B3LYP functional with LANL2DZ basis set within Gaussian09 code *(31)*. Frequencies are determined from the second derivatives of the energy with respect to the atomic positions and then operating transformation to mass-weighted coordinates. Exploring the results especially for the vibrations and their animations with screen captures was done with Gaussview annex module to Gaussian. Video S1 shows the breathing mode and video S2 show the ligand torsion mode. A complete analysis will be published elsewhere.

XANES calculation:

XANES spectra were calculated with the FDMNES program *(32)* for the structures of the LS and HS states and for the transient HS$_t$ state. The input of the calculations were provided by the experimental LS

structure (at 120 K) and HS structure (at 250 K) as obtained by x-ray diffraction and shown in Fig. S7. The HS$_t$ structure was instead constructed with elongated Fe-N$_{phen}$ with the structure of the phen groups similar to the HS state (red) and short Fe-N$_{NCS}$ with the structure of the NCS groups similar to the LS state (blue). The XANES calculations are presented in Figure S7, with LS and HS spectra corresponding well to the ones measured at thermal equilibrium (Fig. 1) and an intermediate change at 7.125 keV between the LS and the HS states for the HS$_t$ structure.
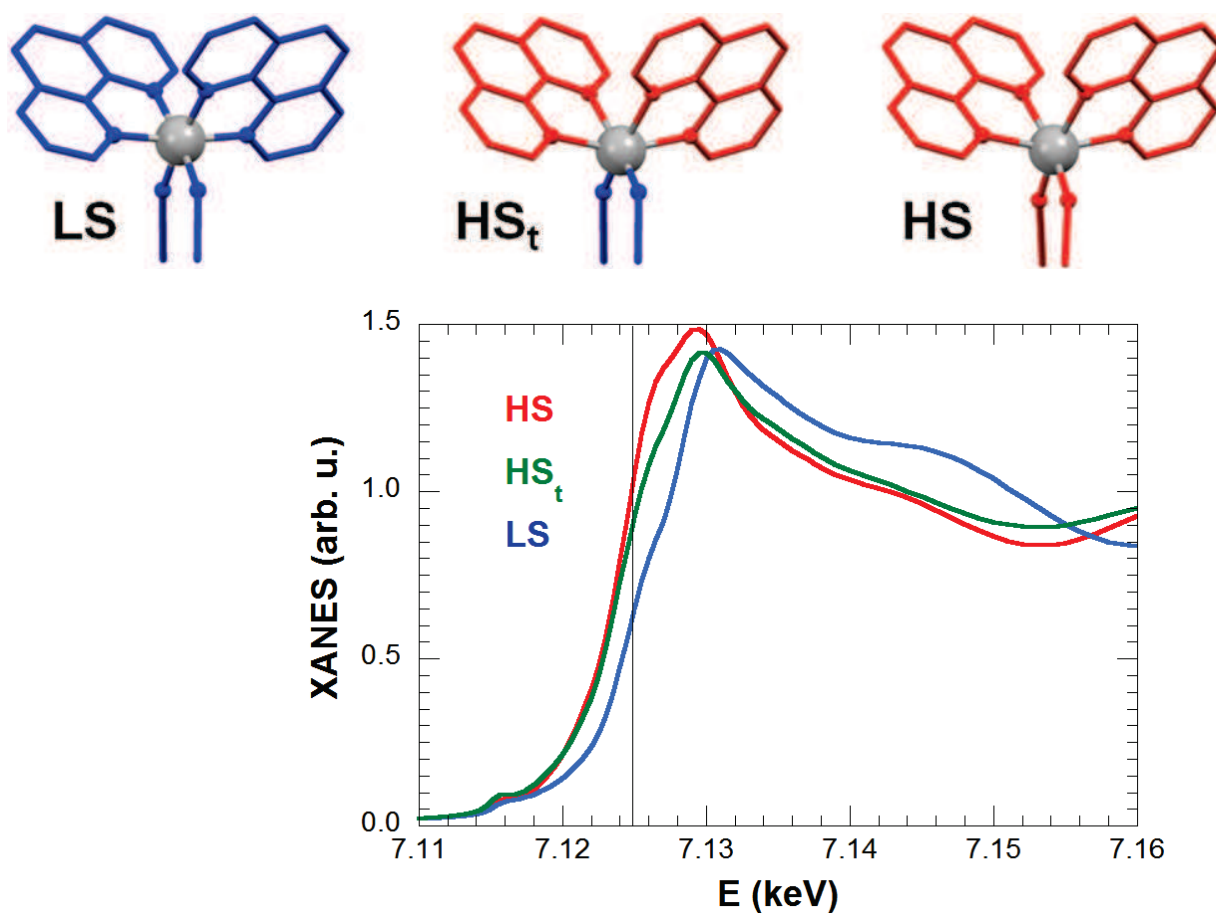
Figure S7. Calculated XANES spectra for the LS and HS structures known at thermal equilibrium and for the transient HS$_t$ states.